Electroweak boson production at small transverse momentum in hadron collisions

Kulesza, Anna K.

Electroweak Boson Production at Small Transverse Momentum in Hadron Collisions

Anna K. Kulesza

A thesis submitted for the degree of
Doctor of Philosophy

University of Durham

Centre for Particle Theory

September 2000

Abstract

The resummation of double-logarithmic perturbative contributions produced by soft-gluon radiation (Sudakov resummation) has proved to be an important tool for enlarging the applications of perturbative QCD to a wider range of kinematical regions. In particular, a complete description of W and Z boson production at high-energy hadron colliders requires the resummation of large double logarithms that dominate the transverse momentum ($p_{\rm T}$) distribution at small $p_{\rm T}$. This can be performed either directly in transverse momentum space or in impact parameter (Fourier transform) b space. The b space method succeeds in resumming all the leading and sub-leading logarithmic terms, but does not allow a smooth transition to fixed-order dominance at high transverse momenta. In contrast, the $p_{\rm T}$ space approach experiences difficulties with resumming more sub-leading logarithms.

This thesis concentrates on developing the $p_{\rm T}$ space formalism which completely resums the first four towers of logarithms. The number of fully resummed towers is the same as for the b space method. The results are compared, both analytically and numerically, with the original b space result as well as with results of other $p_{\rm T}$ space methods. Parametrization of the non-perturbative effects in $p_{\rm T}$ space is discussed. Given recent Tevatron data on Z boson production we find good agreement between the data and the theoretical predictions. Using the same formalism, the transverse momentum distributions are also calculated for W and Z boson production at the LHC. Finally, we discuss production of like-sign W pair production in the context of double parton scattering at the LHC.

Acknowledgements

First and foremost I would like to thank my supervisor, James Stirling, for his continuous guidance and support over the last three years. From the very first moment of encouraging me (no doubt by mistake) to apply for a PhD place in Durham, I have been given much confidence and help. I am indebted to him for sharing his knowledge and physical intuition with me as well as deepening my understanding of particle physics. I greatly appreciate the numerous illuminating discussions and, most of all, his patience to answer my ignorant questions.

My deep gratitude goes to Mike Pennington who, against all the odds, made my PhD studies in Durham possible from the financial point of view. I would also like to express my thanks to all the other members of the staff in the CPT for granting me the opportunity to be part of the group.

To the original, always-ready-for-a-good-distraction, team of room 307 - John, Matt and Pete, thank you very much for putting up with me, my gibberish English and bossy aspirations. I am grateful to Maria-Elena and Martin for bearing the misfortune of sharing the office with me this year. Jeppe and Stephen - thank you for sorting out all my computer worries, no matter how trivial. To all the rest of the students on the top floor I am grateful for making it a friendly place to work and, equally often, to share a good laugh. Particular mention must also go to those from the Maths side of the CPT, specifically Linda and Stuart, on whom one could always rely when it came to solving every Friday's dilemma of choosing between The Swan and The Half Moon...

Special acknowledgements are dedicated to my house-mates last year, Gavin and Michael. Can I also thank Michael for his determination as a squash coach. More on the social side, lots of thanks are addressed to the GradSoc bar crew and the inmates from the Fonteyn Court, in particular Dawn, for keeping me in touch with reality.

Most of all I would like to thank Darrell, for his encouragement, total confidence in me and the heroic ability to stand my endless mourns. Thank you for going through it all with me.

Finally, with all my heart I would very much like to thank my family, in particular my Mum, for the unlimited support and love I was so lucky to have over these years.

* * *

This work has been funded by the Overseas Research Students Award Scheme, University of Durham research studentship and the EU Fourth Framework TMR Programme, contract FMRX-CT98-0194 (DG 12 -MIHT).

Declaration

I declare that no material presented in this thesis has previously been submitted for a degree at this or any other university.

The research described in this thesis has been carried out in collaboration with Prof. W.J. Stirling and has been published as follows:

- A. Kulesza and W.J. Stirling,
  Sudakov logarithm resummation in transverse momentum space for electroweak boson production at hadron colliders,
  Nucl. Phys. **B555** (1999) 279, [hep-ph/9902234].

- A. Kulesza and W.J. Stirling,
  On the resummation of subleading logarithms in the transverse momentum distribution of vector bosons produced at hadron colliders,
  JHEP **0001** (2000) 016, [hep-ph/9909271].

- A. Kulesza and W.J. Stirling,
  Like-sign W boson production at the LHC as a probe of double parton scattering,
  Phys. Lett. **B475** (2000) 168, [hep-ph/9912232].

- A. Kulesza and W.J. Stirling,
  Sudakov logarithm resummation for vector boson production at hadron colliders,
  J. Phys. G **G26** (2000) 637, [hep-ph/9912300].

- A. Kulesza and W.J. Stirling,
  Heavy Gauge Boson Production at Small Transverse Momentum in Hadron-Hadron Collisions,
  in *Particle Physics: Ideas and Recent Developments. Proceedings, NATO Advanced Study Institute, Cargese, France, August 1999.*, ed. J.J. Aubert, Kluwer Academic Publishers (2000).

- S. Catani *et al.*,
  QCD, in *1999 CERN Workshop on SM Physics (and more) at the LHC,*
  CERN-2000-004, [hep-ph/0005025].

Moim Rodzicom

We have a habit in writing articles published in scientific journals to make the work as finished as possible, to cover up all the tracks, to not worry about the blind alleys or describe how you had the wrong idea first, and so on. So there isn't any place to publish, in a dignified manner, what you actually did in order to get to do the work.

Richard P. Feynman (1918 - 1988).

Preface

The foundations of the modern science of particles physics rely on the principle of reduction of all the observable physical phenomena down to four elementary interactions between the constituents of matter. Apart from gravity, the nature of the remaining basic forces: electromagnetism, strong and weak interactions, is described theoretically in the framework of the *Standard Model* (SM) [1] of particle physics.

There are two types of elementary particles: the basic building blocks themselves, i.e. obeying Fermi-Dirac statistics (*fermions*) - the matter particles, and the particles intermediating the interactions, satisfying the Bose-Einstein statistics (*bosons*). The first ones can be classified into *leptons* and *quarks*. In contrast to leptons, quarks interact strongly and are not seen in experiment. They are understood as elementary constituents of *hadrons* – the strongly interacting particles observed in Nature. The existence of all of the SM quarks (u, d, s, c, b, t) and leptons (e, μ, τ, ν_e, ν_μ, ν_τ) is confirmed experimentally, with the recent discovery of ν_τ completing the list.

The SM describes the three interactions in the language of renormalizable, gauge invariant *quantum field theories*. Within the SM, the theory of electromagnetic interactions is given by *Quantum Electrodynamics* (QED). In QED, the interactions between particles carrying electromagnetic charge are mediated by the massless and electrically neutral *photon* γ. The *Electroweak Model* provides a unified description of electromagnetic and weak interactions. The weak force in the broken Electroweak Model is mediated by three massive vector bosons W^+, W^-, Z. The theory of strong interactions, *Quantum Chromodynamics* (QCD) is the main focus of this thesis. Here the strong force is mediated by eight massless, electrically neutral, colour carrying, *gluons*.

From the theoretical point of view, the SM is a field theory based on the *gauge symmetry group* $SU(3)_C \times SU(2)_L \times U(1)_Y$. This gauge group includes the symmetry of the strong interactions $SU(3)_C$ and the symmetry of the electroweak interactions $SU(2)_L \times U(1)_Y$. The group symmetry of the electromagnetic interactions, $U(1)_{EM}$, appears in the SM as a subgroup of $SU(2)_L \times U(1)_Y$ and it is in this sense that the electromagnetic and weak

interactions are said to be unified. More precisely, the existence in Nature of the massive W^+, W^-, Z and the massless photon implies that $SU(2)_L \times U(1)_Y$ symmetry needs to be broken down to $U(1)_{EM}$. By introducing spontaneous symmetry breaking into the gauge theory like the SM, one ensures the renormalizability of the model. The implementation of the symmetry breaking, by the means of the so-called *Higgs mechanism* leaves an aftermath in the form of the prediction of a new scalar and electrically neutral particle, the *Higgs boson*. The Higgs particle is the only remaining element of the SM awaiting experimental confirmation.

The Standard Model provides an elegant theoretical framework and the current precision tests report an excellent agreement between the theory and experimental data. However, it contains some twenty *ad hoc* parameters which need to be extracted from measurement. Any calculations of a theoretical quantity require knowledge of these parameters. Since even a small deviation from the SM predictions observed experimentally could signal new (non-SM) physics, a precise knowledge of the values of the SM parameters is of crucial importance. It can be achieved only by a common effort of improving accuracy of the theoretical calculations and precision of the experimental measurement. In addition to use in background process calculations, knowledge of SM parameters, together with the relations between them, can lead to estimates for the values of the other parameters. In particular, the mass of the W boson, M_W, and the mass of the top quark, m_t, are related to the mass of the Higgs particle.

In this thesis we are concerned with detailed calculations of the transverse momentum distribution of electroweak bosons (virtual photon γ^*, weak boson $W^\pm$, Z) produced in hadron-hadron collisions. The calculations are performed in the framework of QCD. In the course of this thesis it will become obvious that the transverse momentum distribution is a good quantity to test QCD predictions against experimental data. In principle it can be also used for the extraction of the M_W parameter. Furthermore, the transverse momentum distribution may prove extremely convenient to look for possible deviations from the SM, mimicking the effect of SM gauge boson production. A detailed knowledge of vector boson production mechanism becomes mandatory at future hadron colliders, where this process is expected to be one of the major sources of background to new physics processes.

Contents

Chapter 1

Elements of QCD

The first evidence for the substructure of hadrons came from the experiments of the 1960's conducted at the Stanford Linear Accelerator Center (SLAC). It turned out to be a revolutionary milestone on the route to the theory of strong interactions, *Quantum Chromodynamics* (QCD). The substructure of hadrons was, however, already foreseen theoretically. In order to rationalize the observed hadron spectroscopy, Gell-Mann and Zweig proposed that hadrons were made from spin-1/2 particles, *quarks*, the fundamental building blocks of matter. Out of it grew the idea of *colour*, a new quantum number which ensured that the hadronic states assembled from quarks have the right quantum statistics. The property of colour is not observed in Nature, and thus the colours (fictitious red, green and blue) of the constituent quarks must be combined in such a way that only colour-less hadrons are produced.

In the deep inelastic scattering (DIS) experiments at SLAC, electrons were scattered off hydrogen and deuterium targets, probing the structure of nucleons in a way similar to the classic Rutherford experiments. The experimental results suggested that the projectile electrons scattered off almost free point-like constituents, - and this idea was embraced by Feynman's *parton model.* In the parton model, hadrons are imagined as extended objects, made up of constituent partons and held together by their mutual interactions. Moreover, the hadrons can be described in terms of virtual partonic states but one is not in a position

to calculate the structure of these states. On the other hand, it is possible to compute the scattering of a free parton by an electron in the parton model. The partons were later experimentally identified with quarks and *gluons*, carriers of the strong interaction.

The successful description of quark dynamics found its realization in a non-abelian quantum gauge field theory incorporating the property of colour, known as QCD. In this chapter we are going to concentrate only on those aspects of QCD which are crucial for the subject of this thesis.

Detailed surveys of quantum field theory can be found in [2] while excellent reviews of QCD theory and phenomenology are given in [3]-[7].

1.1 The QCD Lagrangian

The theory of strong interactions, QCD, is defined as a field theory by the Lagrange density

$$\mathcal{L}_{\rm QCD} = \mathcal{L}_{\rm classical} + \mathcal{L}_{\rm gauge} + \mathcal{L}_{\rm ghost} \,. \tag{1.1.1}$$

Since the physical content of the theory shows no dependence on redefinitions of colour fields, the Lagrangian (1.1.1) is invariant under colour transformations. This is an example of an internal symmetry of the theory: transformation on internal coordinates (here in the colour space) which transform one field into another with different internal quantum numbers. By imposing the *gauge principle*, i.e. requiring the symmetry to be local and the theory to remain invariant, an originally free theory turns into an interacting theory. In the case of QCD, local colour transformations of the Lagrangian generate the gauge *symmetry group* - the non-abelian Lie group SU(3).

We discuss the symmetry group and the form of particular terms in the Lagrangian (1.1.1) in the following sections.

1.1.1 The symmetry group SU(3)

SU(3) is the Lie group of 3×3 unitary matrices with determinant one. Any element of the group, U, can be constructed given 8 parameters $\Theta_a(x)$

$$U(x) = e^{i\Theta_a(x)T^a} . \tag{1.1.2}$$

T^a are the generators of the group SU(3) obeying the commutation relation

$$[T^a, T^b] = if^{abc}T_c , \tag{1.1.3}$$

which define the Lie algebra of the group SU(3). Real and antisymmetric, the f^{abc} are known as the structure constants of QCD. The matrices T^a give, in the conventional normalization, the following relations for the SU(3) invariant *colour factors* T_R, C_F, C_A

$$\begin{aligned} Tr(T^aT^b) &= T_R\delta^{ab}; & T_R &= \tfrac{1}{2}, \\ \sum_a T^a_{\alpha\beta}T^a_{\beta\gamma} &= C_F\delta_{\alpha\gamma}; & C_F &= \tfrac{4}{3}, \\ \sum_{a,b} f^{abc}f^{abd} &= C_A\delta^{cd}; & C_A &= 3, \\ (a,b,c,d &= 1...8, & \alpha,\beta,\gamma &= 1,2,3) . \end{aligned} \tag{1.1.4}$$

1.1.2 The classical Lagrangian

The classical QCD Lagrangian density reads[1]

$$\mathcal{L}_{\text{classical}} = \sum_f \bar{\psi}_f(i\mathcal{D}^\mu\gamma_\mu - m_f)\psi_f - \frac{1}{4}F^a_{\mu\nu}F^{\mu\nu}_a . \tag{1.1.5}$$

The quark fields are the four-component Dirac spinors ψ_f - vectors in the colour space, so that for each quark flavour

$$\psi_f = \begin{pmatrix} \psi_f^R \\ \psi_f^G \\ \psi_F^B \end{pmatrix} \tag{1.1.6}$$

[1]The metric convention here is $g^{\mu\nu}$ = diag(1,-1,-1,-1) and the gamma matrices satisfy the Clifford algebra relation $\{\gamma^\mu, \gamma^\nu\} = 2g^{\mu\nu}$.

where R, G, B denote quark colour (red, green, blue). There are N_f independent quark flavours which are summed over in (1.1.5). The quark fields transform as the fundamental representation of SU(3)

$$\psi_f(x) \to U(x)\psi_f(x)\,. \tag{1.1.7}$$

The Lagrangian (1.1.5) is invariant under the local gauge transformations if the covariant derivative $\mathcal{D}^\mu$ transforms like the quark field i.e.

$$\mathcal{D}^\mu\psi_f(x) \to U(x)\mathcal{D}^\mu\psi_f(x)\,. \tag{1.1.8}$$

This can be ensured by the definition of the covariant derivative

$$\mathcal{D}^\mu \equiv \partial^\mu + igA_a^\mu T^a\,, \tag{1.1.9}$$

with the spin-1 gauge fields A_a^μ transforming in the adjoint representation of SU(3)

$$A_a^\mu(x)T^a \to U(x)A_a^\mu(x)T^aU^\dagger(x) + \frac{i}{g}[\partial^\mu U(x)]U^\dagger(x)\,. \tag{1.1.10}$$

The field strength tensor describing the dynamics of the gauge fields has the form

$$F_a^{\mu\nu} = \partial^\mu A_a^\nu - \partial^\nu A_a^\mu - g f_{abc} A_b^\mu A_c^\nu\,, \tag{1.1.11}$$

so that the kinetic term $-\frac{1}{4}F_{\mu\nu}^a F_a^{\mu\nu}$ in the Lagrangian (1.1.5) remains gauge invariant.

To summarise, $\mathcal{L}_{\text{classical}}$ describes the matter content of the theory, its interactions with the gauge particles – gluons (first term in (1.1.5)) and the dynamics of the gauge sector (second term). The non-abelian character of the gauge group SU(3) encrypted in the kinetic term generates the cubic and quartic gluon self-interactions. The strength of the interaction is given by the parameter g, also known as the *coupling constant*. Local gauge invariance requires the same coupling for the quartic and triple interactions as for the quark-gluon interactions. The other parameters are the quark masses m_f. Unlike the quarks, gluons cannot have mass if the invariance of the Lagrangian is to be preserved.

The QCD Lagrangian can be understood as the non-abelian generalization of QED. The non-abelian character is necessary for gluons to carry colour charge, as compared to photons and the electric charge in QED. As mediators of strong interactions gluons are

responsible for binding quarks together in hadrons. Since hadrons are colour-less they must be colour singlets in the group theory language. The basic colour singlet states provided by SU(3) are $q\bar{q}$ and qqq combinations, corresponding to the quark structure of mesons and baryons, respectively.

1.1.3 Gauge fixing

The canonical treatment of the Lagrangian (1.1.5) faces several problems. Firstly, the field A_a^0 is a classical quantity and the canonical momentum associated with A_a^0 vanishes. As a result, the canonical quantization procedure fails. Moreover, the field A_a^μ has the freedom of gauge transformations. These two troublesome features can be perceived as an outcome of an attempt to describe a spin-1 massless gluon with two physical degrees of freedom (polarizations) in terms of a four-vector. The remedy to the quantization problem is brought about by constraining A_a^μ, for example by imposing the Lorentz invariant condition [6]

$$\partial_\mu A_a^\mu = 0\,. \tag{1.1.12}$$

This constraint can be implemented in the Lagrangian if a *gauge-fixing term* is added to the Lagrangian

$$\mathcal{L}_{\text{gauge}} = -\frac{1}{2\zeta}(\partial_\mu A_a^\mu)^2\,. \tag{1.1.13}$$

Due to the presence of the gauge-fixing term, the Lagrangian is no longer gauge invariant. The physical observables are, in turn, necessarily gauge independent. Thus the value of ζ is irrelevant to the physical result and can be set arbitrarily. The common choices are $\zeta = 0$ (Landau gauge) and $\zeta = 1$ (Feynman gauge). In the absence of the gauge-fixing term, i.e. $\zeta = \infty$, the gluon propagator is not well defined.

The gauge fixed by the condition (1.1.12) is a *covariant gauge*. Other choices are also possible, for example *axial gauges* with the condition

$$n_\mu A_a^\mu = 0\,, \tag{1.1.14}$$

where n_μ is a fixed vector. Then the gauge-fixing term in the Lagrangian has the form

$$\mathcal{L}_{\text{gauge}} = -\frac{1}{2\zeta}(n \cdot A_a)^2 \,. \tag{1.1.15}$$

Another non-covariant gauge, the planar gauge [8, 29], is defined by

$$n_\mu A_a^\mu = B_a \,, \qquad n^2 < 0 \,, \tag{1.1.16}$$

where the function B_a is arbitrary but independent of the gauge field. This leads to the gauge-fixing term

$$\mathcal{L}_{\text{gauge}} = -\frac{1}{2\zeta n^2} n \cdot A_a \, \partial^2 n \cdot A_a \,, \qquad \zeta = +1 \,. \tag{1.1.17}$$

1.1.4 Ghosts

An additional term in the Lagrangian is required in the covariant gauges to remove unphysical degrees of freedom of the gluon field. The unphysical contributions from the redundant degrees of freedom are canceled if the Lagrangian contains an additional, so-called Faddeev-Popov *ghost term*

$$\mathcal{L}_{\text{ghost}} = \partial_\mu \eta^{a\dagger} (\mathcal{D}^\mu_{ab} \eta^b) \,. \tag{1.1.18}$$

Ghosts are fictitious scalar fields which obey fermionic anti-commuting properties and couple only to gluons. The addition of the ghost term to the Lagrangian is a mathematical procedure allowing one to develop a simple covariant formalism. The non-covariant gauges are ghost-free.

1.2 From the theory to experiment

In particle physics one is interested in calculating physical quantities such as scattering cross sections and decay widths. The road from the Lagrangian density to experimentally observable quantities is well established. Cross sections can be related, through the Feynman amplitudes $\mathcal{M}$, to the *S-matrix* (scattering matrix) elements. An S-matrix element

between an initial and a finite state gives the amplitude for a field configuration that was simple far in the past to evolve into a field configuration that will be simple in the future. Whenever the Lagrangian of the theory is a sum of free (quadratic) Lagrangian and interacting terms then S-matrix elements of the interacting field theory can be expanded around those in the free theory as a power series in the coupling constant. In this approach the interaction emerges as a small perturbation on free theory and the systematic method for expanding in the coupling constant is known as *perturbation theory*.

In practice, calculations of the S-matrix elements, rather than performed *ab initio*, are greatly simplified by using the *Feynman rules* technique. This relies on the one-to-one correspondence between the diagrammatic representation of the basic elements (e.g. *propagators* and *vertices*) of the theory and the equivalent mathematical expressions, giving a simple set of rules. The Feynman rules are derived from the Lagrangian, using for example the path integral formalism. In particular, the free part of the Lagrangian gives rise to propagators while the interacting part is responsible for the form of the vertices. By drawing all possible topologically distinct diagrams of the appropriate order for the specific process and applying the Feynman rules, the transition amplitudes can be calculated. A thorough discussion of Feynman rules in quantum field theories can be found in many textbooks [2].

1.3 Higher order calculations

The current precision of high energy experiments demands an equal accuracy from the theoretical calculations. Therefore higher order terms in the perturbative expansion for physical observables need to be calculated. However, cross sections turn out to be ill-defined (infinite) when loop diagrams are included in the perturbative calculations: a problem characteristic of all quantum field theories. Examples of such loop diagrams in QCD are shown in Fig. 1.1. Consider the one-loop correction to the gluon self-energy,

Fig. 1.1a. Using the QCD Feynman rules one obtains

$$i\Pi^{\mu\nu}_{ab}(q) = -g^2\delta_{ab}T_F \int \frac{d^4k}{(2\pi)^4} \frac{\mathrm{Tr}\left[\gamma^\mu \not{k}\gamma^\nu(\not{k}-\not{q})\right]}{k^2(k-q)^2} \sim \int d^4k \frac{1}{k^2}\,. \tag{1.3.19}$$

This integral is quadratically divergent in the high momentum limit. In general, two types of divergences appear in the higher order calculations:

UV divergences when the integral is divergent in the $k\to\infty$ limit. All three diagrams in Fig. 1.1 are UV divergent.

IR divergences when the integral is divergent in the $k\to 0$ limit. Again, all three diagrams in Fig.1.1 are divergent in the IR limit.

Clearly, the problem is caused by the unconstrained momentum flow in the loop. For the time being we will focus on the UV divergence problem and postpone the discussion of the IR divergences until Section 1.4.

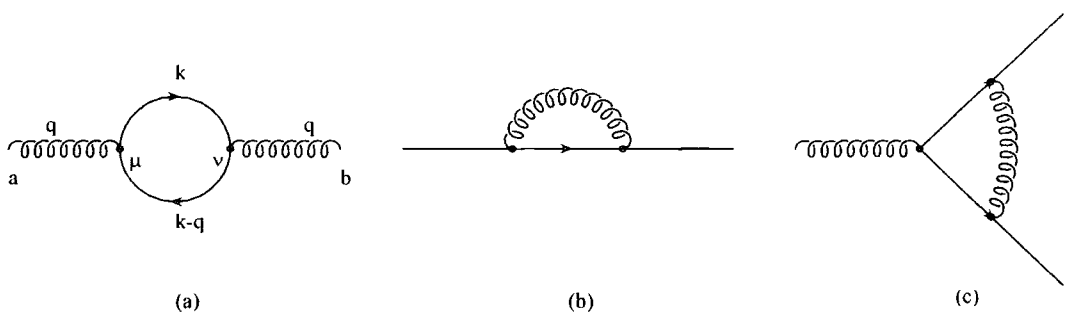

Figure 1.1: The one loop corrections to (a) gluon self-energy, (b) quark self-energy and (c) quark-gluon vertex.

The remedy applied to recover finite values from UV divergent quantities is provided by renormalization theory. But before the execution of the renormalization procedure, it is necessary to regularize the divergences, as the manipulation of infinite integrals is not well defined mathematically.

1.3.1 Regularization

There have been several regularization methods proposed in the literature [9]. The integral (1.3.19) can be, for example, regularized by introducing an upper cut-off, but the most universal method proves to be *dimensional regularization* (DR) [10]. Unlike other methods, it preserves unitarity together with Lorentz and gauge invariance. DR relies on performing an analytic continuation of the divergent integrals in the number of space dimensions D, so that the integrals yield finite values in D dimensions. Returning to the gluon self-energy calculations in $D = 4 - 2\epsilon$ after regularization we have

$$\Pi^{\mu\nu}_{ab} = \frac{4}{3} T_R \delta_{ab} (-q^2 g^{\mu\nu} + q^\mu q^\nu) \left(\frac{g\mu^\epsilon}{4\pi}\right)^2 \left[\frac{1}{\epsilon} - \gamma_E + \ln(4\pi) - \ln(\frac{-q^2}{\mu^2}) + \frac{5}{3} + \mathcal{O}(\epsilon)\right], \tag{1.3.20}$$

where the Euler-Mascheroni constant $\gamma_E = 0.57722....$ Here the arbitrary scale μ has been introduced to preserve the dimensionless nature of the coupling, i.e. in $D = 4 - 2\epsilon$ dimensions $g \to g\mu^\epsilon$, so that $g^2 d^4k \to g^2 \mu^{2\epsilon} d^{4-2\epsilon}k$.

1.3.2 Renormalization

After regularizing the infinities, the perturbation series can be arranged in such a way that the terms divergent in $D = 4$ dimensions are absorbed in the new, redefined parameters of the theory. Then a meaningful physical theory is recovered by removing the regulator, e.g. taking $D \to 4$ in DR. The process of redefining the original, 'bare' fields, masses, gauge parameters and couplings present in the Lagrangian to their physical equivalents is known as *renormalization.* In perturbation theory the renormalization procedure is performed order-by-order and relies on introducing suitable counter-terms in the Lagrangian which results in a modification of the bare parameters. For local gauge theories, such as QCD, the renormalizability of the theory is a consequence of the local gauge invariance.

Unfortunately, the renormalization procedure is not unambiguous. Firstly, it introduces an arbitrary scale μ in the renormalized expression, as seen in (1.3.20). This is the renormalization scale, the scale at which the counter-terms are subtracted. The second

ambiguity is related to the renormalization prescription. Although the singular terms are all removed successfully their definition is not unique. Depending on the convention, different parts of the finite pieces produced by the regularization procedure can be subtracted together with the infinities. For example, in DR, if $D = 4 - 2\epsilon$ then the poles in $1/\epsilon$ always appear in the combination, cf. (1.3.20),

$$\frac{\Gamma(1+\epsilon)}{\epsilon}(4\pi)^{\epsilon} = \frac{1}{\epsilon} + \ln(4\pi) - \gamma_E + \mathcal{O}(\epsilon)\,. \tag{1.3.21}$$

The prescription for how to subtract divergences is called the *renormalization scheme* (RS). Throughout this work we use the *modified minimal subtraction* ($\overline{\text{MS}}$) scheme in which the poles in $1/\epsilon$ are subtracted together with all finite constants appearing on the r.h.s. of Eq. (1.3.21).

1.3.3 Renormalization group

Physical observables are well-defined, measurable quantities. Therefore the corresponding theoretical predictions should not contain ambiguities; in particular they are required to remain independent of the choice of the RS. In other words, all choices of RS must be equivalent and the invariance of the observables under change of RS evokes the mathematical concept of the *renormalization group*. For the time being let us neglect the dependence on the renormalization prescription and concentrate only on the μ dependence first. Consider the dimensionless variable $\mathcal{R}$ at the scale Q. Since after renormalization there would be another scale μ available, $\mathcal{R}$ depends on Q^2/μ^2 and the coupling at the renormalization scale $\alpha_s = \alpha_s(\mu^2) = g(\mu^2)/4\pi$. The independence from μ^2 stems from the following condition

$$\mu^2 \frac{d}{d\mu^2}\mathcal{R}(\frac{Q^2}{\mu^2}, \alpha_s) = \left[\mu^2\frac{\partial}{\partial\mu^2} + \beta\frac{\partial}{\partial\alpha_s}\right]\mathcal{R}(\frac{Q^2}{\mu^2}, \alpha_s) = 0\,, \tag{1.3.22}$$

where we define

$$\beta(\alpha_s) = \mu^2\frac{\partial\alpha_s}{\partial\mu^2}\,. \tag{1.3.23}$$

These equations are the simplest example of the *renormalization group equations* (RGE).

Alas, the independence from the RS holds only for the full theoretical predictions for observables, i.e. for the all order calculated quantities. In perturbation theory we truncate the series expansion at a certain order, violating the cancellation between RS dependent terms of different orders. The price paid is the remaining spurious dependence on the RS in the truncated expression.

1.3.4 Running coupling

The RGE of (1.3.23) leads to a differential equation for the coupling [3]

$$Q^2 \frac{\partial \alpha_s}{\partial Q^2} = \beta(\alpha_s)\,, \tag{1.3.24}$$

describing the *evolution (running)* of the coupling α_s with the scale at which it is evaluated. The QCD β function can be calculated perturbatively

$$\beta(\alpha_s) = -\alpha_s^2(\beta_0 + \alpha_s\beta_1) + ... \tag{1.3.25}$$

while

$$\beta_0 = \frac{1}{4\pi}\left(11 - \frac{2}{3}N_f\right)\,, \qquad \beta_1 = \frac{1}{16\pi^2}\left(102 - \frac{38}{3}N_f\right)\,, \tag{1.3.26}$$

where N_f is the number of active quark flavours.

Solving Eq. (1.3.24) at leading order gives

$$\alpha_s(Q^2) = \frac{\alpha_s(\mu^2)}{1 + \beta_0 \ln\left(Q^2/\mu^2\right)\alpha_s(\mu^2)} \tag{1.3.27}$$

with an expansion

$$\alpha_s(Q^2) = \alpha_s(\mu^2)\left[1 - \alpha_s(\mu^2)\beta_0 \ln\left(\frac{Q^2}{\mu^2}\right)\right] + ... \tag{1.3.28}$$

Originating from the RGE for the coupling, Eq. (1.3.27) is an all-orders expression (up to leading logarithm accuracy). In fact it is the first example of a *resummed quantity* - a quantity arising after reorganization of the perturbative series (which we have not shown here explicitly) and summing an infinite series of otherwise divergent contributions (here terms of the form $\alpha_s^N \ln^{N-1}\left(Q^2/\mu^2\right)$).

The independence of the running coupling from μ can be made explicit by noticing from (1.3.27) that

$$\frac{1}{\alpha_s(Q^2)} - \beta_0 \ln(Q^2) = \frac{1}{\alpha_s(\mu^2)} - \beta_0 \ln(\mu^2) = -\beta_0 \ln(\Lambda^2)\,, \tag{1.3.29}$$

where Λ is a new scale, a constant of the theory. The running of α_s can now be expressed as

$$\alpha_s(Q^2) = \frac{1}{\beta_0 \ln\left(Q^2/\Lambda^2\right)} \tag{1.3.30}$$

and it is clear that α_s depends only on Q. At $Q \sim \Lambda$, $\alpha_s \sim 1$ and the perturbation theory is no longer valid. Thus Λ can be regarded as the transition scale between the perturbative and non-perturbative (short-distance and long-distance) regime. From the formal point of view, it can be also interpreted as a parameterization of a missing boundary condition in (1.3.24). In spite of the fundamental character of Λ, its definition depends on the order up to which β function is evaluated, the choice of the RS, as well as on the number of assumed active quark flavours. The current experimental value for the next-to-next-to-leading order Λ in the $\overline{\text{MS}}$ scheme at five quark flavours is $\Lambda_{\overline{\text{MS}}}^{NNLO}(5) = 208^{+25}_{-23}$ MeV [11]. A more accurate solution for $\alpha_s(\mu^2)$ is obtained including also the β_1 term in the β-function series (1.3.25)

$$\alpha_s(Q^2) = \frac{1}{\beta_0 \ln(Q^2/\Lambda^2)} - \frac{\beta_1 \ln\ln(Q^2/\Lambda^2)}{\beta_0^3 \ln^2(Q^2/\Lambda^2)}\,, \tag{1.3.31}$$

with the expansion

$$\alpha_s(Q^2) = \alpha_s(\mu^2)\left[1 - \alpha_s(\mu^2)\beta_0 \ln\left(\frac{Q^2}{\mu^2}\right) + \alpha_s^2(\mu^2) \ln\left(\frac{Q^2}{\mu^2}\right)\left(\beta_0^2 \ln\left(\frac{Q^2}{\mu^2}\right) - \beta_1\right)\right] + \ldots\,. \tag{1.3.32}$$

1.3.5 Asymptotic freedom and confinement

The behaviour of the running coupling exhibits important properties characterizing QCD.

- With an increasing energy scale Q, the coupling $\alpha_s(Q^2)$ decreases. This property, known as *asymptotic freedom*, ensures that the perturbative treatment of QCD gives reliable predictions at high energy scales. Since the theory approaches a free theory

in the UV region, quarks within behave as asymptotically free particles, in the way assumed by the parton model and observed in high energy processes.

- With a decreasing energy scale, $\alpha_s(Q^2)$ decreases. This signals the breakdown of the validity of the perturbative solution to QCD at $Q \sim \Lambda$. It also suggests that the interaction is strong enough to bind quarks into hadrons so that only hadrons are observed in experiment. Accordingly, the *confinement* at low energies is plausible in QCD, but due to the strength of the coupling cannot be proved using standard perturbative techniques.[2]

The nature of the running of α_s is governed by the β function, Eq. (1.3.25) and (1.3.26). Both asymptotic freedom and confinement arise as a consequence of $\beta_0 > 0$. This is opposite to QED where $\beta_0 < 0$ and the coupling increases (decreases) with the larger (smaller) energy scale. The difference in the behaviour of the coupling can be traced to the nature of the symmetry properties of the theory. In non-abelian theories, such as QCD, gauge particles interact with each other and spread out the charge (colour), generating an anti-screening effect. Technically, the contributions to the β_0 coefficient coming from the glue-glue interactions lead to the positive value of β_0.

1.4 Infrared singularities

Let us now return to the discussion of IR divergences first encountered in Section 1.3. Recall that the higher order corrections in perturbative QCD suffer from divergences in the IR limit. An example of such a divergent correction is given by diagram in Fig 1.1. In general, all possible IR singularities are related to two types of momentum configuration:

Soft divergences arise when a massless on-shell particle emits a massless low momentum, $k^\mu \sim 0$, 'soft' particle and remains on-shell. Integration over k^μ near $k^\mu = 0$ yields a divergent result.

[2]The hypothesis of confinement is confirmed by calculations in lattice QCD, a non-perturbative formulation of QCD.

Collinear divergences arise when an on-shell particle with momentum p^μ emits a massless particle with momentum $k^\mu = \lambda p^\mu$, $0 \leq \lambda \leq 1$ and remains on-shell. Integration over k^μ near $k^\mu \sim \lambda p^\mu$ yields a divergent result.

1.4.1 IR singularities in e^+e^- annihilation

The total hadronic cross section for e^+e^- annihilation provides a good example to discuss the appearance of IR singularities in more detail. The real and virtual $\mathcal{O}(\alpha_s)$ corrections

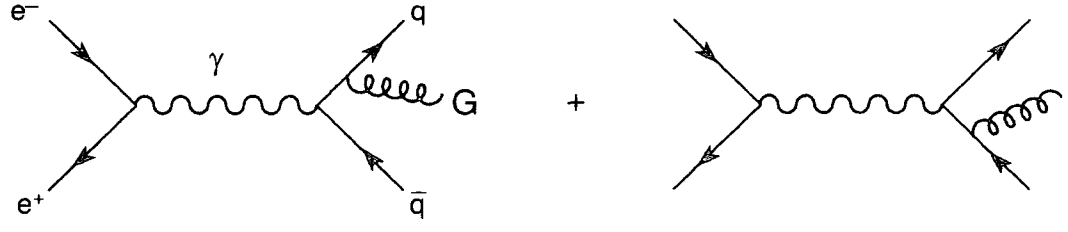

Figure 1.2: The process $e^+e^- \to q\bar{q}g$ to lowest order in α_s.

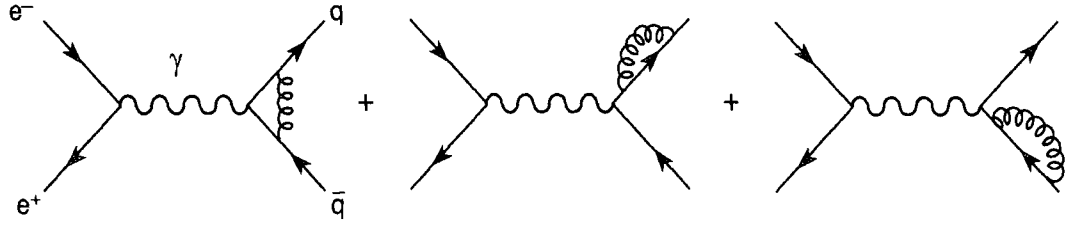

Figure 1.3: The one gluon corrections to $e^+e^- \to q\bar{q}$.

to the total cross section σ are shown in Figs. 1.2 and 1.3, respectively. Consider the real process $e^+e^- \to q\bar{q}g$, Fig. 1.2, first. If we denote the total energy in the c.m. frame by $\sqrt{s}$, the virtual photon (or Z boson) momentum by Q^μ ($Q^2 = s$) and the momenta of the

outgoing particles by p_i^μ, then we can define energy fractions

$$x_i = \frac{2p_i \cdot Q}{s} = \frac{E_i}{\sqrt{s}/2} \,. \tag{1.4.33}$$

The energy fractions are related to the angles θ_{ij} between the momentum of parton i and the momentum of parton j in the following way

$$x_i x_j (1 - \cos\theta_{ij}) = 2(1 - x_k) \,, \tag{1.4.34}$$

where $(i, j, k) = \text{perm}(1, 2, 3)$. In terms of momentum fractions, the differential cross section for $e^+e^- \to q\bar{q}g$ reads

$$\frac{1}{\sigma_0} \frac{d\sigma}{dx_1 dx_2} = \frac{\alpha_s}{2\pi} C_F \frac{x_1^2 + x_2^2}{(1 - x_1)(1 - x_2)} \,, \tag{1.4.35}$$

where $\sigma_0 = (4\pi\alpha^2/s) \sum_f Q_f^2$ is the parton model total cross section for e^+e^- annihilation. The expression (1.4.35) is clearly divergent when $x_1 \to 1$, $x_2 \to 1$ which, from (1.4.34), corresponds to the *collinear singularities* $\theta_{23} \to 0$, $\theta_{13} \to 0$, respectively. There is also a *soft singularity*, given by $x_1 \to 1$ and $x_2 \to 1$

$$1 - x_1 = \frac{x_2 x_3 (1 - \cos\theta_{23})}{2} = \frac{x_2 E_3 (1 - \cos\theta_{23})}{\sqrt{s}} \to 0 \tag{1.4.36}$$

so that $E_3 \to 0$.

Let us now analyze how these divergences arise. If after radiation of a gluon with momentum p_3 the radiating quark has momentum p_1, then the propagator of the parent quark contributes a factor

$$\frac{1}{(p_1 + p_3)^2} = \frac{1}{2E_1 E_3 (1 - \cos\theta_{13})} \sim \frac{1}{E_3 \theta_{13}^2} \,, \tag{1.4.37}$$

which makes it divergent when $\theta_{13} \to 0$ or $E_3 \to 0$. More precisely, the divergent behaviour of the matrix elements $\mathcal{M}$ is given by

$$|\mathcal{M}|^2 \propto \left(\frac{\theta_{13}}{E_3 \theta_{13}^2} \right)^2 . \tag{1.4.38}$$

The integration over the double singular region of the momentum space for the gluon can be written down as

$$\int \frac{d\phi d\theta_{13} dE_3 E_3^2}{E_3} \sim \int d\phi d\theta_{13} dE_3 E_3 \tag{1.4.39}$$

and consequently the divergent contribution to the cross section will come from the integration

$$\sigma \sim \int d\phi \frac{d\theta_{13}^2}{\theta_{13}^2} \frac{dE_3}{E_3} . \tag{1.4.40}$$

The calculations above, although very crude, demonstrate that each type of singularity contributes a *single logarithmic* divergence, leading to a *double logarithmic* divergence in the soft and collinear region.

Despite the divergent contribution, as an observable quantity the total hadronic cross section must certainly be finite. In fact, it can be explicitly demonstrated that the IR singularities *cancel* between real and virtual gluon emission $\mathcal{O}(\alpha_s)$ graphs [3, 6], yielding a finite total cross section. The extension of this statement to any order of the perturbation theory follows from the famous Kinoshita-Lee-Nauenberg (KLN) theorem [12]. The KLN theorem ensures that in a theory with massless fields transition probabilities are free of IR (soft and collinear) divergences if all degenerate initial and final states are taken into account (i.e. summed over). Since there are no hadrons in the initial state for e^+e^- annihilation, it is enough to perform the summation only over final states, i.e. over all hadron states, which is indeed done in the case of the total hadronic cross section. This cross section is an example of a quantity which turns out to be insensitive to the IR effects thus allowing for reliable theoretical predictions: an *infrared safe* quantity.

1.4.2 Infrared safety

The appearance of IR singularities is deeply related to the presence of massless fields in the theory. This can be most easily seen using the mass regularization method while computing the divergent integrals. In the mass regularization method a fictitious mass for the massless particles is introduced; the IR divergences then show up as singularities in mass parameters in their vanishing limit. In particular, soft divergences emerge as a consequence of massless fields like photons in QED or gluons in QCD. Collinear divergences can be shown to arise if the massless field couples to itself or if the matter fields are set massless. Due to the vanishing gluon mass, almost all calculations in perturbative QCD

are plagued with IR divergences, yielding results not defined even in the renormalized theory. This is not, however, the case for infrared safe quantities which are defined as independent of the mass of light partons in the high energy limit. More precisely, a cross section σ is infrared safe if

$$\sigma(Q^2/\mu^2, \alpha_s(\mu^2), m^2/\mu^2) = \bar{\sigma}(Q^2/\mu^2, \alpha_s(\mu^2)) + \mathcal{O}(m^2/Q^2)\,, \tag{1.4.41}$$

where Q is a large invariant scale characteristic of σ and $\bar{\sigma}$ is a finite function. In configuration space an IR safe quantity is correspondingly dependent only on the short-distance behaviour of the theory, not on the long-distance behaviour. If we now consider σ as a perturbative series in α_s

$$\sigma = \sum_{n=0}^{\infty} \alpha_s^n(\mu^2) a_n(Q^2/\mu^2, m^2/\mu^2) \tag{1.4.42}$$

then for the general σ the coefficients a_n can be arbitrary large, spoiling the convergence of the perturbative expansion. However, if σ is an IR safe quantity then the solution for the RGE gives

$$\sigma(Q^2/\mu^2, \alpha_s(\mu^2), 0) = \sigma(1, \alpha_s(Q^2), 0)\,, \tag{1.4.43}$$

i.e. all momentum dependence has been absorbed into the coupling and perturbation theory can be used to obtain reliable predictions. From the technical point of view, IR safety ensures cancellation of the IR divergences. It also means that any IR sensitivity to long-distance physics should cancel after the sum is taken over initial/finite states, leaving only the short-distance cross section. Taking e^+e^- annihilation as an example, we know that after the short-distance creation of the $q\bar{q}$ pair there will be other, long-distance interactions happening. Nevertheless, since to calculate the total hadronic cross section we sum over all finite states and the probability for quarks to evolve into hadrons is one, unitarity ensures that the long-distance interactions leave the short-distance result intact.

1.5 Factorization

The discussion in the previous section concentrated on infrared safe quantities in perturbative QCD. However, not all observable quantities are infrared safe; for example consider

processes with hadrons in the initial state or inclusive cross sections in e^+e^- annihilation with detected hadrons, necessarily involving long-distance interactions. Does perturbative QCD cease to offer meaningful predictions for these observables? The answer is brought by the *factorization theorem* which states that the long-distance effects can be separated from the short-distance physics. The short-distance result comes from perturbative QCD whereas the long-distance quantities are extracted from measurements. In general the factorization theorem is a hypothesis which needs to be proved for each process separately. A detailed discussion of factorization in DIS and hadron-hadron scattering can be found in [13]. This thesis concentrates on a particular example of the latter type of processes: Drell-Yan production. We thus begin with defining the Drell-Yan process and then state the factorization theorem for this specific case.

1.5.1 Drell-Yan production

The hadronic production of a lepton pair (e^+e^-, $\mu^+\mu^-$, $\mu^+\nu_\mu$, etc.) is commonly referred to as the *Drell-Yan process* [14]. The basic electromagnetic reaction occurs through the production of a virtual photon, which decays into the lepton pair, see Fig. 1.4,

$$A + B \to \gamma^* + X \to l^+ + l^- + X\,. \tag{1.5.44}$$

Here X denotes all the undetected particles in the final state so that the process is inclusive.

Because leptons do not interact strongly, in reality the production of lepton pairs signals the production of virtual electroweak bosons: γ^*, $W^\pm$, Z. When the available collision energy permits, the massive W's and Z's can be also produced as physical particles.

In this thesis we will frequently extend the term 'Drell-Yan process' to include production of any spin-1 particle produced by electroweak interactions.

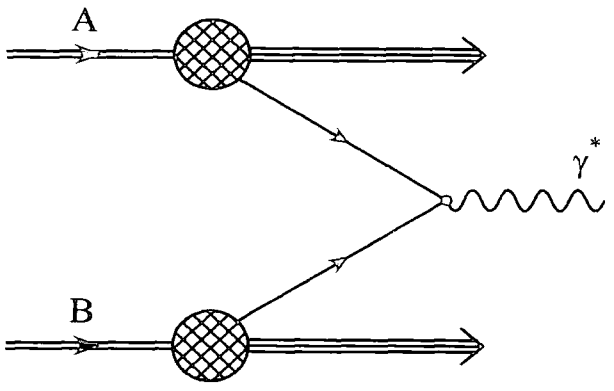

Figure 1.4: The Drell-Yan production of γ^*, as in (1.5.44).

1.5.2 Factorization for the Drell-Yan process

In the framework of perturbative QCD the cross section for the process

$$A(p_a) + B(p_b) \to V(\{Q\}) + X \tag{1.5.45}$$

is given by the factorization theorem[3]

$$\sigma(p_a, p_b, \{Q\}) = \sum_{a,b} \int_0^1 \int_0^1 dx_a dx_b f_{a/A}(x_a, \mu_F) f_{b/B}(x_b, \mu_F) \hat{\sigma}_{ab}(x_a p_a, x_b p_b; Q, \mu_F) \,. \tag{1.5.46}$$

Here the scattering hadrons A and B have momenta p_1 and p_2, respectively, and $\{Q\}$ represents the collection of all relevant kinematic variables of a comparable size with Q being the typical scale of the process. On the l.h.s. of Eq. (1.5.46) V stands for the detected 'hard' particle of interest, e.g. a massive vector boson, while X denotes all other unobserved products of the collision. In the factorization formula $\hat{\sigma}_{ab}$ is the infrared safe hard-scattering cross section. It can be derived from the perturbatively calculable IR divergent partonic cross sections by removing the singularities and absorbing them into the *parton distribution functions* $f_{i/H}$. Since the parton distribution functions contain all the collinear divergences [3], they are susceptible to long-distance physics and as such incalculable in perturbation theory. At present the only way to know their value is

[3]We neglect the so-called 'higher-twist' contributions suppressed by powers of $1/Q^2$.

to measure them in an experiment, for example in DIS. Note that they are universal quantities, i.e. independent of the specific process under investigation.

The factorization theorem provides a generalization of the parton model factorization that uses the assumption that the interactions of the partons among themselves at time-dilated scales before or after the hard-scattering do not interfere with the interaction of a parton with a probe. The cross section can then be calculated by combining probabilities rather than amplitudes. In particular the parton distribution function $f_{i/H}(x)$ has the interpretation of the probability of finding a parton i in hadron H with momentum fraction x of the parent hadron. In perturbative QCD the interpretation essentially stays the same, except with the added restriction that the parton must be off-shell by no more than μ_F^2. Partons of higher virtuality are treated perturbatively and contribute to the scattering cross section $\hat{\sigma}_{ab}$.

The philosophy of incorporating collinear IR divergences into the parton distribution functions resembles the UV renormalization program, cf. Section 1.3.2, where the UV divergences were removed by redefining the bare parameters of the Lagrangian. The 'IR renormalization' introduces an arbitrary scale μ_F: the factorization scale. Akin to the renormalization scale, μ_F is the scale at which factorization is performed. It serves as a separation scale between the long-distance and the short-distance physics. Another ambiguity is again introduced in the prescription for how to define singularities, i.e. how much of the finite contribution should be also absorbed into parton distribution functions. The specific choice of this prescription is termed factorization scale. Both the hard-scattering cross section $\hat{\sigma}_{ab}$ and the parton distribution function $f_{i/H}$ depend on the choice of the scheme. A particular modification of the parton distribution functions defined in the $\overline{\text{MS}}$ scheme used throughout this work is a subject of discussion in Appendix B.

1.5.3 Evolution of the parton distribution functions

Although the r.h.s. of Eq. (1.5.46) exhibits dependence on μ_F, the physical cross section is independent of this parameter. The resulting RGE (cf. Section 1.3.3) tells how the

parton distribution functions change with the scale μ [3]

$$\mu^2 \frac{df_{a/H}(x,\mu^2)}{d\mu^2} = \sum_b \int_x^1 \frac{d\zeta}{\zeta} P_{ab}\left(\frac{x}{\zeta}, \alpha_s(\mu^2)\right) f_{b/H}(\zeta,\mu^2)\,. \tag{1.5.47}$$

Eq. (1.5.47) is known as the *Dokshitzer-Gribov-Lipatov-Altarelli-Parisi* (DGLAP) *evolution equation*. Strictly speaking, it is valid for the non-singlet parton distribution functions defined by

$$\tilde{f}_{q/H} = f_{q/H} - f_{\bar{q}/H}\,, \tag{1.5.48}$$

but the generalization to the singlet case is straightforward, see for example [3]. The *splitting functions* P_{ab} are calculable perturbatively. The leading order P_{ab} can be interpreted as a probability of finding a parton of type a in a parton b. In particular, for the quark-quark splitting we have at the leading order

$$P_{qq}^{(0)}(x) = C_F\left[\frac{1+x^2}{(1-x)_+} + \frac{3}{2}\delta(1-x)\right]\,, \tag{1.5.49}$$

where the '+' prescription is defined as

$$\int_0^1 dx\,[f(x)]_+\, g(x) = \int_0^1 dx f(x)[g(x) - g(1)]\,. \tag{1.5.50}$$

The absorption of collinear divergences into the parton distribution functions provides another example of resummation; the divergences are systematically resummed in the evolved parton distribution functions using the DGLAP equation.[4]

1.6 Soft gluon resummation

The factorization theorem is a powerful tool to calculate cross sections in perturbative QCD, provided that the parton distribution functions are determined experimentally. More precisely, after ensuring that the computed partonic cross section is IR safe by isolating the collinear divergences, there should be no obstacle to obtaining reliable perturbative results. This is, however, only true when all Lorentz invariants defining the

[4] A similar discussion applies to parton fragmentation functions which describe single particle distributions in the final state.

process are large and comparable, except those of the particle masses. If the above mentioned condition does not apply, the convergence of the fixed order expansion, even for IR safe quantities, may be spoiled due to e.g. *soft gluon emission* effects. The theoretical predictions can be improved in these cases by evaluating soft gluon contributions to high orders and possibly resumming them to all orders in α_s. In this section, following the approach of [15], we discuss how large soft gluon contributions can arise and sketch the main idea behind resummation.

1.6.1 Soft gluon emission

Let us revisit the emission of real and virtual gluons from the quark lines, previously discussed for the case of e^+e^- annihilation in Section 1.4.1. Since the nature of this emission is universal we expect to be able to draw conclusions of a general character. However, different types of QCD observables require slightly different treatments of the soft gluon resummation [16]. In this section we will illustrate the resummation of soft gluon radiation using the example of hadronic collisions at threshold. Minor modifications of this treatment are required to handle soft gluon contributions to other observables, like e^+e^- event shapes or transverse momentum distributions p_{T} of systems produced with high mass and small p_{T}.

Consider a quark emitting a real gluon. Let $1-z$ denote the energy fraction radiated by the quark in the hard subprocess. Exactly as shown in (1.4.40), the real gluon emission contribution is divergent in the IR limit. Assuming a regularizing lower cut-off κ on the gluon energy fraction, one obtains the soft and collinear, real gluon emission probability

$$\frac{d\omega_r(z)}{z} = C\frac{\alpha_s}{\pi}\frac{1}{1-z}\ln\frac{1}{1-z}\Theta(1-z-\kappa)\,. \tag{1.6.51}$$

where C is a coefficient depending on the process. In fact, Eq. (1.6.51) can be derived from the cross section (1.4.35) in the soft and collinear limit. On the route to Eq. (1.6.51), the same integration structure as in (1.4.40) is rediscovered. Calculations for the virtual

emission probability are undertaken in a similar way, yielding

$$\frac{d\omega_v(z)}{z} = -C\frac{\alpha_s}{\pi}\delta(1-z)\int_0^{1-\kappa} dz' \frac{1}{1-z'}\ln\frac{1}{1-z'}\,. \tag{1.6.52}$$

Separately, both the real and virtual emission probabilities (1.6.51) and (1.6.52) diverge in the IR limit, as we have already observed. The cancellation of IR singularities in the total emission probability can now be seen clearly

$$\frac{d\omega(z)}{z} = \frac{d\omega_r(z)}{z} + \frac{d\omega_v(z)}{z} = C\frac{\alpha_s}{\pi}\left[\frac{1}{1-z}\ln\frac{1}{1-z}\right]_+\,. \tag{1.6.53}$$

Eq. (1.6.53) is a well-defined distribution, finite in the limit $\kappa\to 0$.

Evidently, the virtual term contributes only at $z = 1$ while the real one, besides regularizing the virtual probability at $z = 1$, is spread out down to $z = 0$. The size of the integrated contributions is however equal, so that

$$\int_0^1 dz \frac{d\omega(z)}{z} = 0\,. \tag{1.6.54}$$

In physical processes, due to the *kinematical boundary* the real contribution stretches down to the same value x, as given by the fraction of the energy carried by the tagged particle in the final state. In this case the total soft gluon contribution is a finite function of x

$$\int_x^1 dz \frac{d\omega(z)}{z} = -C\frac{\alpha_s}{2\pi}\ln^2(1-x)\,. \tag{1.6.55}$$

A residue of the cancellation process, this finite correction can be large when $x\to 1$. (Note that the cancellation of the IR divergences is still preserved!). Physically, the limit $x\to 1$ corresponds to approaching the kinematical boundary in phase space where the suppression of the real gluon emission becomes significant, no longer balancing the virtual emission contribution.

In general we would expect the higher order partonic cross section to behave like

$$\begin{aligned}\hat{\sigma}^{(n+1)}(x) &= \int_x^1 dz\,\hat{\sigma}^{(n)}(x+1-z)\frac{d\omega(z)}{z} \\ &\underset{x\to 1}{\sim} \hat{\sigma}^{(n)}(x)\int_x^1 dz\left[C\frac{\alpha_s}{\pi}\frac{1}{1-z}\ln\frac{1}{1-z}\right]_+ \\ &\sim \hat{\sigma}^{(n)}(x)(-C\frac{\alpha_s}{2\pi}\ln^2(1-x))\,.\end{aligned} \tag{1.6.56}$$

Consequently, in the process where n soft gluons are emitted, the structure of the correction factor to the partonic cross section is believed to have the form

$$\alpha_s^n \sum_{m=1}^{2n} C_{nm} \ln^m(1-x)\,, \tag{1.6.57}$$

which leads to

$$\hat{\sigma}(x) \sim \hat{\sigma}_0(Q^2) \left[1 + \sum_{n=1}^{\infty} \alpha_s^n \sum_{m=1}^{2n} C_{nm} \ln^m(1-x)\right]. \tag{1.6.58}$$

It is clear from (1.6.58) that the logarithmically enhanced terms of infrared origin become relevant near the exclusive phase space boundary, $x \to 1$, even if the coupling constant is in the perturbative regime $\alpha_s \ll 1$. In this case, i.e. when x is close enough to 1 such that $\alpha_s \ln^2(1-x) \gtrsim 1$, the convergence of the fixed-order expansion is spoiled and NLO calculations are certainly insufficient to obtain reliable predictions. Thus the evaluation of soft gluon contributions to all orders in the perturbation theory is required, and whenever possible a suitable reorganization of the perturbative series so that the convergence of the series is restored. This idea is called *resummation.*

1.6.2 Resummation

The previous section focused on the example of threshold logarithmic corrections. Let us now return to the generic hard-scattering case. It still remains true that the large logarithmic factors in (1.6.58) are generated by the suppression of soft gluon emission near the phase space boundary. If the suppression is strong enough then $\alpha_s L^2 \gtrsim 1$ ($L = \ln(1/(1-x))$ for processes at the threshold) and order by order the soft gluon corrections become larger and larger, causing a breakdown of the fixed-order expansion. Since the problem is generated by values of $\alpha_s L^2$, one may want to reorganize the perturbative expansion by selecting and summing classes of logarithmic terms to all orders, so that Eq. (1.6.58) would read

$$\hat{\sigma}(x) \sim \hat{\sigma}_0 \left[T_1(\alpha_s L^2) + \alpha_s L T_2(\alpha_s L^2) + \alpha_s^2 L^2 T_3(\alpha_s L^2) + ...\right]. \tag{1.6.59}$$

The first term in (1.6.59), the function T_1, is actually a sum itself, summing dominant double-logarithmic contributions of the form $\alpha_s^n L^{2n}$. The sub-leading contributions of the

form $\alpha_s^n L^{2n-1}$ are then summed by the term $\alpha_s L T_2(\alpha_s L^2)$, etc. The functions $T_1(\alpha_s L^2)$, $\alpha_s L T_2(\alpha_s L^2)$, etc. are commonly referred in the literature as *towers* of logarithms. At this point we would like to alert the reader that care needs to be taken when performing numerical computations. It is possible that in certain regions of the phase space the most leading tower T_1 may be numerically less relevant than the more sub-leading towers T_2, T_3, ... An example of such a situation in the case of resummation of the transverse momentum logarithms will be given in Chapter 2.

Although the idea behind the resummation procedure seems clear, we have not yet proved that such a reorganization is possible, i.e. that the terms with the structure $\alpha_s^n L^{2n-k}$ can be summed by the functions T_i and that the reformulation (1.6.59) is convergent in the limit $x \to 1$.

To demonstrate this, let us consider a generic hard-scattering process

$$\hat{\sigma}(x) \sim \hat{\sigma}_0 \left[1 + \sum_{n=1}^{\infty} \int_0^1 dz_1 ... dz_n \frac{d\omega_n(z_1, ..., z_n)}{dz_1 ... dz_n} \Theta_{PS}^{(n)}(x, z_1, ..., z_n) \right] . \tag{1.6.60}$$

Here $\frac{d\omega_n(z_1,...,z_n)}{dz_1...dz_n}$ is a multi-gluon emission probability whereas $\Theta_{PS}^{(n)}(x, z_1, ..., z_n)$ denotes the function describing the phase-space available in the process of interest. The multi-gluon emission probability originates from QCD dynamics. It can be proved that due to the properties of gauge-invariance and unitarity, in the soft limit the multi-gluon emission probability factorizes in terms of a single-gluon emission probability [17]

$$\frac{d\omega_n(z_1, ..., z_n)}{dz_1 ... dz_n} = \frac{1}{n!} \prod_{i=1}^{n} \frac{d\omega(z_i)}{dz_i} . \tag{1.6.61}$$

Thus the dynamical factorization (1.6.61) is universal i.e. process independent. The phase-space function Θ_{PS}, in turn, stems from kinematics. More precisely, it contains kinematical constraints defining the physical cross section and is therefore specific to a particular process. Assuming that the phase factorizes in the soft limit $z_i \to 1$ i.e.

$$\Theta_{PS}^{(n)}(x, z_1, ..., z_n) = \prod_{i=1}^{n} \Theta_{PS}(x, z_i) , \tag{1.6.62}$$

the partonic cross section (1.6.60) can be written in the soft limit as

$$\hat{\sigma}(x) \sim \hat{\sigma}_0 \left\{ 1 + \sum_{n=1}^{\infty} \frac{1}{n!} \left[\int_0^1 dz_i \frac{d\omega(z_i)}{dz_i} \Theta_{PS}(x, z_i) \right]^n \right\}$$

$$\sim \hat{\sigma}_0 \exp\left[\int_0^1 dz \frac{d\omega(z)}{dz}\Theta_{PS}(x,z)\right]$$
$$\sim \hat{\sigma}_0 \exp\left[-\alpha_s L^2 - \alpha_s L\right] . \qquad (1.6.63)$$

Expanded, the final result of (1.6.63) reveals the resummed structure of (1.6.59). The exponential factor resumming the logarithmic corrections is known as the *Sudakov factor*.

Thus, in this simplified example we have shown that the resummation is feasible due to the property of *exponentiation* of the single soft gluon emission contribution.

Unfortunately, Θ_{PS} is not necessarily factorizable. In general it depends on multi-gluon configurations and as such can be very complicated. Furthermore, even if factorization occurs it may do so in the space *conjugate* to the space of kinematic variables where the cross section is defined. Thus in practice the generalized exponentiation theorem, and subsequently, resummation, needs to be proved separately for each process. Examples of such processes are event shapes in e^+e^- [18], hadronic collisions at the threshold [19] and the transverse momentum distribution for the Drell-Yan production of massive lepton pairs or electroweak gauge bosons [21].

In general, the resummed cross section is of the form

$$\hat{\sigma} = \int \hat{\sigma}_0 \mathcal{C} \exp(\mathcal{S}) , \qquad (1.6.64)$$

with the Sudakov factor $\exp(\mathcal{S})$ calculated in the conjugate space and the factor $\mathcal{C}$ containing all finite contributions. The inverse transform to the original space is carried out with the help of the integral (1.6.64). It can be shown that the Sudakov factor has typical structure

$$\mathcal{S} = L f_1(\alpha_s L) + f_2(\alpha_s L) + \alpha_s f_3(\alpha_s L) + \ldots , \qquad (1.6.65)$$

where the logarithms L are functions of the conjugated variable. Substituting Eq. (1.6.65) into Eq. (1.6.64) and expanding the exponential yields the tower structure of (1.6.59). While the tower expansion (1.6.59) is in general valid for $\alpha_s L^2 \lesssim 1$, the range of validity of the exponentiated form (1.6.65) is extended up to $\alpha_s L \lesssim 1$. In order to collect maximum information on the perturbative cross section, the resummed expression (1.6.64) must be

matched with the fixed-order result. In Chapter 2 we will discuss matching using the example of the Drell-Yan process.

1.7 Why transverse momentum distribution?

As we will see in Chapter 2 the transverse momentum distribution in vector boson production requires resummation to improve the perturbative QCD predictions. Furthermore, it not only offers a test of the resummation formalism, but also a tool to extract one of the basic parameters of the SM, the mass of the W boson, M_W. A measurement of M_W is one of the most stringent experimental tests of the SM. The existence of yet undiscovered particles that couple to the W boson would modify its mass by radiative electroweak corrections. In particular, measurements of M_W and the mass of the top quark m_t constrain the mass of the Higgs boson, see Fig. 1.5.

After production through $q\bar{q}$ annihilation, W bosons decay into lepton and quark pairs. The $W \to e\nu$ channel provides the cleanest signal and the best resolution. The only quantities directly measured in the experiment are the electron momentum and the transverse momentum of hadrons produced in association with the W, the 'recoil' against the W. Since the apparatus cannot detect the neutrino and cannot measure the longitudinal component of the recoil momentum, there is insufficient information to reconstruct the invariant mass of the W on an event-by-event basis. However, the two-body kinematics of the W decay offers at least two methods of measuring M_W.

The first method relies on constructing the transverse mass of the W event, which is analogous to the invariant mass, except that only components of energy flow transverse to the beamline are used. It is defined as

$$M_T^2 = 2E_T^e E_T^\nu - 2\vec{p}_{\mathrm{T}}^{\,e}\vec{p}_{\mathrm{T}}^{\,\nu} = 2p_{\mathrm{T}}^e p_{\mathrm{T}}^\nu (1 - \cos\phi_{e\nu})\,, \tag{1.7.66}$$

where $p_{\mathrm{T}}^e\,(p_{\mathrm{T}}^\nu)$ is the transverse momentum of the electron (neutrino), $E_T^e\,(E_T^\nu)$ denotes the corresponding transverse energy and $\phi_{e\nu}$ is the azimuthal angle between e and ν. The transverse mass distribution exhibits a kinematic peak at $M_T = M_W$. Precise de-

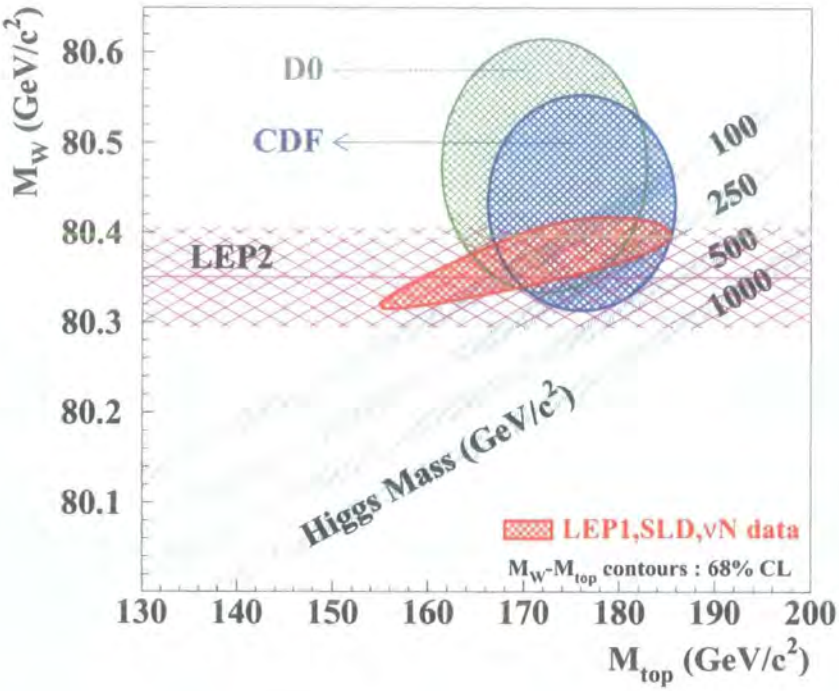

Figure 1.5: The direct measurements of the W and top quark mass from CDF and D0 experiments, the direct measurement of the W mass from LEP2 experiments and the indirect W and top mass measurement from LEP, SLC and Tevatron neutrino experiments. The figure is reproduced form Ref. [82].

termination of M_W must take into account distortion of the M_T distribution due to the finite width Γ_W of the W and its non-zero transverse momentum p_{T}. The M_T spectrum is invariant under p_{T} boosts to leading order in p_{T} and therefore less sensitive to the experimental and theoretical errors.[5]

The second method relies on transverse momentum distribution of the electron, p_{T}^e. It also exhibits a kinematic peak, this time at $M_W/2$. However, resolution effects and non-zero values of p_{T} smear the p_{T}^e spectrum and therefore reduce the use of the peak to determine M_W. This is why the first method has been so far preferred for extracting M_W.

[5]The experimental extraction of W p_{T} from the recoil p_{T}^r suffers from many problems, as discussed in Chapter 5.

This method is nevertheless limited by the missing p_{T}^{ν} measurement. The uncertainty in the detector resolution contributes more uncertainty to M_W using the M_T method than the p_{T}^{e} method [22]. Therefore it is anticipated that in the high statistics p_{T} environment of Run II at the Tevatron it may be more difficult to minimize the systematic uncertainties in the M_T method than theoretical uncertainties due to p_{T}.[6] The work described in this thesis aims to develop a more accurate theoretical description of the p_{T} distribution of W's and Z's produced in hadron-hadron collisions.

1.8 Summary

In this chapter we have presented a short review of some of the aspects of Quantum Chromodynamics as the theory of strong interactions. Using the Feynman rules derived from the QCD Lagrangian density, theoretical expressions for observable quantities can be calculated perturbatively. We have shown that fixed, higher order calculations contain UV divergences which can be removed using the renormalization procedure. As an inevitable consequence of the renormalization, the strong coupling α_s acquires the property of running with the renormalization scale.

Additionally, another type of divergence can be present in higher order diagrams - the IR divergences. Because of the KLN theorem, the IR divergences cancel at each order in perturbation theory for infrared safe quantities. Although not infrared safe, the partonic cross sections in the hadronic collisions can be made infrared safe if the collinear IR singularities are factorized out and absorbed into the parton distribution functions. The feasibility of this procedure is ensured by the factorization theorem which however needs to be proved separately for each process of interest.

Further complexity is introduced by the possible presence of large logarithmic corrections to the infrared safe partonic cross section. These corrections often arise due to

[6] Alternatively, when using the M_T method, the dependence on the detector resolution can be diminished by using the Z p_{T} spectrum and the theoretical ratio of W and Z distributions, see Chapter 5.

emission of soft gluons and the imbalance between real and virtual gluon contributions in certain parts of the phase space. Whenever possible, these logarithmic factors need to be resummed in order to obtain reliable theoretical predictions. Resummation of soft logarithms can be understood as a successful attempt towards improving perturbative predictions, when the fixed-order perturbation theory calculations become precipitously difficult to perform. Although resummation incorporates only the biggest contributions, i.e. the most leading in $\alpha_s L^2$, and only coming from a specific set of diagrams, it does it to all orders, providing a result for the sum over an infinite set of selected terms in the perturbative series. The application of the resummation procedure for one specific type of process, the Drell-Yan process together with the related heavy boson production, occurring at hadron colliders, will be the main subject of this thesis.

Chapter 2

Soft gluon resummation for the Drell-Yan process

For more than two decades the Drell-Yan process has been a benchmark process for all hadron colliders. First observed in proton-nucleus collisions at the Brookhaven National Laboratory, lepton pair production has contributed greatly to the present understanding of high energy physics. Apart from being a crucial process to discover the fourth and fifth quark flavour, c (charm) and b (beauty), it also provided information on parton distributions of the nucleon. Other highlights include one of the first pieces of evidence for the existence of gluons, confirming QCD predictions rather than those of the parton model. The Drell-Yan mechanism for massive gauge boson production played a central role in the discovery of W and Z particles. To this day, the Drell-Yan production of massive lepton pairs or electroweak gauge bosons serves as a test bed for most sophisticated QCD calculations; the resummed calculations being a good example. Moreover, comparison between improved theoretical predictions and data allows for a precise extraction of the W boson mass, see Section 1.7. The experimental programme, started at Brookhaven, has been continued both at the European Laboratory for Particle Physics (CERN) and at the Fermi National Laboratory (Fermilab). A compilation of data on Drell-Yan cross sections can be found in [23]. The Large Hadron Collider (LHC), being currently built

at CERN, will maintain the succession. The abundance of the experimental data from the Tevatron collider at Fermilab necessitates the development of a consistent, accurate description of the Drell-Yan mechanism. Such a description will be undeniably crucial in the case of the LHC where even larger data samples are expected.

In this chapter we are going to discuss effects due to emission of soft gluons in the Drell-Yan process. We will systematically inspect corrections given by such emission and methods to execute the resummation procedure in this case.

2.1 Drell-Yan process in the parton model

In the framework of the parton model, production of a vector boson occurs as a result of interaction between two quarks, each quark coming from a different hadron taking part in a collision. For example, this could be a production of a virtual photon through the annihilation of the quark-antiquark pair. The photon then decays into a lepton pair. The total partonic cross section for the di-lepton production in this case reads

$$\hat{\sigma}_0^\gamma = \frac{4\pi\alpha^2 e_q^2}{9\hat{s}}, \tag{2.1.1}$$

where $\sqrt{\hat{s}}$ is the partonic collision energy in the c.m. frame and e_q is the charge of the annihilating quark (antiquark).

It is straightforward to notice that the production of a lepton pair with a specified invariant mass Q would be given by the differential lepton pair mass distribution of the form

$$\frac{d\hat{\sigma}}{dQ^2} = \frac{4\pi\alpha^2 e_q^2}{9Q^2}\delta(\hat{s} - Q^2)\,. \tag{2.1.2}$$

Analogously, the parton model cross sections for W production subprocess can be easily calculated in the narrow width approximation [3], yielding

$$\hat{\sigma}_0^W = \frac{\pi\ g_W^2 |V_{qq'}|^2}{12}\delta(\hat{s} - M_W^2) \tag{2.1.3}$$

and for Z production

$$\hat{\sigma}_0^Z = \frac{\pi\, g_W^2 M_Z^2 (V_q^2 + A_q^2)}{12 M_W^2} \delta(\hat{s} - M_Z^2)\,. \tag{2.1.4}$$

$V_{qq'}$ in Eq. (2.1.3) denotes the appropriate CKM matrix element while V_q and A_q are the vector and axial couplings of the Z boson to quarks.[1] From this point and without constraining the generality of our discussion we will examine the Drell-Yan process in the form of di-lepton production through a γ^*. The corresponding expressions for the production of massive vector bosons can be obtained by changing the normalization and the appropriate couplings, cf. Eq. (2.1.2), (2.1.3) and (2.1.4).

The parton model framework allows one to write down a leading order (LO) expression for the Drell-Yan process at the hadron level $AB \to \gamma^* \to l^+ l^-$, a simplified version of the equivalent QCD factorization theorem,

$$\frac{d\sigma}{dQ^2} = \sum_{q,\bar{q}} \int dx_a dx_b f_{q/A}(x_a) f_{\bar{q}/B}(x_b) \frac{d\hat{\sigma}}{dQ^2}\,, \tag{2.1.5}$$

where now $\hat{s} = x_a x_b s$. Inserting Eq. (2.1.2) into (2.1.5) gives

$$Q^4 \frac{d\sigma}{dQ^2} = \frac{4\pi\alpha^2}{9} \sum_{q,\bar{q}} \int_\tau^1 \frac{dx_a}{x_a} \tau e_q^2 f_{q/A}(x_a) f_{\bar{q}/B}(\tau/x_a)\,. \tag{2.1.6}$$

The dimensionless quantity $Q^4 d\sigma/dQ^2$ is a function only of the *scaling variable*

$$\tau = \frac{Q^2}{s}\,, \tag{2.1.7}$$

which represents the fraction of the initial c.m. energy $\sqrt{s}$ turned into the produced boson (lepton pair) mass.

The scaling phenomenon, Eq. (2.1.6), is typical for processes considered in the framework of the parton model, the most famous example being DIS. In QCD, scaling is broken due to the appearance of logarithmic contributions to the cross section, proportional to $\alpha_s \ln(Q^2)$.

It is convenient to introduce the *rapidity* variable y defined as

$$y \equiv \frac{1}{2} \ln\left(\frac{E + p_L}{E - p_L}\right)\,, \tag{2.1.8}$$

[1] For more information on the CKM matrix and vector and axial couplings, the reader is referred to the classic reviews of the Standard Model [1].

where E denotes the energy of the lepton pair and p_L its longitudinal momentum. In the Drell-Yan process rapidity is equal to

$$y = \frac{1}{2} \ln \left(\frac{x_a}{x_b} \right) , \tag{2.1.9}$$

which implies the useful relationships

$$x_a = \sqrt{\tau} e^{y} , \qquad x_b = \sqrt{\tau} e^{-y} . \tag{2.1.10}$$

2.2 $\mathcal{O}(\alpha_s)$ corrections in QCD

If we neglect the initial 'primordial' transverse momentum of the incoming partons, in the parton model the produced vector boson (γ^*, W, Z) has no transverse momentum. As we will show explicitly, QCD predicts a non-zero transverse momentum (p_{T}) distribution which behaves like $1/p_{\mathrm{T}}^2$ at large p_{T}. In QCD, the non-zero p_{T} can arise if a quark emits a gluon before the collision. In this light, observation of a non-zero transverse momentum signals the existence of gluons. The first order $\mathcal{O}(\alpha_s)$ QCD corrections to the parton model cross section for $AB \to \gamma^* + X$ include the gluon bremsstrahlung process $q\bar{q} \to \gamma^* g$ together with the virtual corrections to the basic qqg vertex. Additionally, there are two new channels for the process $AB \to \gamma^* + X$ to occur: $qg \to q\gamma^*$ and $\bar{q}g \to \bar{q}\gamma^*$. Exact calculations of the Feynman diagrams presented in Fig. 2.1 give [7]

$$\frac{d\sigma}{dQ^2 d\hat{t}}^{q\bar{q} \to l^+ l^- g} = \frac{\alpha^2 \alpha_s e_q^2}{Q^2 \hat{s}^2} \frac{8}{27} \left[\frac{\hat{t}^2 + \hat{u}^2 + 2Q^2 \hat{s}}{\hat{t}\hat{u}} \right] , \tag{2.2.11}$$

and

$$\frac{d\sigma}{dQ^2 d\hat{t}}^{qg \to l^+ l^- q} = \frac{\alpha^2 \alpha_s e_q^2}{Q^2 \hat{s}^2} \frac{1}{9} \left[\frac{\hat{t}^2 + \hat{s}^2 + 2Q^2 \hat{u}}{-\hat{t}\hat{s}} \right] . \tag{2.2.12}$$

The Mandelstam invariants are defined in the following way for (2.2.11)

$$\hat{s} = (q_q + q_{\bar{q}})^2 , \tag{2.2.13}$$

$$\hat{t} = (p_\gamma - q_q)^2 , \tag{2.2.14}$$

$$\hat{u} = (k_g - q_q)^2 , \tag{2.2.15}$$

$$\tag{2.2.16}$$

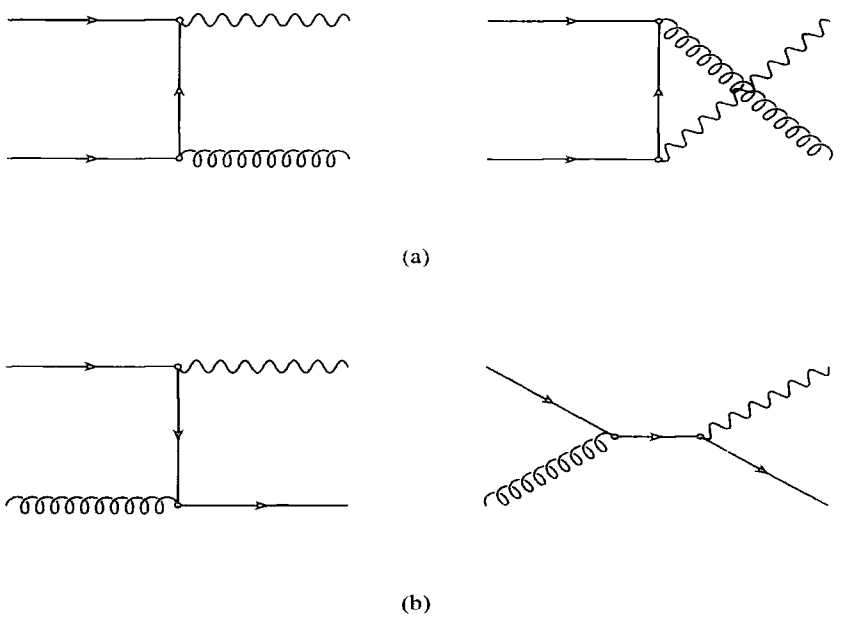

Figure 2.1: Real diagrams *(a)* for the process $q\bar{q}\to\gamma^* g$, *(b)* for the process $qg\to\gamma^* q$

and for (2.2.12)

$$\hat{s} = (q_q + k_g)^2 , \tag{2.2.17}$$

$$\hat{t} = (p_\gamma - q_q)^2 , \tag{2.2.18}$$

$$\hat{u} = (p_\gamma - k_g)^2 . \tag{2.2.19}$$

The matrix elements exhibit poles at $\hat{t} = 0$ and $\hat{u} = 0$. Consequently, the integration over $\hat{t}$ in (2.2.11) and in (2.2.12) yields infinity. This divergence is a collinear divergence and, according to the factorization theorem, can be factorised out into the parton distribution functions, i.e. for the hadronic cross-section $AB\to\gamma^* + X$ and choosing $\mu_F = Q$ we have

$$\frac{d\sigma}{dQ^2}\Big|_{\mathcal{O}(\alpha_s)} = \sum_{a,b} \int dx_a dx_b f_{a/A}(x_a, Q) f_{b/B}(x_b, Q) \frac{d\sigma^{ab\to l^+ l^- c}}{dQ^2 d\hat{t}} d\hat{t} , \tag{2.2.20}$$

where $(a,\, b,\, c) = \{q,\, \bar{q},\, g\}$ and the integrated cross sections $\int d\hat{t}(d\sigma_{a,b}/dQ^2 d\hat{t})$ are made infrared safe. The exact formulae for the $\mathcal{O}(\alpha_s)$ corrections can be found in [3, 4, 7].

In order to extract information on the transverse momentum distribution one of the integrations in the cross section (2.2.20) needs to be undone. In particular, using the relation

$$dx_b d\hat{t} = dy dp_T^2 \frac{x_a x_b}{x_a - x_1} \tag{2.2.21}$$

with

$$x_1 = e^y \sqrt{\frac{p_{\rm T}^2}{s} + \tau}\,, \qquad x_2 = e^{-y} \sqrt{\frac{p_{\rm T}^2}{s} + \tau}\,, \tag{2.2.22}$$

it can be shown [7] that for the $q\bar{q}\to l^+l^-g$ process

$$\begin{aligned} \frac{d\sigma}{dQ^2 dy dp_{\rm T}^2}^{q\bar{q}\to l^+l^-g} &= \frac{\alpha^2\alpha_s}{sQ^2}\frac{8}{27}\frac{1}{p_{\rm T}^2}\int_{x_a^{min}}^1 dx_a \frac{x_a x_b}{x_a - x_1}\sum_{q,\bar{q}} e_q^2 f_{q/A}(x_a,Q) f_{\bar{q}/B}(x_b,Q) \\ &\times \left[1 - \frac{2p_{\rm T}^2}{x_a x_b s} + \left(\frac{\tau}{x_a x_b}\right)^2\right], \end{aligned} \tag{2.2.23}$$

where

$$x_a^{min} = \frac{x_1 - \tau}{1 - x_2}, \qquad x_b = \frac{x_a x_2 - \tau}{x_a - x_1}. \tag{2.2.24}$$

Thus, at high values of $p_{\rm T}$ the annihilation contribution ($q\bar{q}\to l^+l^-g$) gives a $p_{\rm T}^{-2}$ tail to the $p_{\rm T}$ distribution. The Compton contribution ($q\bar{g}\to l^+l^-q$) behaves in a similar way. On the other hand, at small $p_{\rm T}$ the cross section diverges. Although it would naively appear that the divergence is quadratic ($\sim p_{\rm T}^{-2}$) , in fact another singular contribution comes from the integral in (2.2.23). As $p_{\rm T}\to 0$, from (2.2.22) $x_1\to\sqrt{\tau}e^y$ and also, from (2.2.24) $x_a^{min}\to\sqrt{\tau}e^y$. Since for $p_{\rm T}\to 0$ the term in the square brackets in (2.2.23) goes to 2, the most important contribution comes from integrating $x_a x_b/(x_a - x_1)$. In this limit, the low end of the integration range x_a^{min} equals x_1. As a result, the logarithmic term proportional to $-\ln(x_a^{min} - x_1)$, arising from the integration over x_a, exhibits a singularity. Moreover,

$$-\ln(x_a^{min} - x_1) = -\ln\left(\frac{x_1 x_2 - \tau}{1 - x_2}\right) = \ln\left(\frac{s\,(1 - \sqrt{\tau}e^{-y})}{p_{\rm T}^2}\right), \tag{2.2.25}$$

and the cross section (2.2.23) behaves like

$$\frac{\ln(s/p_{\rm T}^2)}{p_{\rm T}^2}. \tag{2.2.26}$$

Let us remind the reader that the divergence (2.2.26) stems from the $\mathcal{O}(\alpha_s)$ real emission contribution. The virtual contributions, according to the KLN theorem, cancel

the singularities from the real diagrams. Indeed, due to their nature, the virtual contributions are dependent on p_{T}^2 only proportionally to $\delta(p_{\mathrm{T}}^2)$ and, when added to the real terms, regularize the logarithmic divergence at $p_{\mathrm{T}} = 0$ in terms of a plus prescription, see Section 1.5.3. As a result the distribution $d\sigma/dQ^2dydp_{\mathrm{T}}^2$ remains infrared safe. Furthermore, the integral over dp_{T}^2 for the annihilation process returns a finite result. In other words undoing this integration provides an insight into the structure of the divergences, allowing us to probe the imbalance between real and virtual contributions discussed in Section 1.6.1. The strongest imbalance occurs when $p_{\mathrm{T}} \to 0$ which, in the language of Section 1.6.1, refers to limited phase space available for the k_{T} of the emitted gluon close to the kinematical boundary.

2.3 Higher orders

The $\mathcal{O}(\alpha_s)$ corrections to the Drell-Yan cross section $AB \to \gamma^* + X$ involve a real gluon emission process. As always, there is a possibility that the radiated gluon can have small energy or momentum collinear with the parent quark. Such a possibility reflects itself in the presence of logarithmic divergences, cf. Chapter 1.6.1. By the means of the factorization theorem, the collinear divergence is taken care of by absorbing it into the parton distribution functions. If more gluons are emitted, some of them can be soft. Furthermore, since the soft gluons may at the same time be collinear, they potentially contribute *double logarithmic* divergences. Therefore, in the approximation of taking only the most divergent terms at each order of α_s, the structure of the soft gluon contributions can be investigated by performing the analysis for the appropriate partonic subprocesses. Contributing single logarithms, collinear divergences are thus not of interest in this approximation.

The nature of the soft gluon effects can be studied most easily working in a general planar gauge, see Section 1.1.3, and using a *Sudakov parameterization* of the gluon's momenta

$$k = \mu q_q + \theta q_{\bar{q}} + k_T \,, \tag{2.3.27}$$

where $k_T \cdot q_q = k_T \cdot q_{\bar{q}} = 0$. With the help of the above parameterization the exact $\mathcal{O}(\alpha_s)$ result for the reaction $q\bar{q} \to \gamma^* g$ reads [25, 26]

$$\begin{aligned} \frac{d\hat{\sigma}}{dp_{\mathrm{T}}^2} &= \frac{\sigma_0}{\hat{s}} \frac{\alpha_s C_F}{2\pi} \int d\theta d\mu \delta \left(\theta\mu - \frac{p_{\mathrm{T}}^2}{\hat{s}} \right) \Theta(1-\theta-\mu) \frac{(1-\theta)^2 + (1-\mu)^2}{\theta\mu} \\ &= \sigma_0 \frac{\alpha_s C_F}{\pi} \frac{1}{p_{\mathrm{T}}^2} \left[\ln \left(\frac{\sqrt{\hat{s}} + \sqrt{\hat{s} - 4p_{\mathrm{T}}^2}}{\sqrt{\hat{s}} - \sqrt{\hat{s} - 4p_{\mathrm{T}}^2}} \right) - \frac{3}{2} \sqrt{1 - \frac{4p_{\mathrm{T}}^2}{\hat{s}}} \right] , \end{aligned} \tag{2.3.28}$$

where now $\sigma_0 = 4\pi\alpha^2/9\hat{s}$. It follows from (2.3.27) that a gluon is soft and collinear if both $\mu \ll 1$, $\theta \ll 1$. The condition of collinearity, but not softness, is imposed if only one of the parameters μ or θ is $\ll 1$. Expanding (2.3.28) in terms of $p_{\mathrm{T}}^2/\hat{s}$ recovers the same result as (2.2.26) i.e. the largest contribution in the limit $p_{\mathrm{T}} \to 0$ is given by

$$\frac{d\hat{\sigma}}{dp_{\mathrm{T}}^2} \sim \sigma_0 \frac{\alpha_s C_F}{\pi} \frac{1}{p_{\mathrm{T}}^2} \left[\ln \left(\frac{\hat{s}}{p_{\mathrm{T}}^2} \right) - \frac{3}{2} \right] . \tag{2.3.29}$$

As can be seen from the form of (2.3.28), the term $\sim \ln(\hat{s}/p_{\mathrm{T}}^2)/p_{\mathrm{T}}^2$ comes from the emission of a soft and collinear gluon. The term $\sim 3/2p_{\mathrm{T}}^2$ arises when the gluon is allowed to be collinear, but not soft.

Analogously, the most leading contribution to the transverse momentum distribution in the process when two real gluons are radiated, $q\bar{q} \to \gamma^* gg$, is given by [27, 28]

$$\frac{d\hat{\sigma}}{dp_{\mathrm{T}}^2}\Big|_{\mathcal{O}(\alpha_s^2)} \sim -\sigma_0 \frac{\alpha_s^2 C_F^2}{2\pi^2} \frac{1}{p_{\mathrm{T}}^2} \ln^3 \left(\frac{\hat{s}}{p_{\mathrm{T}}^2} \right) . \tag{2.3.30}$$

The above result (2.3.30) is derived under assumption that the two emitted gluons are soft and collinear, μ_1, θ_1, μ_2, $\theta_2 \ll 1$. Additionally it is required that $k_{T\,1,2}^2 \ll k_{T\,2,1}^2 \sim p_T^2$. Assuming the soft and collinear limit in the matrix element, but taking into account transverse momentum conservation, the calculations give [27]

$$\frac{d\hat{\sigma}}{dp_{\mathrm{T}}^2}\Big|_{\mathcal{O}(\alpha_s^2)} \approx \sigma_0 \frac{\alpha_s^2 C_F^2}{\pi^2} \frac{1}{p_{\mathrm{T}}^2} \left[-\frac{1}{2} \ln^3 \left(\frac{\hat{s}}{p_{\mathrm{T}}^2} \right) + 2\zeta(3) \right] . \tag{2.3.31}$$

If the approximation of softness and collinearity is relaxed, then other, less leading logarithmic terms appear, e.g. such as a term $\sim \alpha_s^2 \ln^2(\hat{s}/p_{\mathrm{T}}^2)/p_{\mathrm{T}}^2$. Nevertheless, in order $\mathcal{O}(\alpha_s^2)$, there are no sub-leading logarithmic terms related to transverse momentum conservation. As we will see in Chapter 3, this result foretells a general property of the p_{T}

distribution for multi-gluon emission: the first sub-leading logarithms of $\hat{s}/p_{\mathrm{T}}^2$ *related to transverse momentum conservation* appear no sooner than three towers down from the leading logarithms.

Let us now return to the most leading contributions. Due to the radiation of soft and collinear gluons we expect the subsequent terms in the perturbative $\mathcal{O}(\alpha_s)$ expansion to behave like $\alpha_s^N \ln^{2N-1}(\hat{s}/p_{\mathrm{T}}^2)$, cf. (2.3.30). An example diagram representing a contribution coming from the emission of only real gluons is shown in Fig 2.2. In the approximation

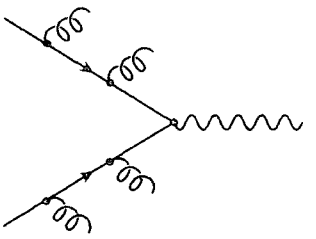

Figure 2.2: One of the diagrams which needs to be taken into account while calculating real gluon emission at higher orders.

of soft and collinear gluons, calculations for the process $q\bar{q}\to\gamma^* + Ng$ are undertaken in the planar gauge and using the Sudakov parameterization (2.3.27). The gluons are soft and collinear if the corresponding parameters θ_i, μ_i are small, i.e θ_i, $\mu_i \ll 1$. In this limit the most leading contributions are obtained after approximating the matrix element by its most singular piece and by requiring that the soft gluons are emitted completely independently, ignoring energy conservation [27]. The independent emission of gluons leads to the factorised form of the final expression (dynamical factorization, cf. Section 1.6.2). Evaluation of the θ_i and μ_i integrals gives

$$\frac{1}{\sigma_0}\frac{d\hat{\sigma}}{dp_{\mathrm{T}}^2}\Big|_{\mathcal{O}(\alpha_s^N)} = \frac{1}{N!}\left(\frac{\alpha_s C_F}{\pi}\right)^N \prod_{i=1}^{N}\left[\int \frac{d^2k_{Ti}}{\pi k_{Ti}^2}\ln\frac{\hat{s}}{k_{Ti}^2}\right]\pi\delta^{(2)}(\sum_i \vec{k}_{Ti} + \vec{p_{\mathrm{T}}})\,. \qquad (2.3.32)$$

Note that (2.3.32) has a structure of the N-th order contribution to (1.6.63) with the delta function of transverse momentum conservation being the phase-space constraint Θ_{PS}.

If in addition to the requirement of softness and collinearity we also impose *strong ordering* of the gluons momenta, i.e.

$$k^2_{T_{i1}} \ll k^2_{T_{i2}} \ll ... \ll k^2_{T_{iN}} \lesssim p^2_{\rm T} \ll \hat{s}\,, \tag{2.3.33}$$

the coupled integrals in (2.3.32) factorise to give

$$\frac{1}{\sigma_0}\frac{d\hat{\sigma}}{dp^2_{\rm T}}\Big|_{\mathcal{O}(\alpha_s^N)} = \frac{\alpha_s C_F}{\pi}\frac{1}{p^2_{\rm T}}\ln\left(\frac{\hat{s}}{p^2_{\rm T}}\right)\frac{1}{(N-1)!}\left(\frac{\alpha_s C_F}{\pi}\int^{p^2_{\rm T}}\frac{dk^2_T}{k^2_T}\ln\frac{\hat{s}}{k^2_{Ti}}\right)^{N-1}. \tag{2.3.34}$$

Owing to the presence of virtual corrections, the integral (2.3.34) is finite. Performing the integration and summing over N yields

$$\begin{aligned}\frac{1}{\sigma_0}\frac{d\sigma}{dp^2_{\rm T}} &= \frac{1}{p^2_{\rm T}}\left[\alpha_s\frac{A^{(1)}}{2\pi}\ln\left(\frac{\hat{s}}{p^2_{\rm T}}\right) - \alpha_s^2\frac{(A^{(1)})^2}{8\pi^2}\ln^3\left(\frac{\hat{s}}{p^2_{\rm T}}\right) + ...\right.\\ &+ \left.\alpha_s^N\frac{(-1)^{N-1}(A^{(1)})^N}{2^{2N-1}(N-1)!\pi^N}\ln^{2N-1}\left(\frac{\hat{s}}{p^2_{\rm T}}\right) + ...\right],\end{aligned} \tag{2.3.35}$$

where $A^{(1)} = 2C_F$. The above approximation to the $q\bar{q}\to\gamma^* + X$ cross section, Eq. (2.3.35), is commonly known as the *Double Leading Logarithm Approximation* (DLLA). For $\alpha_s\ln(\hat{s}/p^2_{\rm T}) \sim 1$ the series in (2.3.35) diverges, i.e. the higher-order terms become dominant.[2] Since the DLLA expression arises as a result of dynamical and kinematical factorization, we expect that the cross section exponentiates, cf. Section 1.6.2. In fact, under the assumption of strong ordering, the $k^2_{\rm T}$ of the gluon corresponds to the variable $1-z$, reaching the phase space boundary at $z = 1$ ($k_{\rm T} = 0$). A closer inspection of (2.3.35) reveals that it is an exponential power series and as such can be resummed, giving

$$\frac{1}{\sigma_0}\frac{d\sigma}{dp^2_{\rm T}} = \frac{\alpha_s A^{(1)}}{2\pi p^2_{\rm T}}\ln\left(\frac{\hat{s}}{p^2_{\rm T}}\right)\exp\left(\frac{-\alpha_s A^{(1)}}{4\pi}\ln^2\left(\frac{\hat{s}}{p^2_{\rm T}}\right)\right). \tag{2.3.36}$$

Eq. (2.3.36) has been firstly derived by Dokshitzer, Dyakonov and Troyan [29] and is often referred in the literature as the *DDT formula.*

All orders resummation of logarithmic divergences in (2.3.35) leads to a drastically different behaviour of (2.3.36) as compared to the LO expression (2.3.29), cf. Fig. 2.3. Clearly it recovers the finite result in the small $p_{\rm T}$ limit. In particular, the resummed cross section vanishes when $p_{\rm T}\to 0$.

[2]This is particularly important in the case of the W, Z production, where $Q \sim M_W, M_Z$. The condition $\alpha_s\ln(Q^2/p^2_{\rm T}) \sim 1$ corresponds to $p_{\rm T} \sim 10 \div 15$ GeV. The majority of collected data lies below this limit.

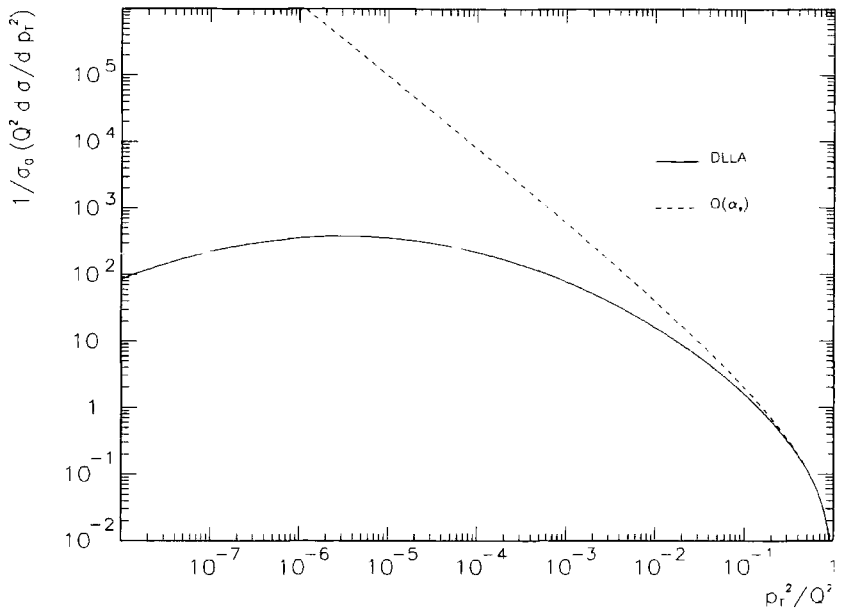

Figure 2.3: Comparison of LO perturbative calculation (only logarithmic part) and DLLA (2.3.36), for the parton subprocess.

2.4 The impact parameter space

Although the DLLA succeeds in resumming the most leading logarithmic contributions to the p_T distribution it returns a result which is suppressed in the limit $p_T \to 0$.[3] The suppression arises directly from imposing the strong ordering condition (2.3.33). According to (2.3.33), if a vector boson is produced with a very small p_T then there is no phase space left for the production of soft gluons and the cross section becomes naturally suppressed. In reality, the same vector boson can be, for example, produced in association with two almost back-to back gluons with non-negligible transverse momentum. In fact the only requirement for the production of a vector boson with $p_T \sim 0$ is that the vector sum over the gluons' momenta, $\sum_i \vec{k}_{Ti}$ is small. Therefore one can suspect that the DLLA

[3]In principle one should also take into account the non-perturbative contribution to the transverse momentum distribution, which causes the distribution to be non-zero in the $p_T \to 0$ limit. These non-perturbative effects are discussed in Section 2.5.

suppression is simply an artifact of the approximation, in which the transverse momentum conservation condition is destroyed by strong ordering. Moreover, we would expect the sub-leading corrections resulting from the correct implementation of the transverse momentum conservation to modify the behaviour of $d\sigma/dp_{\mathrm{T}}^2$ at small p_{T}.

The exact $\mathcal{O}(\alpha_s)$ calculations for the p_{T} distribution were performed in [30], whereas [31, 32] presents a derivation of the $\mathcal{O}(\alpha_s^2)$ result. Unfortunately, owing to the delta function of transverse momentum conservation coupling the integrals, it is very difficult to calculate (2.3.32) *exactly* beyond $\mathcal{O}(\alpha_s^2)$ in p_{T} space. In [33] it was proposed to perform soft gluon emission calculations in the impact parameter b space, the Fourier conjugated space to the p_{T} space. The advantage of the b space method is that it allows correct implementation of the transverse momentum conservation condition [27, 28]. In the Fourier conjugated space the phase-space constraint Θ_{PS} factorises, cf. Section 1.6.2

$$\Theta_{PS}(\vec{p_{\mathrm{T}}}, \vec{k}_{T\,1}, ...) = \delta^2\left(\vec{p_{\mathrm{T}}} - \sum_{i=1}^{N} \vec{k}_{T\,i}\right) = \int d^2b \frac{1}{4\pi^2} e^{i\vec{b}\vec{p_{\mathrm{T}}}} \prod_{i=1}^{N} e^{-i\vec{b}\vec{k}_{T\,i}}\,, \tag{2.4.37}$$

This suggests that in order to properly take into account sub-leading kinematical effects related to transverse momentum conservation, resummation should be carried out in impact parameter space.

2.4.1 Resummation in impact parameter space

Summarizing the discussion above, the following programme accomplishing resummed calculations conserving transverse momentum for any differential cross section in p_{T}, i.e. $d\sigma/dp_{\mathrm{T}}$ or $d\sigma/dQ^2dydp_{\mathrm{T}}^2$, emerges:

- First the cross-section (with a delta function conserving transverse momentum implemented) is transformed into the Fourier conjugate, $b-$space,

$$\tilde{\sigma}_r(b) = \int d^2p_{\mathrm{T}} e^{-i\vec{b}\vec{p_{\mathrm{T}}}} \sigma(p_{\mathrm{T}}^2) \tag{2.4.38}$$

- then the conjugated cross-section $\tilde{\sigma}(b)$ is computed (resummed) and finally trans-

formed back to momentum space

$$\sigma_r(p_{\rm T}) = \frac{1}{4\pi^2}\int d^2b e^{i\vec{b}\vec{p_{\rm T}}}\tilde{\sigma}_r(b)\,. \tag{2.4.39}$$

- The resulting $\sigma_r(p_{\rm T})$ is a resummed distribution.

The use of the b space technique allows for a development of a general expression resumming all terms of the perturbation series which are at least as singular as $1/p_{\rm T}^2$ when $p_{\rm T}\to 0$ [21]. For the process $AB\to\gamma^*(\to l^+l^-)+X$ Collins, Soper and Sterman proposed the general formalism [21] (*CSS formalism*)

$$\frac{d\sigma}{dQ^2dydp_{\rm T}^2} = \frac{\sigma_0}{4\pi Q^2}\int d^2b e^{ip\vec{_{\rm T}}\vec{b}}\tilde{\sigma}_r(b,Q,x_a,x_b) + \frac{\sigma_0\pi}{Q^2}\sigma_f(p_{\rm T},Q,x_a,x_b)\,. \tag{2.4.40}$$

The form of (2.4.40) stems from the standard perturbative formula for the Drell-Yan cross section to which the factorization theorem is applied

$$\frac{d\sigma}{dQ^2dydp_{\rm T}^2} = \frac{\sigma_0\pi}{Q^2}\sum_{a,b}\int_{x_a}^1\frac{d\zeta_a}{\zeta_a}\int_{x_b}^1\frac{d\zeta_b}{\zeta_b}T_{ab}(p_{\rm T},Q,x_a/\zeta_a,x_b/\zeta_b,\mu_F)f_{a/A}(\zeta_a,\mu_F)f_{b/B}(\zeta_b,\mu_F)\,. \tag{2.4.41}$$

The short-distance contribution to the cross section T_{ab} has a perturbative expansion

$$T_{ab}(p_{\rm T},Q,x_a/\zeta_a,x_b/\zeta_b,\mu_F) = \sum_{N=0}^{\infty}\bar{\alpha_s}^N(\mu_R)T_{ab}^{(N)}(p_{\rm T},Q,x_a/\zeta_a,x_b/\zeta_b,\mu_R,\mu_F)\,. \tag{2.4.42}$$

where $\bar{\alpha_s}=\alpha_s/2\pi$. In the lowest order

$$T_{ab}^{(0)} = e_a^2\delta_{a,b}\delta\left(\frac{x_a}{\zeta_a}-1\right)\delta\left(\frac{x_b}{\zeta_b}-1\right)\delta(p_{\rm T})\,, \tag{2.4.43}$$

and we discussed the exact form of $T_{ab}^{(1)}$ in Section 2.3. We also know that in each order of α_s the corresponding $T_{ab}^{(N)}$ is singular with the strongest double logarithmic singularity of the form $(1/p_{\rm T}^2)\alpha_s^N\ln^{(2N-1)}(p_{\rm T}^2/Q^2)$, cf. Section 1.6.1. Apart from logarithmic singularities coming from the real emission diagrams and the $\delta(p_{\rm T})$ singularities from the virtual diagrams, $T_{ab}^{(N)}$ contains also regular terms

$$\begin{aligned} T_{ab}^{(N)}(p_{\rm T},Q,x_a/\zeta_a,x_b/\zeta_b,\mu_R,\mu_F) &= \mathcal{V}^{(N)}(Q,x_a/\zeta_a,x_b/\zeta_b,\mu_R,\mu_F)\delta(p_{\rm T}) \\ &+ \sum_{m=0}^{2N-1}T_{ab}^{(N,m)}(Q,x_a/\zeta_a,x_b/\zeta_b,\mu_R,\mu_F)\frac{1}{p_{\rm T}^2}\ln^m\left(\frac{Q^2}{p_{\rm T}^2}\right) \\ &+ R_{ab}^{(N)}(p_{\rm T},Q,x_a/\zeta_a,x_b/\zeta_b,\mu_R,\mu_F)\,. \end{aligned} \tag{2.4.44}$$

The regular part $R_{ab}^{(N)}$ is defined as a set of terms which are less singular that $p_{\rm T}^{-2}$ or $\delta(p_{\rm T})$ as $p_{\rm T}\to 0$. Putting back (2.4.44) into (2.4.41), one recovers (2.4.40), under the condition that the function σ_f assembles the regular parts $R_{ab}^{(N)}$ to all orders

$$\sigma_f(p_{\rm T},Q,x_a,x_b)=\sum_{a,b}\int_{x_a}^1\frac{d\zeta_a}{\zeta_a}\int_{x_b}^1\frac{d\zeta_b}{\zeta_b}\sum_{N=0}^{\infty}\ \bar{\alpha_s}^N(\mu_R)R_{ab}^{(N)}(p_{\rm T},Q,x_a/\zeta_a,x_b/\zeta_b,\mu_R,\mu_F)$$
$$f_{a/A}(\zeta_a,\mu_F)f_{b/B}(\zeta_b,\mu_F)\,. \qquad (2.4.45)$$

The singular terms of (2.4.44) are then collected in the function $\sigma_r(p_{\rm T},Q,x_a,x_b)$ which is Fourier conjugated to $\sigma_r(b,Q,x_a,x_b)$, cf. (2.4.39).

To resum logarithmically divergent terms the perturbation series in $\tilde{\sigma}_r(b,Q,x_a,x_b)$ needs to be reorganized. It can be argued [20, 21] that the x_a/ζ_a and a dependence factorises from the x_b/ζ_b and b dependence in $\tilde{\sigma}_r(b,Q,x_a,x_b)$:

$$\begin{aligned}\tilde{\sigma}_r(b,Q,x_a,x_b) &= \sum_{a,b}\int_{x_a}^1\frac{d\zeta_a}{\zeta_a}\int_{x_b}^1\frac{d\zeta_b}{\zeta_b}f_{a/A}(\zeta_a,\mu_F)f_{b/B}(\zeta_b,\mu_F)\\ &\times\ \sum_j e_j^2 C_{ja}(x_a/\zeta_a,b,Qb,\mu_F)C_{jb}(x_b/\zeta_b,b,Qb,\mu_F)\,, \qquad (2.4.46)\end{aligned}$$

where j stands for the flavour of the annihilating quark and antiquark. The functions C_{ja} are calculable in perturbation theory and we discuss them in detail in Appendix B. As functions in b space, they contain logarithms of Q^2b^2. Since arbitrarily large values b are allowed, it is possible that $\alpha_s\ln^2(Q^2b^2)\gtrsim 1$. In this way spoiling of the convergence of the fixed order expansion, observed already in $p_{\rm T}$ space, manifests itself in b space.

Notwithstanding, it follows from the results of [20, 34] that $\tilde{\sigma}_r$ obeys the evolution equation

$$\frac{\partial}{\partial\ln Q^2}\tilde{\sigma}_r(b,Q,x_a,x_b)=\{K(b\mu,\alpha_s(\mu))+G(Q/\mu,\alpha_s(\mu))\}\tilde{\sigma}_r(b,Q,x_a,x_b)\,, \qquad (2.4.47)$$

where again K and G have expansions in $\alpha_s(\mu)$. Note that the b and Q dependences are isolated in Eq. (2.4.47). Furthermore, the functions K and G satisfy renormalization group equations

$$\mu\frac{d}{d\mu}K(b\mu,\alpha_s(\mu)) = -\gamma_K(\alpha_s(\mu)) \qquad (2.4.48)$$

$$\mu\frac{d}{d\mu}G(b\mu,\alpha_s(\mu)) = +\gamma_K(\alpha_s(\mu)) \qquad (2.4.49)$$

with the anomalous dimension γ_K being calculable perturbatively [35]. Describing the evolution of the functions K and G, the RGE's (2.4.48), (2.4.49) can be used to retain control over the large logarithmic terms. By changing the scale in K to $\mu \sim 1/b$ while changing the scale in G to $\mu \sim Q$, the large logarithms disappear. In other words the solution of (2.4.48), (2.4.49) yields

$$\begin{aligned} K(b\mu, \alpha_s(\mu)) + G(Q/\mu, \alpha_s(\mu)) = & - \int_{C_1^2/b^2}^{C_2^2 Q^2} \frac{d\bar{\mu}^2}{\bar{\mu}^2} \frac{1}{2} \gamma_K(\alpha_s(\bar{\mu})) \\ & + K(C_1, \alpha_s(C_1/b)) + G(1/C_2, \alpha_s(C_2 Q)) \,, \end{aligned} \tag{2.4.50}$$

and the evolution equation for $\tilde{\sigma}_r$ can be written down in a compact way

$$\frac{\partial}{\partial \ln Q^2} \tilde{\sigma}_r(b, Q, x_a, x_b) = -\tilde{\sigma}_r(b, Q, x_a, x_b) \int_{C_1^2/b^2}^{C_2^2 Q^2} \frac{d\bar{\mu}^2}{\bar{\mu}^2} \left[A(\alpha_s(\bar{\mu}), C_1) + B(\alpha_s(C_2 Q), C_1, C_2) \right] . \tag{2.4.51}$$

The descendants of K, G and γ_K functions, the A and B functions can be calculated reliably in fixed-order perturbation theory.

Finally, solving the evolution equation (2.4.51) gives the expression for the $AB \to \gamma^* + X$ cross section

$$\begin{aligned} \frac{d\sigma}{dQ^2 dy dp_{\mathrm{T}}^2} = & \frac{\sigma_0}{4\pi Q^2} \int d^2 b e^{i\vec{p}_{\mathrm{T}}\vec{b}} \sum_j e_j^2 \sum_{a,b} \int_{x_a}^1 \frac{d\zeta_a}{\zeta_a} \int_{x_b}^1 \frac{d\zeta_b}{\zeta_b} f_{a/A}(\zeta_a, \mu_F) f_{b/B}(\zeta_b, \mu_F) \\ & \times e^{\mathcal{S}(Q,b,C_1,C_2)} C_{ja}(x_a/\zeta_a, b, C_1/C_2, \mu_F) C_{jb}(x_b/\zeta_b, b, C_1/C_2, \mu_F) \\ & + \frac{\sigma_0 \pi}{Q^2} \sigma_f(p_{\mathrm{T}}, Q, x_1, x_2) \,, \end{aligned} \tag{2.4.52}$$

with the Sudakov factor of the form

$$\mathcal{S}(Q, b, C_1, C_2) = - \int_{C_1^2/b^2}^{C_2^2 Q^2} \frac{d\bar{\mu}^2}{d\bar{\mu}^2} \left[A(\alpha_s(\bar{\mu}), C_1) \ln \left(\frac{C_2^2 Q^2}{\bar{\mu}^2} \right) + B(\alpha_s(\bar{\mu}), C_1, C_2) \right] . \tag{2.4.53}$$

and

$$A(\alpha_S) = \sum_{i=1}^{\infty} (\bar{\alpha}_s)^i A^{(i)} \quad B(\alpha_S) = \sum_{i=1}^{\infty} (\bar{\alpha}_s)^i B^{(i)} . \tag{2.4.54}$$

The canonical choice of the constants C_1, C_2 is

$$C_1 = C_2 b_0 = b_0 = 2 \exp^{-\gamma_E} . \tag{2.4.55}$$

The first two coefficients in each series (2.4.54) can be obtained [35] from the exact $\mathcal{O}(\alpha_s)$ and $\mathcal{O}(\alpha_s^2)$ perturbative calculation by comparing the logarithmic terms therein with the corresponding logarithms generated by the first three terms of the expansion of $\exp(\mathcal{S}(Q, b, C_1, C_2))$ in (2.4.52). With the canonical choice of C_1, C_2 (2.4.55)

$$\begin{aligned}
A^{(1)} &= 2C_F \\
A^{(2)} &= 2C_F \left(N_c \left(\frac{67}{18} - \frac{\pi^2}{6} \right) - \frac{10}{9} T_R N_f \right) \\
B^{(1)} &= -3C_F \\
B^{(2)} &= C_F^2 \left(\pi^2 - \frac{3}{4} - 12\zeta(3) \right) + C_F N_c \left(\frac{11}{9}\pi^2 - \frac{193}{12} + 6\zeta(3) \right) \\
&+ C_F T_R N_f \left(\frac{17}{3} - \frac{4}{9}\pi^2 \right) ,
\end{aligned} \tag{2.4.56}$$

where $N_c = 3$. The $\mathcal{O}(\alpha_s)$ expansion of the function C_{ij}, cf. (2.4.46), assuming (2.4.55), is given in Appendix B, whereas the regular coefficients $R^{(1)}$, $R^{(2)}$ of the σ_f part (2.4.45) are listed in [21, 24, 36].

The derivation of (2.4.52) ensures that the CSS formula resums all sub-leading logarithms in p_{T} space by the means of the b space technique.[4] Additionally, the resummed part of the cross section has been proved to be renormalization group invariant. In Chapter 3 we discuss the logarithmic structure of the cross section in p_{T} space. Nonetheless it can be already seen from the form of (2.4.52), (2.4.53) and (2.4.54) that the perturbation series indeed undergoes reorganization (1.6.59) into towers of logarithms. The current knowledge of only the first two coefficients in the expansion of A, B and C functions allows resummation of the first four towers of logarithms; the fifth tower contains the first unknown coefficient $A^{(3)}$ [36]. We will explicitly demonstrate this in Chapter 3.

[4] Another method of soft gluon resummation for vector boson production was proposed in [24]. As explained in [36], the formalism of [24] and the CSS formalism differ by terms coming from the sub-leading, lower than the fourth tower, towers of logarithms, provided α_s in the formalism of [24] is evaluated at b_0/b^2.

2.4.2 Matching

The resummed expression $\sigma_r(p_{\rm T})$ is expected to give correct predictions for the $p_{\rm T}$ distribution in the small $p_{\rm T}$ region, $p_{\rm T} \ll Q$. The region of large $p_{\rm T}$, $p_{\rm T} \sim Q$, is well described by fixed-order results, known up to $\mathcal{O}(\alpha_s^2)$. Collecting only a particular subset of terms in the perturbative expansion for the cross section, both approaches fail to provide an expression valid for all values of $p_{\rm T}$. Such an expression is proposed by (2.4.52), derived for the general case of full all-order perturbative expansion incorporating all the terms. It contains the resummed part σ_r and the part σ_f, defined as a sum of all regular terms in the perturbative series. In other words, σ_f is equivalent to the difference between the fixed-order perturbative contribution and its asymptotic approximation in the limit $p_{\rm T} \to 0$, gathering terms at least as divergent as $p_{\rm T}^{-2}$. When all orders are considered, the asymptotic approximation is obviously identical with σ_r. Since knowledge of σ_f requires knowledge of the fixed-order result, σ_f defined as above, i.e.

$$\sigma_f = \frac{d\sigma}{dQ^2 dy dp_{\rm T}^2}\Big|_{\text{fixed-order}} - \frac{d\sigma}{dQ^2 dy dp_{\rm T}^2}\Big|_{\text{fixed-order, asymptotic}} \tag{2.4.57}$$

is known only up to $\mathcal{O}(\alpha_s^2)$. Given the truncated σ_f, σ_f^{trunc}, the cross section can be written as

$$\frac{d\sigma}{dQ^2 dy dp_{\rm T}^2} = \sigma_r + \sigma_f^{trunc}. \tag{2.4.58}$$

Eq. (2.4.58) defines the matching prescription. At low $p_{\rm T}$ the fixed-order and the asymptotic pieces effectively cancel, leaving the resummed; at high $p_{\rm T}$ the resummed and the asymptotic pieces cancel to a certain order, leaving the fixed-order result. This method of matching has been first proposed at $\mathcal{O}(\alpha_s)$ in [24] and then extended to $\mathcal{O}(\alpha_s^2)$ in [36]. It is characterized by a smaller theoretical error than simple choosing some moderate value $p_{\rm T} = p_{\rm T}^{cut}$ and applying the resummation expression σ_r for $p_{\rm T} < p_{\rm T}^{cut}$ and the fixed-order result for $p_{\rm T} > p_{\rm T}^{cut}$ [36].

The matching procedure (2.4.58) is bound to fail eventually since the cancellation between the resummed part and the asymptotic, fixed-order part is not *complete*. In particular, resummation introduces terms such as $\alpha_s^3 \ln^5(Q^2/p_{\rm T}^2)$ which are not cancelled by the second-order asymptotic expression. The uncancelled resummed part is strong enough

to cause negative values of the cross section at $p_{\rm T} \sim Q$ [36]. This can be understood easily if one realizes that due to the presence of the Bessel function in σ_r and the kinematical boundary $p_{\rm T} \leq Q$, σ_r is forced to oscillate at large values of $p_{\rm T}$. To overcome the problem, usually a prescription is provided for how to switch from the matched result to the pure fixed-order result [36, 37].

2.4.3 Large b treatment

The CSS resummation formalism involves the non-perturbative regime of large b. More precisely, the integration in (2.4.53) extends from 0 to ∞. When $b \to 1/\Lambda$ then $\alpha_S(1/b)$ grows large entering the non-perturbative regime. Consequently, the result of the integration (2.4.53) is made invalid. Therefore it is necessary to enrich the CSS formalism by a prescription for how to deal with the non-perturbative regime of large b. One approach is to artificially forbid b from reaching large values by replacing it with a new variable b_* which serves to 'freeze' the perturbative calculations at a certain point b_{lim},

$$b_* = \frac{b}{\sqrt{1+(b/b_{\rm lim})^2}}, \qquad b_* < b_{\rm lim}\,, \tag{2.4.59}$$

with the parameter $b_{\rm lim} \sim 1/\Lambda$ separating the perturbative and non-perturbative physics. This prescription enables us to perform the integration in (2.4.53). Of course, with such a prescription, the resulting theoretical predictions should not be expected to agree with data at small $p_{\rm T}$ where the contribution of the large b region is the biggest. This problem is normally overcome by parameterizing the non-perturbative effects in the large b region in terms of the form-factor $F_{ab}^{NP}(b,Q,x_a,x_b)$ so that the cross section (2.4.52), after integrating over rapidity, followed by integrating over angles using

$$\int_0^{2\pi} e^{ip_{\rm T}b\cos\phi} d\phi = 2\pi J_0(p_{\rm T}b)\,, \tag{2.4.60}$$

and choosing $\mu_F = b_0/b_*$, reads

$$\begin{aligned}\frac{d\sigma}{dQ^2dp_{\rm T}^2} &= \frac{\sigma_0}{2Q^2}\sum_q e_q^2 \int_0^1 dx_a dx_b\, \delta\left(x_a x_b - \frac{Q^2}{s}\right) \\ &\times \int db\, b\, J_0(p_{\rm T}b)\, e^{S(Q,b_*)} F_{ab}^{NP}(b,Q,x_a,x_b) f'_{q/A}(x_a,b_0/b_*) f'_{\bar{q}/B}(x_b,b_0/b_*) \\ &+ \frac{\sigma_0\pi}{Q^2}\sigma_f(p_{\rm T},Q,x_1,x_2)\,,\end{aligned} \tag{2.4.61}$$

where the functions f' are defined as a convolution of the C functions with the parton distribution functions, see Appendix B. We discuss specific choices for the form of the non-perturbative function in Section 2.5.

2.4.4 Small b treatment

The resummation formalism (2.4.61) does not uniquely specify how to treat the small b region. Although this region does not contribute large logarithmic terms, no numerical predictions can be obtained without an unambiguous prescription.

The problem arises because (2.4.61) allows for any small value of b to be considered as an argument of the integrand. The limits of integration in (2.4.53) imply, however, that $b_* \geq b_0/Q$ and smaller values of b ($b_* \sim b$ in this limit) are clearly unphysical. Various solutions have been proposed. For example one can replace the lower limit of integration in (2.4.53) by [38]

$$\frac{b_0}{b_*} \to \frac{b_0}{b_*} \frac{1}{\sqrt{1 + b_0^2/(b^2 Q^2)}}, \tag{2.4.62}$$

which ensures that the scale $\bar{\mu}$ in the integral (2.4.53) never exceeds Q. The authors of [37] proposed a more sophisticated treatment, involving changing the form of the Sudakov factor, which, when expanded, enabled them to correctly recover the $\mathcal{O}(\alpha_s)$ fixed coupling result.

In practice, various treatments of the small b region cause differences in the p_{T} distribution at the large p_{T} end of the spectrum. For such p_{T}, the resummed calculations on their own are not expected to provide reliable predictions and need to be matched with the fixed order result, as described in Section 2.4.2. It is then necessary to ensure that matching is performed according to a particular prescription applied to the small b regime. Thus the choice of prescription has not much relevance if followed by an appropriate matching strategy.[5] In this thesis, for the numerical results obtained with the help of the b space expression (2.4.61) we use the 'minimal' prescription of disregarding the

[5]The analysis in [39] suggest that the method of continuation of the Sudakov factor in (2.4.61) for b from $1/Q$ to 0 makes no numerical difference for $p_{\mathrm{T}} < Q/5$.

values of the integral (2.4.61) for $b < b_0/Q$, i.e. we effectively change the lower limit of the integral from 0 to b_0/Q.

2.5 Intrinsic transverse momentum of partons

The cross section expression (2.4.61) is not complete without specifying the form of the function F_{NP}. It is introduced in (2.4.61) to account for the *initial, non-perturbative* $q_{\rm T}$ distribution of incoming partons which contributes to the final $p_{\rm T}$ of a produced boson. Intrinsic $q_{\rm T}$ is a consequence of the Fermi motion of partons confined within a hadron. As it is uncorrelated with the momentum of the hadron, the Fermi motion manifests itself as momentum fluctuations in the transverse direction. Based on renormalization group analysis arguments, in [21] a universal form of F_{NP} has been proposed

$$F_{ab}^{NP}(Q, b, x_a, x_b) = \exp\left[-h_Q(b)\ln\left(\frac{Q}{2Q_0}\right) - h_a(b, x_a) - h_b(b, x_b)\right] . \qquad (2.5.63)$$

where Q_0 is an arbitrary constant indicating the smallest scale at which the perturbation theory is reliable, $Q_0 \sim 1/b_{\rm lim}$. The functions h_Q, h_a, h_b are to be extracted by comparing theoretical predictions with experimental data. It is, however, inherent in their definitions that

$$h_Q(0) = h_a(0, x_a) = h_b(0, x_b) = 0\,, \qquad (2.5.64)$$

since as $b \to 0$, $\tilde{\sigma}_r(b_*) \approx \tilde{\sigma}_r(b)$ and the $p_{\rm T}$-integrated cross section should remain unchanged, so that we require $F^{NP}(b = 0) = 1$. As postulated in [21] the flavour dependence of F^{NP} can be ignored. The $\ln(Q/Q_0)$ dependence in (2.5.63) is required to balance the Q dependence of the Sudakov factor. Additionally, h_Q was proved to be universal and its leading b^2 behaviour is suggested by the analysis of the infrared renormalon contribution [40], as well as recent analysis of the dispersive approach to power corrections [41].

However, the detailed form of the non-perturbative function $F_{ab}^{NP}(Q, b, x_a, x_b)$ remains a matter of theoretical dispute. Early studies on the fixed-target experiments, see e.g. [3], suggested that a Gaussian parameterization of an intrinsic $q_{\rm T}$ distribution provided a good

description of data in the low p_{T} (1-2 GeV) regime.[6] Motived by this result, Davies et al. (DSW) [39] approximated the function F^{NP} by

$$F_{ab}^{NP}(Q, b, x_a, x_b) = \exp\left[-g_2 b^2 \ln\left(\frac{Q}{2Q_0}\right) - g_1 b^2\right] . \tag{2.5.65}$$

The g_1 parameter in (2.5.65) has a interpretation of a measure of the intrinsic transverse momentum whereas g_2 stands for a contribution coming from unresolved gluons with $k_{\mathrm{T}} < Q_0$ as the structure functions evolve from scales $\mathcal{O}(Q_0)$ to $\mathcal{O}(Q)$. Assuming (2.5.65), with a particular choice of $Q_0 = 2$ GeV, $b_{\mathrm{lim}} = 0.5$ GeV^{-1}, and using the Duke-Owens parton distribution functions [42] the DSW analysis gave

$$g_1 = 0.15\,\mathrm{GeV}^2, \qquad g_2 = 0.40\,\mathrm{GeV}^2 . \tag{2.5.66}$$

An alternative parameterization, proposed by Ladinsky and Yuan (LY) [43], incorporates a possible dependence on $\tau = x_a x_b$

$$F_{ab}^{NP}(Q, b, x_a, x_b) = \exp\left[-g_2 b^2 \ln\left(\frac{Q}{2Q_0}\right) - g_1 b^2 - g_1 g_3 b \ln(100\tau)\right] . \tag{2.5.67}$$

Choosing $Q_0 = 1.6$ GeV, $b_{\mathrm{lim}} = 0.5$ GeV^{-1} and using the CTEQ2M parton distribution functions, the parameters in (2.5.67) were determined

$$g_1 = 0.11^{+0.04}_{-0.03}\,\mathrm{GeV}^2, \qquad g_2 = 0.58^{+0.1}_{-0.2}\,\mathrm{GeV}^2, \qquad g_3 = -1.5^{+0.1}_{-0.1}\,\mathrm{GeV}^{-1} . \tag{2.5.68}$$

Both parameterizations were recently revisited in [44]. Using modern, high-statistics samples of Drell-Yan data the values of the DSW parameters were updated

$$g_1 = 0.24\,\mathrm{GeV}^2, \qquad g_2 = 0.34\,\mathrm{GeV}^2 , \tag{2.5.69}$$

as well as the LY parameters

$$g_1 = 0.15^{+0.04}_{-0.03}\,\mathrm{GeV}^2, \qquad g_2 = 0.48^{+0.04}_{-0.05}\,\mathrm{GeV}^2, \qquad g_3 = -0.58^{+0.26}_{-0.20}\,\mathrm{GeV}^{-1} . \tag{2.5.70}$$

[6] For low energy Drell-Yan experiments (e.g. $\sqrt{s} \sim 30$ GeV), the perturbative fixed-order result combined with the non-perturbative model alone tends to describe data quite well [3, 7], making the effect of the resummed calculations insignificant.

The analysis of [44] found that currently available experimental data show no preference in the form of the parameterization, i.e. both parameterizations can be considered to describe data equally well. However, the form of the non-perturbative function is expected to be extremely important for obtaining accurate predictions at the LHC. Given that existing data concentrated roughly around same value of τ, the dependence on τ is difficult to determine, as opposed to the dependence on Q. The expected values of τ at the LHC will be very different from the currently achievable values, presenting the problem of the non-perturbative function in a new light.

2.6 Numerical results

In this section we briefly present numerical results for the $d\sigma/dp_{\rm T}$ distribution. Since the CSS formalism itself is rather a starting point, not a main focus of our study, the results shown here are mostly for the future reference. We compare the theoretical predictions for the resummed part of the cross section $d\sigma/dp_{\rm T}$ with the recent sets of data on Z boson production from the D0 and CDF experiments at the Fermilab Tevatron [45, 46]. As the resummed part description is valid for small values of $p_{\rm T}$, we consider only data in the range $0 - 25$ GeV.

In our analysis we use the first order expansion of α_s and a continuously changing number of flavours N_f, explained in Section 5.2. To improve the speed of the numerical calculations while evaluating numerous integrals over the slowly decreasing Bessel function, we use the ansatz function, see Appendix C, calculated at the scale b_0/b_*. The relative normalization between the experimental and theoretical distributions is found taking into account only those experimental points with $p_{\rm T} < 15$ GeV and using a method based on minimizing the χ^2 parameter, as outlined in Section 5.5.2. We consider both DSW and LY parameterization functions at $Q = M_Z$, $\sqrt{s} = 1.8$ TeV. In Figs. 2.4, 2.5, the CDF and D0 experimental points are compared with the theoretical distribution, obtained with the effective gaussian (LY) parameterization and MRST98 [47] (CTEQ4M [48]) parton distribution functions. In agreement with the D0 analysis [45] we find that the LY non-

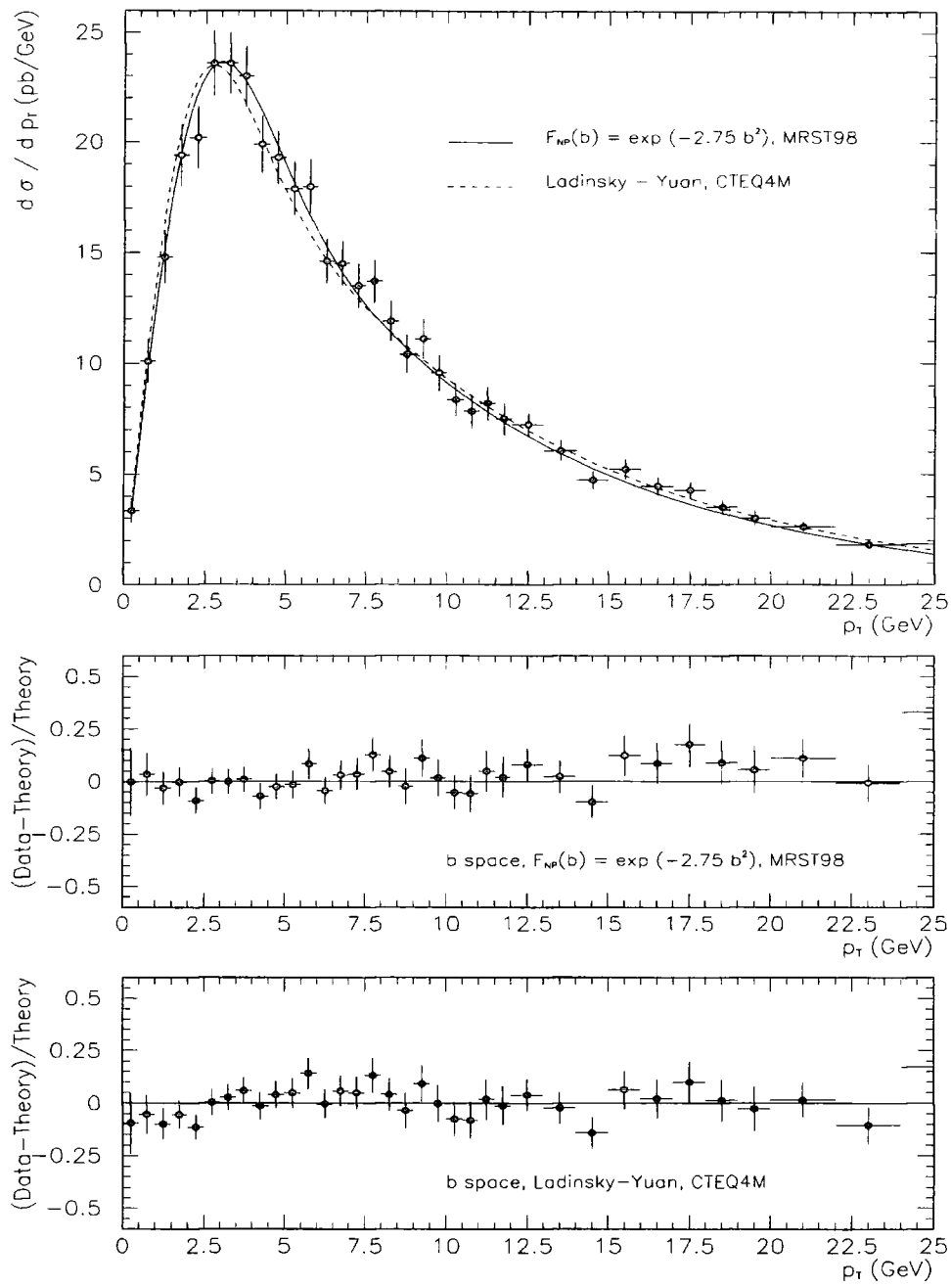

Figure 2.4: Theoretical cross section in b space vs. CDF data. The predictions were obtained using the effective gaussian form of the non-perturbative function with $g_2' = 2.75$ GeV^2, $b_{\rm lim} = 0.5$ GeV-1 and MRST98 parton distribution functions (solid line) as well as the LY non-perturbative function with parameters given by (2.5.68) and CTEQ4M parton distribution functions (dashed line).

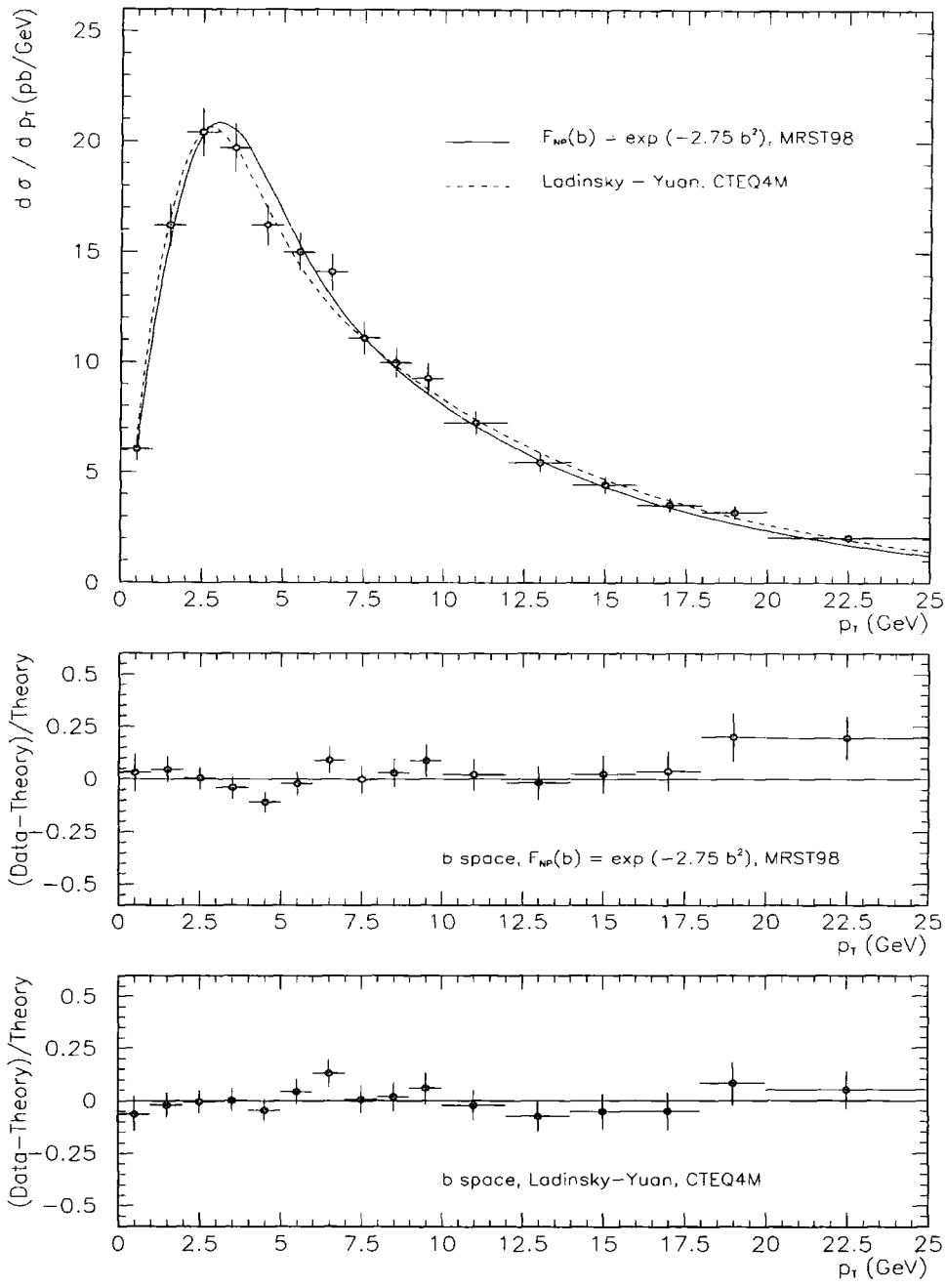

Figure 2.5: Theoretical cross section in b space vs. D0 data. The predictions were obtained using the effective gaussian form of the non-perturbative function with $g_2' = 2.75$ GeV^2, $b_{\rm lim} = 0.5$ GeV-1 and MRST98 parton distribution functions (solid line) as well as the LY non-perturbative function with parameters given by (2.5.68) and CTEQ4M parton distribution functions (dashed line).

perturbative function describe the data well. We also find that even better agreement (i.e. a better value of χ^2) can be obtained using the effective Gaussian function

$$F^{NP}(b) = \exp(-g_2' b^2)\,, \tag{2.6.71}$$

with $g_2' = 2.75$ GeV^2. [7] The validity of the LY form was also questioned in [37] and thus we believe that the form of the non-perturbative function remains a open question.

Note: The most up-to-date numerical programs, incorporating the CSS formalism in b space, matched to the fixed-order $\mathcal{O}(\alpha_s)$ result have been developed in [37, 49]. These codes calculate distributions for the hadronic production of a vector boson, accounting for its decay kinematics.

2.7 Summary

In this chapter we presented the soft gluon emission problem in the widely understood context of the Drell-Yan process. Starting from the discussion of the parton model Drell-Yan cross section, we investigated the $\mathcal{O}(\alpha_s)$ QCD corrections to di-lepton production through the creation of a virtual photon γ^*. In particular we focused on the real gluon emission process, showing that it contributes a logarithmic correction divergent in the $p_{\rm T}\to 0$ limit. Emission of a larger number of gluons results in higher order corrections characterized by stronger logarithmic divergences, with the leading contribution of the form $\alpha_s^N \ln^{2N-1}(Q^2/p_{\rm T}^2)$. The logarithms arise because every factor of α_s corresponds to an addition of a real or virtual gluon in diagrams, and each gluon potentially has both soft and collinear singularities. Since the KLN theorem is valid to all orders in perturbation theory the cancellation of singularities between real and virtual contributions takes place. This gives us a regularized (infrared safe) expression at $p_{\rm T} = 0$ so that the integral over $p_{\rm T}^2$ is finite. By examining the $p_{\rm T}$ distribution one develops an insight into the structure of

[7] In fact the value of $g_2' = 2.75$ GeV^2 was obtained as a result of fitting the effective gaussian function to the data. It is almost twice as big as the corresponding g_2' incurred from the original DSW non-perturbative function. However, the DSW analysis was performed in a narrow range of small Q with large errors on the experimental data.

the singularities, in particular the imbalance between the real and virtual contributions as functions of p_{T}. The perturbation series for the imbalanced contributions coming from the real gluon emission diagrams can be reorganized and resulting subsets of terms resummed, either via the DLLA expression (if only the most leading logarithmic contributions are taken into account), or generally, in the b space based CSS formalism. Once again utilising the idea of the RGE equation analysis, cf. Chapter 1, the CSS formalism succeeds in resumming all the sub-leading terms which are at least as divergent as p_{T}^{-2}. Subsequently, as discussed in Sections 2.4.2, 2.4.4, the formalism must be completed with a matching prescription and a parameterization of non-perturbative effects.

In the above analysis of the full resummation formalism we were not concerned with the effect of the vector boson decay into leptons or quarks. In particular, we do not discuss distributions of the final state particles, after the decay of the boson. Moreover, for massive vector bosons, we assume a narrow width approximation. The inclusion of the decay effects is not complicated and details can be found in [37].

At this point it is worthwhile to mention the existence of another approach to evaluating soft gluon radiation effects. It relies on Monte Carlo simulations, as opposed to exact analytic calculations presented above. The parton shower packages like HERWIG [50], ISAJET [51] or PYTHIA [52] incorporate the backward evolution technique to simulate soft gluon emission. Parton showers resum only the leading logarithms together with some of the sub-leading logarithms. Nevertheless much progress has been achieved recently in incorporating the matrix element corrections for the vector boson production to HERWIG [53] and PYTHIA [54, 55].

In the following chapters we will develop, discuss and apply an analytical approximation of the CSS formalism in p_{T} space.

Chapter 3

Sudakov logarithm resummation in transverse momentum space

The impact parameter method provides a fine example of the resummation of logarithmically enhanced contributions in perturbative QCD. As we have seen in Chapter 2 the b space formalism achieves satisfactory agreement between theoretical predictions and experimental data. Nevertheless, the formalism suffers from certain deficiencies and theoretical drawbacks which need to be 'fixed' in order to obtain desirable agreement with the data. Thus, although its theoretical importance is unquestionable, the b space method can be considered as not fully satisfactory. Let us now briefly examine the disadvantages of the b space method.

- *Non-perturbative ambiguities*

  The final expression (2.4.61) generated by the b space formalism contains a Fourier transform integral over b which extends from 0 to ∞. As a result no predictions can be made without an 'ansatz' prescription for how to deal with the non-perturbative region. The usual method is to artificially prevent b from reaching large values by replacing it with a new variable b_*, and parametrising the non-perturbative large b region in terms of a form factor $F^{NP}(b)$. As we have discussed in Chapter 2, this method is not free from ambiguities. In fact we would particularly like to stress

that it is *impossible* to make an unambiguous prediction, not only for small p_{T}, but for *any* value of p_{T}, without having a prescription for the non-perturbative regime of large b.

- *Matching ambiguities*

  The resummed expression, σ_r, cannot describe the cross section for the whole range of p_{T}. It automatically sums all known logarithmic terms (i.e. those containing logarithms of $\ln(Q^2/p_{\mathrm{T}}^2)$), but does not take into account full fixed-order corrections, which become increasingly important at large p_{T}. A feature of the b space method, due to properties of the Bessel function in (2.4.61), is that σ_r oscillates at large p_{T}, leading to a *negative* cross section. Therefore in order to obtain a consistent description of the data both at small and large p_{T}, one needs to match the resummed predictions σ_r, enriched by the finite part σ_f, with fixed order predictions at some intermediate value of p_{T}, as discussed in Section 2.4.2. Since it is impossible to select any particular subset of logarithmic corrections in σ_r, there is no unambiguous prescription for matching; existing prescriptions require unsmooth or even discontinuous switching from resummed to fixed-order calculation at some value of p_{T}. This results in unphysical predictions for the cross section around the matching point. Additionally, the cancellation between terms in the resummed part and in the fixed order part are undermined by the presence of the non-perturbative function $F^{NP}(b)$, which distorts the resummed part.

- *Numerical evaluation*

  Because of the oscillatory nature of the integrand in the Fourier transform, the numerical evaluation of the integral (2.4.61) has proved to be enormously difficult and lengthy [56]. The large cancellations between many cycles of the Bessel function (as it is a slowly vanishing function in the limit $b\to\infty$) are difficult to implement and create a potential source of numerical errors. To make things worse, the unknown non-perturbative parameters, like b_*, g_1 and g_2, need to be extracted from data. In order to find the best fit to the data, calculations of the Bessel integral have to be repeated many times, once for each different set of the non-perturbative parameters.

The above mentioned difficulties of the b space method would be naturally circumvented if one had a resummed expression for σ_r in transverse momentum space. First, the non-perturbative prescription would be required in, and would affect only, the very lowest values of p_{T}. This means that outside the non-perturbative region the predictions would be based on the perturbative theory alone. Secondly, since the resummed and the fixed order part would both be calculated in p_{T} space, it would be straightforward to distinguish between terms which are or are not resummed. Merging with the fixed order large p_{T} expression is in principle *direct*, since the p_{T} logarithms in σ_r can simply be removed from the finite order pieces to avoid double counting. Using the former terminology, σ_f can now be defined as the difference between the fixed order expression and the asymptotic form of the p_{T} space resummed σ_r. Then matching of $\sigma_r + \sigma_f$ to the fixed-order part would be explicit, returning a smooth cross section. Together with the non-perturbative input influencing only the small p_{T} limit, this should lead to a unified description of vector boson transverse momentum at both small and large p_{T}.

Since the Fourier integral in the b space method leading to the exact p_{T} expression cannot be performed analytically, the question is whether it is possible to develop a p_{T} space expression approximating the full b space result sufficiently well in the region of p_{T} relevant for comparison with data. The goal is to achieve a p_{T} space resummed expression reproducing all the good features of the b space resummation without the drawbacks related to this method.

Various techniques have been proposed for carrying out resummation in p_{T} space [57, 58]. All of them resum different subsets of logarithmic terms and we will discuss the differences between them in more detail in Chapter 4. Here we present the derivation of a method which allows resummation of the first four towers of logarithms.

3.1 The formalism of the transverse momentum space resummation

The springboard for our approach is the general expression (2.4.61) in impact parameter space for the Drell-Yan cross section [21]. For simplicity, throughout this chapter we shall restrict our attention to the parton-level subprocess cross section. Parton distribution functions can in principle be incorporated to yield the hadron level cross section without significantly changing the conclusions on resummation. We will discuss hadron cross sections in detail in Chapter 5. Suffice it to say here that the subprocess cross section can be factored out if one takes τ^N *moments* ($\tau = Q^2/s$) of the hadron cross section. Then the subprocess cross section corresponds to the $N = 0$ moment, $\frac{1}{\sigma_0}\frac{d\sigma}{dp_{\rm T}^2} \equiv \frac{1}{p_{\rm T}^2}\Sigma(0, \frac{Q^2}{p_{\rm T}^2}, \frac{Q^2}{\mu^2}, \alpha_S(\mu^2))$, as in Ref. [35]. To begin with, we will not include any non-perturbative treatment in the small $p_{\rm T}$ region.

The parton level b space formula reads, cf. (2.4.61)

$$\frac{d\sigma}{dp_{\rm T}^2} = \frac{\sigma_0}{2}\int_0^\infty bdb\, J_0(p_{\rm T}b)e^{\mathcal{S}(b,Q^2)}\,, \tag{3.1.1}$$

where, assuming the canonical choice of the constant C_1, C_2 (2.4.55)

$$\mathcal{S}(b,Q^2) = -\int_{\frac{b_0^2}{b^2}}^{Q^2}\frac{d\bar{\mu}^2}{\bar{\mu}^2}\left[\ln\left(\frac{Q^2}{\bar{\mu}^2}\right)A(\alpha_s(\bar{\mu}^2)) + B(\alpha_s(\bar{\mu}^2))\right], \tag{3.1.2}$$

$$A(\alpha_s) = \sum_{i=1}^{\infty}\bar{\alpha_s}^i A^{(i)} \quad B(\alpha_s) = \sum_{i=1}^{\infty}\bar{\alpha_s}^i B^{(i)}\,. \tag{3.1.3}$$

The first two coefficients in each of the series in (3.1.3), i.e. $A^{(1)}$, $A^{(2)}$, $B^{(1)}$, $B^{(2)}$ are given in (2.4.56).

It is instructive to see how the logarithms in b space generate logarithms in $p_{\rm T}$ space. For illustration, we take only the leading coefficient $A^{(1)} = 2C_F$ to be non-zero in $\exp(\mathcal{S}(b,Q^2))$, and assume a fixed coupling α_s. This corresponds to

$$\frac{d\sigma}{dp_{\rm T}^2} = \frac{\sigma_0}{2}\int_0^\infty bdb\, J_0(p_{\rm T}b)\exp\left(-\frac{\alpha_s C_F}{2\pi}\ln^2\left(\frac{Q^2b^2}{b_0^2}\right)\right). \tag{3.1.4}$$

The expressions are made more compact by defining new variables $\eta \equiv p_{\rm T}^2/Q^2$, $\lambda \equiv \alpha_s C_F/\pi$, $x \equiv bp_{\rm T}$. Then

$$\frac{1}{\sigma_0}\frac{d\sigma}{d\eta} = \frac{1}{2\eta}\int_0^\infty dx x J_0(x) \exp\left[-\frac{\lambda}{2}\ln^2\left(\frac{x^2}{\eta b_0^2}\right)\right] \tag{3.1.5}$$

and we encounter the same expression as in [27], which describes the emission of soft and collinear gluons with transverse momentum conservation taken into account. The result of numerically integrating (3.1.5) and its comparison with the DLLA approximation (2.3.36) is shown in Fig. 3.1.[1]

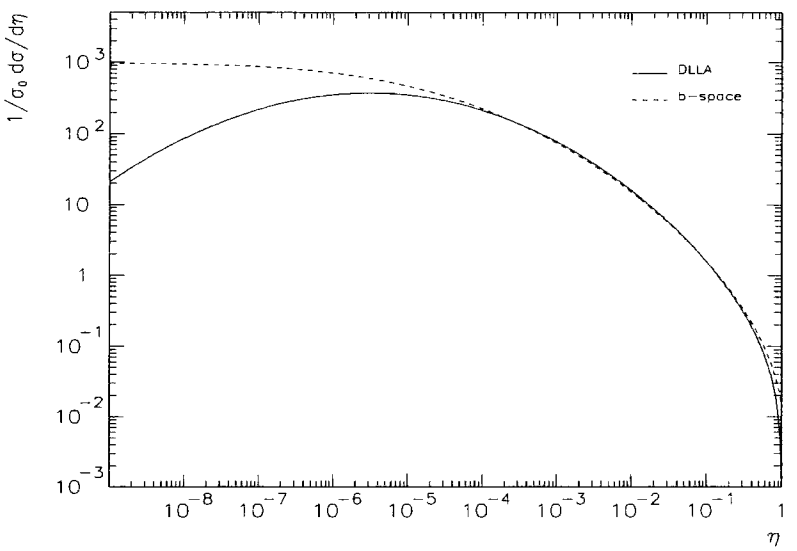

Figure 3.1: DLLA (2.3.36) and b-space (3.1.5) results for the transverse momentum distribution $(1/\sigma_0)(d\sigma/d\eta)$.

The cross sections are similar over a broad range in η: the main differences occur at (i) small η, where the DLLA curve is suppressed to zero and the b space curve tends to a finite value, as predicted in [33], and (ii) at large η (strictly, outside the domain of validity of either expression). The physical reasons for recovering the finite positive

[1]For all our studies with a fixed value of the coupling we take $\lambda = \alpha_s C_F/\pi = 0.085$, $N_f = 4$.

result in the limit $\eta \to 0$ were already discussed in Section 2.4: the contributions due to transverse momentum conservation fill the DLLA dip at $p_{\rm T} \to 0$. Mathematically, it can be seen from (3.1.1). In the limit $p_{\rm T} \to 0$ the Bessel function tends to unity and the integral over b yields a finite positive value.

At $\eta = 1$ the $p_{\rm T}$ space cross section vanishes by virtue of the overall factor of $\ln(1/\eta)$. This is a crude approximation to the (formally correct) vanishing of the leading-order cross section at the kinematic limit $p_{\rm T} \sim Q$. In contrast, the b space cross section has no information about this kinematic limit, and is non-zero at $\eta = 1$. Furthermore, at large $p_{\rm T}$ the b space cross section *oscillates* about 0. This can be seen in Fig. 3.2, which extends the cross section of Fig. 3.1 to large η on a linear scale. The first zero of the oscillation is clearly evident. Now since this occurs far outside the physical region it might be argued that it is not a problem in practice. However, when the first sub-leading logarithm $B^{(1)}$ is included, the first zero moves *inside* the physical region, as shown in the figure. It is this behaviour which causes problems in merging the large $p_{\rm T}$ fixed-order result with the resummed expression, which develops negative values for large $p_{\rm T}$, see Chapter 2.

The expression (3.1.5) can be integrated by parts using the relationship $\frac{d}{dx}\left[xJ_1(x)\right] = xJ_0(x)$ so that it transforms into

$$\frac{1}{\sigma_0}\frac{d\sigma}{d\eta} = -\frac{1}{2\eta}\int_0^\infty dx x J_1(x) \frac{d}{dx}\left[\exp\left(-\frac{\lambda}{2}\left(L + L_b\right)^2\right)\right], \tag{3.1.6}$$

where $L \equiv \ln(1/\eta) = \ln(Q^2/p_{\rm T}^2)$, $L_b \equiv \ln(x^2/b_0^2)$. Expansion of the exponential in (3.1.6) leads to

$$\frac{1}{\sigma_0}\frac{d\sigma}{d\eta} = \frac{1}{\eta}\sum_{N=1}^{\infty} \lambda^N \frac{(-1/2)^{N-1}}{(N-1)!} \sum_{m=0}^{2N-1} 2^m \tau_m \binom{2N-1}{m} L^{2N-1-m}, \tag{3.1.7}$$

which is now a perturbation series in $p_{\rm T}$ space. Here the numbers τ_m are defined by

$$\tau_m \equiv \int_0^\infty dy J_1(y) \ln^m\left(\frac{y}{b_0}\right), \tag{3.1.8}$$

and can be calculated explicitly from the generating function

$$\sum_{m=0}^{\infty} \frac{1}{m!} t^m \tau_m = e^{t\gamma_E} \frac{\Gamma(1+t/2)}{\Gamma(1-t/2)} = \exp\left[-2\sum_{k=1}^{\infty} \frac{\zeta(2k+1)}{2k+1}\left(\frac{t}{2}\right)^{2k+1}\right], \tag{3.1.9}$$

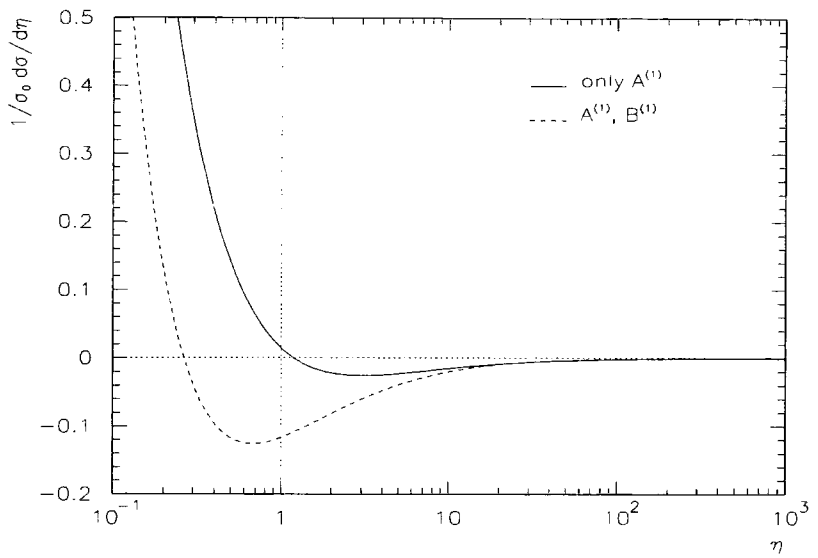

Figure 3.2: Extension of the b space cross section presented in Fig. 3.1 to large values of η.

so that e.g. $\bar{b}_0(\infty) = 1$, $\bar{b}_1(\infty) = \bar{b}_2(\infty) = 0$, $\bar{b}_3(\infty) = -\frac{1}{2}\zeta(3)$ etc.

Due to the $\alpha_s^N L^{2N-1-m}$ structure of the summation (3.1.7) the accuracy is limited by the condition $\alpha_s L^2 \lesssim 1$. This accuracy can be improved by extracting the Sudakov factor $\exp\left(-\frac{\lambda}{2}L^2\right)$ from the sum to get

$$\frac{1}{\sigma_0}\frac{d\sigma}{d\eta} = \frac{\lambda}{\eta} e^{\frac{-\lambda}{2}L^2} \sum_{N=1}^{\infty} \frac{(-2\lambda)^{(N-1)}}{(N-1)!} \sum_{m=0}^{N-1} \left(\begin{array}{c} N-1 \\ m \end{array} \right) L^{N-1-m} \left[2\tau_{N+m} + L\tau_{N+m-1} \right] . \tag{3.1.10}$$

Clearly, the resummation formula (3.1.10) is now well-behaved provided $\alpha_s L \lesssim 1$. In section 3.2 we study the two expressions (3.1.7) and (3.1.10) in more detail.

Before doing so, it is worthwhile comparing the expression for the differential cross section (3.1.1) with the expressions (3.1.7) and (3.1.10). The first, in b space, calculates the cross section in terms of a one-dimensional integral. The cross section is well defined at all values of $p_{\rm T}$, and in particular at $p_{\rm T} = 0$. In practice, however, non-perturbative

effects have to be taken into account in this region, as discussed in Chapter 2.

On the other hand, the large $p_{\rm T}$ behaviour of (3.1.1) is not physical: the integral has no knowledge of the exact kinematic upper limit on $p_{\rm T}$, although numerically it becomes small when $p_{\rm T} \sim Q$. More problematically, as $p_{\rm T}$ is increased the distribution starts to *oscillate*, and it is this feature (built-in via the Bessel function) which makes it difficult to merge with the finite-order large $p_{\rm T}$ cross section.

In contrast, the $p_{\rm T}$ space cross section of (3.1.7) (or (3.1.10)) is an *asymptotic* series. The logarithms are singular at $p_{\rm T} = 0$, although as argued above this is in any case the region where non-perturbative effects dominate. As with any asymptotic series, care must be taken with the number of terms retained.

3.2 Quantitative study of resummed cross sections

As has been outlined in Chapter 2 the b space formalism allows resummation of *all* logarithmic terms in the cross section. This naturally includes sub-leading logarithmic contributions. Let us remind the reader that the leading terms can be resummed on their own in $p_{\rm T}$ space giving the DLLA expression 2.3.36. The sub-leading logarithmic terms, which can thus also be viewed as corrections to (2.3.36), have three origins. First, there are sub-leading terms arising from the matrix elements that are associated with the coefficients $B^{(1)}, A^{(2)}$, etc. Secondly, there are sub-leading effects resulting from the running of the strong coupling α_s. Finally, there are also sub-leading terms in the form of kinematic logarithms, which as we will see later, always appear with τ_m $(m \geq 1)$ coefficients. In the following subsection we focus on this particular type of sub-leading effect and assess its importance. We isolate the effects induced by kinematic logarithms by fixing the coupling and taking only leading terms arising from the matrix element. Then, in the following subsections, we progressively switch on running coupling effects and sub-leading logarithms from the matrix element.

3.2.1 Fixed coupling analysis

We begin our study of (3.1.7) by performing the resummation for the simple case $m = 0$. This is the DLLA of Eq. (2.3.35), i.e. all radiated gluons are soft and collinear with strong transverse momentum and energy ordering, and no account taken of transverse momentum conservation:

$$\frac{1}{\sigma_0}\frac{d\sigma}{d\eta} = \frac{1}{\eta}\sum_{N=1}^{\infty} \lambda^N \frac{(-1/2)^{N-1}}{(N-1)!}\tau_0 L^{2N-1}\,. \tag{3.2.11}$$

Being a simple expansion of the exponential function, the sum (2.3.35) converges to (2.3.36) with increasing number of terms taken into account, see Fig. 3.3.

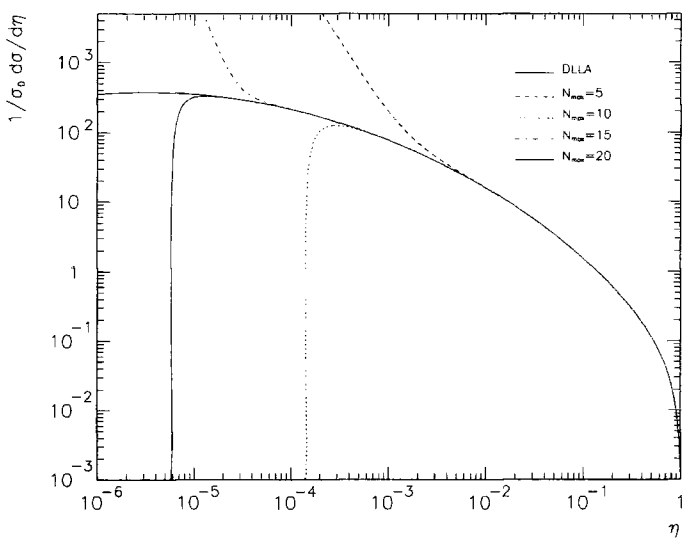

Figure 3.3: Convergence of the series (3.2.11) to DLLA expression (2.3.36).

Next we investigate the effect of including all the $m \geq 0$ terms in (3.1.7). (To be approximated numerically the series has to be truncated at some $N_{\max}$. Thus full evaluation of (3.1.7) up to the $N_{\max}$-th term requires knowledge of the first $2N_{\max} - 1$ coefficients τ_m.) The first 20 coefficients, calculated according to (3.1.9), are listed in Table 3.1. We find (see Fig. 3.4) that for large m the coefficients behave as $\tau_m \approx C\,(-1)^m m!\, 2^{-m}$, where C is a constant.

m	τ_m	m	τ_m
0	1.0	10	1122.9875510
1	0	11	−6141.3046770
2	0	12	36851.269530
3	−.601028451	13	−239674.372200
4	0	14	1677209.4750
5	−1.555391633	15	−12580409.1300
6	3.612351995	16	100640859.60
7	−11.343929370	17	−855451267.600
8	52.350738970	18	7.699062951e+09
9	−218.6078590	19	−7.314109389e+10

Table 3.1: The first 20 coefficients τ_m, calculated according to (3.1.9).

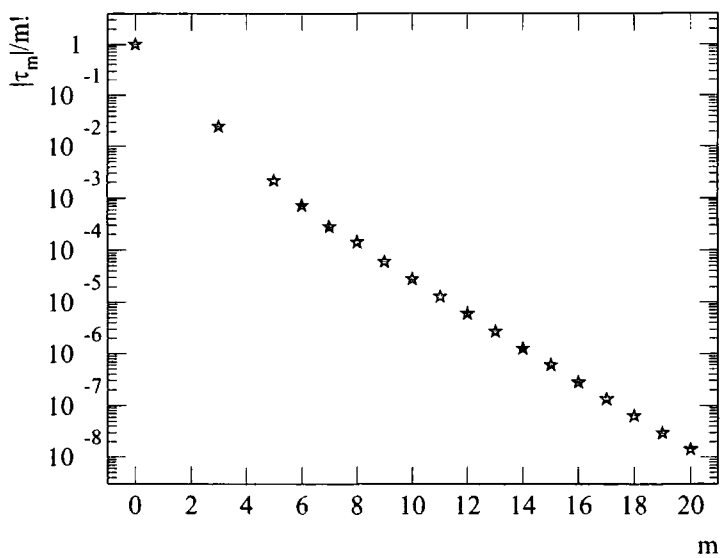

Figure 3.4: The behaviour of $|\tau_m|/m!$.

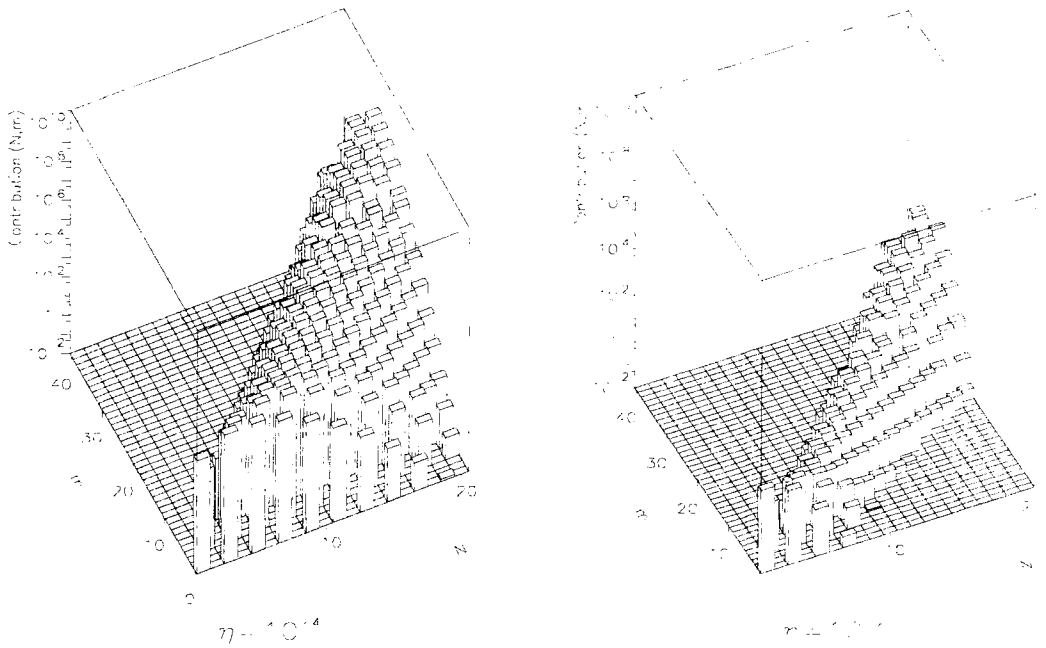

Figure 3.5: Contributions (3.2.12) to the cross section (3.1.7). Only positive contributions plotted here.

Taking more terms into account, i.e. $m \geq 1$, we find that, as expected, the sum (3.1.7) exhibits behaviour consistent with an asymptotic series. A single (N, m) contribution to (3.1.7) is of the form

$$\frac{1}{\eta}\lambda^N \frac{(-1/2)^{N-1}}{(N-1)!} 2^m \tau_m \begin{pmatrix} 2N-1 \\ m \end{pmatrix} L^{2N-1-m} , \tag{3.2.12}$$

and to show the complexity of the resummation (3.1.7) we display these individual contributions in Fig. 3.5. For all η the biggest contributions arise when $m \sim 2N-1$, since the coefficients τ_m are largest there. As η decreases, contributions with smaller m become more significant due to the terms with L^{2N-m-1}.

Our first task is to investigate numerically the dependence of (3.1.7) on the point of truncation $N_{\max}$, i.e. the order of the perturbative expansion, and the number of terms included in the internal summation (3.1.7) – the 'cut-off' value $m_{\max}$, equivalent to the

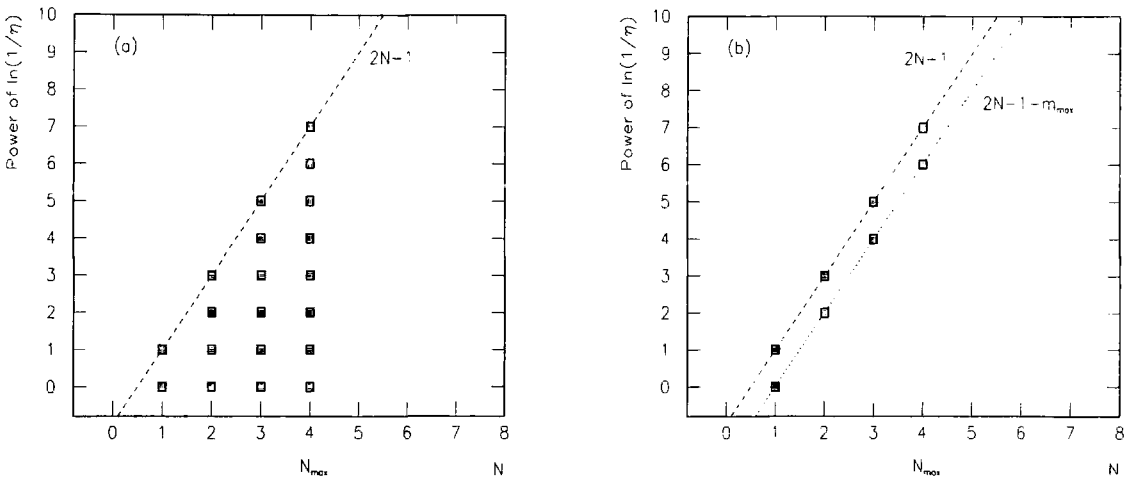

Figure 3.6: Resummation of (3.2.12). Each point corresponds to a contribution (3.2.12) summed in (3.1.7) when (a): 'all' $m_{max} \geq 2N_{\max} - 1$ coefficients τ_m are known and (b): only $m_{max} < 2N_{\max} - 1$ are known. In particular here $N_{\max} = 4$ and $m_{\max} = 7, 1$ for the case (a),(b), respectively. Here N equals power of the coupling α_s.

number of resummed (truncated) 'towers' of logarithms down from leading. Obviously for different pairs $(N_{\max}, m_{\max})$ different contributions (3.2.12) are summed, see Fig. 3.6. In Fig. 3.7 we show a 3D cumulative plot of (3.1.7) which illustrates some of the features discussed below. Each plotted value for a given point $(N_{\max}, m_{\max})$ represents the sum (3.1.7), truncated at $N_{\max}$ and calculated with $\tau_m = 0$ for $m > m_{\max}$. The distinctive plateau present for large values of $N_{\max}$ and small $m_{\max}$ is equivalent to recovering the b space result for various η. Notice how for smaller η this plateau has a tendency to contract. If all $2N_{\max} - 1 = m_{\max}$ coefficients τ_m are taken into account (see Fig. 3.6a), it seems that the b-space result cannot be approximated for any value of $N_{\max}$, except for the region of large η. This should not be surprising, considering that the 'towers' of logarithms have been *truncated.* Conversely, if only the first few coefficients $(m_{\max} < 2N_{\max} - 1)$ are known (Fig. 3.6b) and the rest of them are set to zero, then in some sense one is closer

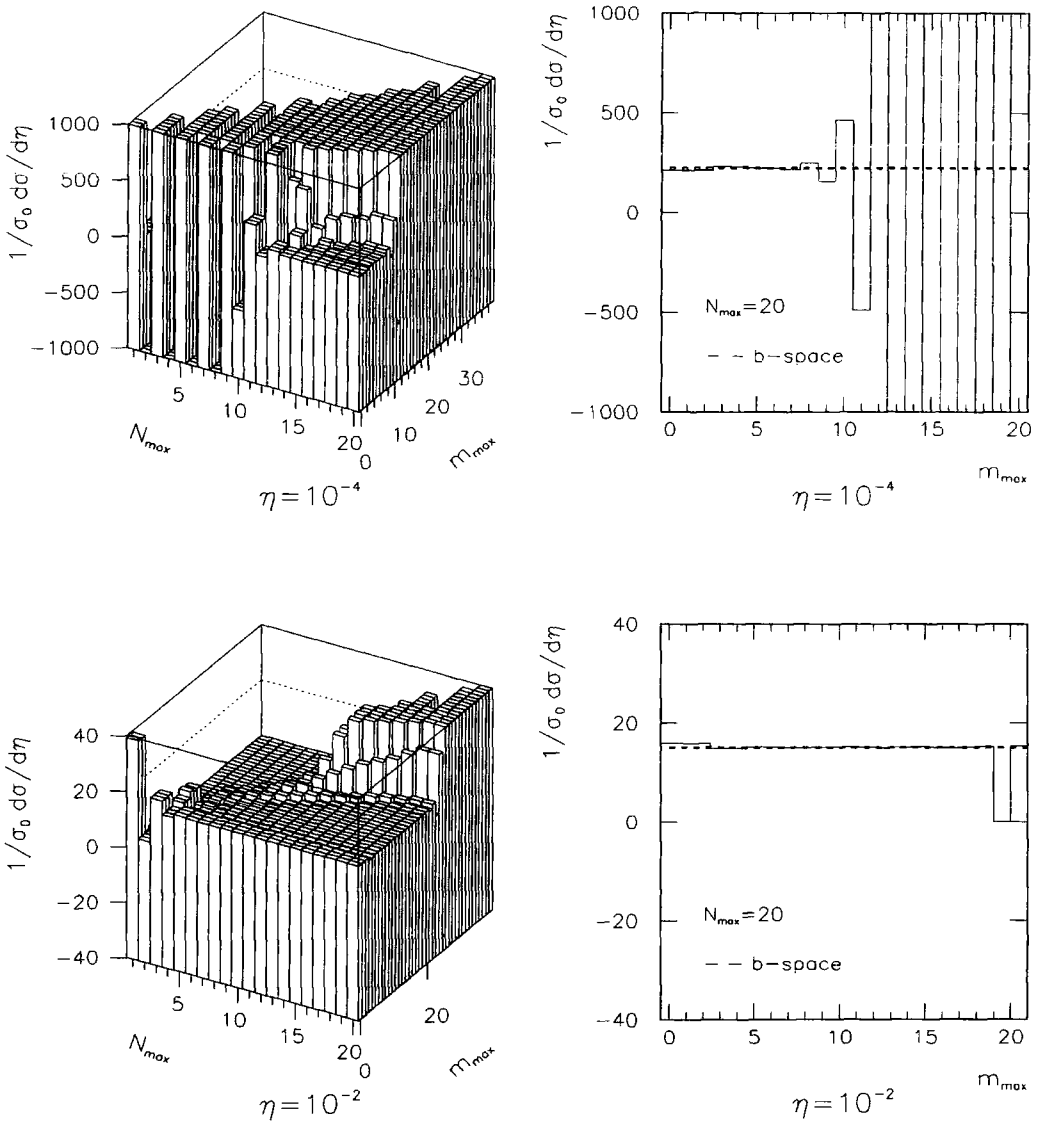

Figure 3.7: The cumulative plot of (3.1.7) for $\eta = 10^{-4}, 10^{-2}$ and its section along $N_{\max} = 20$.

to the DLLA situation and it is possible to find $N_{\max}$ such that the cross section (3.1.7) approaches the b-space result, at least at large enough values of η. Moreover, it can be seen from Fig. 3.7 that it is necessary to consider the first *few* factors τ_m, i.e. more then one logarithmic tower, to achieve the best approximation of the b-space result.

It is interesting to see whether factorizing out the resummed DLLA piece from (3.1.7) in (3.1.10) leads to an improvement in the approximation of the b space result. As we have already noticed, a key feature of (3.1.10) is that after extracting the Sudakov factor, the residual perturbation series has at most $N+1$ logarithms of $1/\eta$ at Nth order in perturbation theory, i.e. the leading terms are now $\lambda^N L^{N+1}$. This obviously extends the validity of the resummation formula (3.1.10) down to values of η satisfying the condition $\alpha_s L \lesssim 1$. However we know that the terms in the residual sum must give a large contribution as $\eta \to 0$ in order to compensate the overall suppression from the Sudakov factor. The terms which contribute to the new series (3.1.10) are illustrated schematically in Fig. 3.8. Notice that the extraction of the Sudakov factor results in an ability to sum an *infinite* subseries of logarithms. This observation constitutes a basis for our further analysis. However, there is a shortcoming: in order to sum the first m towers *fully* we need to take $N_{\max} = m$ which leads us to include extra sub-leading contributions from more than the first m towers, cf. Fig. 3.8b.

The individual contributions to the summation (3.1.10),

$$\frac{1}{\eta} e^{-\frac{\lambda}{2}L^2} \frac{(-2)^{(N-1)}\lambda^N}{m!(N-1-m)!} L^{N-1-m}\left[2\tau_{N+m} + L\tau_{N+m-1}\right], \tag{3.2.13}$$

are presented in Fig. 3.9. As was the case for (3.2.12), the importance of the $\ln(1/\eta)$ factors diminishes for small m and large η. Note that for small η the sizes of the contributions are much smaller here than for (3.1.7).

Next we perform the same analysis as for (3.1.7), i.e. we study the dependence of (3.1.10) on $N_{\max}$ and on the 'cut-off' value $m_{\max}$. Comparing the cumulative plot for (3.1.10), Fig. 3.10, with Fig. 3.7, we note that the b space result is now better approached close to the line $m_{\max} = N_{\max} - 1$, which corresponds to resummation of all $N_{\max}$ infinite towers. Such an effect can be observed in the case of (3.1.7) only for large

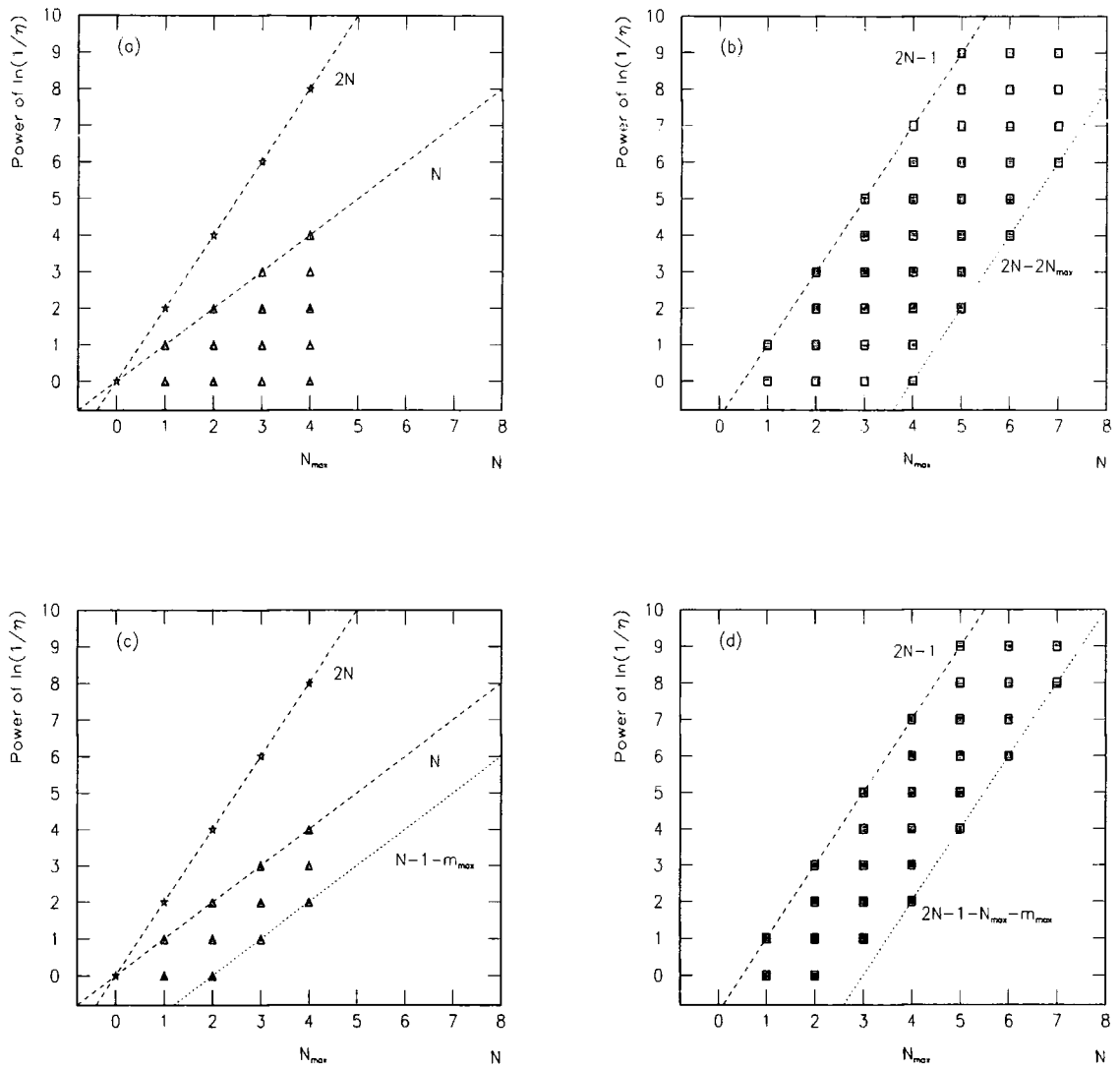

Figure 3.8: Resummation of Eq. (3.2.13). Each point corresponds to a contribution (3.2.13). The points along the straight line 'power of $\ln(1/\eta) = 2N$' represent terms coming from the Sudakov factor. Figures (b) and (d) illustrate contributions summed when this factor is expanded. In particular, here $N_{\max} = 4$ and $m_{\max} = 7$ for the case (a),(b) and $m_{\max} = 1$ in (c), (d). Note that only the $N_{\max}$, $\min(N_{\max}, 2 + 2m_{\max})$ first towers are fully summed in (b), (d), respectively.

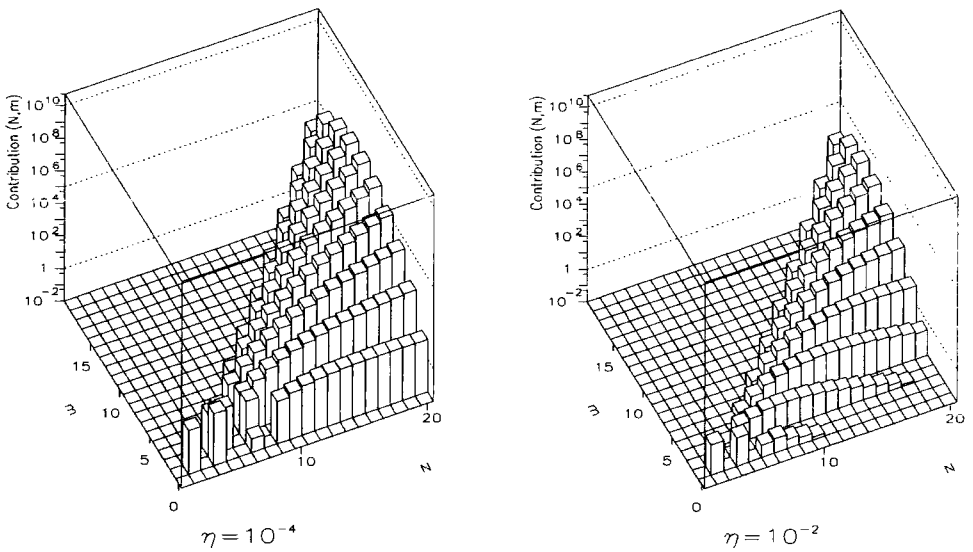

Figure 3.9: Contributions (3.2.13) to the cross section (3.1.10). Only positive contributions plotted here.

η. Here the b space result can be reproduced even for very small η given sufficiently large $N_{\max}$, see Fig. 3.11. When $m_{\max} < N_{\max} - 1$ the balance between different contributions is apparently spoiled until $m_{\max}$ becomes considerably small. Again, it turns out that it is necessary to incorporate at least the first *few* sub-leading towers (i.e. some moderate $N_{\max}$) to obtain the best approximation of the b space result, cf. Fig 3.11.

The asymptotic properties of (3.1.10) can be most easily seen for large values of η and large $N_{\max}$. The apparent discrepancy between the b space result and the summation (3.1.10) is caused here by contributions with $m = N - 1$, i.e. terms proportional to τ_{2N-1}. The other terms are negligible as they contain powers of L which for these η are very small. The dominant contribution is then proportional to $(-1)^{N_{\max}-1}2^{N_{\max}}\tau_{2N_{\max}-1}/(N_{\max}-1)!$, i.e. the sign varies as $(-1)^{N_{\max}}$. Fortunately, the range of η for which the discrepancy occurs is outside the region of interest for the present discussion. Also, in practice we

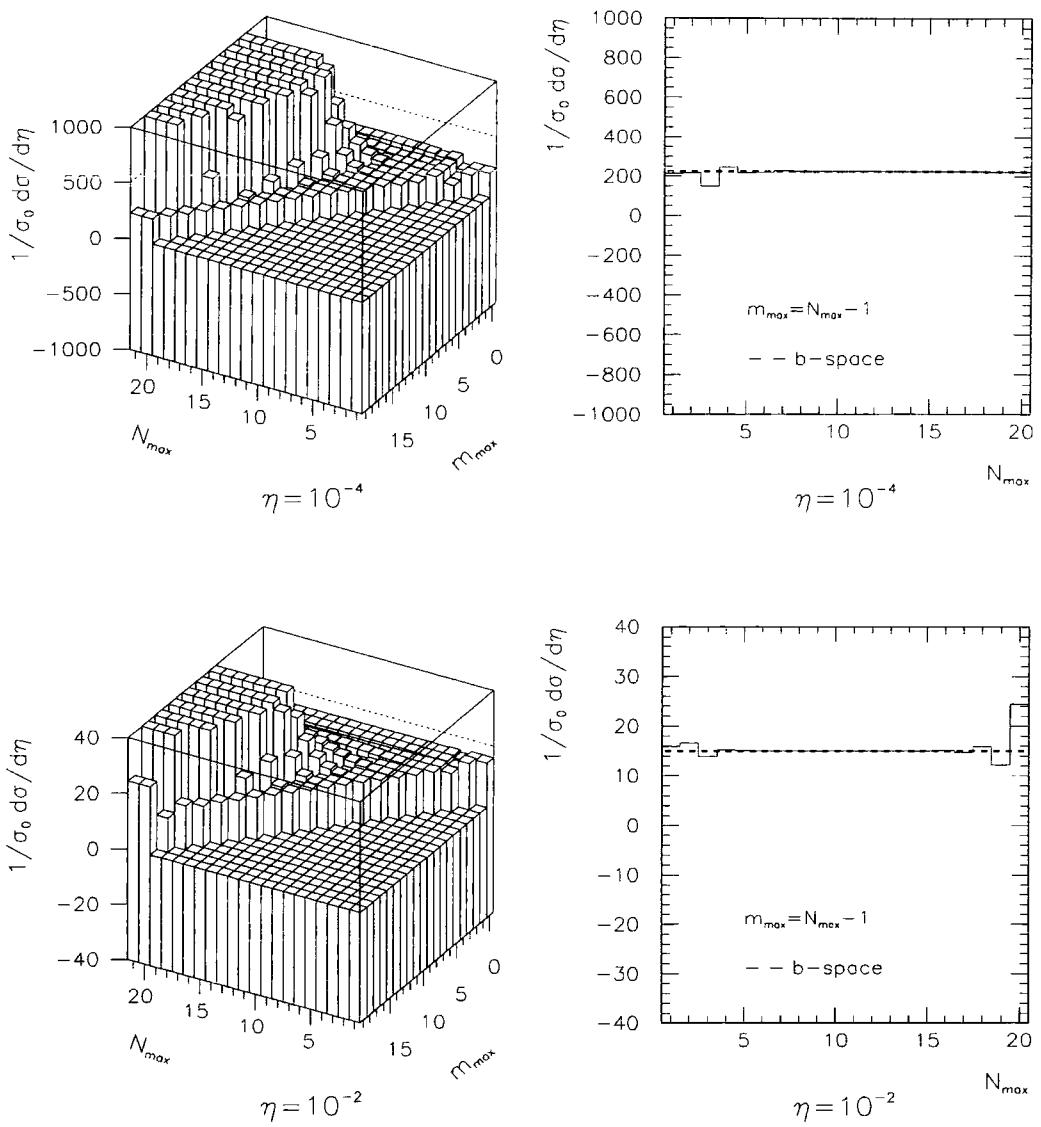

Figure 3.10: The cumulative plot of (3.1.10) for $\eta = 10^{-4}, 10^{-2}$ and its section through the line $m_{\max} = N_{\max} - 1$.

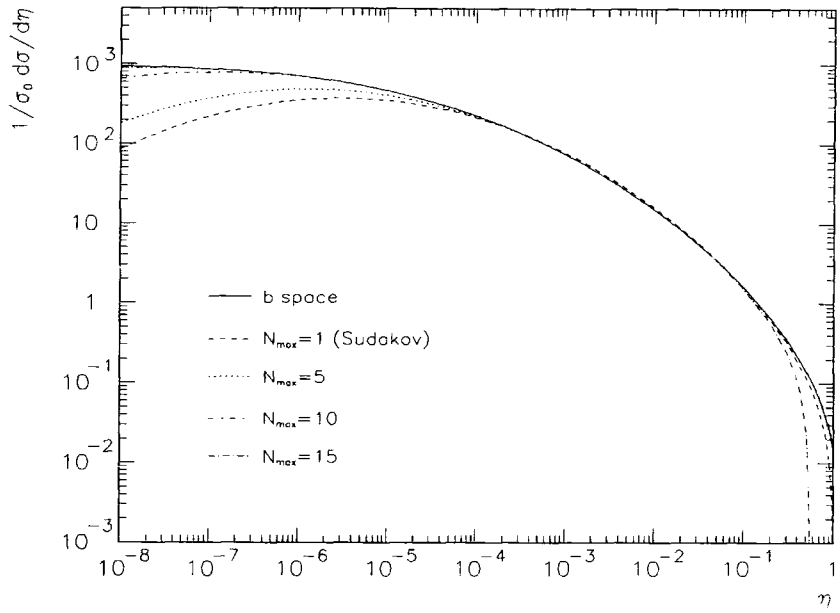

Figure 3.11: The b space result (parton level, fixed coupling, only $A^{(1)}$) compared to the expression (3.1.10), calculated for various values of $N_{\max}$. This plot corresponds to the $m_{\max} = N_{\max} - 1$ section in 3.10 for selected $N_{\max}$ and various η.

never take $N_{\max}$ so large as to make this effect substantial. Nevertheless, it emphasises the necessity of performing a careful matching with the fixed-order perturbative result.

Let us now return to the relation between the DLLA cross section and the expression resumming sub-leading logarithmic corrections (3.1.10). We have already noticed that if the double sum in (3.1.10) is reduced to a single sum of terms with $m = 0$ then the DLLA formula is recovered. This obviously corresponds to setting all τ_m coefficients (except τ_0) to zero. Since in this calculation only $A^{(1)}$ is kept nonzero and the coupling is fixed, there are no sources of sub-leading logarithms in (3.1.5) (and correspondingly in (3.1.10)) other than those related to kinematics. In other words these sub-leading logarithms are related to conservation of transverse momentum, which is preserved in the original b space expression. The presence of the τ_m coefficients must then correspond to relaxing the strong-ordering condition. This can be checked explicitly by performing the 'exact'

$\mathcal{O}(\alpha_s^2)$ calculation in transverse momentum space, see also (2.3.31):

$$\int d^2k_{T1}d^2k_{T2}\left[\frac{\ln(Q^2/k_{T1}^2)}{k_{T1}^2}\right]_+\left[\frac{\ln(Q^2/k_{T2}^2)}{k_{T2}^2}\right]_+\delta^{(2)}(\vec{k_{T1}}+\vec{k_{T2}}-\vec{p_{\rm T}}) = \frac{\pi}{p_{\rm T}^2}\left(-L^3+4\zeta(3)\right). \qquad (3.2.14)$$

Strong ordering is equivalent to replacing the $\delta-$function by $\delta^{(2)}(\vec{k_{T1}}-\vec{p_{\rm T}})\times\theta(k_{T1}^2-k_{T2}^2)$ $+(1\leftrightarrow 2)$. This gives only the leading L^3 term on the right-hand side. The $\zeta(3)$ term represents the first appearance of the kinematic τ_3 ($\tau_3=-\zeta(3)/2$) coefficient of (3.1.10).

We may therefore conclude that the expression (3.1.10), with the Sudakov factor resummed and factored out, enables us to resum an infinite series of logarithms while at the same time allowing for the inclusion of kinematic sub-leading logarithms. By explicitly including τ_m coefficients in $p_{\rm T}$ space we are able to take transverse momentum conservation into account. Moreover, Eq. 3.1.10 has very good convergence properties over a large range of η, even while summing the sub-leading logarithmic terms. The b space result can be adequately (for phenomenological purposes) approximated by retaining sufficiently many terms, see Fig. 3.11. The expression (3.1.10) is thus well suited for the purposes of this analysis, i.e. reproducing the b space result by explicit resummation in $p_{\rm T}$ space, and we will continue to use this expression for the rest of this study.

3.2.2 Running coupling analysis

The ultimate goal of the work presented here is to obtain a more accurate description, if possible, of the W production distribution. To this end, one has to incorporate various other sub-leading effects in addition to the kinematic logarithms discussed in the previous subsection. One example is the incorporation of the running of the strong coupling α_s into the cross section expression. This is achieved by substituting Eq. (1.3.32) in (3.1.10).[2] The effect on the DLLA form factor is to introduce a sequence of sub-leading logarithms whose coefficients depend on the $\beta-$function coefficients. If only the 1-loop running of α_s

[2]In fact, for the purpose of this calculation we extracted the factors $(1/\pi)$, $(1/\pi^2)$ from the β_0, β_1 coefficients in the expansion (1.3.32), so that from now on $\beta_0=\pi\beta_0$(1.3.26) and $\beta_1=\pi^2\beta_1$(1.3.26).

is introduced then the cross section expression (3.1.10) reads

$$\begin{aligned}\frac{1}{\sigma_0}\frac{d\sigma}{d\eta} &= \frac{\alpha_s(\mu^2)A^{(1)}}{2\pi\eta}e^{-\frac{\alpha_s(\mu^2)A^{(1)}}{4\pi}L^2\left[1+\frac{1}{3\pi}\beta_0\alpha_s(\mu^2)\left(2L-3L_\mu\right)\right]} \\ &\times\sum_{N=1}^{\infty}\left(-\frac{\alpha_s(\mu^2)A^{(1)}}{\pi}\right)^{N-1}\frac{1}{(N-1)!}\sum_{m=0}^{N-1}\left(\begin{array}{c}N-1\\ m\end{array}\right)\sum_{k=0}^{N-m-1}\left(\begin{array}{c}N-m-1\\ k\end{array}\right) \\ &c_2^m c_3^k c_1^{N-m-k-1}\times\left[3c_3\tau_{N+m+2k+1}+2c_2\tau_{N+m+2k}+c_1\tau_{N+m+2k-1}\right], \qquad (3.2.15)\end{aligned}$$

with

$$\begin{aligned}c_3 &= \frac{4}{3\pi}\beta_0\alpha_s(\mu^2)\,, \\ c_2 &= \frac{1}{\pi}\left[\pi+\beta_0\alpha_s(\mu^2)\left(2L-L_\mu\right)\right]\,, \\ c_1 &= \frac{1}{\pi}\ln\left(\frac{1}{\eta}\right)\left[\pi+\beta_0\alpha_s(\mu^2)\left(L-L_\mu\right)\right]\,, \qquad (3.2.16)\end{aligned}$$

and $L_\mu \equiv \ln(Q^2/\mu^2)$. Notice the appearance in (3.2.15) of sub-leading $\mathcal{O}\left(\alpha_s^2 L^3\right)$ terms in the exponent of the Sudakov form factor. Interestingly, these logarithms can be eliminated by a particular scale choice: $\mu^2 = Q^2\,\eta^{2/3}$. This restores the same form as in (3.1.10) i.e. $\exp\left(-\frac{\alpha_s A^{(1)}}{\pi}L^2\right)$, but now with a coupling which also depends on η.[3] However not all β_0–dependent logarithms are eliminated. For example, we can see from (3.2.16) that corrections of order $\beta_0\alpha_s L$ remain. Of course in a complete calculation the dependence on the scale choice should disappear. To illustrate the residual dependence on the scale of the cross section (3.2.15) we show (Fig. 3.12) results for two different choices: $\mu^2 = \eta\,Q^2 = p_{\rm T}^2$ and $\mu^2 = Q^2\,\eta^{2/3} = Q^{2/3}p_{\rm T}^{4/3}$. Also shown is the effect of truncating the sum in (3.2.15) at first, second and third order.[4]

We see that with $\mu^2 = Q^{2/3}\,p_{\rm T}^{4/3}$ there is slightly less stability with respect to the truncation point than there is with the choice $\mu^2 = p_{\rm T}^2$. Note also that now the plots of $(1/\sigma_0)(d\sigma/d\eta)$ are no longer explicitly independent of Q, as was the case when α_s was taken to be constant. The additional dependence on Q enters into (3.2.15) via the

[3]There is an analogous $y_{\rm cut}$–dependent scale choice for resummed jet cross sections in e^+e^- annihilation, see for example [59].

[4]Obviously, now we truncate the sum in (3.2.15) at a certain order of $\alpha_s(\mu^2)$, so that 'N' in Fig. 3.8 should be read as 'power of α_s'.

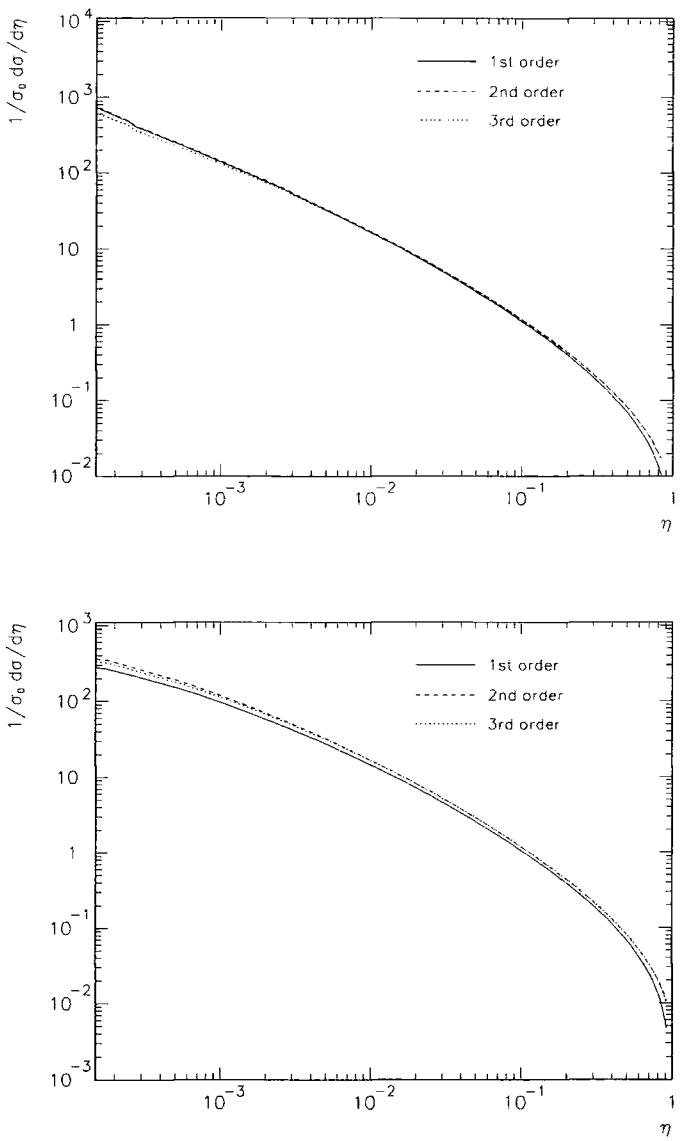

Figure 3.12: Comparison between the resummed (3.2.15) using two different choices of renormalization scale: $\mu^2 = p_{\rm T}^2$ (top figure) and $\mu^2 = Q^{2/3} p_{\rm T}^{4/3}$ (bottom figure), and the first three orders in $\alpha_s(\mu^2)$ in (3.2.15) (i.e. the orders in $\alpha_s(\mu^2)$ at which the residual sum is truncated). Here $Q = M_Z = 91.187$ GeV, $\alpha_s(M_Z^2) = 0.113$.

coupling $\alpha_s(\mu^2) = \alpha_s(Q^{2/3}p_{\rm T}^{4/3})$. For values of $p_{\rm T}$ where perturbative QCD can safely be applied (e.g. $p_{\rm T} \geq 3$ GeV) and the energies considered here, the resulting scale μ is bigger than the b quark mass, and we therefore avoid evolving the coupling through any quark mass thresholds.

An extension of this analysis for the case of the two-loop running coupling is straightforward and gives

$$\begin{aligned}
\tfrac{1}{\sigma_0}\tfrac{d\sigma}{d\eta} &= \frac{\alpha_s(\mu^2)A^{(1)}}{2\pi\eta} e^{\mathcal{S}_\eta} \sum_{N=1}^{\infty} \left(-\frac{\alpha_s(\mu^2)A^{(1)}}{\pi} \right)^{N-1} \frac{1}{(N-1)!} \sum_{m=0}^{N-1} \binom{N-1}{m} \\
&\times \sum_{k=0}^{N-m-1} \binom{N-m-1}{k} \sum_{l=0}^{N-m-k-1} \binom{N-m-k-1}{l} c_2^m c_3^k c_4^l c_1^{N-m-k-l-1} \\
&\times \Big[4c_4 \tau_{N+m+2k+3l+2} + 3c_3 \tau_{N+m+2k+3l+1} + 2c_2 \tau_{N+m+2k+3l} \\
&+ c_1 \tau_{N+m+2k+3l-1} \Big] .
\end{aligned} \tag{3.2.17}$$

Here

$$\begin{aligned}
\mathcal{S}_\eta &= -\frac{\alpha_s(\mu^2)A^{(1)}}{4\pi} L^2 \Big[1 + \frac{1}{3\pi} \Big(\beta_0 \alpha_s(\mu^2) + \frac{1}{\pi} \beta_1 \alpha_s^2(\mu^2) \Big) (2L - 3L_\mu) \\
&+ \frac{1}{6\pi^2} \alpha_s^2(\mu^2) \beta_0^2 \left(3L^2 - 8LL_\mu + 6L_\mu^2 \right) \Big] , \\
c_4 &= \frac{2}{\pi^2} \alpha_s^2(\mu^2) \beta_0^2 , \\
c_3 &= \frac{4}{3\pi^2} \Big[\beta_0 \alpha_s(\mu^2)\pi + \beta_1 \alpha_s^2(\mu^2) + \beta_0^2 \alpha_s^2(\mu^2) (3L - 2L_\mu) \Big] , \\
c_2 &= \frac{1}{\pi^2} \Big[\pi^2 + \Big(\beta_0 \alpha_s(\mu^2)\pi + \beta_1 \alpha_s^2(\mu^2) \Big) (2L - L_\mu) \\
&+ \beta_0^2 \alpha_s^2(\mu^2) \left(3L^2 - 4LL_\mu + L_\mu^2 \right) \Big] , \\
c_1 &= \frac{1}{\pi^2} L \Big[\pi^2 + \Big(\beta_0 \alpha_s(\mu^2)\pi + \beta_1 \alpha_s^2(\mu^2) \Big) (L - L_\mu) \\
&+ \beta_0^2 \alpha_s^2(\mu^2) \left(L^2 - 2LL_\mu + L_\mu^2 \right) \Big] .
\end{aligned}$$

Now, after fixing the choice of scale as described above, a new term proportional to $\beta_0^2 \alpha_s^3(\mu^2) L^4$ appears in the exponential. As a result, the line of points corresponding to terms of the form $\alpha_s^N L^{2N-1}$ in Figs. 3.8a, 3.8c will now change to the set of points

corresponding to $\alpha_s^{3N} L^{4N}$ or higher powers of L. Unlike the L^3 terms, those with L^4 do *not* cancel when $\mu^2 = Q^{2/3} p_{\rm T}^{4/3}$ is chosen. It is impossible to cancel these terms by *any* choice of the renormalization scale. On the other hand, the choice which eliminates those terms with L^3 is also the one that minimizes the coefficient of the L^4 terms.

3.2.3 Resummation including all types of sub-leading logarithms

A derivation of the expression for the cross section for the case when all known leading and sub-leading coefficients, i.e. $A^{(1)}, B^{(1)}, A^{(2)}, B^{(2)}$, are taken into account follows the method introduced above and gives (fixed coupling to begin with)

$$\begin{aligned} \tfrac{1}{\sigma_0}\tfrac{d\sigma}{d\eta} &= \frac{\alpha_s A^{(1)}}{2\pi\eta} e^{\mathcal{S}_\eta} \sum_{N=1}^{\infty} \left(-\frac{\alpha_s A^{(1)}}{\pi} \right)^{N-1} \frac{1}{(N-1)!} \sum_{m=0}^{N-1} \binom{N-1}{m} \\ &\quad \times c_2^m c_1^{N-m-1} \Big[2c_2 \tau_{N+m} + c_1 \tau_{N+m-1} \Big] , \end{aligned} \tag{3.2.18}$$

with

$$\begin{aligned} \mathcal{S}_\eta &= -\frac{\alpha_s A^{(1)}}{4\pi} \Big[L^2 \Big(1 + \frac{\alpha_s}{2\pi} \frac{A^{(2)}}{A^{(1)}} \Big) + L \Big(2\frac{B^{(1)}}{A^{(1)}} + \frac{\alpha_s}{\pi} \frac{B^{(2)}}{A^{(1)}} \Big) \Big] , \\ c_1 &= \Big(1 + \frac{\alpha_s}{2\pi} \frac{A^{(2)}}{A^{(1)}} \Big) L + \frac{B^{(1)}}{A^{(1)}} + \frac{\alpha_s}{2\pi} \frac{B^{(2)}}{A^{(1)}} , \\ c_2 &= 1 + \frac{\alpha_s}{2\pi} \frac{A^{(2)}}{A^{(1)}} . \end{aligned}$$

Now each logarithmic term in the sum (3.2.18) acquires a factor which is a combination of the As, Bs and τ's. Notice that although the various sub-leading logarithms are mixed together, they have a distinctive origin. We have mentioned already that the DLLA (i.e. retaining only terms of the form $A^{(1)} \alpha_s^N L^{2N-1}$) corresponds to the situation where all gluons are soft and collinear and where strong ordering of the transverse momenta and energies is imposed. We also know that other terms with $A^{(1)}$ multiplied by the τ_m arise from using the soft and collinear approximation for the matrix element but relaxing the strong-ordering condition. The sub-leading terms with $B^{(1)}$ etc. correspond to the situation where at least one gluon is collinear but energetic [39], cf. Section 2.3.

6	0	0	0
5	0	0	$\frac{1}{8}A^{(1)^3}$
4	0	0	$\frac{5}{8}A^{(1)^2}B^{(1)}$
3	0	$-\frac{1}{2}A^{(1)^2}$	$A^{(1)}B^{(1)^2} - A^{(1)}A^{(2)}$
2	0	$-\frac{3}{2}A^{(1)}B^{(1)}$	$-\frac{3}{2}B^{(1)}A^{(2)} + 10A^{(1)^3}\tau_3 + \frac{1}{2}B^{(1)^3} - \frac{3}{2}A^{(1)}B^{(2)}$
1	$A^{(1)}$	$A^{(2)} - B^{(1)^2}$	$-2B^{(1)}B^{(2)} + 20A^{(1)^2}B^{(1)}\tau_3$
0	$B^{(1)}$	$-4A^{(1)^2}\tau_3 + B^{(2)}$	$4A^{(1)^3}\tau_5 - 8A^{(1)}A^{(2)}\tau_3 + 8A^{(1)}B^{(1)^2}\tau_3$
	1	2	3

Table 3.2: Coefficients of the logarithmic terms in (3.2.18), with the Sudakov factor expanded, for the first three orders in $\bar{\alpha}_s$. The rows correspond to powers of $\bar{\alpha}_s$, the columns to powers of L.

In addition, extracting a Sudakov form factor from the sum (3.2.18) 'squeezes' it down to a summation over m from 0 to $N-1$, thereby reducing the number of fully known 'towers' of logarithms (in the residual sum): from the first four to the first two. This can be appreciated by comparing the logarithmic coefficients appearing in the expansion of the cross section up to and including the first three orders in α_s with (Table 3.3) and without (Table 3.2) the Sudakov form factor extracted.

These tables also reveal another relevant property: sub-leading coefficients like $A^{(2)}$ are associated with τ factors whose indices are not as high as those which accompany $A^{(1)}$. Both L terms and τ factors originate from the same $\ln(Q^2b^2/b_0^2)$ terms appearing

3	0	0	0
2	0	0	$8A^{(1)^3}\tau_3$
1	$A^{(1)}$	$A^{(2)}$	$16A^{(1)^2}B^{(1)}\tau_3$
0	$B^{(1)}$	$-4A^{(1)^2}\tau_3 + B^{(2)}$	$4A^{(1)^3}\tau_5 - 8A^{(1)}A^{(2)}\tau_3 + 8A^{(1)}B^{(1)^2}\tau_3$
	1	2	3

Table 3.3: Coefficients of logarithmic terms in the residual sum in (3.2.18) for the first three orders in $\bar{\alpha}_s$. The rows correspond to powers of $\bar{\alpha}_s$, the columns to powers of L. Because $\tau_1 = \tau_2 = \tau_4 = 0$, the coefficients of $\bar{\alpha}_s{}^2L^2$ and $\bar{\alpha}_s{}^3L^3$ are zero, and for higher orders the biggest power of L is equal to the order in $\bar{\alpha}_s$.

at the very early stage of the derivation. In particular, let us focus on a term with a particular power of α_s and L. To reproduce such a term one has to take $\ln(Q^2b^2/b_0^2)$ up to the appropriate power, depending on its associated coefficient (i.e. A or B). For sub-leading coefficients this power will be obviously lower than for more leading ones. Hence the indices of the corresponding τ factors are lower for more sub-leading coefficients. For example, the index of τ accompanying the first sub-leading unknown coefficient $A^{(3)}$ would be at least four less than the index of a corresponding τ for the $A^{(1)}$ coefficient, for given powers of α_s and L. This observation provides us with a strong argument for justifying the inclusion of known *parts* of logarithmic terms from sub-leading towers lower than NNNLL. Physically, the τ factors are of kinematic origin and as such they are much more relevant to the cross section than perturbative lower order coefficients in the expansion of $A(\alpha_s(\mu^2))$ and $B(\alpha_s(\mu^2))$. While, as we have shown earlier, resummation of the terms containing τ factors with higher indices can still be of numerical importance for the final result, especially for small values of η, terms with unknown higher-order perturbative

coefficients seem to contribute corrections of much smaller size.

A comparison of effects induced by the inclusion of successive sub-leading coefficients in (3.2.18) is demonstrated in Fig. 3.13. Also shown are the results of an exact integration in b space. The agreement for low values of η is excellent. At high η we encounter a discrepancy of the same nature as that discussed for the case of the leading coefficient $A^{(1)}$, i.e. for large $N_{\max}$ the expression (3.2.18) either grows significantly or acquires negative values, depending on the number of terms at which the expression is truncated. For the values of $N_{\max}$ we use in our calculations this behaviour does not occur.[5]

With the above prescriptions for the sub-leading logarithmic terms, kinematic effects and running coupling, we finally obtain a 'complete' expression for the cross section:

$$\begin{aligned}
\frac{1}{\sigma_0}\frac{d\sigma}{d\eta} &= \frac{\alpha_s(\mu^2)A^{(1)}}{2\eta\pi} e^{\mathcal{S}_\eta} \sum_{N=1}^{\infty} \left(\frac{-\alpha_s(\mu^2)A^{(1)}}{\pi}\right)^{N-1} \frac{1}{(N-1)!} \sum_{m=0}^{N-1} \binom{N-1}{m} \\
&\times \sum_{k=0}^{N-m-1} \binom{N-m-1}{k} \sum_{l=0}^{N-m-k-1} \binom{N-m-k-1}{l} \\
&\times \sum_{j=0}^{N-m-k-l-1} \binom{N-m-k-l-1}{j} \sum_{i=0}^{N-m-k-l-j-1} \binom{N-m-k-l-j-1}{i} \\
&\times c_2^m c_3^k c_4^l c_5^j c_6^i c_1^{N-m-k-l-j-i-1} \sum_{n=1}^{6} n c_n \tau_{N+m+2k+3l+4j+5i+n-2} \,. \qquad (3.2.19)
\end{aligned}$$

The expressions for $\mathcal{S}_\eta$ and the c_i are now of course much more complicated. Explicit expressions up to fifth order in the coupling constant $\alpha_s(\mu^2)$ are presented in the Appendix A. The fifth order appears here as a consequence of using the two-loop expansion of the running coupling and including the first two terms in the expansion of $A(\alpha_s)$, $B(\alpha_s)$, cf. (3.1.3). The contributions resummed in (3.2.19) and in the b space expression (2.4.61) are schematically illustrated in Fig. 3.14.

Numerical results based on the complete expression are displayed in Figs. 3.15 and 3.16, for the scale choice $\mu^2 = Q^{2/3}p_{\mathrm{T}}^{4/3}$. First, Fig. 3.15 gives the cross section with all four A_i, B_i coefficients included, together with the first three orders in $\alpha_s(\mu^2)$ in the entire sum

[5]This is also true for the case of the running coupling.

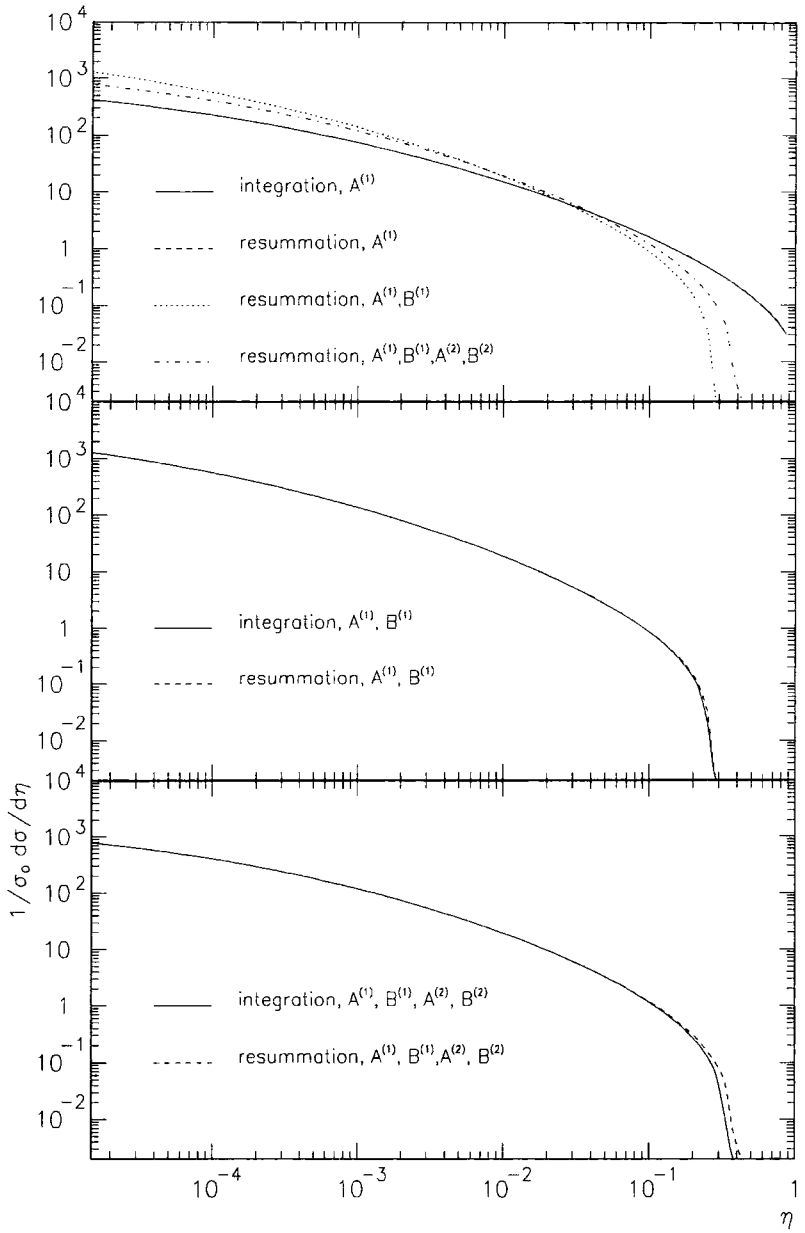

Figure 3.13: The resummed cross section (3.2.18), truncated at $N_{\max} = 10$, compared to the results of integration. Top figure: only $A^{(1)}$ coefficient non-zero, middle figure: $A^{(1)}, B^{(1)}$ non-zero, bottom figure: $A^{(1)}, B^{(1)}, A^{(2)}, B^{(2)}$ non-zero. The top figure also shows a comparison of the effects induced when subsequent coefficients are introduced.

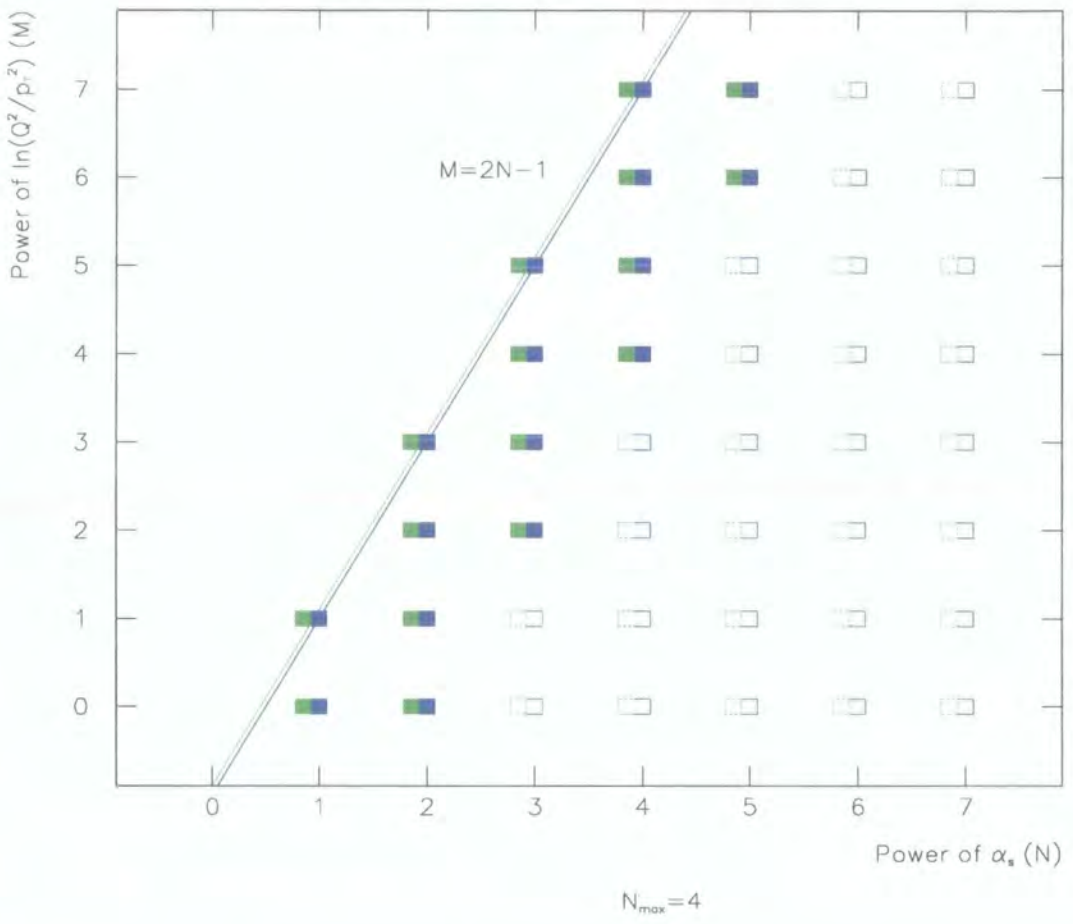

Figure 3.14: Schematic representation of contributions to b space method (2.4.61) (green) and to expression (3.2.19) (blue) for $N_{\max} = 4$. An empty box of a certain colour means that there exist other contributions in the perturbative series with the same power of α_s and L which are not included in an expression coded with that colour. A full box means all contributions are taken into account.

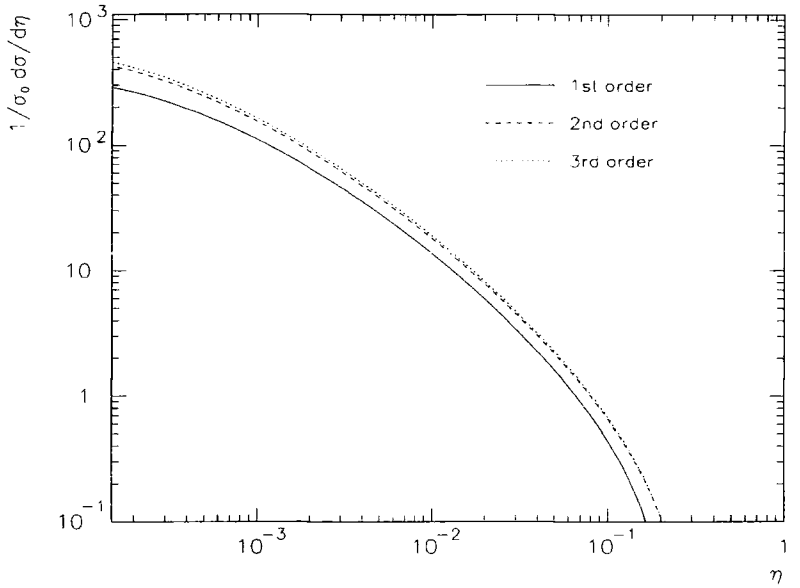

Figure 3.15: Resummation of (3.2.19) for the first three orders in $\alpha_s(\mu^2)$ in the residual sum. Here $\mu^2 = Q^{2/3}p_{\mathrm{T}}^{4/3}$, $Q = M_Z = 91.187$ GeV, $\alpha_s(M_Z^2) = 0.113$.

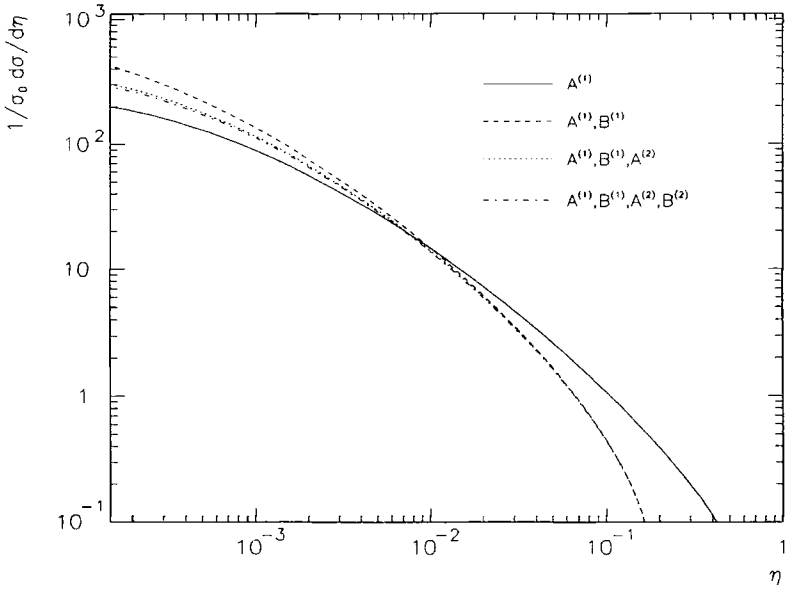

Figure 3.16: Resummation of (3.2.19) for different subsets of nonzero coefficients, with only $\mathcal{O}(\alpha_s(\mu^2))$ terms in the residual sum considered. Here $\mu^2 = Q^{2/3}p_{\mathrm{T}}^{4/3}$, $Q = M_Z = 91.187$ GeV, $\alpha_s(M_Z^2) = 0.113$.

over N in (3.2.19). Notice the rapid convergence when the higher-orders are included. Fig. 3.16 shows how the first-order cross section is influenced by the various A_i, B_i coefficients. Note how the relative impact on the leading-order A_1 result is essentially $B_1 > A_2 > B_2$, as might be expected. The effect of including B_2 is numerically small, indicating a reasonable degree of convergence from the higher-order coefficients.

Formally our expression allows the inclusion of *any* number of sub-leading kinematic logarithms, defined by the cut-off value $N_{\max}$, which determines the number of fully resummed towers of logarithms.[6] In reality, however, due to the lack of knowledge of $A^{(3)}$, $B^{(3)}$, etc. it is only possible to obtain a result where no more than the first four towers of logarithms are fully resummed. Fig. 3.17 shows the effect of including 3, 5, 6, 7 and 8 towers, normalised to the 4th-tower result, for the scale choice $\mu^2 = Q^{2/3}p_{\mathrm{T}}^{4/3}$. The

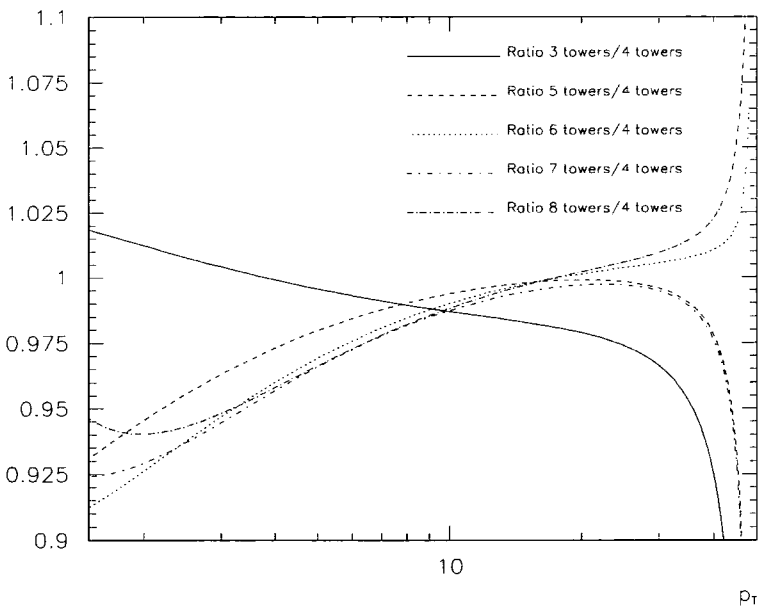

Figure 3.17: Ratio of the results for 3,5,6,7,8 towers of logarithms, normalised to the 4-th tower result, for $\mu^2 = Q^{2/3}p_{\mathrm{T}}^{4/3}$, $Q = M_Z = 91.187$ GeV, $\alpha_s(M_Z^2) = 0.113$.

[6]The numerical programme, used to obtain all results presented here, takes into account only $\mathcal{O}(\alpha_s^{N_{\max}})$ or lower order terms in the sum in (3.2.19). This forces the number of fully resummed towers to be $N_{\max}$.

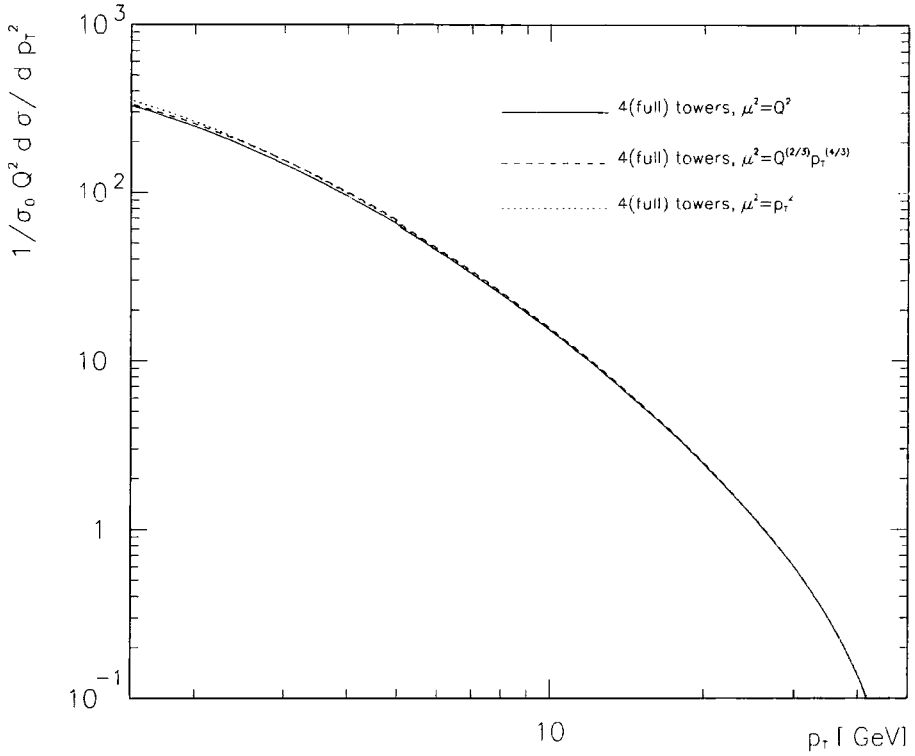

Figure 3.18: Dependence of the resummed result for the first four towers of logarithms in (3.2.19) on the renormalization scale μ.

figure clearly shows the numerical importance of the kinematic logarithms of the higher towers, and also the stability over a broad range of relevant p_T as more towers are included. However, this difference is of approximately the same magnitude as the one observed on changing the renormalization scale. In particular, for the first four towers of logarithms, changing the scale from our default $\mu^2 = Q^{2/3}p_T^{4/3}$ to the (lower) scale $\mu^2 = p_T^2$ and the (higher) scale $\mu^2 = Q^2$ alters the p_T distribution by less than $\pm 3\%$ over the considered low-p_T range, cf. Fig. 3.18.

3.3 Summary

In this chapter we have developed the p_{T} space approach for resumming logarithmic corrections to the transverse momentum distribution in the Drell-Yan process. The formalism is well behaved provided $\alpha_s L \lesssim 1$. We have carefully studied the effect of various sub-leading contributions: higher-order perturbative coefficients, the running coupling, and kinematic logarithms. We have confirmed that the kinematic logarithms are particularly important at small p_{T}, where they serve to cancel the suppressing effect of the Sudakov form factor.

Our technique enables us to resum the first four logarithmic towers *including* the NNNLL series, together with the first few sub-leading kinematic logarithms. The convergence of our expansion is certainly adequate for phenomenological applications. We note that a drawback of this method is the inability to select particular towers to be fully resummed.

Here we have concentrated only on the perturbative contributions to the parton level cross section. Non-perturbative effects ('q_{T}'-smearing), as well as parton distribution functions, must be taken into account before assessing the impact of the sub-leading logarithmic contributions on the physical cross section. We will address these issues in forthcoming chapters.

Chapter 4

Methods of transverse momentum space resummation

Although the resummation of the soft gluon contributions is achieved most naturally in impact parameter space, there are certain advantages in performing the resummation directly in transverse momentum space. In Chapter 3 we demonstrated the potential of the $p_{\rm T}$ space resummation while deriving and discussing our formalism. The resummation of large logarithms directly in $p_{\rm T}$ space received much attention, starting from the early work of Ellis, Fleishon and Stirling [27]. More recently, Ellis and Veseli revisited the idea of the $p_{\rm T}$ space resummation and proposed their own (EV) formalism [57]. Almost concurrently, Frixione, Nason and Ridolfi were working on a different approach (FNR) to the $p_{\rm T}$ space resummation [58]. Our technique, which from now on we will refer to as the KS technique, has roots in the Ellis *et al.* work.

In this chapter we will examine theoretical differences between various approaches and study them numerically. All approaches originate from the general expression in impact parameter space for the Drell-Yan process (2.4.52). In order to highlight the differences we shall examine the resummation methods in their most simplified version, i.e. we will restrict ourselves to the parton level cross section and ignore certain sub-leading corrections, as described below.

4.1 EV formalism

4.1.1 Theoretical properties

For the full derivation of the EV formalism the reader is referred to [57]. The EV formula for the Drell-Yan subprocess cross section reads[1]

$$\frac{1}{\sigma_0}\frac{d\sigma}{dp_{\rm T}^2} = \frac{d}{dp_{\rm T}^2}\exp[\mathcal{T}(p_{\rm T},Q)]\,, \tag{4.1.1}$$

where

$$\mathcal{T}(p_{\rm T},Q) = -\int_{p_{\rm T}^2}^{Q^2}\frac{d\bar{\mu}^2}{\bar{\mu}^2}\left[\tilde{A}(\bar{\alpha}_s(\bar{\mu})\ln\frac{Q^2}{\bar{\mu}^2}+\tilde{B}(\bar{\alpha}_s(\bar{\mu}))\right], \tag{4.1.2}$$

$$\tilde{A}(\bar{\alpha}_s(\bar{\mu})) = \sum_{i=1}^{\infty}\bar{\alpha}_s{}^i\tilde{A}^{(i)}\,, \qquad \tilde{B}(\bar{\alpha}_s(\bar{\mu})) = \sum_{i=1}^{\infty}\bar{\alpha}_s{}^i\tilde{B}^{(i)}\,, \tag{4.1.3}$$

and

$$\begin{aligned}
\tilde{A}^{(1)} &= A^{(1)}\,,\\
\tilde{B}^{(1)} &= B^{(1)}\,,\\
\tilde{A}^{(2)} &= A^{(2)}\,,\\
\tilde{B}^{(2)} &= B^{(2)}+2(A^{(1)})^2\zeta(3)\,.
\end{aligned} \tag{4.1.4}$$

It is clear that the EV method succeeds in developing a fully resummed expression. Contrary to the KS expression, there is no explicit sum but instead a resummed Sudakov form factor of a specific form. In order to derive this (4.1.1) analytic approximation of the b space method one uses an approximation

$$\int_0^{\infty}dx J_1(x)\ln^m\left(\frac{x}{b_0}\right)\approx 0 \qquad\qquad \text{for } m\geq 3\,.$$

This means that all the τ_m coefficients, except τ_0, in the KS formula (3.2.19) are now set to zero. As we have seen in Chapter 3, the presence of the τ_m coefficients is always related to kinematic logarithms, which in turn appear if the transverse momentum is conserved. Therefore the EV technique does not provide a proper treatment of kinematic effects.

[1] Again, we take the zero-th moment of the hadron level expression, in the way described in Chapter 3.

The correspondence between the EV and the KS method can be easily illustrated if one takes a fixed α_s and sets all coefficients $\tilde{A}^{(i)}$, $\tilde{B}^{(i)}$ to be zero, except $\tilde{A}^{(1)}$. Then it follows from (4.1.1) that

$$\frac{1}{\sigma_0}\frac{d\sigma}{d\eta} = \frac{A^{(1)}\bar{\alpha}_s}{\eta} L \exp\left[-\frac{1}{2}A^{(1)}\bar{\alpha}_s L^2\right] = \frac{1}{\eta}\sum_{N=1}^{\infty}\frac{\lambda^N}{(N-1)!}\left(-\frac{1}{2}\right)^{N-1} L^{2N-1}, \qquad (4.1.5)$$

which is exactly the KS expression (3.1.7) taken for $m = 0$. Here $L = \ln(p_{\mathrm{T}}^2/Q^2) = \ln(1/\eta)$. More precisely, in this limit Eq. (4.1.5) corresponds to the DLLA approximation (2.3.35).

The non-trivial τ_m coefficients first appear in the fourth tower of logarithms. Therefore the EV formalism fully resums only the first three towers and does not include known contributions from sub-leading NNNLL series of (kinematic) logarithms. This is partially compensated by a redefinition $B^{(2)} \to \tilde{B}^{(2)} = B^{(2)} + 2(A^{(1)})^2\zeta(3)$ which, although correctly accounting for a $\alpha_s^2 L^0$ term in the NNNLL tower, as can be seen from (3.2.14) and (2.3.31), distorts other terms in this series, cf. Table 3.2. Furthermore, it also distorts terms from more sub-leading towers wherever the $B^{(2)}$ coefficient appears. With the help of the KS method, one can obtain the first four series *fully* resummed. Nevertheless, it should be remembered that generally both approaches do not give 'pure' results, i.e. when other than kinematic sub-leading effects are taken into account (running coupling, matrix element) then the additional terms, coming from more sub-leading towers than NNLL or NNNLL, will also be resummed. The contributions resummed in both approaches are schematically presented in Fig. 4.1.

4.1.2 Numerical comparison

We begin our investigations by comparing the two methods in the limit of a fixed coupling and only one non-zero coefficient $A^{(1)}$. With these assumptions the EV expression is equivalent to the DLLA, and as we have already discussed in Chapter 3, the kinematic logarithms included in the KS formula serve to cancel the suppressing effect of the DLLA Sudakov factor, leading to a better approximation of the b space result, cf. Fig. 4.2.

In a more complicated case, when other sub-leading contributions are also resummed,

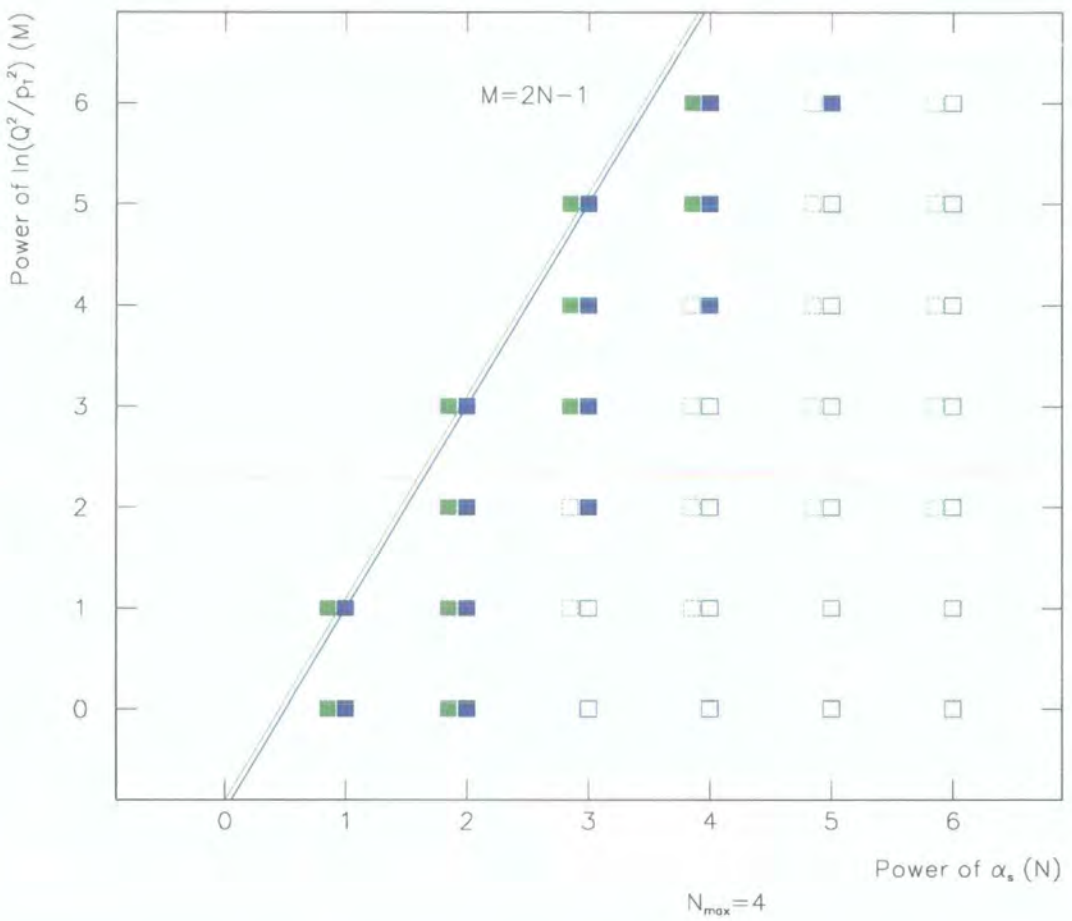

Figure 4.1: Schematic representation of contributions to (4.1.1) (green) and (3.2.19) (blue). An empty box of a certain colour means that there exist other contributions in the perturbative series with the same power of α_s and L which are not included in an expression coded with that colour. A full box means all contributions are taken into account.

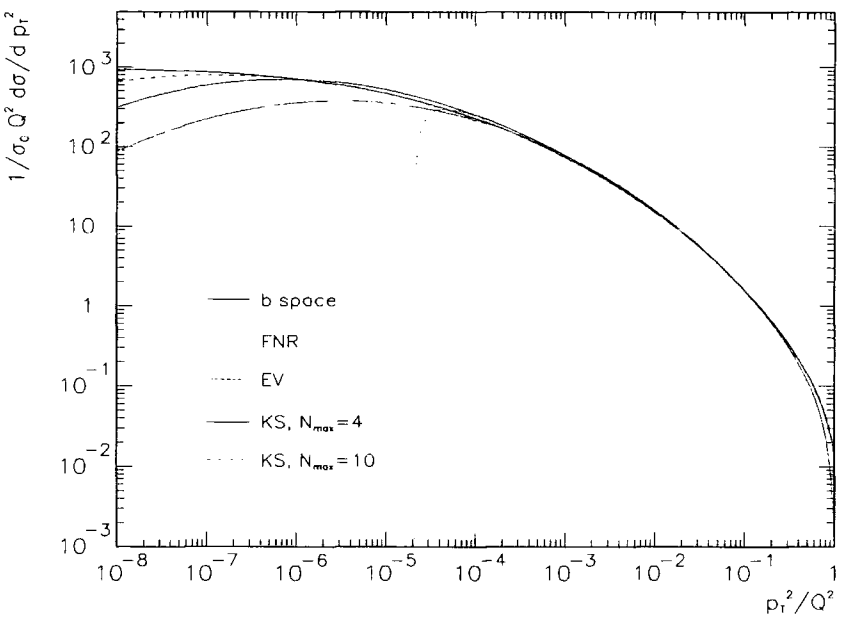

Figure 4.2: Comparison between various p_{T} space resummation approaches and the b space method. Here $\alpha_s = 0.2$, $A^{(1)} \neq 0$ only.

the effect introduced by the redefinition of $B^{(2)}$ in (4.1.1) seems to be comparable with that caused by summing additional, more than NNLL sub-leading terms when only $\mathcal{O}(\alpha_s^3)$ contributions are taken into account in (3.2.19), cf. Fig 4.3. Fig 4.3 shows also the comparison between the KS result (3.2.19) with the fourth tower resummed and the EV result (4.1.1). Numerically we encounter an increase in the cross section of approximately 3% for all values of p_{T}, when the scale equals $\mu = Q$.

4.2 FNR formalism

4.2.1 Theoretical properties

The complete FNR formalism for the Drell-Yan cross section can be found in [58]. Again, it is easier to discuss the properties of this approach, and the differences with respect to

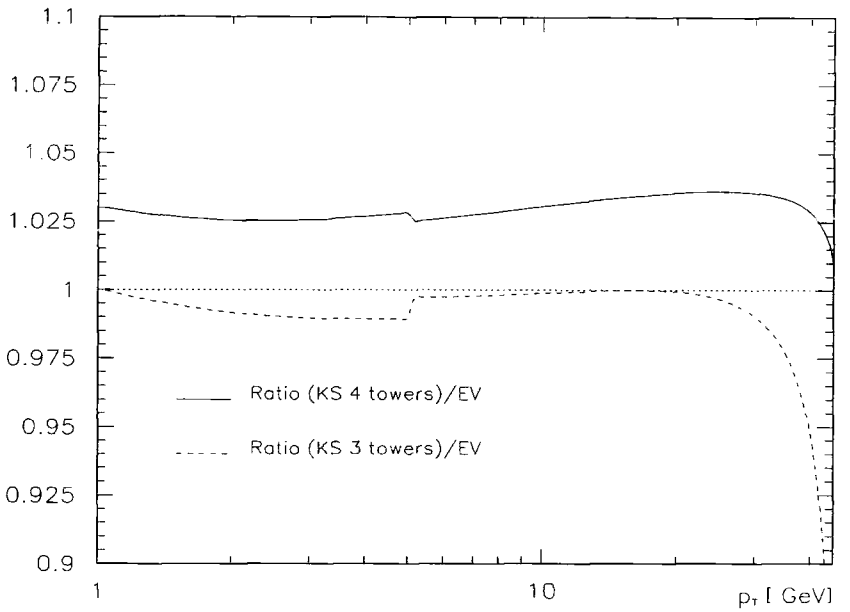

Figure 4.3: Resummation of the L, NL, NNL and NNNL towers of logarithms (solid line) and resummation of the L, NL, NNL towers (dashed line) according to (3.2.19) versus EV result (4.1.1). Here $\mu^2 = p_{\rm T}^2$, $\alpha_S(M_Z^2) = 0.113$. The approximation of the step-like behaviour of N_f results in an artificial 'kink' at $p_{\rm T} = m_b$.

the KS approach (3.2.19) in the approximation of a fixed α_s and only one non-vanishing coefficient $A^{(1)}$. Then the FNR expression has the form

$$\frac{1}{\sigma_0}\frac{1}{dp_{\rm T}^2} = \frac{d}{dp_{\rm T}^2}\left\{\exp\left[-\frac{\bar{\alpha}_s A^{(1)}}{2}L^2\right] 2^{-2\bar{\alpha}_s A^{(1)}L}\frac{\Gamma(1-\bar{\alpha}_s A^{(1)}L)}{\Gamma(1+\bar{\alpha}_s A^{(1)}L)}\right\}. \tag{4.2.6}$$

In a manner similar to the EV approach, the FNR resummation method is characterized by a compact form, avoiding the infinite summation. Using the notation of Chapter 3, Eq. (4.2.6) reads[2]

$$\frac{1}{\sigma_0}\frac{d\sigma}{d\eta} = \frac{d}{d\eta}\left[\exp\left(-\frac{\lambda}{2}L^2\right)\left(\frac{2}{b_0}\right)^{-2\lambda L}\frac{\Gamma(1-\lambda L)}{\Gamma(1+\lambda L)}\right]. \tag{4.2.7}$$

[2]The value of the lower limit of integration in (3.1.2) is b_0^2/b^2. This is different from [58] where the constant C_1 in (2.4.53) is chosen to be $C_1 = 1$. Therefore the expression (4.2.7) differs from the original expression in [58], i.e. Eq. (4.2.6), by a constant.

To derive the FNR expression (4.2.7) one expands the exponent in (3.1.6)

$$\exp\left(-\frac{\lambda}{2}\ln^2\left(\frac{x}{\eta b_0^2}\right)\right) = \exp\left(-\frac{\lambda}{2}\left(L^2 + 2L\,L_b + L_b^2\right)\right), \tag{4.2.8}$$

where $L_b = \ln(x^2/b_0^2)$, and retains only the first two terms (defined as 'NLL' approximation in [58]):

$$\frac{1}{\sigma_0}\frac{d\sigma}{d\eta} = \frac{d}{d\eta}\int_0^\infty dx J_1(x)\exp\left(-\frac{\lambda}{2}L^2 - \lambda L\,L_b\right). \tag{4.2.9}$$

This is a point where the FNR approach departs from its common roots with the KS (EV) technique; the KS technique involves exact integration in (3.1.6). The 'NLL' approximation is applied here in the spirit of (1.6.65), i.e. taking only the functions f_1 and f_2, which ensures the validity of such approximation for $\alpha_s L \lesssim 1$. Note that keeping only the leading $\sim L^2$ term in the exponent (4.2.8) corresponds to the DLLA. A great advantage of the 'NLL approximation' is that the x integral can be performed analytically, leading to (4.2.7). There is in fact a direct link between the KS and FNR approaches. If instead of performing the integration in (4.2.9) one expands the $x-$dependent terms in the exponent and then performs the integration, the result is

$$\frac{1}{\sigma_0}\frac{d\sigma}{d\eta} = \frac{\lambda}{\eta}e^{-\frac{\lambda}{2}L^2}\sum_{N=1}^{\infty}\frac{(-2\lambda)^{(N-1)}}{(N-1)!}L^{N-1}\left[2\tau_N + L\tau_{N-1}\right]. \tag{4.2.10}$$

Clearly this is just the expression (3.1.10) taken at $m = 0$. Indeed the same result can be derived from the resummed expression (4.2.7) by recalling the definition of the generating function (3.1.9) and using the relation

$$\ln\Gamma(1+x) = -\ln(1+x) + x(1-\gamma_E) + \sum_{n=2}^{\infty}(-1)^n[\zeta(n)-1]\frac{x^n}{n}, \quad |x| < 2. \tag{4.2.11}$$

The contributions being resummed in both KS and FNR approaches are illustrated schematically in Fig. 4.4. The terms presented there are the terms emerging in the *full* perturbative expansion, i.e after expanding and multiplying in the Sudakov factor. Note that summing over all logarithmic terms with a given power of α_S must result in the perturbative expansion coefficient of the same order, up to logarithmic accuracy. Of course a formula with an expanded Sudakov factor is valid only when $\alpha_S L^2 \lesssim 1$. The only reason for expanding the Sudakov factor here is to determine which terms in the overall perturbation series are actually being resummed in (3.1.10) and (4.2.7). It is these latter

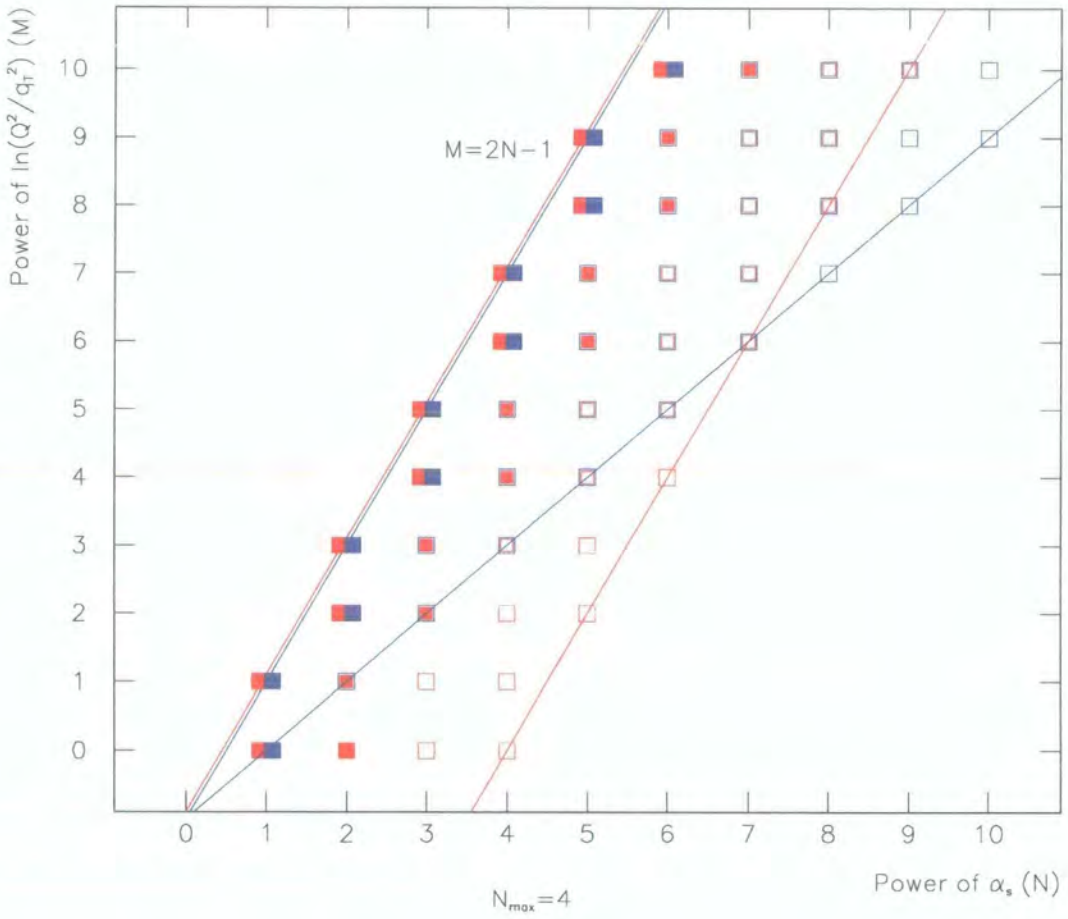

Figure 4.4: Schematic representation of contributions to (4.2.7) (red) and (3.1.10) (blue). An empty box of a certain colour means that there exist other contributions in the perturbative series with the same power of α_s and L which are not included in an expression coded with that colour. A full box means all contributions are taken into account. Here we assume a fixed coupling α_s, only $A^{(1)} \neq 0$ and $N_{\max} = 4$. Note that due to $\tau_1 = \tau_2 = \tau_4 = 0$ all contributions to the 2nd, 3rd and 5th tower are zero in this approximation.

expressions, which can be regarded as the 'master equation' of the two approaches, that we use to obtain numerical results, and both approaches remain well-behaved provided $\alpha_S L \lesssim 1$.

Unfortunately, the range of applicability of the FNR resummed formula (4.2.7) is seriously restricted. As pointed out in [58], the expression (4.2.7) suffers from singularities at $\lambda L = 1, 2, ...$ (In fact these singularities are poles of order two.) Therefore the first pole encountered as η decreases is at $\eta^{\rm crit} = \exp(-1/\lambda)$, i.e. $p_{\rm T}^{\rm crit} = Q \exp(-\pi/2\alpha_S C_F)$. [3]

A natural extension of the approach of [58] would be a resummed analytic expression also including $m = 1$ terms in the classification of (4.2.10). In fact one can systematically include the sub-leading 'NNLL' terms of (4.2.8) using the identity

$$\exp\left(-\frac{\lambda}{2}\left(2L\,L_b + L_b^2\right)\right) = \sum_{j=0}^{\infty} \frac{1}{j!}\left(-\frac{\lambda}{2}\right)^j \frac{d^{2j}}{d^{2j}(\lambda L)} \exp\left(-\lambda L\, L_b\right) , \qquad (4.2.12)$$

which generates more sub-leading terms as derivatives of the FNR analytic 'NLL' result. In particular, including the $m = 0, 1$ contributions yields

$$\frac{1}{\sigma_0}\frac{d\sigma}{d\eta}\Big|_{m=0,1} = \frac{d}{d\eta}\left\{\exp\left(-\frac{\lambda}{2}L^2\right)\left(1 - \frac{\eta^2}{2\lambda}\frac{d^2}{d^2\eta} - \frac{\eta}{2\lambda}\frac{d}{d\eta}\right)\left[\left(\frac{2}{b_0}\right)^{-2\lambda L}\frac{\Gamma(1-\lambda L)}{\Gamma(1+\lambda L)}\right]\right\} . \qquad (4.2.13)$$

This, however, does not cure the singularity problem but makes it even worse. It turns out that if the upper limit of the sum over m increases by 1, the order of the poles increases by 2, e.g. the formula (4.2.13) has poles of order four at $\eta^{\rm crit}$. Effectively, as this upper limit increases, the region where the approximation of the b–space result becomes better contracts. This signals the instability of the FNR expansion. Consequently, it does not seem possible to extend the FNR approach beyond the 'NNL' approximation in a systematic way.

[3] This may appear to be an irrelevantly small value but, as shown in [58], when the running coupling constant is used the pole moves significantly towards higher values of $p_{\rm T}$.

4.2.2 Numerical studies

In Fig. 4.2 we present the resummed FNR result (4.2.7) as a function of η. The pole at $\eta^{\rm crit}$ is evident (the distribution $\to -\infty$ as the singularity is approached from above). Since the position of the pole moves towards higher $p_{\rm T}^{\rm crit}$ with increasing Q, one should be very careful when applying the FNR formalism to describe production of a of very heavy particle, e.g. the hypothetical Z' boson. On the contrary, the KS formalism does not have problems with recovering the resummed result in this limit, provided sufficient number of towers is considered. This is because the KS approach takes into account terms $\sim L_b^2$ in the exponent (4.2.8) which arise as a consequence of the transverse momentum conservation.

The resummed FNR result can also be compared to the 'truncated' expression (4.2.10), cf. Fig. 4.5, for various values of the cut-off parameter $N_{\rm max}$. This shows the effect of

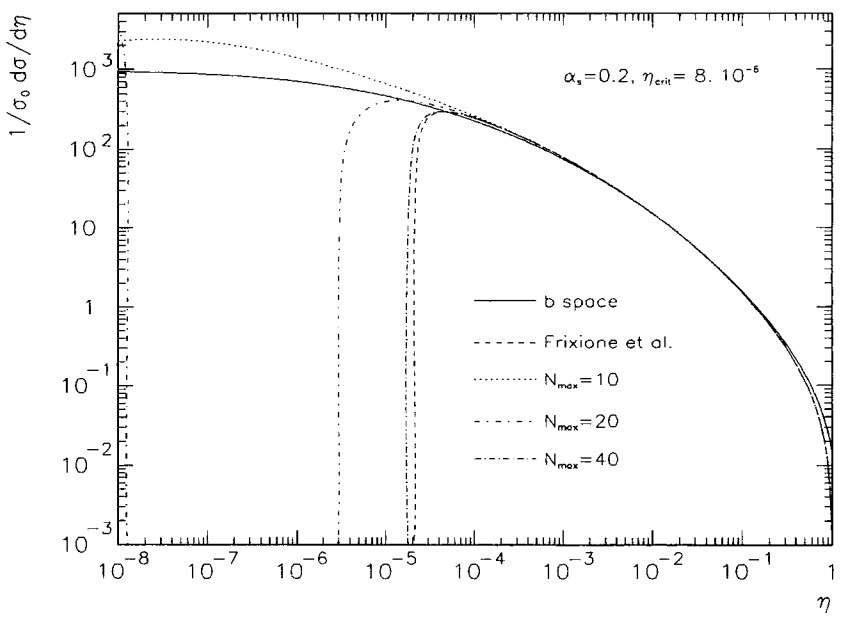

Figure 4.5: The b space result compared to the expression (4.2.7)and (4.2.10), calculated for various values of $N_{\rm max}$. With the choice $\alpha_s = 0.2$, (4.2.7) is only applicable for $\eta \gtrsim 8. \times 10^{-6}$.

successively adding more and more of the sub-leading '$m = 0$' terms, starting from the DLLA expression for $N_{\max} = 1$. Convergence to the (singular) resummed FNR result (4.2.7) for large $N_{\max}$ is clearly evident.

The singularity problem in the FNR approach is illustrated in Fig. 4.6. We show there the ratio of the numerically calculated expressions (4.2.7), (4.2.13) to the 'full' b space result. Because the singularity is stronger in (4.2.13) than in (4.2.7) the applicability of the former expression is restricted to a smaller region of η.

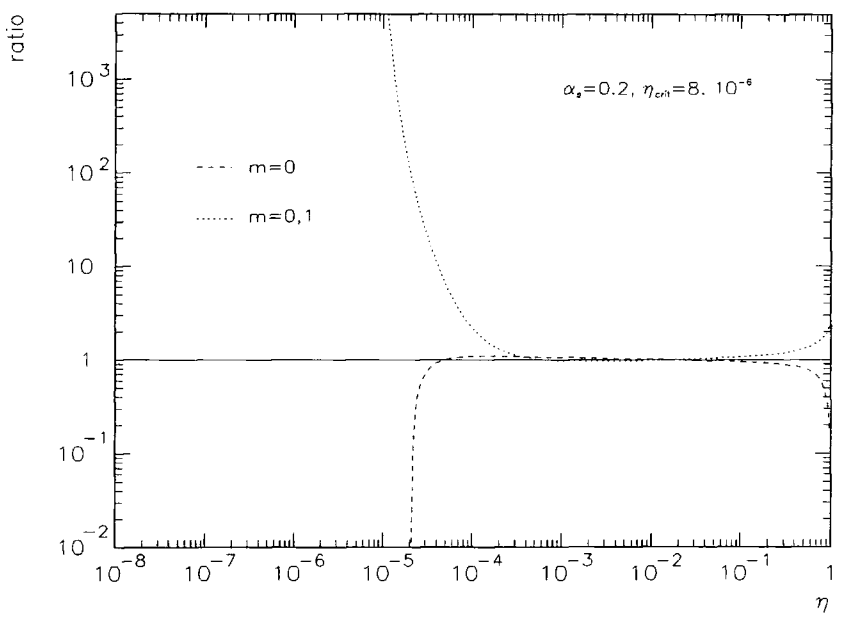

Figure 4.6: The ratio of the numerically calculated (4.2.7) (m=0 curve) and (4.2.13) (m=0,1 curve) to the b space result.

4.3 Summary

In this chapter we have shown that the EV, KS and FNR approaches start from the same expression for the cross section in b space, but organise the perturbative expansion

in p_T space in different ways such that different sub-leading p_T logarithms are included. In the KS approach, towers of sub-leading logarithms fill in the Sudakov (DLLA) dip at small p_T. Whereas up to the first four towers can be successfully resummed in this way, the EV technique is limited only to the three most leading series. In the FNR approach, a particular subset of sub-leading logarithms is resummed to all orders, but the resulting expression has a singularity at $p_T = p_T^{crit}$, below which the cross section is not defined. The pole at p_T^{crit} does not have any physical meaning and can be treated as an artifact of the FNR approximation. Since we have shown that attempts systematically to include the 'NNLL' contributions in this approach lead to even more singular behaviour than that observed in the 'NLL' case, this may cast doubt on the validity of the 'NLL' approximation used in the FNR approach. Both EV and FNR results can be obtained in the KS approach by including only the appropriate sub-leading terms. In this sense the KS approach can be considered as the most universal.

Chapter 5

Vector boson production at hadron colliders

About 90% of all W and Z bosons produced at the Tevatron have a transverse momentum smaller than 20 GeV. These bosons mostly acquire their transverse momentum as a result of the radiation of soft gluons by their parent partons. The correct theoretical description of a process involving emission of soft gluons requires the resummation of large logarithmic corrections. Having studied in the previous chapters various resummation formalisms, with particular focus on those in $p_{\rm T}$ space, we now turn to the phenomenology of the process.

First we derive the hadron level cross section in the KS approach using the Mellin transform method. It needs to be stressed that here we investigate only the resummed part of the cross section and do not perform matching with the fixed order calculations. The resummed part accounts for almost the entire cross section in the $p_{\rm T}$ range of interest. For the b space method it is estimated that the σ_f piece of the cross section contributes less that 10% to $d\sigma/dp_{\rm T}$ at $p_{\rm T} \sim 20$ GeV and the total contribution of the σ_r term to $\int_0^{30\,\mathrm{GeV}} dp_{\rm T} \frac{d\sigma}{dp_{\rm T}}$ is less than 1% [60].

In a manner similar to the b space formalism, the $p_{\rm T}$ space formalism is incomplete

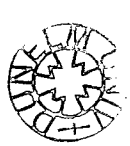

without a prescription for dealing with the non-perturbative region of small $p_{\rm T}$. Hence we first discuss the possible forms of the non-perturbative inputs. This is followed by a comparison with the Tevatron data on Z boson production. We finish our investigations by commenting on W production and the ratio of W to Z $p_{\rm T}$ distributions.

5.1 Theoretical cross section for $p\bar{p}\to W, Z + X$

In analogy with the parton level expression, the derivation of the resummed part of the theoretical cross section for the Drell-Yan process follows from the b space formula, cf. Chapter 2[1]

$$\begin{aligned}\frac{d\sigma}{dp_{\rm T}^2\, dQ^2} &= \frac{\sigma_0}{Q^2}\sum_q e_q^2 \int_0^1 dx_A\, dx_B\, \delta\left(x_A x_B - \frac{Q^2}{s}\right) \times \\ &\quad \frac{1}{2}\int_0^\infty db\, b\, J_0(p_{\rm T} b)\, \exp[\mathcal{S}(b,Q)]\, \tilde{f}'_{q/A}\left(x_A, \frac{b_0}{b}\right)\, \tilde{f}'_{\bar{q}/B}\left(x_B, \frac{b_0}{b}\right) .\end{aligned} \tag{5.1.1}$$

At the moment we focus on the non-singlet (NS) cross-section, i.e.

$$\tilde{f}'_{q/H} = f'_{q/H} - f'_{\bar{q}/H}$$

are the modified higher order NS structure functions, defined as in Appendix B. The N-th moment of the cross section with respect to $\tau = Q^2/s$ has the form

$$\begin{aligned}\mathcal{M}(N) &= \int d\tau\, \tau^N \frac{Q^2}{\sigma_0}\frac{d\sigma}{dp_{\rm T}^2\, dQ^2} \\ &= \sum_q e_q^2 \frac{1}{2}\int_0^\infty db\, b\, J_0(p_{\rm T} b)\, \exp\left[\mathcal{S}(b,Q)\right] \tilde{f}'_{q/A}(N, \frac{b_0}{b})\, \tilde{f}'_{\bar{q}/B}(N, \frac{b_0}{b}) .\end{aligned} \tag{5.1.2}$$

Solving the DGLAP equation for the N-th moment of the modified structure function $\tilde{f}'_{q/H}(N,Q) = \int_0^1 dx_H x_H^N \tilde{f}'_{q/H}(x_H, Q)$ yields (cf. Appendix B)

$$\tilde{f}'_{q/H}(N, \frac{b_0}{b}) = \exp\left[-\int_{(b_0/b)^2}^{Q^2} \frac{d\bar{\mu}^2}{\bar{\mu}^2}\gamma'_N(\bar{\alpha}_s(\bar{\mu}))\right] \tilde{f}'_{q/H}(N,Q)\,, \tag{5.1.3}$$

[1] Here we mostly adopt the method presented in [57] with modifications necessary for the KS method.

which leads to

$$\mathcal{M}(N) = \sum_q e_q^2 \, \tilde{f}'_{q/A}(N,Q)\tilde{f}'_{\bar{q}/B}(N,Q) \times \frac{1}{2}\int_0^\infty db\, b\, J_0(p_{\rm T} b)\, \exp\left[\mathcal{S}(b,Q) - 2\int_{b_0^2/b^2}^{Q^2} \frac{d\bar{\mu}^2}{\bar{\mu}^2}\gamma'_N(\bar{\alpha}_s(\bar{\mu}))\right] . \quad (5.1.4)$$

Integration by parts, familiar from the derivation of the parton level expression, see Eq. 3.1.6, allows us to write

$$\begin{aligned}
\mathcal{M}(N) &= -\frac{1}{2p_{\rm T}^2}\sum_q e_q^2 \, \tilde{f}'_{q/A}(N,Q)\tilde{f}'_{\bar{q}/B}(N,Q) \\
&\quad \times \int_0^\infty dx\, x\, J_1(x)\, \frac{d}{dx}\exp\left[\mathcal{S}(x,Q) - 2\int_{\frac{b_0^2 p_{\rm T}^2}{x^2}}^{Q^2} \frac{d\bar{\mu}^2}{\bar{\mu}^2}\gamma'_N(\bar{\alpha}_s(\bar{\mu}))\right] \\
&= \frac{d}{dp_{\rm T}^2}\Bigg\{ \sum_q e_q^2 \, \tilde{f}'_{q/A}(N,Q)\tilde{f}'_{\bar{q}/B}(N,Q) \\
&\quad \times \int_0^\infty dx\, J_1(x)\, \exp\left[\mathcal{S}(x,Q) - 2\int_{\frac{b_0^2 p_{\rm T}^2}{x^2}}^{Q^2} \frac{d\bar{\mu}^2}{\bar{\mu}^2}\gamma'_N(\bar{\alpha}_s(\bar{\mu}))\right]\Bigg\} \\
&= \frac{d}{dp_{\rm T}^2}\Bigg\{ \sum_q e_q^2 \, \tilde{f}'_{q/A}(N,p_{\rm T})\tilde{f}'_{\bar{q}/B}(N,p_{\rm T}) \\
&\quad \times \int_0^\infty dx\, J_1(x)\, \exp\left[\mathcal{S}(x,Q) - 2\int_{\frac{b_0^2 p_{\rm T}^2}{x^2}}^{p_{\rm T}^2} \frac{d\bar{\mu}^2}{\bar{\mu}^2}\gamma'_N(\bar{\alpha}_s(\bar{\mu}))\right]\Bigg\} ,
\end{aligned}$$

where $x = p_{\rm T} b$. In the second transformation we used the identity first derived by the authors of [57], (Eq.(25) of [57]), whereas the last transformation was made possible by applying the solution of the DGLAP equation.

In order to proceed with developing an expression for the hadron level cross section, the following approximation is introduced

$$\exp\left[\mathcal{S}(x,Q) - 2\int_{\frac{b_0^2 p_{\rm T}^2}{x^2}}^{p_{\rm T}^2} \frac{d\bar{\mu}^2}{\bar{\mu}^2}\gamma'_N(\bar{\alpha}_s(\bar{\mu}))\right] \approx \exp\left[\mathcal{S}(x,Q)\right] . \quad (5.1.5)$$

The above equality is exact for the first four towers of logarithms; it is the fifth tower which will contain the first modified anomalous dimension coefficient γ'_N. This can be easily seen by expanding the exponential in (5.1.5) (assuming fixed coupling constant)

$$\begin{aligned}
&\exp\left[\mathcal{S}(x,Q) - 2\int_{\frac{b_0^2 p_{\rm T}^2}{x^2}}^{p_{\rm T}^2} \frac{d\bar{\mu}^2}{\bar{\mu}^2}\gamma'_N(\bar{\alpha}_s(\bar{\mu}))\right] = \\
&\sum_{N=0}^{\infty}\frac{(-1)^N}{N!}\Big[\frac{1}{2}(A^{(1)}\alpha_s + A^{(2)}\alpha_s^2 + ...)(L+L_b)^2 + (B^{(1)}\alpha_s + B^{(2)}\alpha_s^2)(L+L_b) \\
&\qquad +2(\gamma_N'^{(1)}\alpha_s + \gamma_N'^{(2)}\alpha_s^2 + ...)L_b\Big]^N ,
\end{aligned}$$

where $L = \ln(Q^2/p_{\rm T}^2)$ and $L_b = \ln(x^2/b_0^2)$, as in Chapter 3 and Chapter 4. The first term containing $\gamma_N^{\prime(1)}$ which does not vanish after integration over x is of the form $\bar{\alpha_s}^N A^{(1)N-1} \gamma_N^{\prime(1)} L^{2(N-2)} L_b^3$. The same statement holds also for the singlet parton distribution functions. Therefore from now on we will perform resummation only for the first four towers of logarithms, meaning $N_{\rm max} = 4$ in the KS parton level formula (3.1.10).[2] The resulting expression

$$\mathcal{M}(N) = \frac{d}{dp_{\rm T}^2}\left\{ \sum_q e_q^2 \, \tilde{f}'_{q/A}(N, p_{\rm T}) \tilde{f}'_{\bar{q}/B}(N, p_{\rm T}) \int_0^\infty dx \, J_1(x) \, \exp[\mathcal{S}(x, Q)] \right\} \qquad (5.1.6)$$

can now be transformed back to momentum space by the means of the inverse Mellin transform

$$\begin{aligned} \frac{d\sigma}{dp_{\rm T}^2 \, dQ^2} &= \frac{\sigma_0}{Q^2} \sum_q e_q^2 \int_0^1 dx_A \, dx_B \, \delta\left(x_A x_B - \frac{Q^2}{s}\right) \times \\ &\quad \frac{d}{dp_{\rm T}^2}\left\{ \int_0^\infty dx \, J_1(x) \, \exp[\mathcal{S}(x, Q)] \, \tilde{f}'_{q/A}(x_A, p_{\rm T}) \, \tilde{f}'_{\bar{q}/B}(x_B, p_{\rm T}) \right\}. \end{aligned} \qquad (5.1.7)$$

At the parton level we calculated the quantity, see Eq. 3.2.19

$$\begin{aligned} \frac{1}{\sigma_0}\frac{d\sigma}{d\eta} &= -\frac{Q^2}{2p_{\rm T}^2} \int_0^\infty dx \, x \, J_1(x) \frac{d}{dx} \exp[\mathcal{S}(x, Q)] \\ &= -\frac{Q^2}{2p_{\rm T}^2} \exp(\mathcal{S}_\eta(Q)) \int_0^\infty dx \, x \, J_1(x) \frac{d}{dx} \exp[\tilde{\mathcal{S}}(x, Q)] \\ &\equiv -\frac{Q^2}{2p_{\rm T}^2} \Sigma_1(p_{\rm T}, Q) \end{aligned}$$

in terms of resummed towers of logarithms in $p_{\rm T}$ space. Here $\tilde{\mathcal{S}}(x, Q) = \mathcal{S}(x, Q) - \mathcal{S}_\eta(Q)$. The expression for $\int_0^\infty dx J_1(x) \exp[\mathcal{S}(x, Q)]$ can be derived in a similar manner

$$\begin{aligned} \int_0^\infty dx J_1(x) \exp[\mathcal{S}(x, Q)] = \exp(\mathcal{S}_\eta) \sum_{N=1}^{\infty} \left(\frac{-\alpha_S(\mu^2) A^{(1)}}{\pi}\right)^{N-1} \frac{1}{(N-1)!} \sum_{m=0}^{N-1} \binom{N-1}{m} \\ \times \sum_{k=0}^{N-m-1} \binom{N-m-1}{k} \sum_{l=0}^{N-m-k-1} \binom{N-m-k-1}{l} \\ \times \sum_{j=0}^{N-m-k-l-1} \binom{N-m-k-l-1}{j} \sum_{i=0}^{N-m-k-l-j-1} \binom{N-m-k-l-j-1}{i} \end{aligned}$$

[2] In any case, the fifth tower of logarithms cannot be fully taken into account due to the lack of knowledge of $A^{(3)}$.

$$\times \; c_2^m c_3^k c_4^l c_5^j c_6^i c_1^{N-m-k-l-j-i-1} \tau_{N+m+2k+3l+4j+5i-1}$$
$$\equiv \; \Sigma_2(p_{\rm T}, Q)\,, \tag{5.1.8}$$

with $\mathcal{S}_\eta$ and c coefficients defined in Appendix A. Finally we arrive at the $p_{\rm T}$ space formula for the Drell-Yan cross section at the hadron level

$$\frac{d\sigma}{dp_{\rm T}^2\, dQ^2} = \frac{\sigma_0}{Q^2} \sum_q e_q^2 \int_0^1 dx_A\, dx_B\, \delta\left(x_A x_B - \frac{Q^2}{s}\right) \times \frac{d}{dp_{\rm T}^2}\left\{\Sigma_2(p_{\rm T}, Q)\, f'_{q/A}(x_A, p_{\rm T})\, f'_{\bar{q}/B}(x_B, p_{\rm T})\right\}\,. \tag{5.1.9}$$

From now on we will refer to above Eq. (5.1.9) as the KS hadron-level formula in $p_{\rm T}$ space.

Analogously the transverse momentum distribution for a massive vector boson V produced in $p\bar{p}\to V + X$ reads

$$\frac{d\sigma}{dp_{\rm T}} = \sigma_0 \sum_{qq'} U^V_{qq'} \int_0^1 dx_A\, dx_B\, \delta\left(x_A x_B - \frac{M_V^2}{s}\right) \times \frac{d}{dp_{\rm T}}\left\{\Sigma_2(p_{\rm T}, M_V)\, f'_{q/A}(x_A, p_{\rm T})\, f'_{q'/B}(x_B, p_{\rm T})\right\}\,, \tag{5.1.10}$$

where

$$\sigma_0 = \frac{\pi\sqrt{2}G_F}{N}$$
$$U^V_{qq'} = \begin{cases} |V_{qq'}|^2 & V = W^\pm\,, \\ (V_q^2 + A_q^2)\delta_{qq'} & V = Z\,, \end{cases} \tag{5.1.11}$$

with $V_{qq'}$, V_q, A_q defined in Chapter 2.

In practice it is better to split the differentiation in (5.1.10) into two terms

$$\frac{d\sigma}{dp_{\rm T}} = \sigma_0 \sum_{qq'} U^V_{qq'} \int_0^1 dx_A\, dx_B\, \delta\left(x_A x_B - \frac{M_V^2}{s}\right) \times \left\{-\frac{1}{p_{\rm T}}\Sigma_1(p_{\rm T}, M_V) f'_{q/A}(x_A, p_{\rm T})\, f'_{q'/B}(x_B, p_{\rm T}) + \Sigma_2(p_{\rm T}, M_V)\frac{d}{dp_{\rm T}}\left[f'_{q/A}(x_A, p_{\rm T})\, f'_{q'/B}(x_B, p_{\rm T})\right]\right\}\,. \tag{5.1.12}$$

This trick allows us to apply an inevitable numerical derivative only to the product of the structure functions, not to the whole expression, leading to a reduction of the numerical error.

A dramatic improvement in the amount of computing time used can be achieved, at a low cost in terms of the accuracy, by parameterizing the integral over the partons' momenta fractions x_A, x_B in (5.1.12) by an ansatz function (typically a polynomial of the 5th order in $\ln(p_{\rm T})$), see Appendix C. The usefulness of this solution relies on the absence of x_A, x_B anywhere in (5.1.10) except in the structure functions.[3]

5.2 Treatment of the quark mass thresholds effects

The Drell-Yan cross section 5.1.9 has been derived in the limit of the fixed number of quark flavours, N_f, which implies no quark mass thresholds are considered. However, the original b space expression depends on N_f, which is taken to be the number of quark flavours active at the scale at which α_s is evaluated. The dependence on N_f enters in the Sudakov factor through the $A^{(2)}$, $B^{(2)}$ coefficients and through the β function in the expansion of α_s. Consequently one would expect the $p_{\rm T}$ space method to have some form of dependence on N_f as well. Nevertheless, there are no indications that the treatment of N_f in b space is universal or unique. Additionally, if taken literally, it poses technical problems while deriving the $p_{\rm T}$ space expression. Therefore for our $p_{\rm T}$ space method we propose to change N_f according to the number of flavours active at the renormalization scale at which α_s is calculated while the expression is derived in the massless quarks limit. With the choices of the scale we use this roughly corresponds to the energy scale of the emitted gluons and fits into the physical picture of the process. It is reassuring that the quantity $\zeta(3)$, ($\tau_3 = -\zeta(3)/2$), which also appears in the fixed-order expression (2.3.31), is retrieved in our method when the above treatment of N_f is applied. This would not be possible if we transferred the b space treatment of N_f strictly into our method.

Changing the number of active quark flavours N_f immediately leads to a problem of obtaining reliable predictions free of unphysical discontinuities. The running coupling $\alpha_s^{\overline{\rm MS}}$ is traditionally constructed by solving the renormalization group equations using

[3]This is not true if the non-perturbative parameterization depends on the partons' momenta fractions, see Chapter 2, Section 2.5.

perturbative approximants to the β function which change discontinuously at the quark mass thresholds. This is equivalent to using effective Lagrangians with a fixed number of completely massless fermions and a fixed number of infinitely massive fermions in each energy range between quark mass thresholds. Although the continuity of the coupling is not required by the theory, a standard procedure is to impose matching conditions at the thresholds. This ensures an equivalence between the effective theories and relates the values of the coupling for different energy regions. Depending on the accuracy (in the sense of the order of calculations) of the matching conditions in the $\overline{\rm MS}$ scheme, different problems arise, like lack of analyticity, differentiability or even continuity of the coupling. For example the one-loop matching conditions require $\alpha_s^{\overline{\rm MS}}$ to be continuous at each quark threshold, but leave its derivative discontinuous.

In a recent work [61], Brodsky *et al.* proposed to analytically extend the $\alpha_s^{\overline{\rm MS}}$ scheme so that it incorporates the finite-mass quark threshold effects into the running of the coupling. By connecting the coupling directly to the analytic and physically-defined effective charge α_V scheme the authors obtain an analytic expression for the effective number of flavours which is a continuous function of the renormalization scale μ and the quark mass m_i. As a result, the evolution of the analytically extended coupling $\tilde{\alpha}_s^{\overline{\rm MS}}$ in the intermediate regions reflects the actual mass dependence of a physical effective charge and the analytic properties of the particle production in a physical process. Attracted by the advantages of the analytically extended $\overline{\rm MS}$ scheme, we employ it to calculate the values of N_f and $\alpha_s(\mu_R) = \tilde{\alpha}_s(\mu_R)$ to obtain results in the KS approach. Of course, our technique is not theoretically strict, since up to this point we performed all calculations in the $\overline{\rm MS}$ scheme. For our purposes the number of active flavours N_f is taken as the lowest order expression for $N_{f,\overline{\rm MS}}^{(0)}$ from [61]

$$N_{f,\overline{\rm MS}}^{(0)} \approx \sum_{i=1}^{6} \left(1 + \frac{5m_i^2}{\mu^2 \exp(5/3)}\right)^{-1} . \tag{5.2.13}$$

Solving the renormalization group equation for the analytic extension of the $\overline{\rm MS}$ coupling $\tilde{\alpha}_s^{\overline{\rm MS}}$

$$\frac{d\tilde{\alpha}_s^{\overline{\rm MS}}(\mu)}{d\ln\mu} = -\tilde{\psi}_{\overline{\rm MS}}^{(0)}(\mu)\frac{\tilde{\alpha}_s^{\overline{\rm MS}^2}(\mu)}{\pi} + \dots , \tag{5.2.14}$$

with

$$\tilde{\psi}^{(0)}_{\overline{\rm MS}}(\mu) = \frac{11}{2} - \frac{1}{3}\tilde{N}^{(0)}_{f,\overline{\rm MS}}(\mu) \tag{5.2.15}$$

gives

$$\tilde{\alpha}_s^{\overline{\rm MS}}(\mu) = \frac{2\pi}{\ln\left(\frac{\mu^2}{\tilde{\Lambda}^2}\right)\left[\frac{11}{2} - \frac{1}{3}\sum_{i=1}^{6}\frac{\ln(\mu^2\exp(5/3)+5m_i^2)}{\ln(\mu^2/\tilde{\Lambda}^2)}\right]}. \tag{5.2.16}$$

For the sake of numerical calculations we use the value (at one-loop) $\tilde{\Lambda} = 98.5$ MeV to restore the current world average estimate of the strong coupling at the M_Z scale, $\tilde{\alpha}_s^{\overline{\rm MS}}(M_Z) = 0.1175$.

5.3 Inclusion of the non-perturbative effects in $p_{\rm T}$ space

In Chapter 2 we thoroughly discussed problems related to modeling the non-perturbative contribution in the b space method. Let us remind the reader that the non-perturbative ansatz in $p_{\rm T}$ space is expected to be required only where the perturbation theory fails i.e. at the very low values of $p_{\rm T} \leq 2 - 3$ GeV. In this way a region of higher $p_{\rm T}$ can be described purely by the resummed perturbative QCD. Still, the W mass measurement is made in the region of $p_{\rm T} < 30$ GeV [63], and thus correct inclusion of the non-perturbative effects will play a significant role in achieving good accuracy of the measurement.

Unfortunately, the form of the prescription for how to deal with the non-perturbative region in $p_{\rm T}$ space remains an open theoretical issue. So far there has been only one method proposed which addresses this problem. The authors of [57] advocate the following alteration of the EV approach in order to incorporate the low energy effects

$$\begin{aligned} &f'_{a/A}(x_A, p_{\rm T})\, f'_{b/B}(x_B, p_{\rm T})\, \exp\left[\mathcal{T}(p_{\rm T}, Q)\right] \rightarrow \\ &\quad f'_{a/A}(x_A, p_{\rm T*})\, f'_{b/B}(x_B, p_{\rm T*})\, \exp\left[\mathcal{T}(p_{\rm T*}, Q)\right] \tilde{F}^{NP}(p_{\rm T}), \end{aligned} \tag{5.3.17}$$

with the $p_{\rm T}$ space non-perturbative function $\tilde{F}^{NP}(p_{\rm T})$ defined as

$$\tilde{F}^{NP}(p_{\rm T}) = 1 - \exp\left[-\tilde{a}\, p_{\rm T}^2\right] \tag{5.3.18}$$

and the 'freezing' prescription

$$p_{\mathrm{T}*} = \sqrt{p_{\mathrm{T}}^2 + p_{\mathrm{T}\,\mathrm{lim}}^2 \exp\left[-\frac{p_{\mathrm{T}}^2}{p_{\mathrm{T}\,\mathrm{lim}}^2}\right]}\,. \tag{5.3.19}$$

Adopting this approach for the KS technique leads to

$$\begin{aligned}\frac{d\sigma}{dp_{\mathrm{T}}} &= \sigma_0 \sum_{qq'} U_{qq'}^V \int_0^1 dx_A\, dx_B\, \delta\left(x_A x_B - \frac{M_V^2}{s}\right) \times \\ &\Bigg\{ -\frac{1}{p_{\mathrm{T}*}} \frac{dp_{\mathrm{T}*}}{dp_{\mathrm{T}}} \Sigma_1(p_{\mathrm{T}*}, M_V) f'_{q/A}(x_A, p_{\mathrm{T}*})\, f'_{q'/B}(x_B, p_{\mathrm{T}*}) \tilde{F}^{NP}(p_{\mathrm{T}}) \\ &+\Sigma_2(p_{\mathrm{T}*}, M_V) \frac{dp_{\mathrm{T}*}}{dp_{\mathrm{T}}} \frac{d}{dp_{\mathrm{T}*}} \left[f'_{q/A}(x_A, p_{\mathrm{T}*})\, f'_{q'/B}(x_B, p_{\mathrm{T}*})\right] \tilde{F}^{NP}(p_{\mathrm{T}}) \\ &+\Sigma_2(p_{\mathrm{T}*}, M_V) f'_{q/A}(x_A, p_{\mathrm{T}*})\, f'_{q'/B}(x_B, p_{\mathrm{T}*}) \frac{d}{dp_{\mathrm{T}}} \tilde{F}^{NP}(p_{\mathrm{T}}) \Bigg\}\,. \end{aligned} \tag{5.3.20}$$

Subsequently we discuss the choice of the form of $\tilde{F}^{NP}(p_{\mathrm{T}})$ and the freezing prescription.

5.3.1 Non-perturbative function $\tilde{F}^{NP}(p_{\mathrm{T}})$

The above method of incorporating the low p_{T} effects is somewhat arbitrary. Although the presence of the non-perturbative contribution in p_{T} space is mandatory, in the above approach it is introduced on an *ad hoc* basis; the main motivation being to obtain phenomenologically plausible results. This brings about the freedom in choosing the form of the non-perturbative function of $\tilde{F}^{NP}(p_{\mathrm{T}})$, except for the few necessary conditions such a function must obey, see [57]. It can be argued that the simplest possible $\tilde{F}^{NP}(p_{\mathrm{T}})$ satisfying the listed conditions is of the form (5.3.18). In Fig. 5.1 we compare the parton level results $(1/\sigma_0)(d\sigma/dp_{\mathrm{T}})$ for the EV approach for different values of $\tilde{a}$. As expected from (5.3.17) and (5.3.18), smaller values of $\tilde{a}$ lead to broader distributions and shift the distribution peak towards higher values of p_{T}.

Contrary to the b space case, the simple form of $\tilde{F}^{NP}(p_{\mathrm{T}})$ in the present framework does not take into account a possible dependence on Q and x. In other words, existence of an x-dependent linear term in the b space parameterization would suggest an x dependent correction to the presently used form of $\tilde{F}^{NP}(p_{\mathrm{T}})$. Identically to the b space case, it may prove to be of significant importance for making theoretical predictions at the LHC.

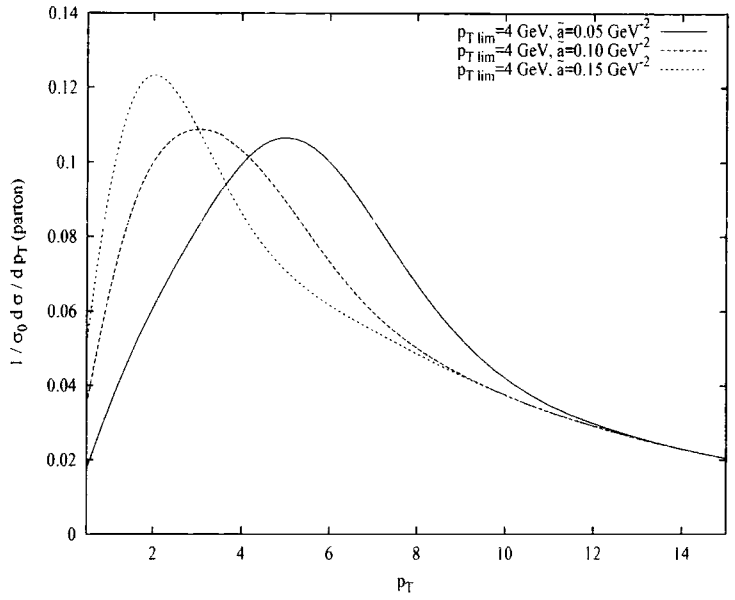

Figure 5.1: Predictions for $(1/\sigma_0)(d\sigma/dp_{\rm T})$ calculated at the parton level in the EV approach with various values of $\tilde{a}$. Here $Q = M_Z$.

5.3.2 Freezing of perturbative results in the low $p_{\rm T}$ limit

Analogously to the b space concept of b_*, $p_{\rm T*}$ never falls below the value of $p_{\rm T\,lim}$ and ensures that the perturbative calculations are not performed in the region where perturbative QCD is invalid. In Fig. 5.2 we present the parton level predictions for $\frac{1}{\sigma_0}\frac{d\sigma}{dp_{\rm T}}$ for a fixed value of $\tilde{a}$ and various choices of $p_{\rm T\,lim}$. As illustrated on the plot, the $\tilde{F}^{NP}(p_{\rm T})$ and the freezing effect can interfere in a complicated way, leading to considerable correlations between $\tilde{a}$ and $p_{\rm T\,lim}$.

The form of $p_{\rm T*}$ (5.3.19) provides a very efficient freezing of $p_{\rm T}$ so that the change from the region where perturbative theory is in full use and to the region where its ghostly existence contributes only a constant value is quite abrupt, although certainly continuous. However, the abruptness of $p_{\rm T*}$ (5.3.19) is a worrying feature as it may manifest itself in an unphysical shape of the cross section. Moreover the discussed freezing prescription is

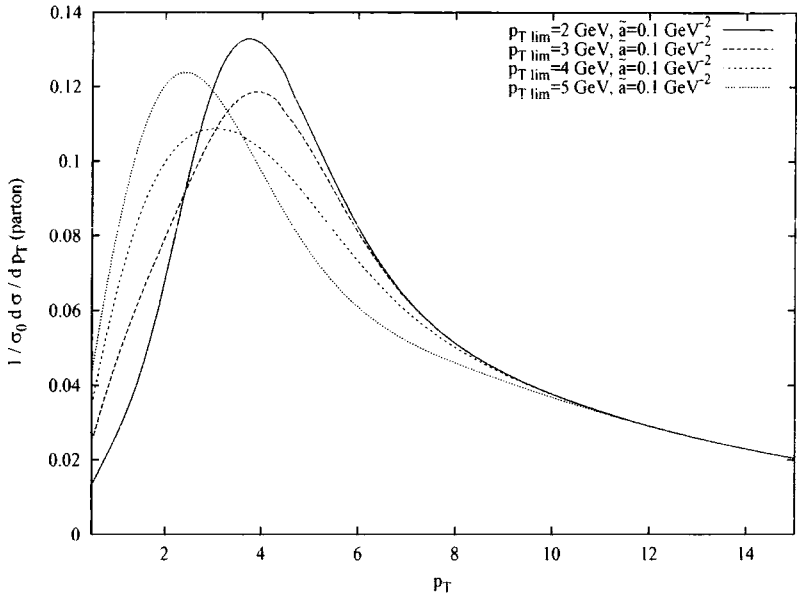

Figure 5.2: Predictions for $(1/\sigma_0)(d\sigma/dp_{\rm T})$ calculated at the parton level in the EV approach with various values of $p_{\rm T\,lim}$. Here $Q = M_Z$.

very different from the b space method (2.4.61), in fact the freezing suggested by the form of b_* would be much slower and have a power-law character, e.g.

$$p_{\rm T*} = \sqrt{p_{\rm T}^2 + p_{\rm T\,lim}^2}\,, \tag{5.3.21}$$

The two methods of freezing (5.3.19) and (5.3.21) are compared in Fig. 5.3. For comparison we also plot results obtained with an 'instant' method of freezing

$$p_{\rm T*} = \begin{cases} p_{\rm T\,lim} & p_{\rm T} \le p_{\rm T\,lim} \\ p_{\rm T} & p_{\rm T} > p_{\rm T\,lim}\,. \end{cases} \tag{5.3.22}$$

For $p_{\rm T} < p_{\rm T\,lim}$ the cross section (5.3.20) effectively reduces to the perturbative part calculated at $p_{\rm T*}$ times the derivative of $\tilde{F}^{NP}(p_{\rm T})$ (the other terms are practically negligible since they contain derivatives of the 'frozen' quantities). Therefore the slower the freezing, the bigger the cross section, and hence the inequality

$$p_{\rm T*}|_{(5.3.21)} > p_{\rm T*}|_{(5.3.19)} > p_{\rm T*}|_{(5.3.22)} \tag{5.3.23}$$

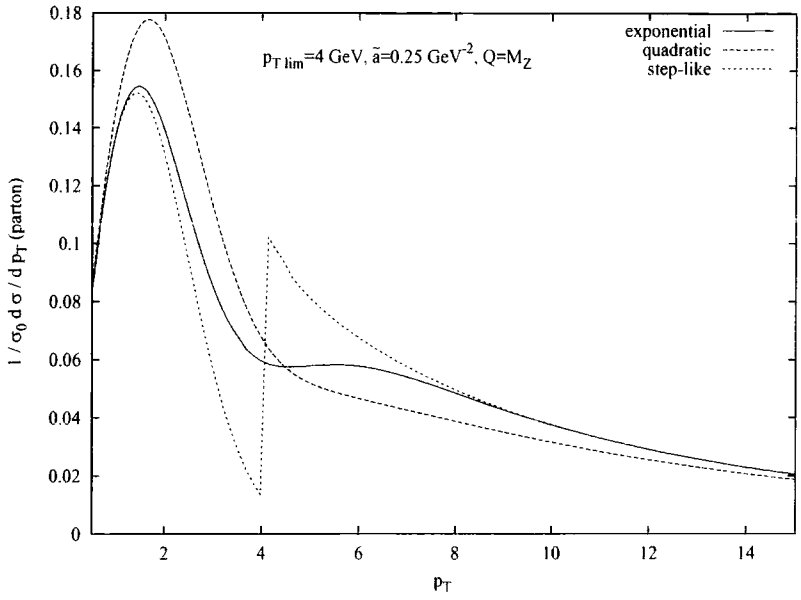

Figure 5.3: Predictions for $(1/\sigma_0)(d\sigma/dp_{\mathrm{T}})$ calculated at the parton level in the EV approach with various methods of freezing for Q=91.187 GeV (solid line: Eq. 5.3.19, dashed line: Eq. 5.3.21, dotted line: Eq. 5.3.22).

is reflected in the order of curves in Fig. 5.3. For higher p_{T} other terms become equally important. The size of the remaining terms is closely related or, depending on the freezing method, corresponds to the height of the discontinuity produced by the step-like method (5.3.22). This discontinuity signals potential problems for the other methods of freezing, i.e. unphysical humps in the distribution, as illustrated in Fig. 5.3. Obviously, the quicker the freezing, the closer resemblance to the step-like freezing (5.3.22) and the distribution is thus more likely to suffer from humps. This is exactly what happens in Fig. 5.3: large discontinuity for (5.3.22), hump for (5.3.19) and a legitimate curve obtained with (5.3.21). To obtain a valid prediction for a certain value of $p_{\mathrm{T\,lim}}$ the gap caused by the aforementioned discontinuity has to be small. Since the size of the discontinuity is partially governed by the size of $\tilde{F}^{NP}(p_{\mathrm{T}})$, this imposes a small $\tilde{a}$ for the exponential method to be correct. For particular values of $p_{\mathrm{T\,lim}} = 2,\ 3,\ 4$ GeV we find (for the

parton level cross section) corresponding maximum values of $\tilde{a} \leq 0.55,\ 0.3,\ 0.2\ \mathrm{GeV}^{-2}$. We expect to retain similar numbers for the case of hadron-level distributions. The above findings suggest that the quadratic method of freezing is theoretically preferable, although for large enough values of $\tilde{a}$ a deep gap at $p_{\mathrm{T\,lim}}$ causes the distribution obtained with the quadratic method to be unphysical too. Nevertheless quadratic freezing seems to allow for a bigger region in parameter space ($\tilde{a},\ p_{\mathrm{T\,lim}}$) to recover a physical shape of a distribution. Unfortunately, as discussed later, it poses problems when fitting predictions to data.

The appearance of humps is less likely for lower values of Q, e.g. in the Drell-Yan pair production process. Smaller values of $\ln(Q^2/p_{\mathrm{T}}^2)$ diminish the contribution of the first two terms in (5.3.20), resulting in a lowering of the height of the gap and enlargement of the allowed region in parameter space, see Fig. 5.4. On the other hand, this also means that for higher values of Q than considered here, e.g. for a hypothetical massive Z' boson production, the 'freezing issue' should be treated with greater care.

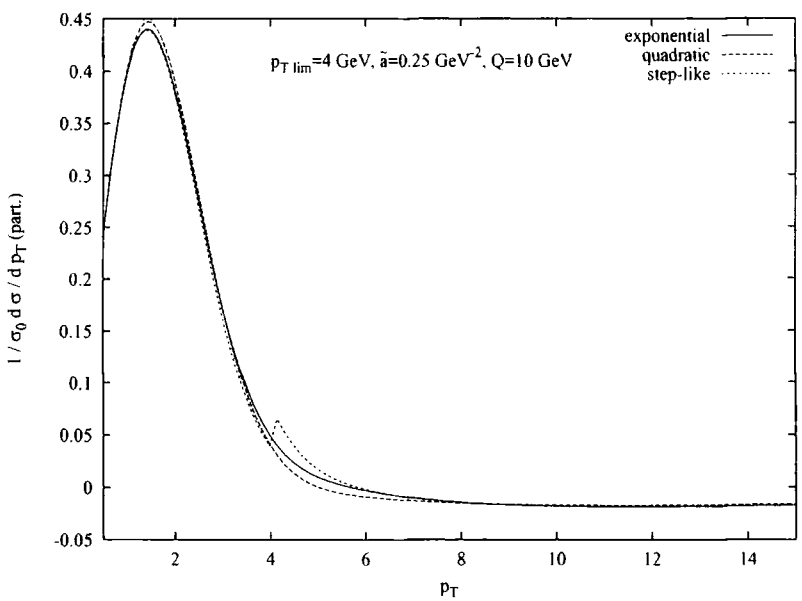

Figure 5.4: Predictions for $(1/\sigma_0)(d\sigma/dp_{\mathrm{T}})$ calculated at the parton level in the EV approach with various methods of freezing for Q=10 GeV (solid line: Eq. (5.3.19), dashed line: Eq. (5.3.21), dotted line: Eq. (5.3.22).

5.4 Alternative method of including non-perturbative effects

The EV scenario offers a conceptually simple method for including non-perturbative effects in $p_{\rm T}$ space, affecting the perturbative result only in the small $p_{\rm T}$ limit. Nevertheless its introduction may be seen as being 'too phenomenological'. The EV scenario incorporates almost arbitrary, or only phenomenologically based, choices of the form of the non-perturbative function and the freezing method – choices which may prove to be responsible for significant limitations, if not failure, of the method, e.g. for higher Q . Although the implementation of the non-perturbative effects in $p_{\rm T}$ space remains an open question, one could attempt to deduce its universal features from the general b space solution. Here we will shortly present a derivation of an alternative scenario, based closely on the original b space approach, for including the low $p_{\rm T}$ physics in $p_{\rm T}$ space. For the sake of simplicity we neglect freezing effects.

Again, we treat the Drell-Yan cross section in b space as a springboard

$$\frac{d\sigma}{dp_{\rm T}^2\,dQ^2} = \int_0^\infty db\, b\, J_0(p_{\rm T}b)\; P(b)\, F^{NP}(b)\,, \tag{5.4.24}$$

where $P(b)$ depends on b, Q and $p_{\rm T}$

$$\begin{aligned} P(b) &= \frac{1}{2}\frac{\sigma_0}{Q^2}\sum_q e_q^2 \int_0^1 dx_A\, dx_B\, \delta\left(x_A x_B - \frac{Q^2}{s}\right) \\ &\times \exp[\mathcal{S}(b,Q)]\, f'_{q/A}\left(x_A, \frac{b_0}{b}\right)\, f'_{\bar{q}/B}\left(x_B, \frac{b_0}{b}\right)\,. \end{aligned} \tag{5.4.25}$$

The convolution theorem allows us to write

$$\begin{aligned} \frac{d\sigma}{dp_{\rm T}^2\,dQ^2} &= \frac{1}{2\pi}\int d^2b e^{-i\vec{b}\vec{p}_{\rm T}} P(\vec{b}) F^{NP}(\vec{b}) \\ &= \frac{1}{2\pi}\int d^2p'_{\rm T}\tilde{P}(\vec{p}_{\rm T}{}')\tilde{F}^{NP}(\vec{p}_{\rm T} - \vec{p}_{\rm T}{}')\,, \end{aligned} \tag{5.4.26}$$

or

$$\frac{d\sigma}{dp_{\rm T}^2\,dQ^2} = \frac{1}{2\pi}\int d^2p'_{\rm T}\tilde{P}(\vec{p}_{\rm T} - \vec{p}_{\rm T}{}')\tilde{F}^{NP}(\vec{p}_{\rm T}{}')\,, \tag{5.4.27}$$

where now $\tilde{P}(\vec{p}_{\rm T})$ and $\tilde{F}^{NP}(\vec{p}_{\rm T})$ are defined as the Fourier transforms of the perturbative $P(b)$ and non-perturbative $F^{NP}(b)$ parts of the b space expression (5.4.24)

$$\tilde{P}(\vec{p}_{\rm T}) = \frac{1}{2\pi}\int d^2b e^{-i\vec{b}\vec{p}_{\rm T}} P(\vec{b}), \tag{5.4.28}$$

$$\tilde{F}^{NP}(\vec{p}_{\rm T}) = \frac{1}{2\pi}\int d^2b e^{-i\vec{b}\vec{p}_{\rm T}} F^{NP}(\vec{b}), \tag{5.4.29}$$

and we used the property $P(\vec{b}) \equiv P(b)$, $F^{NP}(\vec{b}) \equiv F^{NP}(b)$. It is clear from (5.4.28) that $\tilde{P}(\vec{p}_{\rm T})$ corresponds to the previously calculated expression in $p_{\rm T}$ space without the non-perturbative contribution. The Fourier transform of the non-perturbative contribution is easy to calculate when $F^{NP}(b)$ is a gaussian, but leads to a very sophisticated function if an extra linear term in b is assumed in the exponential of $F^{NP}(b)$. Due to the difficulties and uncertainties concerning the presence of a linear term in $F^{NP}(b)$ we assume

$$F^{NP}(\vec{b}) = \exp(-g\vec{b}^{\,2}), \tag{5.4.30}$$

which leads to

$$\tilde{F}^{NP}(\vec{p}_{\rm T}) = \frac{1}{2g}\exp\left(-\frac{\vec{p}_{\rm T}^{\,2}}{4g}\right). \tag{5.4.31}$$

Two different forms of the result, i.e. (5.4.26) and (5.4.27), generate two different scenarios for numerical calculations. Given (5.4.31), it follows from (5.4.27)

$$\begin{aligned}\frac{d\sigma}{dp_{\rm T}^2\, dQ^2} &= \frac{1}{4\pi g}\int d^2p'_{\rm T}\tilde{P}(\vec{p}_{\rm T}-\vec{p}\,'_{\rm T})\exp\left(-\frac{p'^{\,2}_{\rm T}}{4g}\right) \\ &= \frac{1}{2\pi}\int_0^1 dr\int_0^{2\pi} d\theta\tilde{P}\left(\left(p_{\rm T}^2 - 4g\ln(r) - 4\sqrt{g\ln(1/r)}p_{\rm T}cos(\theta)\right)^{\frac{1}{2}}\right)\end{aligned} \tag{5.4.32}$$

while to obtain (5.4.32) we made the substitution $p'_{T1} = \sqrt{4g\ln(1/r)}\cos(\theta)$, $p'_{T2} = \sqrt{4g\ln(1/r)}\sin(\theta)$.

The results obtained using Eq. 5.4.32 combined with the KS approach, for the simplified case of fixed α_s and only one nonzero coefficient in the Sudakov factor $A^{(1)} \neq 0$, are presented in Fig. 5.5. Although the results in Fig. 5.5 are valid only for the parton subprocess, the conclusions should also hold at the hadron level. The approximation of

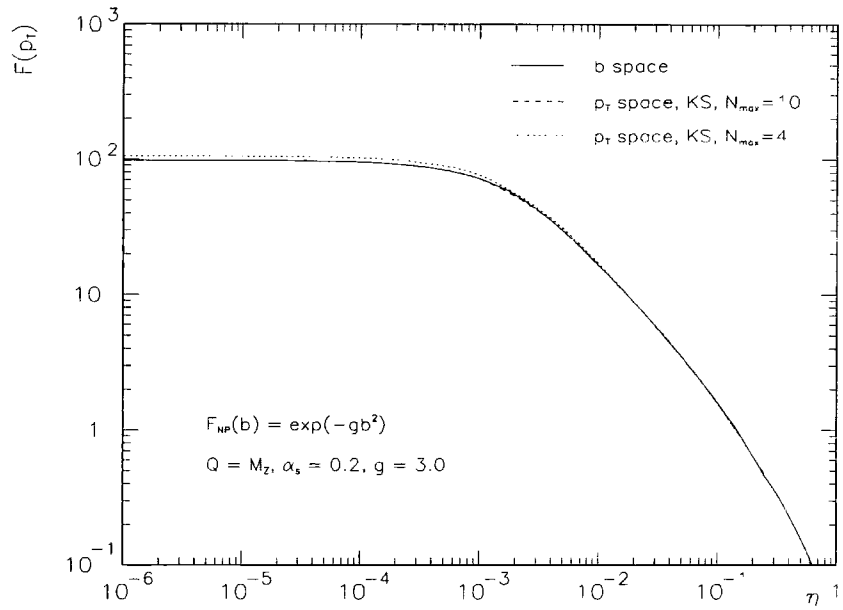

Figure 5.5: Comparison between the b space result including the non-perturbative contribution $F_{NP}(b)$ (5.4.24) and the p_{T} space result (5.4.32) in the KS approach, calculated at the parton level. Here $F(p_{\mathrm{T}}) \equiv F^{q_T}(q_T)$ as defined in [57], Eq. 37.

the b space result incorporating the non-perturbative smearing by the p_{T} space expression (5.4.32) seems to be promisingly good, and most importantly, improves notably with an increasing number of towers N_{max} in the KS approach.

The result derived in this way is definitely closer to the original b space method and a direct link between $F^{NP}(b)$ and $F^{NP}(p_{\mathrm{T}})$ lies at the heart of the scenario proposed above. Unfortunately, and in similar manner to b space, the non-perturbative contribution affects the result for *all* values of p_{T}, which can be considered a disadvantage. Needless to say, the non-perturbative function $\tilde{F}^{NP}(p_{\mathrm{T}})$ that in this scenario arises as a Fourier conjugate of the $F_{NP}(b)$, inherits all the ambiguities related to our current lack of understanding of the x and Q dependence of the non-perturbative contribution.

5.5 Results and discussion

Due to a rapid (already in the detector) decay of bosons produced in hadron collisions their properties are inferred from the measurement of the decay products. Because of the inaccuracies related to the measurement of jet properties it is normally the lepton decay channel, $Z \to l^+l^-$ and $W^\pm \to l^\pm \nu$, which is investigated. Thus the p_{T} distribution of Z is determined by measuring two final-state charged leptons, and can be determined at Tevatron with a resolution of $1 - 2$ GeV [63]. In contrast the measurement of W p_{T} poses a serious problem, due to the final state neutrino. Its transverse momentum is deduced by imposing a condition of the conservation of momentum on the momenta of all the final state particles produced in association with the W ('recoil' against the W), including the fragmentation products of the initial state gluon radiation. Since they normally carry very low momentum, it is extremally difficult experimentally to perform an accurate measurement (for a detailed disscussion, see [63]). Consequently, to compare experimental results and theory, the W data (or W theoretical predictions) have to be heavily corrected for detector effects. The Z measurements require no detector simulation in order to be compared with the theoretical predictions. As investigating detector effects lies beyond the scope of this work, we first focus on obtaining and discussing theoretical results for the case of Z production; a comment on W production follows.

The results presented below are for Tevatron experiments, CDF and D0, at $\sqrt{s} = 1.8$ TeV. Unless stated otherwise we use the factorization scale $\mu_f = p_{\mathrm{T}}$, continuous treatment of N_f, as described in Section 5.2, MRST99 parton distribution functions [74] (central gluon), branching ratio $BR(Z \to e^-e^+) = 3.366\%$ and the world average value of the strong coupling $\alpha_s = 0.1175$.

5.5.1 Theoretical uncertainties

In the following we discuss potential sources of uncertainties on the theoretical cross section. At low p_{T} the non-perturbative part of the cross section is believed to contribute

significantly to the theoretical uncertainty. Unfortunately, there are no theoretical suggestions on the general form of the non-perturbative function in p_{T} space. So far the only proposed form of $\tilde{F}^{NP}(p_{\mathrm{T}})$ (5.3.18) does not include any dependence on Q and/or x. Moreover, the value of the coefficient $\tilde{a}$ of (5.3.18) was obtained in [57] as a result of only one fit, to CDF Run 0 data. Therefore at this point we do not have enough information to estimate the size of the error caused by the non-perturbative contribution. Instead we fit the coefficient of $\tilde{F}^{NP}(p_{\mathrm{T}})$ to the newest set of the Tevatron data in the next section, see 5.5.2.

Dependence on the renormalization scale

A free parameter in the calculations, the renormalization scale determines the strength of the coupling in the theoretical predictions. For the process we investigate, the interaction strength must somehow depend on the size of the transverse momentum and we require the choice of the scale to reflect this fact. In particular, at the parton level cross section we advocated the use of the renormalization scale $\mu_R = p_{\mathrm{T}}^{(2/3)} Q^{(1/3)}$ as a means of eliminating certain logarithmic terms from the Sudakov factor and thus increasing the reliability of our approach. Moreover, for values of p_{T} where perturbative QCD can be safely applied and values of Q considered here, such μ_R is always bigger then the b quark mass, thus lessening the relevance of the correction due to the quark mass thresholds treatment. Another obvious choice of the scale is $\mu_R = p_{\mathrm{T}}$.[4] In Fig. 5.6 we present results calculated in the KS approach for the scales $\mu_R = p_{\mathrm{T}}$ and $\mu_R = p_{\mathrm{T}}^{(2/3)} Q^{(1/3)}$. It is clear that without any non-perturbative effects included, the results are significantly different, especially for small p_{T}. However, if the non-perturbative effects are taken into account, the difference almost disappears, cf. Fig. 5.7. Subjected to freezing, the perturbative part of the cross section no longer shows dependence on μ_R at small p_{T}. The presence of the derivative $dp_{\mathrm{T}*}/dp_{\mathrm{T}}$ is expected to provide a rapid suppression independently of the scale. From now on we decide to use $\mu_R = p_{\mathrm{T}}^{(2/3)} Q^{(1/3)}$ as a default choice for the KS approach.

[4] Other choices of μ_R were also considered in the literature, for example the authors of [31] proposed to take $\mu_R = \sqrt{p_{\mathrm{T}}^2 + Q^2}$.

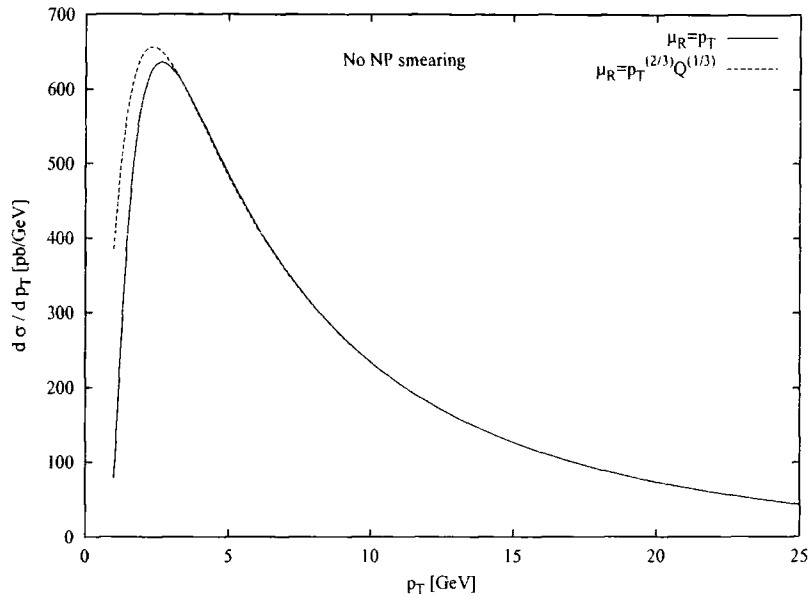

Figure 5.6: Theoretical predictions for Z production and two different choices of the renormalization scale when no non-perturbative contribution is taken into account .

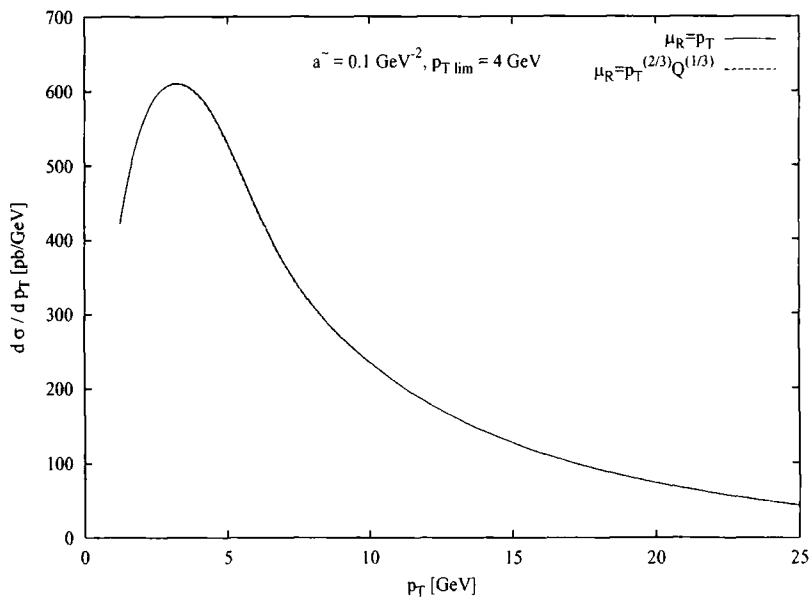

Figure 5.7: Theoretical predictions for Z production and two different choices of the renormalization scale with nonzero non-perturbative contribution ($\tilde{a} = 0.1\,\mathrm{GeV}^{-2}$, $p_{\mathrm{T\,lim}} = 4\,\mathrm{GeV}$, exponential freezing).

The choice of the scale is a source of minor theoretical errors only in the resummed part of the entire cross section. The fixed-order part of the cross section should be calculated with the same scale μ_R (for the studies of the dependence on μ_R for the fixed-order part see e.g. [31]). This will certainly increase the dependence on μ_R of the entire cross section.

Dependence on $\alpha_s(M_Z)$

The theoretical predictions prove to be significantly susceptible to the value of $\alpha_s(M_Z)$, see Fig. 5.8. Contrary to the situation when μ_R is varied, this behaviour persists after incorporating low p_{T} effects, cf. Fig. 5.8. A variation of $\alpha_s(M_Z)$ by ± 0.005 around its average value, 0.1175, causes over $\pm 8\%$ change in results. The dependence of the cross section on $\alpha_s(M_Z)$ is magnified by the change in the parton distribution functions due to the change of $\alpha_s(M_Z)$. We discuss the dependence on the choice of parton distribution functions in more detail in Appendix C.

5.5.2 Comparison of the theoretical results with data

Normalisation

The most recent sets of data on Z production come from the Run 1b (D0 collaboration [45]) and combined Run Ia+Ib (CDF [46]) at the Fermilab Tevatron $p\bar{p}$ collider. Although both experiments measure roughly the same number of events, they differ in the luminosity measurement. This obviously results in a difference in the reported cross sections, at the level of 6.2% [62]. Therefore it is necessary to normalise both data sets and theory predictions in order to make comparisons. This can be achieved by dividing by the measured or predicted total cross section, respectively. Alternatively, the normalisation factor can be found using the χ^2 method. By minimizing the χ^2, i.e. by imposing $\frac{\partial \chi^2(N)}{\partial N} = 0$ we find the normalization factor N for the theoretical predictions to be

$$N = \frac{\sum_i \frac{\sigma_i^{th}\sigma_i^{exp}}{(\Delta\sigma_i^{exp})^2}}{\sum_i \frac{(\sigma_i^{th})^2}{(\Delta\sigma_i^{exp})^2}}, \tag{5.5.33}$$

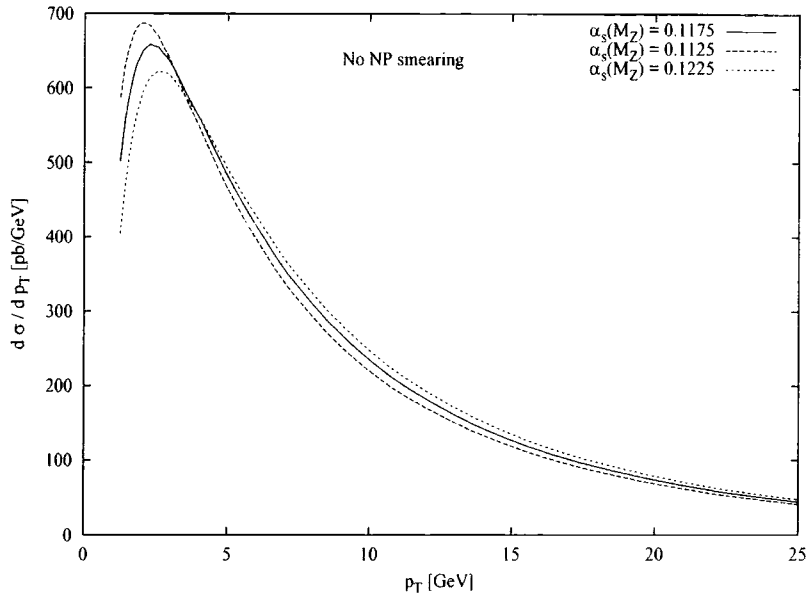

Figure 5.8: Theoretical predictions in the KS approach ($\mu_R = p_T^{(2/3)} Q^{(1/3)}$) for Z production and different values of $\alpha_s(M_Z)$ when no non-perturbative contribution is taken into account.

where σ_i^{th} (σ_i^{exp}) is the value of the theoretical (experimental) cross section - here the differential distribution in p_T, and $\Delta\sigma_i^{exp}$ is the experimental error.[5] The normalization factor is calculated separately for the D0 and CDF sets of data. Moreover, since we are not in a possession of a full matched cross section, the experimental points considered to determine N have $p_T < 15$ GeV. For the typical choice of the non-perturbative parameters [57], $\tilde{a} = 0.1$ GeV^{-2}, $p_{T\,\mathrm{lim}} = 4$ GeV, the normalization factors N_{CDF} and N_{D0} vary by around 10%, as expected. In Figs. 5.9, 5.10 we compare the CDF and D0 data with the KS predictions with these specific parameters.

[5]The main contribution to the experimental error comes, unsurprisingly, from the uncertainties in the luminosity measurement: ±4.4% for D0 [45] and ±3.9% for CDF.

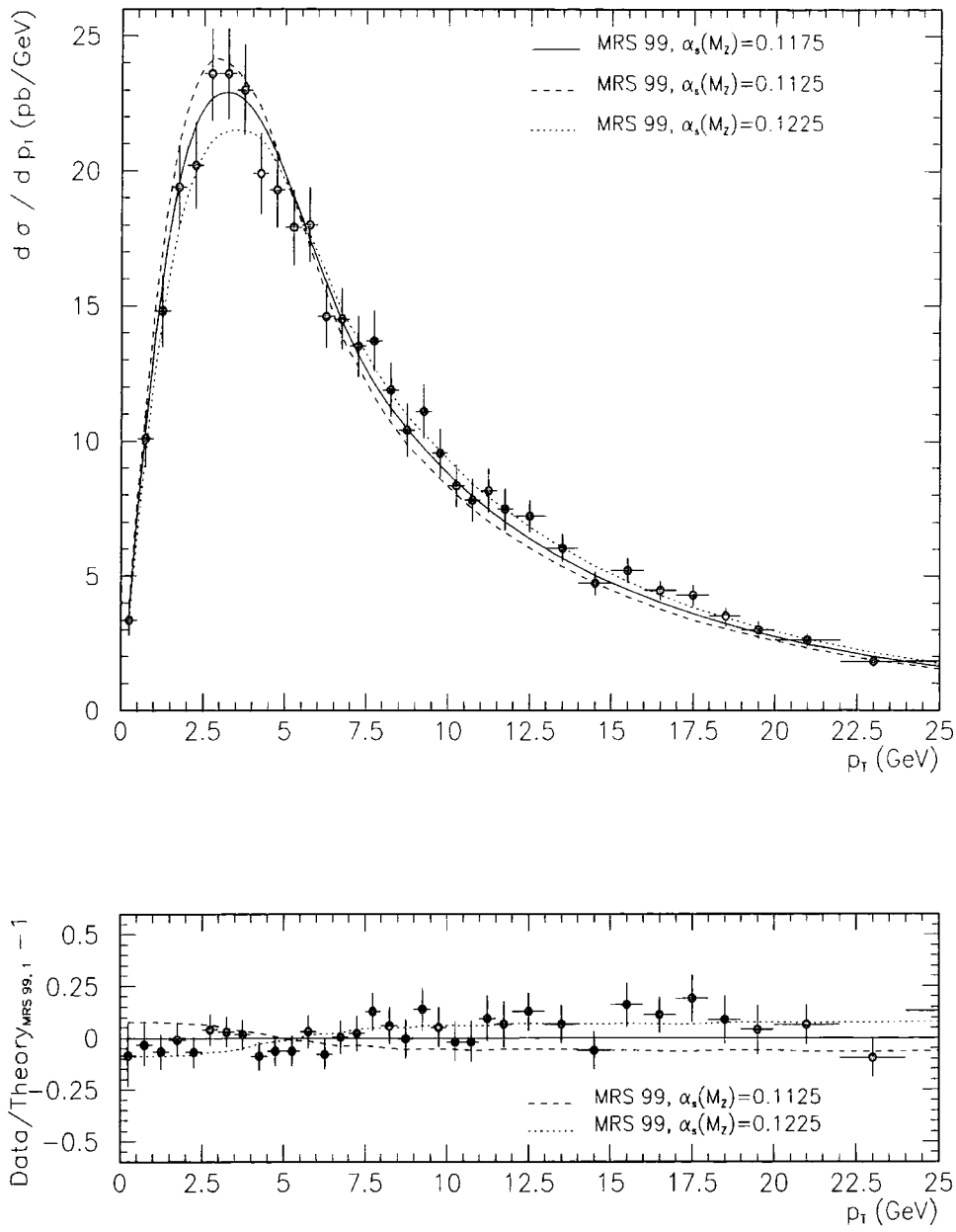

Figure 5.9: Theoretical cross section in p_{T} space (KS approach) vs. CDF data. The predictions were obtained using the EV form of the non-perturbative function with $\tilde{a} = 0.1$ GeV^{-2}, $p_{\mathrm{T\,lim}} = 4$ GeV. Also shown are the fractional differences between the data together with predictions for two more extreme choices of α_s and the predictions for the central value of α_s.

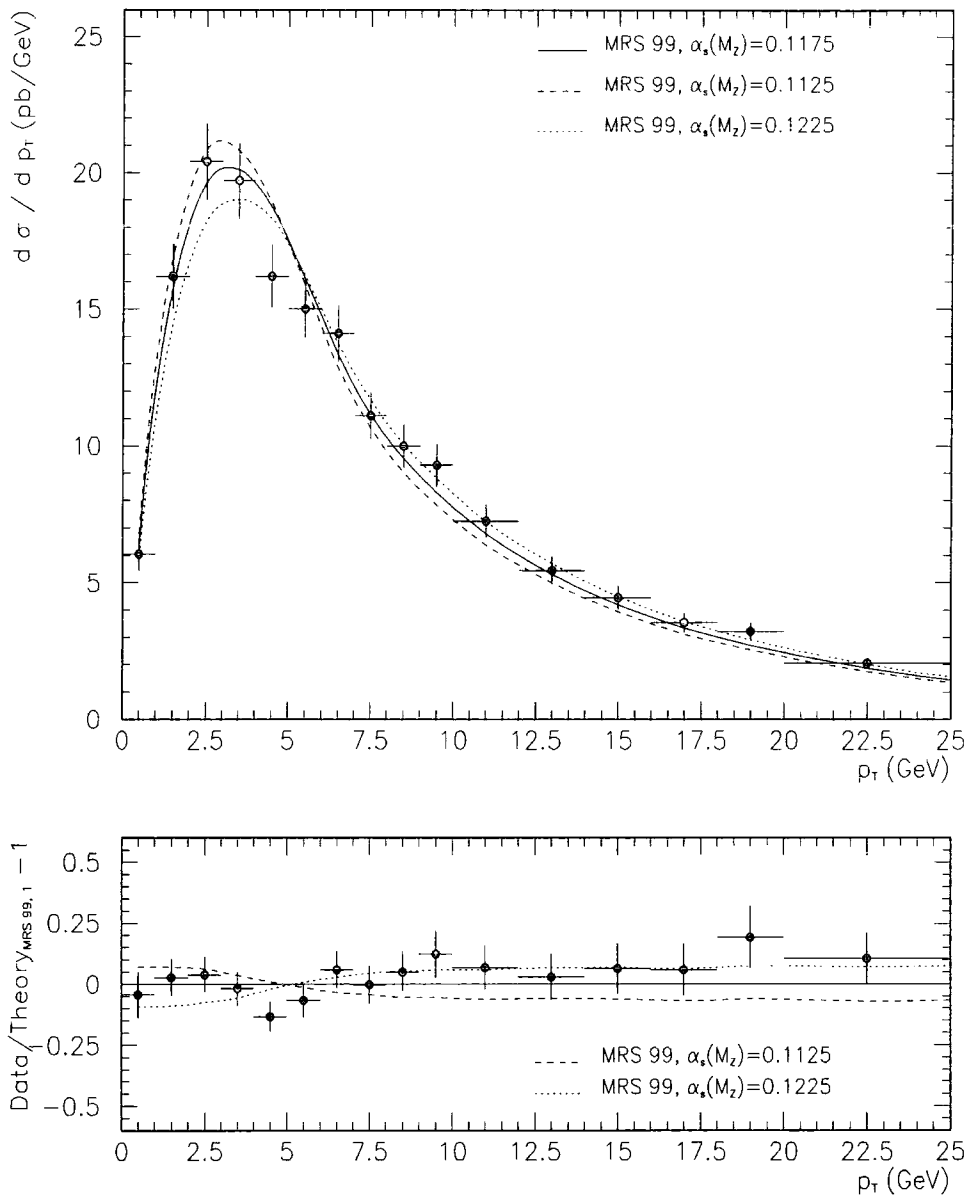

Figure 5.10: Theoretical cross section in p_{T} space (KS predictions) vs. D0 data. The predictions were obtained using the EV form of the non-perturbative function with $\tilde{a} = 0.1$ GeV^{-2}, $p_{\mathrm{T\,lim}} = 4$ GeV. Also shown are the fractional diffrences between the data together with predictions for two more extreme choices of α_s and the predictions for the central value of α_s.

Small $p_{\rm T}$ treatment

Non-perturbative parameters

Given that the Tevatron data are the most recent set of results on Z production, it is compelling to infer values of the non-perturbative parameters from the fits to the data. In order to do so we use the χ^2 method. Since our theoretical results do not include the fixed-order part we consider only those experimental points with $p_{\rm T} < 15$ GeV. Generally we find that the best $\chi^2/d.o.f.$ value is returned by the smaller values of $\tilde{a}$ and larger $p_{\rm T\,lim}$, see Fig. 5.11. In this context the values proposed by the EV collaboration $\tilde{a} = 0.1$ GeV^{-2}, $p_{\rm T\,lim} = 4$ GeV provide one of the best fits, $\chi^2/d.o.f. = 0.67$, and describe the data well. This is in agreement with the CDF and D0 analyses, cf. [45, 46]. The average value of the intrinsic momenta of partons is then

$$< q_{\rm T} >= \frac{1}{\sqrt{\pi\tilde{a}}} \qquad \Longrightarrow \qquad < q_{\rm T} >= 1.8\,{\rm GeV}. \tag{5.5.34}$$

We also find that there is a wide range of strongly correlated values of larger $\tilde{a}$ and smaller $p_{\rm T\,lim}$ for which $\chi^2/d.o.f.$ is only minimally worse, see Fig. 5.11. The correlations suggest that smaller values of $p_{\rm T\,lim}$ support smaller $< q_{\rm T} >$. First observed at the parton level (Section 5.3.2), the strong correlations come here as no surprise. The change in shape of the theoretical distribution induced by varying the non-perturbative parameters, compared to the CDF data, is shown in Fig. 5.12. Due to the experimental errors it is difficult to estimate the predictive power of these results, although it certainly is an indication that the next generation of measurements may cause changes in the widely accepted values of $\tilde{a}$, $p_{\rm T\,lim}$. In summary, a satisfactory agreement between data and theory can be achieved for quite a wide range of parameters $\tilde{a}$, $p_{\rm T\,lim}$. We also find that with the current experimental evidence there is no need to introduce additional overall smearing, as proposed in [57].

Linear term in $\tilde{F}^{NP}(p_T)$

Analogously to the b space method, one may consider modifications to the gaussian form of the non-perturbative function in $p_{\rm T}$ space, for example adding an extra term in

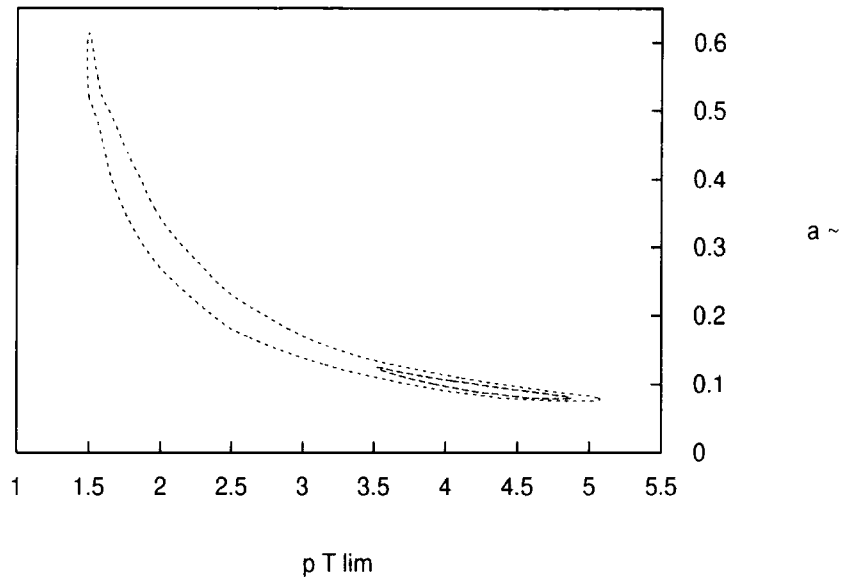

Figure 5.11: The contours of equal χ^2 in the $\tilde{a}$, $p_{\mathrm{T\,lim}}$ plane for the KS p_{T} space approach with the non-perturbative input of the form (5.3.18). Both CDF and D0 data (with separate normalization) for $p_{\mathrm{T}} < 15$ GeV are used here. The outer line is $\chi^2/d.o.f. = 1$, the inner $\chi^2/d.o.f. = 0.75$.

the exponential, linear in $p_{\mathrm{T\,lim}}$. Thus such a function would have a form

$$\tilde{F}_{NP}(p_{\mathrm{T}}) = 1 - \exp(-\tilde{a}p_{\mathrm{T}}^2 - \tilde{d}p_{\mathrm{T}})\,. \tag{5.5.35}$$

Following this analogy to b space, the parameter $\tilde{d}$ would be expected to have dependence on x, whereas $\tilde{a}$ would in general be Q dependent. However we find that introducing the linear term does not yield a great improvement. The value of χ^2 becomes negligibly lower when a very small positive term in $\tilde{d}$ is included in $\tilde{F}^{NP}(p_{\mathrm{T}})$. Unfortunately, an improvement of this size may equally well be caused by the presence of additional parameter in the overall fit. For smaller negative (cf. Fig 5.13) and all positive (cf. Fig 5.14) values of $\tilde{d}$ there is a significant discrepancy between data and theory. Moreover the size of the experimental errors does not allow for a precise enough analysis. In view of the above, we do not find any evidence for the existence of an extra linear term in p_{T} space, using

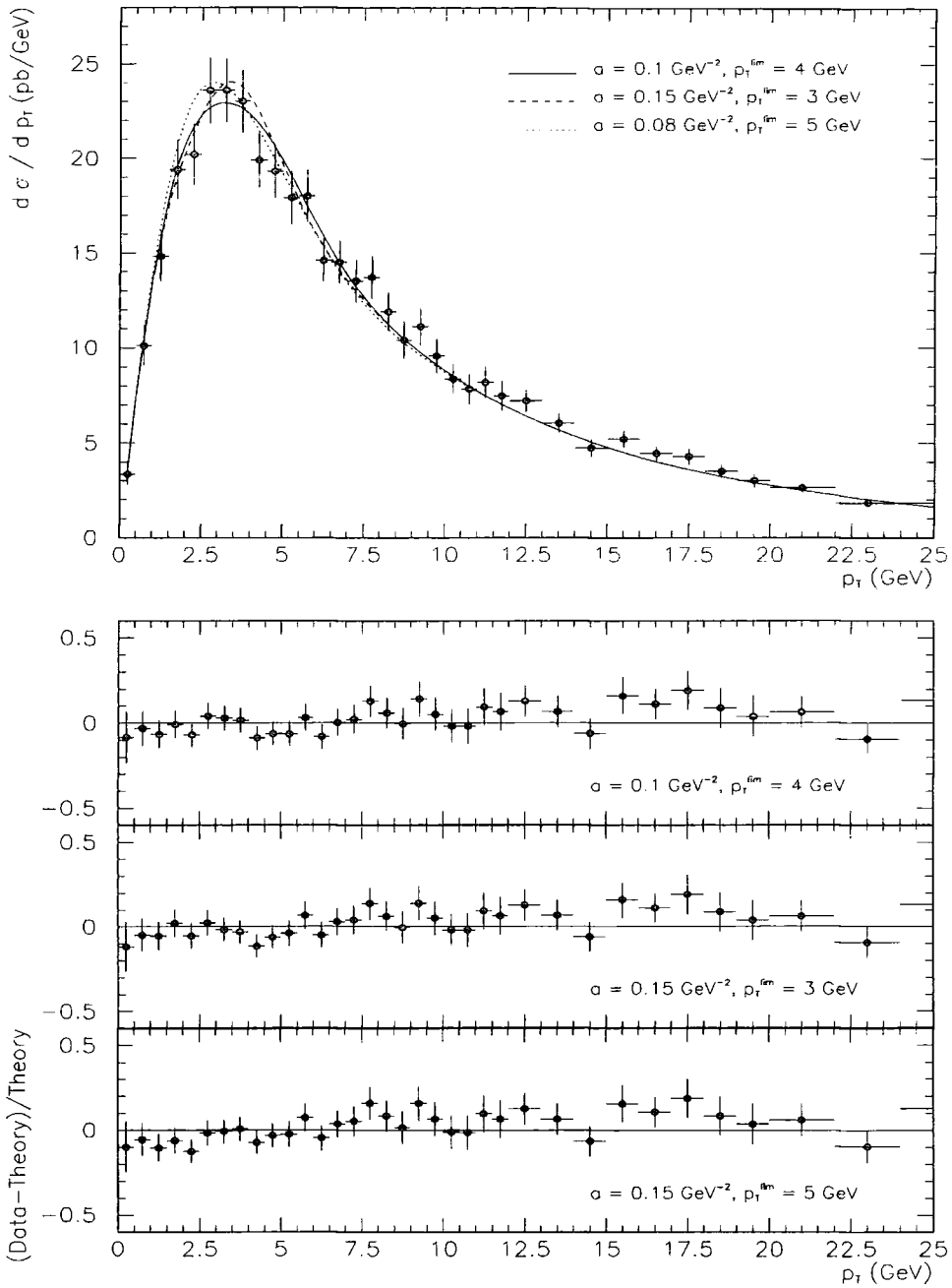

Figure 5.12: Comparison between CDF data and theoretical predictions for the KS approach with various choices of non-perturbative parameters. Also shown are the fractional differences between the data and theory.

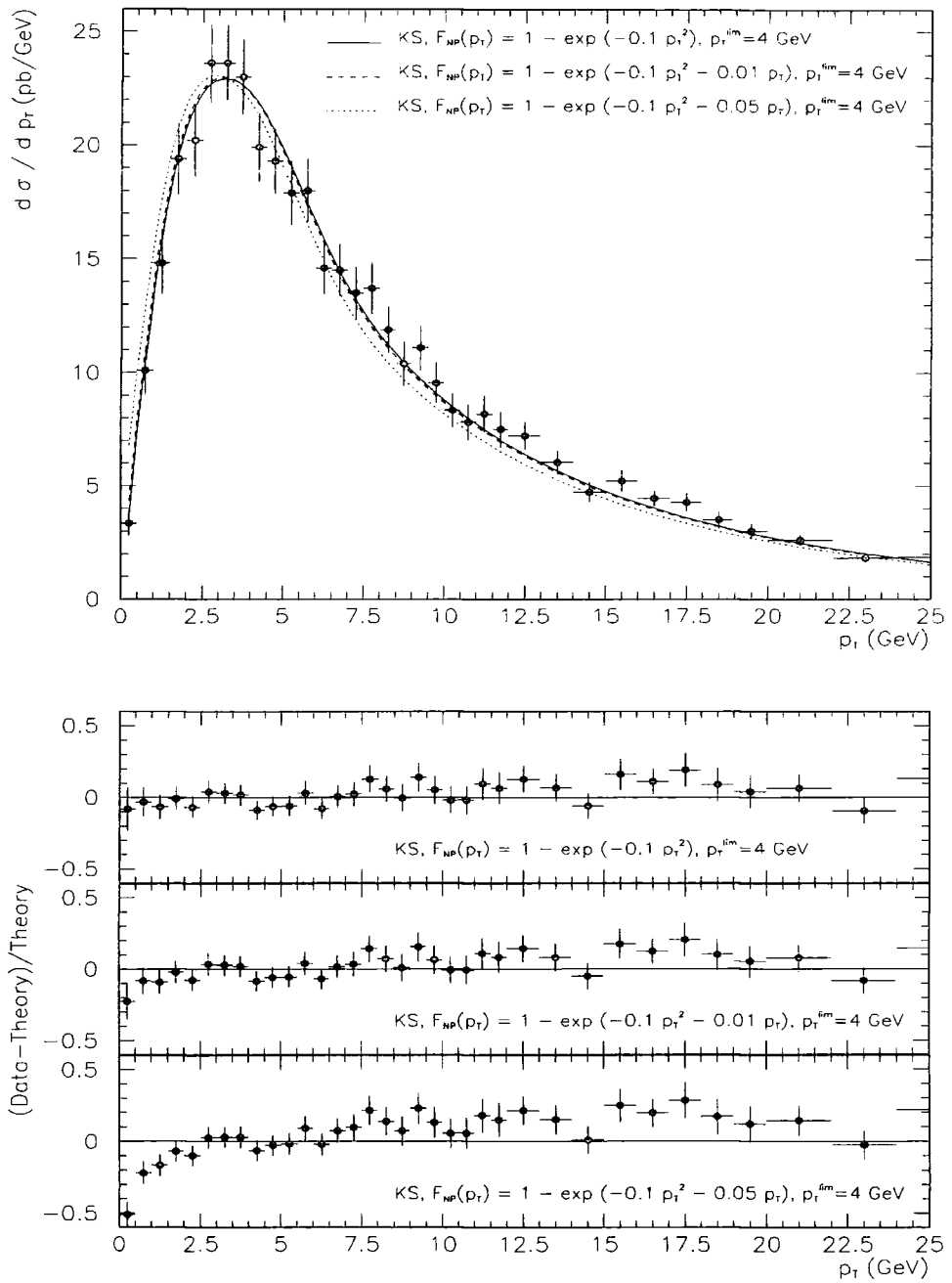

Figure 5.13: Comparison between CDF data and theoretical predictions for the KS approach when the non-perturbative contribution contains a negative linear term. Also shown are the fractional differences between the data and theory.

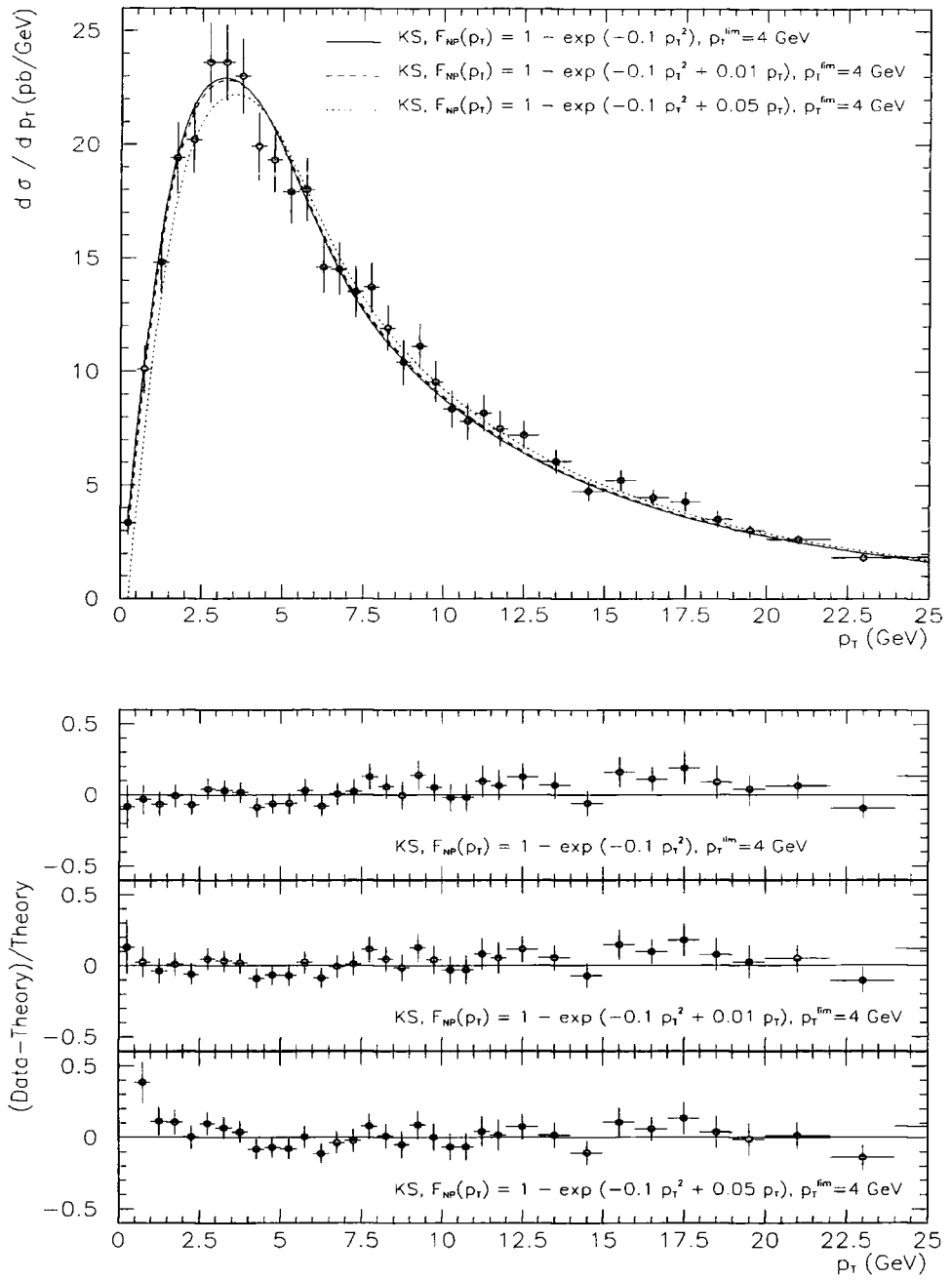

Figure 5.14: Comparison between CDF data and theoretical predictions for the KS approach when the non-perturbative contribution contains a positive linear term. Also shown are the fractional differences between the data and theory.

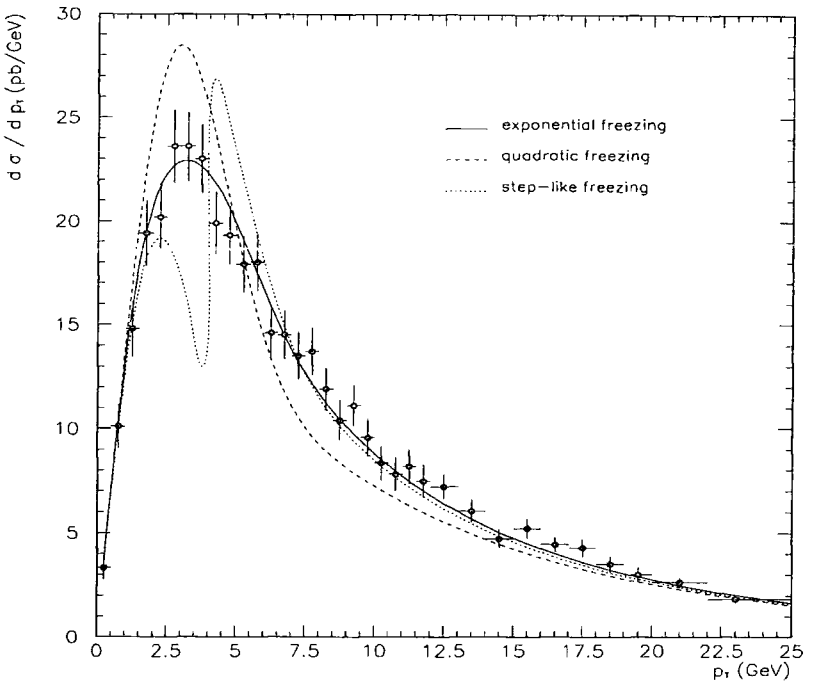

Figure 5.15: Comparison between CDF data and theoretical predictions for the KS approach when various methods of freezing are used (for the standard choice of non-perturbative parameters $\tilde{a} = 0.1$ GeV^{-2}, $p_{\mathrm{T\,lim}} = 4$ GeV).

the (5.3.18) parameterization of the non-perturbative effects.

Freezing method

The results presented so far were obtained using the exponential freezing method (5.3.19). As we pointed out already, there is a problem related to this method, i.e. the risk of producing unphysical distributions for certain values of $\tilde{a}$, $p_{\mathrm{T\,lim}}$ coefficients. In particular, we find out that the previous, derived at the parton level, limit values of the parameters still apply. Although they are not contained in the $\chi^2/d.o.f$ ellipse, they are alarmingly close. Therefore we next turn to investigate distributions obtained with the quadratic method of freezing (5.3.21). Unfortunately, the theoretical curve obtained with this method is in much poorer agreement with the data, cf. Fig 5.15.

Moreover, we could not find other values of the parameters $\tilde{a}$, $p_{\mathrm{T}\,\mathrm{lim}}$ which would result in a better χ^2 fit to the data. Naively one may apply a broad gaussian smearing but that certainly shifts the peak of a distribution towards higher p_{T}.

This lack of success may prompt us to conclude that the current form of $\tilde{F}_{NP}(p_{\mathrm{T}})$ and the choice parton distribution functions requires an exponential method of freezing.

Comparison between b space, p_{T} space results and Z data

In Figs. 5.16, 5.17 we present a comparison between experimental data on Z production as measured by CDF and D0, and a theoretical distribution, calculated using the b space method, EV p_{T} space method and KS p_{T} space method. We observe an agreement between the data and the theoretical predictions for all three methods, in the range of $p_{\mathrm{T}} = 0 \sim 25$ GeV. In general, the b space distribution is more 'peaked' than the p_{T} space equivalents. This effect is, however, very susceptible to the choice of the non-perturbative function and values of the non-perturbative parameters. The b space distribution is also higher in the intermediate range of $p_{\mathrm{T}} = 10 \sim 20$ GeV, where the non-perturbative physics does not influence the resummed perturbative result. In this region the KS distribution approximates the b space result better than the corresponding EV distribution. Given that the KS formalism resums more towers of logarithms than the EV formalism, this is an expected result. The increase of the cross section due to incorporating the fourth, NNNL, tower can be as big as 4% for some values of p_{T}, which remains in agreement with our result at the parton subprocess level, see Chapter 3.

5.5.3 W production at the Fermilab Tevatron

In Section 5.5 we explained some difficulties underlying predicting the W p_{T} distribution. Let us remind the reader that the knowledge of the transverse momentum of the produced W relies on the measurement of the non-leptonic p_{T} in the event, which in turn, carries a large experimental error due to acceptance loss, detector resolution effects and background

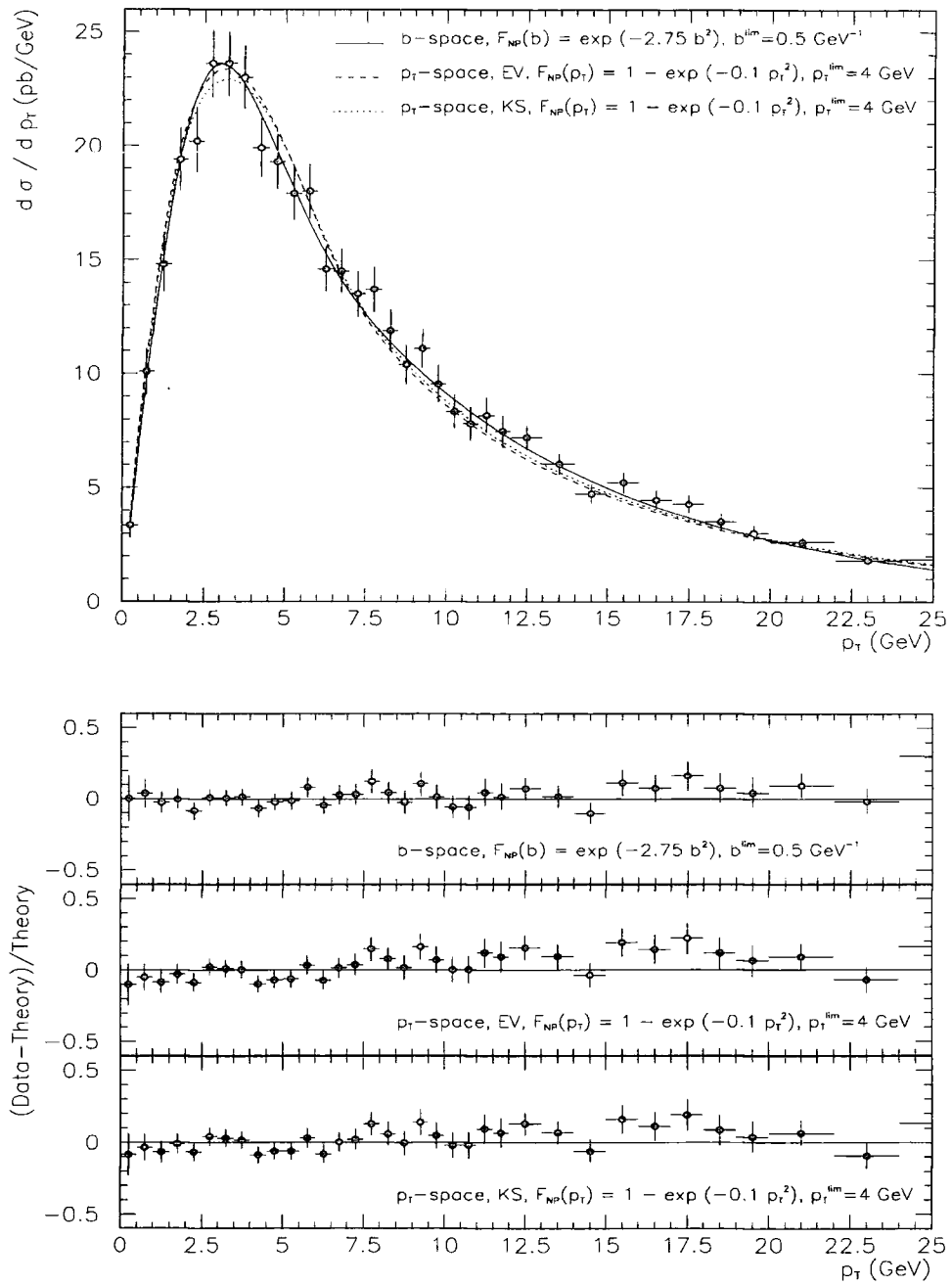

Figure 5.16: Comparison between CDF data and theoretical predictions for the b space method, p_T space method in the EV approach and in the KS approach.

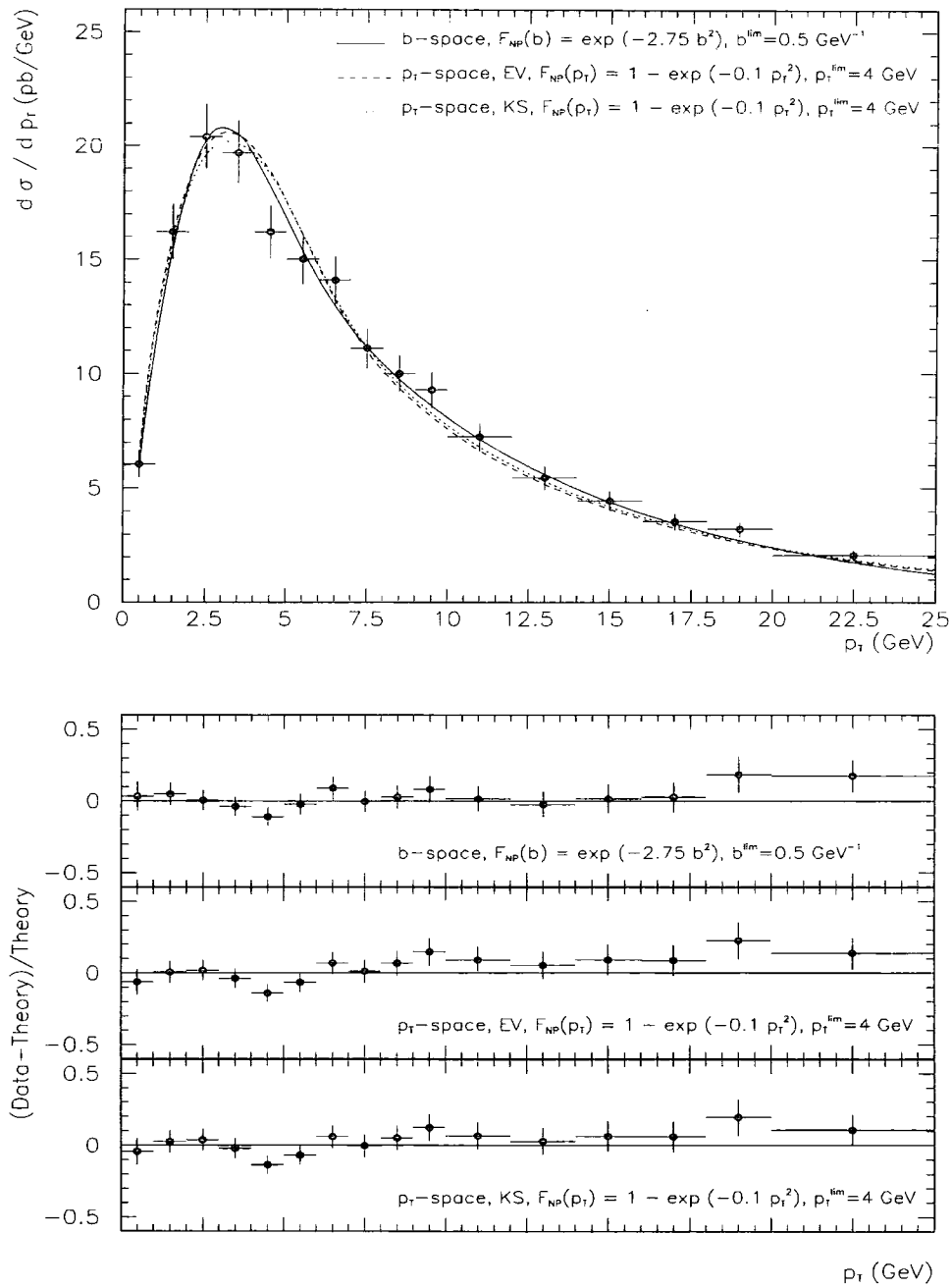

Figure 5.17: Comparison between D0 data and theoretical predictions for the b space method, p_T space method in the EV approach and in the KS approach.

contributions. As a result, the data should be unfolded from these large corrections before making any comparisons with theory. To complicate things further, the corrections depend quite strongly on the W $p_{\rm T}$ distribution, i.e. precisely the quantity one wants to extract. There is only one set of unfolded data on W $p_{\rm T}$ – the very first Run 0 CDF measurement [64], characterised by large statistical uncertainties. The level of difficulty faced when unfolding the $p_{\rm T}$ measurement has gradually become exposed with improving statistics. For that reason the current experiments do not attempt to unfold the data, leaving it rather in a 'raw' form of non-leptonic $p_{\rm T}$. Now, these measurements can still be compared with theory, under the condition that the theoretical distribution is subjected to a detector simulation. This, however, is beyond the scope of this thesis.

In Fig 5.18a we show a comparison between the theoretical predictions and the old (Run 0) CDF unfolded data. Large experimental errors prevent us from making any definite statements, but the resummed part of the cross section reflects the shape of the data and correctly locates the position of the distribution peak. For comparison, we also plot the theoretical predictions versus D0 Run Ia 'raw' data on W $p_{\rm T}$ [65], see Fig 5.18b. It is clear that the data and theory are shifted with respect to each other – an effect of the presence of the unfolding corrections. To obtain the theoretical distributions we use the non-perturbative smearing function of the form (5.3.18) for the EV and KS $p_{\rm T}$ space approaches and (2.6.71) for the b space method together with the same non-perturbative parameters as used for Z production predictions i.e. $\tilde{a} = 0.1$ GeV^{-2} and $p_{\rm T\,lim} = 4$ GeV, $g_2 = 2.75$ GeV^2, respectively. In principle the values of these parameters could change with Q but due to the small difference between M_W and M_Z and the logarithmic dependence on Q one would expect the W non-perturbative parameters to be close to the Z parameters currently used. As such, this should be sufficient for the present analysis.

5.5.4 Ratio of W and Z transverse momentum distributions

The transverse momentum distribution is a basic quantity for extracting the mass of the W. We have discussed problems arising when determining the W $p_{\rm T}$ distribution from the

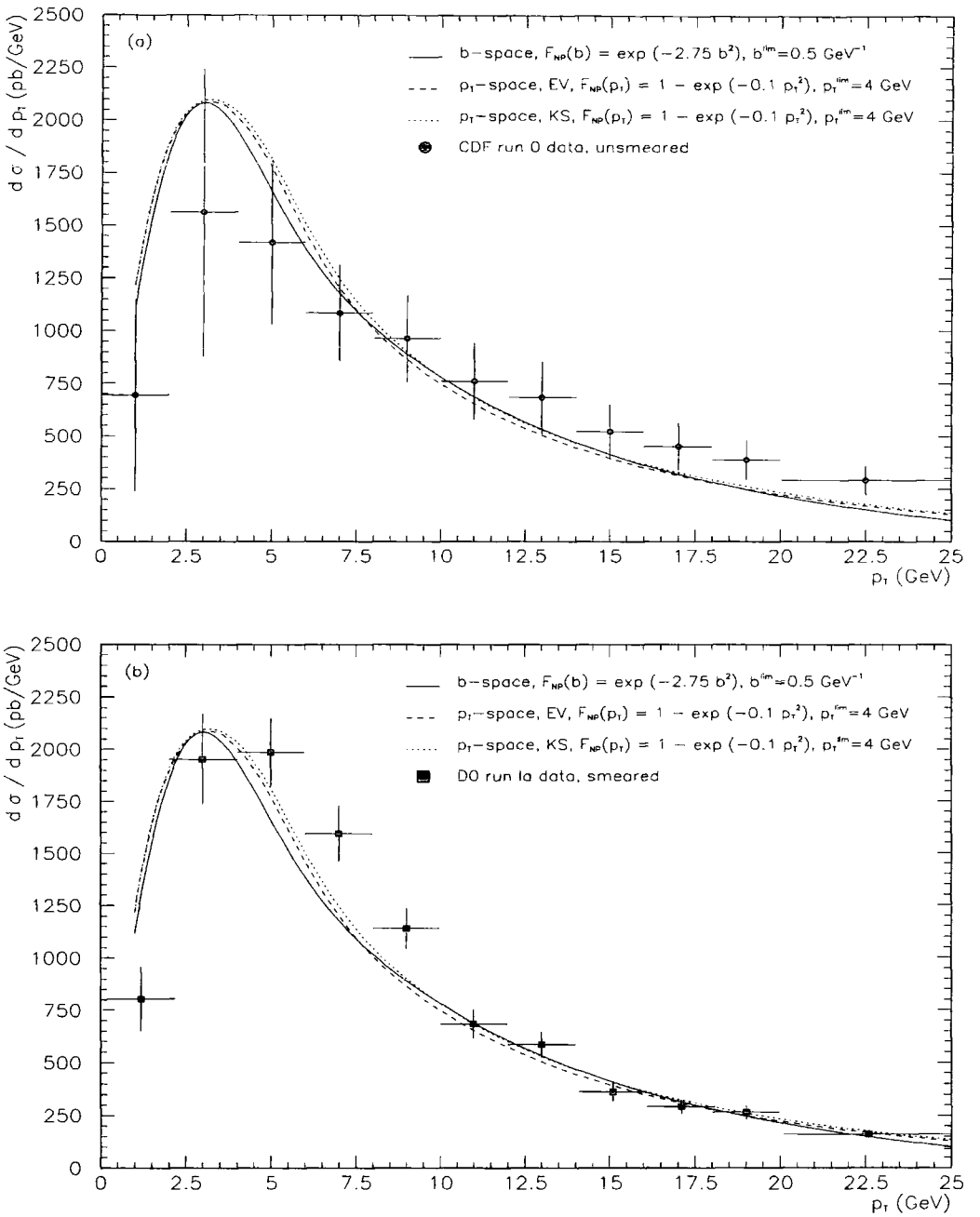

Figure 5.18: (a) Comparison between unfolded CDF W data, Run 0, and theoretical predictions in the b and p_{T} space approach. (b) Comparison between uncorrected W D0 data, Run Ia, and theoretical predictions in the b and p_{T} space approach.

measured data. Because of these problems the present hadron collider analyses use the relatively well measured Z p_{T} distribution and then apply the theoretical ratio of $\frac{d\sigma_W}{dp_{\mathrm{T}}} / \frac{d\sigma_Z}{dp_{\mathrm{T}}}$ to obtain the W p_{T} distribution.

The current Tevatron measurement of M_W, combining the CDF and D0 analyses, is

$$M_W = 80.450 \pm 0.063 \text{ GeV}.$$

With the large amount of luminosity expected for the Run 2 Tevatron programme, a further significant reduction in the W mass uncertainty $\Delta M_W < 20$ MeV will require progress to be made on the number of systematic error sources. (The statistical uncertaintity is expected to be $\sim$ 10 MeV.) At present these errors contribute 25 MeV out of total 60 MeV error. Parton shower Monte Carlo (HERWIG, PYTHIA) predctions, augmented by an exact matrix element calculations at high p_{T}, cf. Chapter 2, provide a reasonable description of the data. However, for a precision W mass measurement it is believed that they do not describe the data accurately enough and one must use theoretical calculations to obtain a W p_{T} distribution. Therefore it is absolutely necessary that the input theoretical quantity $\frac{d\sigma_W}{dp_{\mathrm{T}}} / \frac{d\sigma_Z}{dp_{\mathrm{T}}}$ is well known and does not create a large systematic error. Even more crucial, one has to make certain that it stays robust as p_{T} approaches 0, and an instability of the numerical programs in this particular limit has been reported [66].

It is a well known result [33, 57] that the b space distribution $d\sigma/dp_{\mathrm{T}}^2$ yields a constant intercept at $p_{\mathrm{T}} = 0$, and so does the ratio $\frac{d\sigma_W}{dp_{\mathrm{T}}} / \frac{d\sigma_Z}{dp_{\mathrm{T}}}$. This holds independently of the presence of the non-perturbative contribution. Things are different in the case of the p_{T} space method. Here the limited number of towers of logarithms being summed by the EV and KS methods causes the ratio to be of the type $\frac{0}{0}$. This is because the p_{T} space methods always fail to approximate the b space (which sums all possible towers of logarithms) for small enough p_{T}. In consequence, due to the relation between M_W and M_Z the ratio approaches 0 when $p_{\mathrm{T}} \to 0$, see Fig. 5.19. Note that the KS ratio depart from the stable horizontal line later then the EV ratio, illustrating that inclusion of more towers of logarithms better approximates the b space result. However, when the non-perturbative treatment is introduced, it freezes the perturbative part and damps it with

the smearing function, so that the ratio retains its constant value, cf. Fig. 5.20. More precisely, from (5.3.20)

$$\frac{\frac{d\sigma_W}{dp_{\rm T}}|_{p_{\rm T}=0}}{\frac{d\sigma_Z}{dp_{\rm T}}|_{p_{\rm T}=0}} = \frac{\sum_{qq'} U^W_{qq'} \int_0^1 dx_A\, dx_B\, \delta\left(x_A x_B - \frac{M_W^2}{s}\right) \left\{\Sigma_2(p_{\rm T\,lim}, M_W) f'_{q/A}(x_A, p_{\rm T\,lim})\, f'_{q'/B}(x_B, p_{\rm T\,lim})\right\}}{\sum_{qq'} U^Z_{qq'} \int_0^1 dx_A\, dx_B\, \delta\left(x_A x_B - \frac{M_Z^2}{s}\right) \left\{\Sigma_2(p_{\rm T\,lim}, M_Z) f'_{q/A}(x_A, p_{\rm T\,lim})\, f'_{q'/B}(x_B, p_{\rm T\,lim})\right\}}. \tag{5.5.36}$$

This value is in the proximity of $\sigma^W_{total}/\sigma^Z_{total}$. In fact, it follows from (5.1.10)

$$\frac{\frac{d\sigma_W}{dp_{\rm T}}|_{p_{\rm T}=0}}{\frac{d\sigma_Z}{dp_{\rm T}}|_{p_{\rm T}=0}} \sim \frac{\sigma^{res}_W}{\sigma^{res}_Z}, \tag{5.5.37}$$

where by σ^{res}_V we mean the resummed contribution to the total cross section. The closeness of the $p_{\rm T}$ space and b space results proves the success of the $p_{\rm T}$ space method.

One of the major sources of uncertainty in the ratio relates to the lack of a definitive prescription of how to treat the non-perturbative component. It is clear that the effective non-perturbative parameters e.g. g, $\tilde{a}$ must be different for W and Z production, but we would expect the general form of the non-perturbative function to be the same, together with the 'general' non-perturbative parameters (e.g. g_1, g_2 in (2.5.65)). In principle, they should be extractable from the Z distribution, but how accurately do we know the general form of the non-perturbative function?

5.5.5 Vector boson production at the LHC

QCD dynamics is expected to play an important role at the LHC, both for testing the theoretical predictions and for estimating the background to new physics [16]. Since the W and the Z will be produced profusely at the LHC, it is essential to investigate characteristics of these production processes. The transverse momentum distribution of

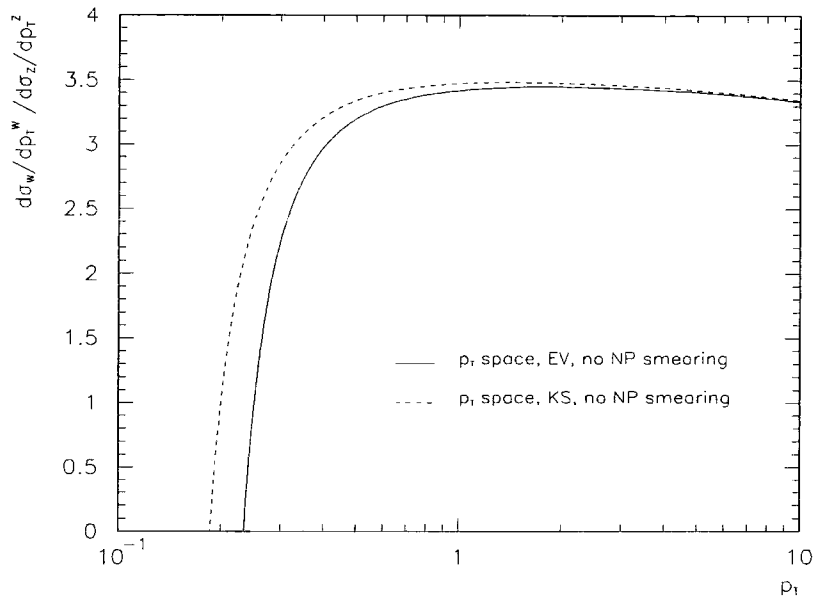

Figure 5.19: Ratio $\frac{d\sigma_W}{dp_T} / \frac{d\sigma_Z}{dp_T}$ for the p_T space calculations when no non-perturbative function is introduced.

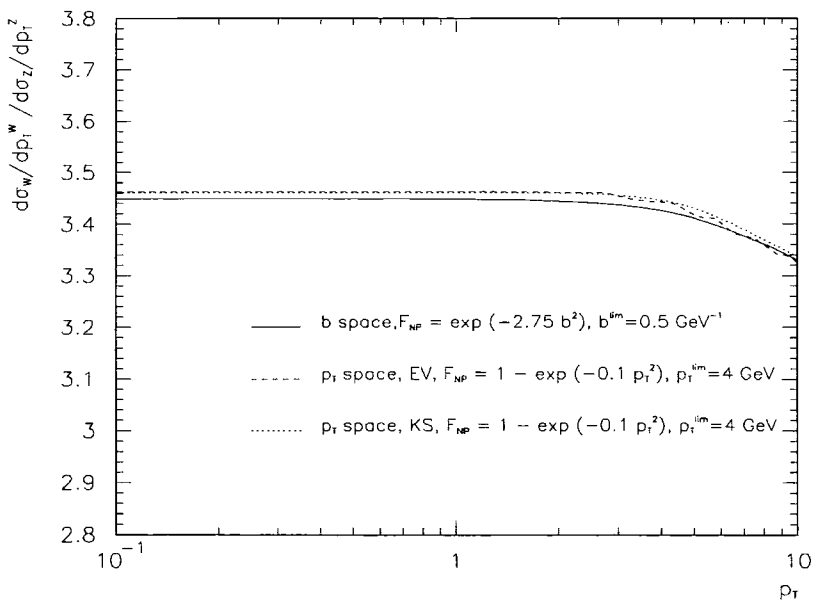

Figure 5.20: Ratio $\frac{d\sigma_W}{dp_T} / \frac{d\sigma_Z}{dp_T}$ for the b and p_T space calculations with nonzero non-perturbative component.

W and Z's, predicted in the $p_{\rm T}$ space formalism (KS), is shown in Fig 5.21. The results agree with similar analyses performed using the b space method [67]. As expected, the shape of the distribution echoes the shape obtained for the distribution at the Tevatron collider. The cross section is naturally higher than the Tevatron cross section though, due to higher parton distributions at smaller x ($x \sim M_V/\sqrt{s}$). For the sake of this analysis we used the standard Tevatron values of the non-perturbative parameters $\tilde{a} = 0.1$ GeV^{-2} and $p_{\rm T\,lim} = 4$ GeV in $p_{\rm T}$ space. This may prove to be a very unwise assumption if the non-perturbative parameterization depends significantly on the partons momenta fractions, for example in the way it was proposed for the b space method (2.5.67).

5.6 Summary

In this Chapter we applied the KS resummation technique in $p_{\rm T}$ space, developed in Chapter 3, to the hadronic production of vector bosons. At the hadron level our approach retains the potential of full resummation of the first four towers of logarithms. Additionally, we discussed how to supplement the hadron-level expressions presented in Section 5.1 with the treatment of the quark mass thresholds and parameterization of non-perturbative effects. The numerical results generally show good agreement with the recent sets of data on Z boson production from the Tevatron collider.

The theoretical uncertainties were examined in Section 5.5.1. For the resummed part of the $d\sigma/dp_{\rm T}$ distribution we observed very small dependence on the renormalization scale μ_R. Much higher uncertainty arises from the error in the value of $\alpha_s(M_Z)$. The remaining sources of theoretical uncertainty include the choice of the factorization scale μ_F, treatment of the quark mass thresholds and the choice of the parameterization of parton distribution functions. We did not attempted to estimate the error due to the non-perturbative parameterization uncertainty. Instead we fitted a simple Gaussian form, proposed originally by the EV collaboration, to the Z boson data. We confirmed the EV values of the parameters $\tilde{a}$, $p_{\rm T\,lim}$. Moreover, we found strong correlations between $\tilde{a}$, $p_{\rm T\,lim}$. This leads us to believe that the next generation of measurements may significantly change

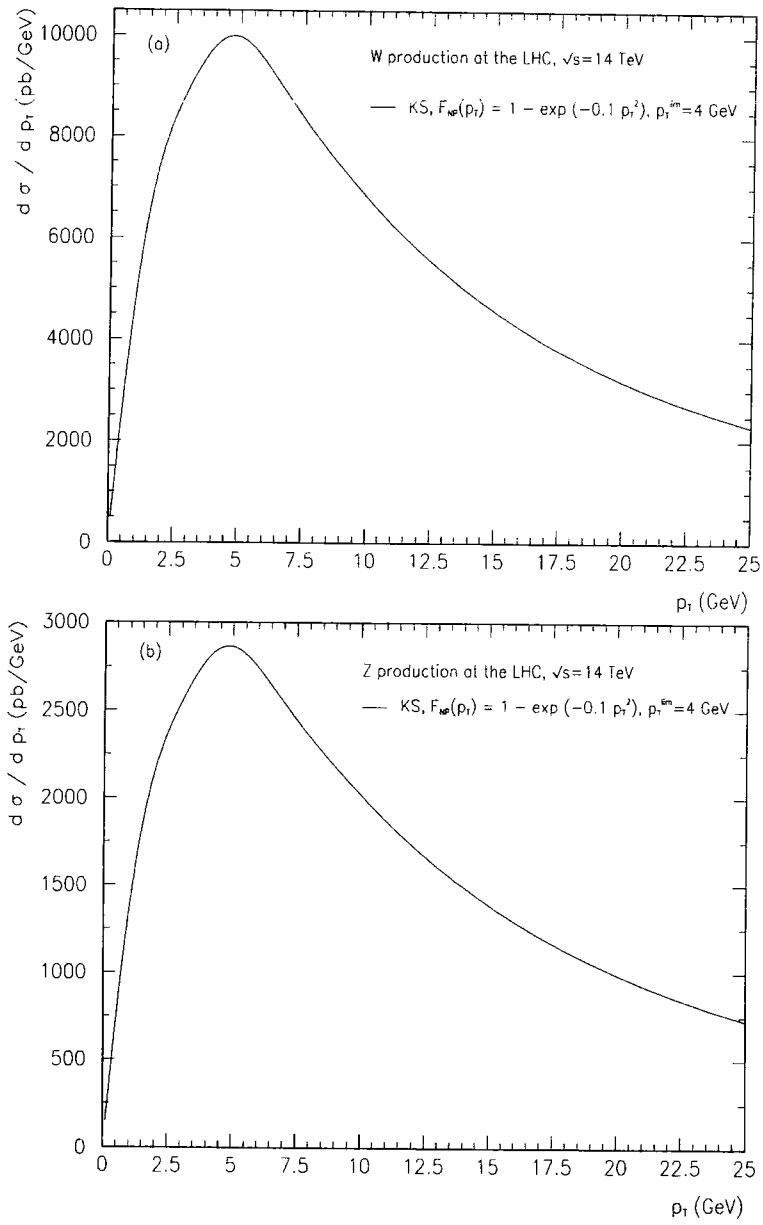

Figure 5.21: p_{T} space predictions (KS formalism) for the transverse momentum distribution at the LHC of: (a) W boson, (b) Z boson.

these values. We also investigated other possible methods of 'freezing' and forms of the non-perturbative function $\tilde{F}^{NP}(p_{\rm T})$. As a result we concluded that in the approach we work with, the exponential freezing combined with the Gaussian form of $\tilde{F}^{NP}(p_{\rm T})$ provides the best fit to the data. We were not able, however, to confirm the necessity of the additional overall smearing. In Section 5.4 another approach for implementing the non-perturbative effects, closely based to the original b space approach, was proposed. The parton level implementation of this approach into the $p_{\rm T}$ space formalism yielded encouraging results.

Due to large experimental errors, the current experimental method of measuring the W $p_{\rm T}$ distribution relies on knowledge of the theoretical ratio $\frac{d\sigma_W}{dp_{\rm T}} / \frac{d\sigma_Z}{dp_{\rm T}}$. In Section 5.5.4 we resolved the existing controversy, showing that the ratio remains constant in the limit $p_{\rm T} \to 0$, as opposed to reported divergent behaviour. Finally we applied our formalism to predict W and Z $p_{\rm T}$ distributions at the LHC.

Chapter 6

Like-Sign W Boson Production at the LHC as a Probe of Double Parton Scattering

In previous chapters we have been discussing electroweak boson production as an example of the Drell-Yan mechanism at the Tevatron and the LHC. At the energies accessible at these machines, in particular at the LHC, another type of scattering phenomenon is expected to significantly contribute to the total cross section: hadron-hadron collisions with multiple parton interactions. Thus, in the case of two (several) electroweak bosons production there would be two competing mechanisms: single scattering and double (multiple) scattering featuring two (several) Drell-Yan processes happening simultaneously. Although both of them result in the same final state, it turns out that they can be differentiated by their production characteristics; for example using the transverse momentum distributions which we have studied in the previous chapters.

In general, multiple parton scattering becomes important as a potential background to many processes of interest at the LHC. For example, it has been pointed out recently [68] that double parton scattering may constitute a significant background to Higgs boson production and decay via the $b\bar{b}$ decay channel, which, for a Higgs mass below the W^+W^-

threshold, is one of the most promising discovery channels. Similar analyses have been also performed in the past for other processes in hadron collisions at lower energies [69]. However, the LHC and its discovery potential necessitates a very accurate estimation of backgrounds where double scattering may provide a significant contribution. Therefore it is essential to obtain a better quantitative understanding of double parton scattering and a more precise estimation of the effect. Of course, this would be the best done using a well-understood Standard Model process. In the case of single scattering processes, the benchmark process at the LHC is W boson production, see for example Ref. [74]. This suggests that W *pair* production could be used to calibrate double parton scattering. In the Standard Model, like-sign W pair production is much smaller than opposite-sign production, which hints that the former channel is the best place to look for additional double scattering contributions.

In the following we will consider the expected cross sections for like- and opposite-sign W pair production at the LHC, from both the single and double scattering mechanisms. We shall also explore differences in the distributions of the final state particles using the results discussed in Chapter 5.

The possibility of double scattering background contributions to like-sign W pair production was noticed some time ago [71], when this process was considered as one of the most promising channels for searching for strong scattering in the electroweak symmetry breaking sector [72].

6.1 Double parton scattering

Double scattering occurs when two different pairs of partons scatter independently in the same hadronic collision, see Fig. 6.1. With increasing collision energy the accessible fractional momenta of the probed partons become smaller (smaller x) whereas the parton distributions become correspondingly higher. Consequently the large flux of partons must result in an increased probability of multiple scattering events. Generally, the many-body

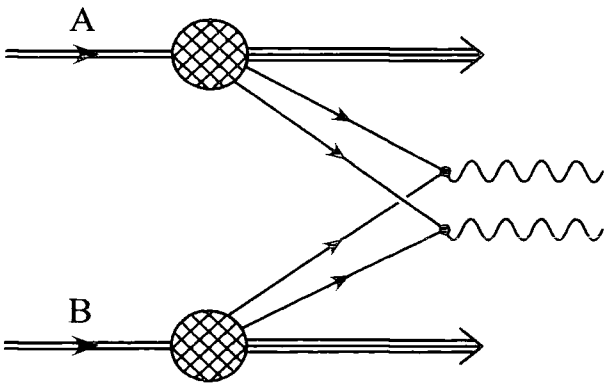

Figure 6.1: Double parton scattering producing two vector bosons in the final state (double Drell-Yan process).

parton distributions considered in the multiple parton scattering are correlated. These parton distributions depend on the fractional momenta of all the interacting partons x and, additionally, on their distance in transverse space $\hat{b}$ which has to be the same for both the target and the projectile partons in order for the collisions to occur. The inclusive cross section of a double parton scattering then reads

$$\sigma_{\mathrm{DS}} = \sum_{i,j,k,l} \int dx_1 dx_2 dx_1' dx_2' d^2b \, \Gamma_A^{ij}(x_1, x_2; \hat{b}) \hat{\sigma}_{ik}^a(x_1, x_1') \hat{\sigma}_{jl}^b(x_2, x_2') \Gamma_B^{kl}(x_1', x_2'; \hat{b}) \qquad (6.1.1)$$

where $\hat{\sigma}^a(x, x')$, $\hat{\sigma}^b(x, x')$ are two distinguishable partonic cross sections and the two-body parton distributions $\Gamma(x_1, x_2; \hat{b})$ contain all non-perturbative information. Thus double scattering probes correlations between partons in the hadron in the transverse plane, providing important additional information on hadron structure [73].

These correlations can be assumed to be negligible if a scattering event is characterized by high centre-of-mass energy and relatively modest partonic subprocess energy, which happens for example in the production of heavy gauge bosons or a Higgs boson at the LHC. Then the two-body parton distribution functions factorise $\Gamma(x_1, x_2; \hat{b}) = f(x_1) f(x_2) F(\hat{b})$ so that $f(x)$ is the usual one-body parton distribution and $F(\hat{b})$ describes the distribution of partons in the transverse plane. This leads to a simplified expression for the double

scattering cross section in the case of two distinguishable parton interactions

$$\sigma_{\rm DS} = \frac{\sigma^a_{\rm SS}\sigma^b_{\rm SS}}{\sigma_{\rm eff}}\,, \tag{6.1.2}$$

If the two interactions are indistinguishable, double counting is avoided by replacing Eq. (6.1.2) with

$$\sigma_{\rm DS} = \frac{\sigma^2_{\rm SS}}{2\sigma_{\rm eff}}\,. \tag{6.1.3}$$

Here $\sigma_{\rm SS}$ represents the single scattering cross section

$$\sigma_{\rm SS} = \sum_{i,j}\int dx_A dx_B f_i(x_A) f_j(x_B)\hat{\sigma}_{ij}\,, \tag{6.1.4}$$

with $f_i(x_A)$ being the standard parton distribution of parton i in hadron A and $\hat{\sigma}_{ij}$ representing the partonic cross section. The parameter $\sigma_{\rm eff} = 1/\int d^2\hat{b}F^2(\hat{b})$, the effective cross section, now contains all information on the spatial distribution of partons in this simplified approach. Depending on the parton spatial density, the probability of hard scattering b taking place given a, $\sigma^b_{\rm SS}/\sigma_{\rm eff}$ in (6.1.2), becomes larger or smaller. In other words, larger $\sigma_{\rm eff}$ means more evenly distributed partons whereas smaller $\sigma_{\rm eff}$ hints that distributions are fairly localised. Since in a double scattering event the different pairs of interacting partons are separated in transverse space by a distance of the order of the hadron radius, $\sigma_{\rm eff}$ represents a rough estimate of the size of the hadron. The geometrical origin of $\sigma_{\rm eff}$ suggests independence on the centre-of-mass energy of the collision and on the nature of the partonic interactions (for a detailed discussion the reader is referred to [73]). The factorisation hypothesis appears to be in agreement with the experimental data on the $p\bar{p}\to\gamma + 3\,jets$ process as measured by the CDF collaboration [70]: in the limited range of experimentally accessible x, $\sigma_{\rm eff}$ shows no evidence for dependence on the fractional momenta. The CDF measurement yields $\sigma_{\rm eff} = 14.5 \pm 1.7^{+1.7}_{-2.3}$ mb and we shall use this value throughout this study.[1] This, in a simple model of proton structure [46], corresponds to the proton radius of 0.73 ± 0.07 fm.

[1] Recently it has been argued that the current value of $\sigma_{\rm eff}$ is significantly smaller than naively expected and indicates the presence of correlation effects [80, 81].

6.2 Total cross sections

The predicted rate of single W production at the LHC is naturally very high, resulting in a significant double scattering cross section. Since the W^+ and W^- single scattering cross sections are comparable in magnitude, the same will be true for the double scattering $\sigma_{\rm DS}(W^+W^+)$, $\sigma_{\rm DS}(W^-W^-)$ and $\sigma_{\rm DS}(W^+W^-)$ cross sections. However, for single scattering we would expect $\sigma(W^-W^-) < \sigma(W^+W^+) \ll \sigma(W^+W^-)$. The reason is that while the latter is $\mathcal{O}(\alpha_W^2)$ at leading order, same-sign inclusive W pair production is a mixed strong-electroweak process with leading contributions of $\mathcal{O}(\alpha_S^2\alpha_W^2)$ and $\mathcal{O}(\alpha_W^4)$. Hence we might expect that like-sign W pair production, with its relatively larger double scattering component, could give a clean measurement of $\sigma_{\rm eff}$.

We begin our analysis by calculating the total single-scattering cross sections for single W and (opposite-sign and like-sign) W pair production in pp and $p\bar{p}$ collisions at scattering energy $\sqrt{s}$. For consistency, we consider only *leading-order* cross sections for all processes studied, i.e. we use leading-order subprocess cross sections with leading-order parton distributions. [2]

As already noted, in the context of leading-order single parton scattering, opposite-sign W pair production in hadron-hadron collisions arises from the $\mathcal{O}(\alpha_W^2)$ subprocess

$$q + \bar{q} \to W^+ + W^- \tag{6.2.5}$$

In contrast, like-sign W pair production is an $\mathcal{O}(\alpha_S^2\alpha_W^2)$ or $\mathcal{O}(\alpha_W^4)$ process at leading order:

$$q + q \to W^+ + W^+ + q' + q' \tag{6.2.6}$$

with $q = u, c, \ldots$, $q' = d, s, \ldots$, together with the corresponding crossed processes. Charge conjugation gives a similar set of subprocesses for W^-W^- production. The Feynman diagrams split into two groups: the first set corresponds to the $\mathcal{O}(\alpha_S^2\alpha_W^2)$ gluon exchange process $qq \to qq$ where a single W is emitted from each of the quark lines, see Fig. 6.2(a).

[2] We note that the full $\mathcal{O}(\alpha_S^2)$ corrections to single W [75] and $\mathcal{O}(\alpha_S)$ corrections to W pair production [76] have been calculated.

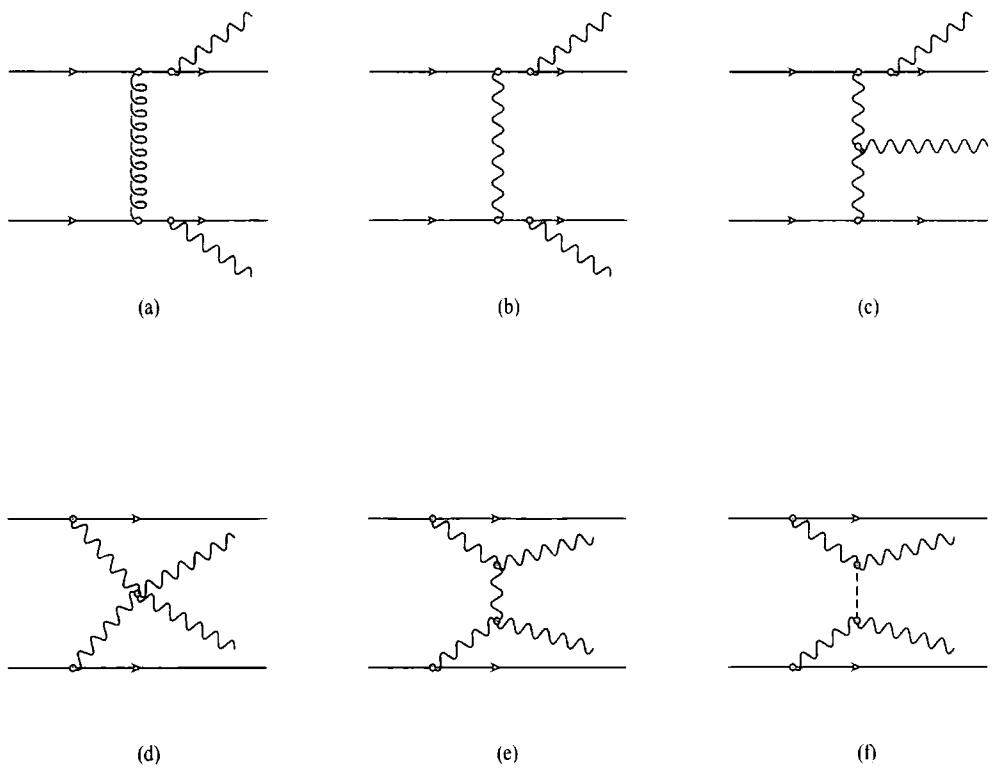

Figure 6.2: Examples of Feynman diagrams for the $uu \to W^+W^+dd$ scattering process, $\mathcal{O}(\alpha_S^2\alpha_W^2)$ (a) and $\mathcal{O}(\alpha_W^4)$ (b-f).

The second, $\mathcal{O}(\alpha_W^4)$, set contains analogous electroweak diagrams, i.e. $t-$channel γ or Z exchange, as well as WW scattering diagrams, including also a $t-$channel Higgs exchange contribution, see Fig. 6.2(b-f). Note that the corresponding cross sections are infra-red and collinear safe: the total rate can be calculated without imposing any cuts on the final-state quark jets. We would therefore expect naive coupling constant power counting to give the correct order of magnitude difference between the like-sign and opposite-sign cross sections, i.e. $\sigma(W^+W^+) \sim \alpha_{S,W}^2\, \sigma(W^+W^-)$. Given the excess of u quarks over d quarks in the proton, we would also expect $\sigma(W^+W^+) > \sigma(W^-W^-)$.

Figure 6.3 shows the total single W and W pair cross sections in proton–antiproton and proton–proton collisions as a function of the collider energy. No branching ratios are

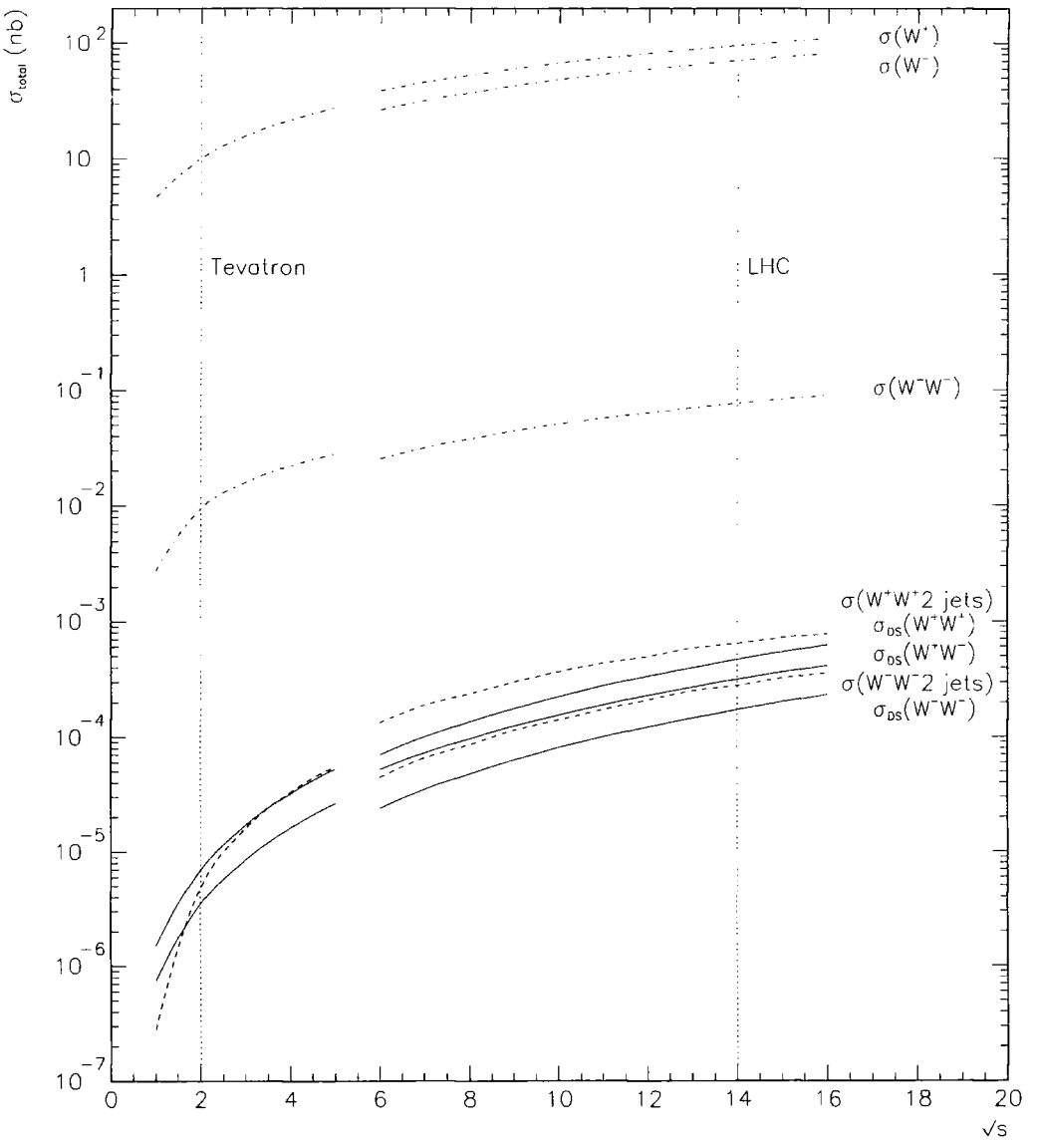

Figure 6.3: Total cross sections for single W and W pair production in pp (in the range 6-16 TeV) and $p\bar{p}$ (in the range 1-5 TeV)collisions. The dashed and dot-dashed lines correspond to single parton scattering, and the solid lines to double parton scattering assuming $\sigma_{\text{eff}} = 14.5$ mb.

included, and there are no cuts on any of the final state particles. The matrix elements are obtained using MADGRAPH [77] and HELAS [78]. We use the MRST leading-order parton distributions from Ref. [74], and the most recent values for the electroweak parameters. [3] Note that for $p\bar{p}$ collisions, $\sigma(W^+) \equiv \sigma(W^-)$ and $\sigma(W^+W^+) \equiv \sigma(W^-W^-)$. The like-sign and opposite-sign cross sections differ by about two orders of magnitude, as expected. Despite the fact that $\alpha_S > \alpha_W$, the electroweak contribution to the single scattering like-sign WW production cross section is similar in size to the strong contribution. This is due to the relatively large number of diagrams (e.g. 86 for $uu \to W^+W^+dd$), as compared to the gluon exchange contribution (16 for the same process). A total annual luminosity of $\mathcal{L} = 10^5$ pb^{-1} at the LHC would yield approximately 65 thousand W^+W^+ events and 29 thousand W^-W^- events, before high-order corrections, branching ratios and acceptance cuts are included, see Table 6.1.

	$N(W^+W^-)$	$N(W^+W^+)$	$N(W^-W^-)$
single scattering	7,500,000	65,000	29,000
double scattering	46,000	31,000	17,000

Table 6.1: The expected number of WW events expected for $\mathcal{L} = 10^5$ pb^{-1} at the LHC from single and double scattering, assuming $\sigma_{\text{eff}} = 14.5$ mb for the latter.

We turn now to the double parton scattering cross sections. As discussed above, we estimate these by simply multiplying the corresponding single scattering cross sections and normalising by $2\sigma_{\text{eff}}$ for the like-sign W pair production, see Eq. 6.1.3 and σ_{eff} for the opposite-sign case, Eq. 6.1.2. The factorisation assumption holds since the energy required to produce a vector boson is much lower than the overall centre of mass energy. Figure 6.3 shows the resulting total $\sigma_{\text{DS}}(W^+W^-)$ and $\sigma_{\text{DS}}(W^\pm W^\pm)$ cross sections as a function of $\sqrt{s}$. Note that for $p\bar{p}$ reactions $\sigma_{\text{DS}}(W^+W^+) \equiv \sigma_{\text{DS}}(W^-W^-) \neq \sigma_{\text{DS}}(W^+W^-)$.

[3] Note that the same-sign cross sections are weakly dependent on the Higgs mass: varying the mass from $M_H = 125$ GeV to $M_H = 150$ GeV leads to only a 2% change in the total rate at the LHC. We use $M_H = 125$ GeV as the default value.

The opposite-sign single scattering and double scattering cross sections differ by two orders of magnitude. However for like-sign W^+W^+ (W^-W^-) production the double scattering contribution is only a factor 2.1 (1.7) smaller than the single scattering contribution, cf. Table 6.1. [4] A simple consequence of the quadratic dependence of $\sigma_{\rm DS}$ on $\sigma_{\rm SS}$, the double scattering cross section increases faster with collision energy $\sqrt{s}$ than single scattering .

6.3 Production characteristics

The production characteristics of the Ws in like- and opposite-sign single scattering production are somewhat different. In particular, the presence of two jets in the final state for the former leads to a broader transverse momentum distribution, as illustrated in Fig. 6.4. Also of interest is the jet transverse momentum distribution in $W^\pm W^\pm$ production, shown in Fig. 6.5. This indicates that a significant fraction of the jets would pass a detection p_T threshold, and could be used as an additional 'tag' for like-sign single scattering production. Of course one also expects large p_T jets in opposite-sign W production via higher-order processes, e.g. $q\bar{q} \to W^+W^-g$ at $\mathcal{O}(\alpha_S)$, but these have a steeply falling distribution reflecting the underlying infra-red and collinear singularities at $p_T = 0$.

In turn, a double scattering event signature differs significantly from the single scattering case. In particular, the W transverse momentum distribution from double scattering has a very pronounced, steep peak for small values of p_T (see Fig. 6.4), inherited from the single scattering p_T distribution [5], in contrast to the broader single-scattering distributions. Obviously, similar features will characterize the p_T spectra of leptons originating from W decay, allowing for additional discrimination between double and single scattering events.

[4] In a recent work the authors of [81], consider the dependence of $\sigma_{\rm eff}$ on parton correlations and conclude that its value in the WW channel at the LHC can be almost twice the size assumed here. Clearly, this would result in even smaller double scattering cross sections.

[5] We are assuming here that the non-perturbative 'intrinsic' transverse momentum distributions of the two partons participating in the double parton scattering are uncorrelated.

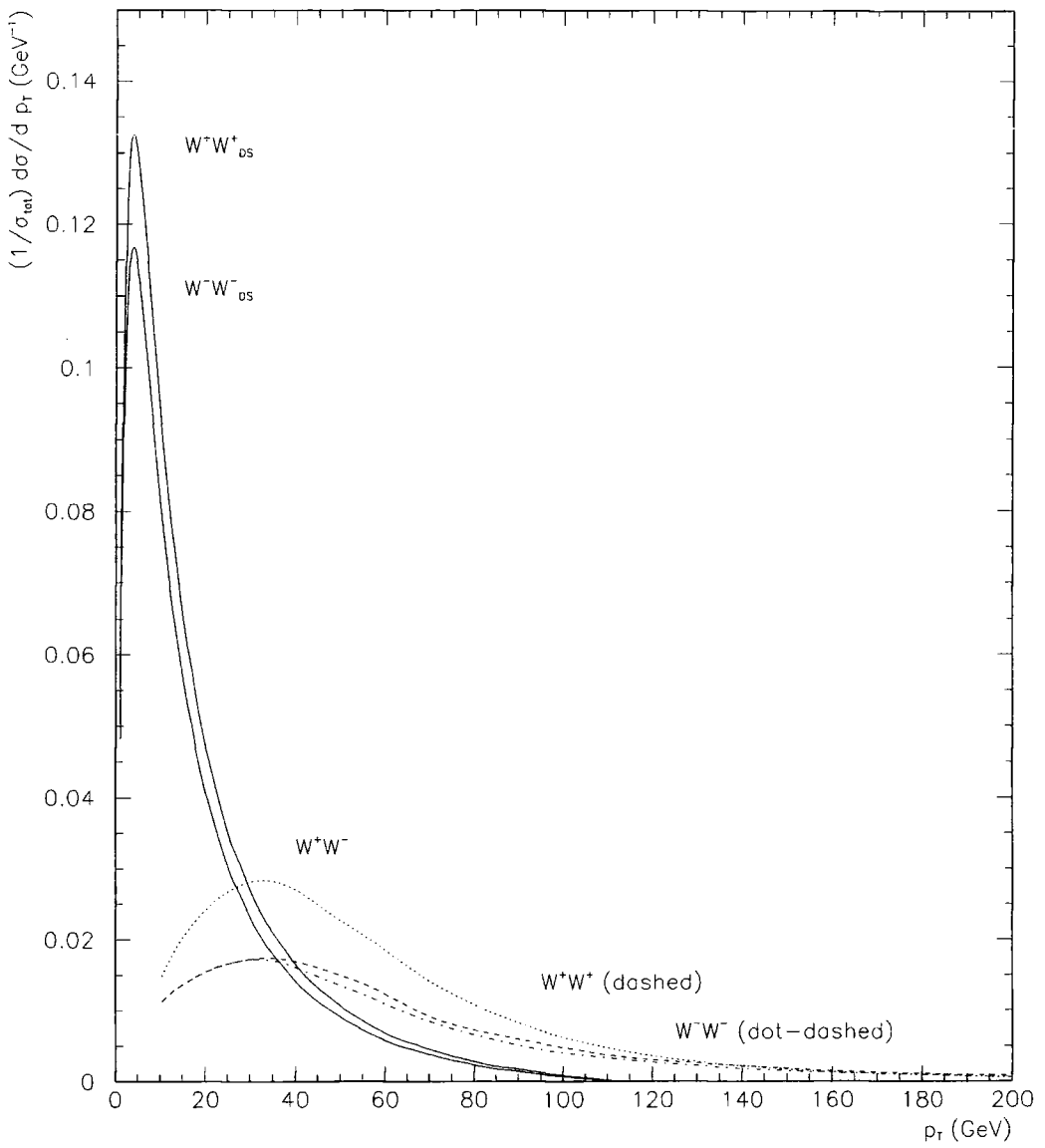

Figure 6.4: Transverse momentum distributions for W^+W^+, W^-W^-, W^+W^- (dashed, dot-dashed and dotted lines, respectively) single parton scattering and W^+W^+, W^-W^- double parton scattering (solid lines) at the LHC. The double scattering predictions are obtained using the p_T-space resummation method described in Chapter 5 (with neither smearing nor matching included).

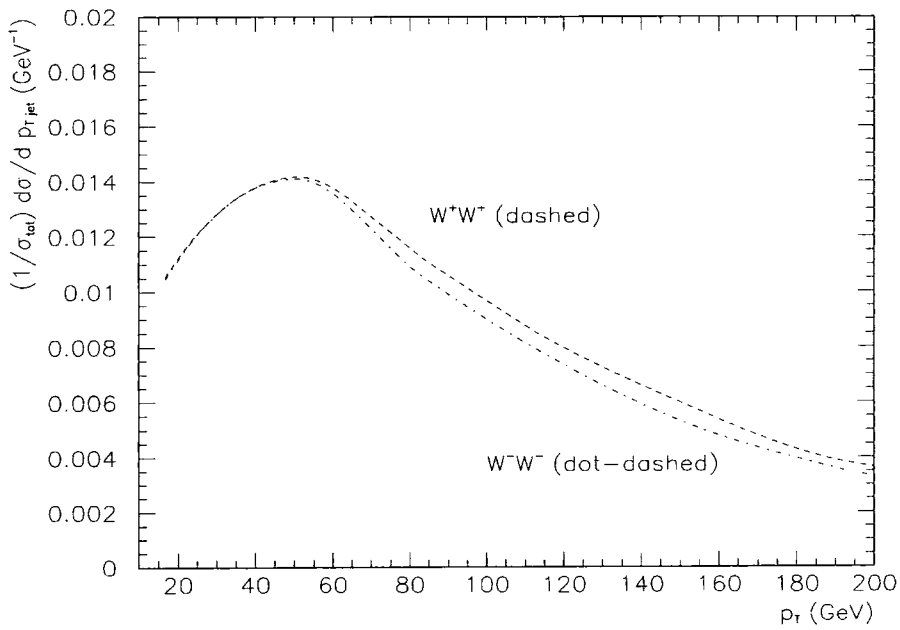

Figure 6.5: Jet transverse momentum distributions in like-sign single scattering WW production at the LHC.

6.4 Measurement of $\sigma_{\rm eff}$ at the LHC

We conclude that the absolute rate of like-sign W^+W^+ and W^-W^- pair production can provide a relatively clean measure of $\sigma_{\rm eff}$ at LHC energies. Table 6.1 summarizes the number of expected events in the various WW channels (recall these are leading-order estimates only, with no branching ratios), assuming $\sigma_{\rm eff} = 14.5$ mb. However, since the absolute event rates shown in Table 6.1 are sensitive to overall measurement and theoretical uncertainties, it may be more useful to consider cross section *ratios*. Consider for example the ratio of the like- to opposite-sign event rates

$$\begin{aligned} \mathcal{R} &= \frac{N(W^+W^+) + N(W^-W^-)}{N(W^+W^-)} \\ &= \frac{\sigma(W^+W^+) + \sigma(W^-W^-) + (2\sigma_{\rm eff})^{-1}\left[\sigma(W^+)^2 + \sigma(W^-)^2\right]}{\sigma(W^+W^-) + \sigma_{\rm eff}^{-1}\sigma(W^+)\sigma(W^-)} \end{aligned} \tag{6.4.7}$$

with both single and double scattering contributions included. The ratio $\mathcal{R}$ for the LHC is shown as a function of $\sigma_{\rm eff}$ in Fig. 6.6.

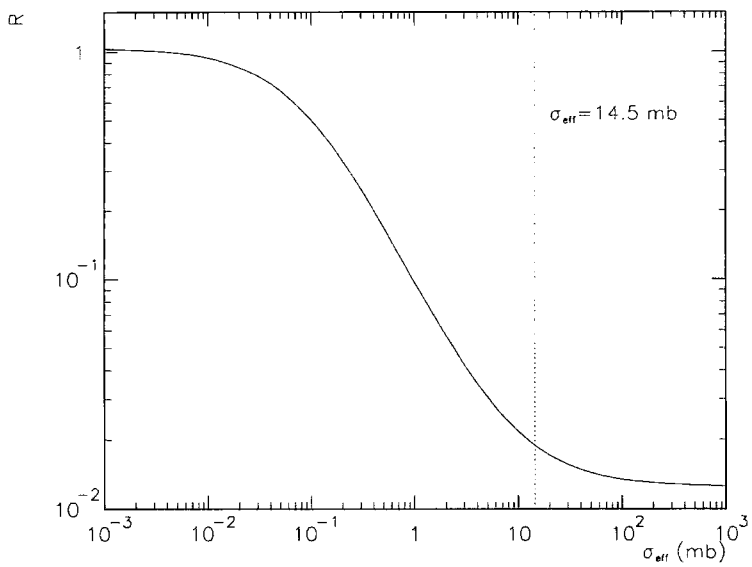

Figure 6.6: The dependence of the ratio $\mathcal{R}$ of like-sign to opposite-sign W pair event rates on the effective cross section $\sigma_{\rm eff}$ at the LHC.

The limit $\sigma_{\text{eff}} \to \infty$ corresponds to the (very small, $\mathcal{R} = 0.0125$) single scattering ratio,

$$\mathcal{R} = \frac{\sigma(W^+W^+) + \sigma(W^-W^-)}{\sigma(W^+W^-)},$$

while $\sigma_{\text{eff}} \to 0$ corresponds to the ratio (≈ 1.05) of the *single* W production cross sections in pp collisions,

$$\mathcal{R} = \frac{1}{2}\left(\frac{\sigma(W^+)}{\sigma(W^-)} + \frac{\sigma(W^-)}{\sigma(W^+)}\right).$$

The CDF measured value [46] of $\sigma_{\text{eff}} = 14.5$ mb gives $\mathcal{R} = 0.019$.

6.5 Summary and outlook

In conclusion, we have shown that like-sign W pair production provides a relatively clean environment for searching for and calibrating double parton scattering at the LHC. A measurement of σ_{eff} from this process would allow the double scattering backgrounds to new physics searches to be calibrated with precision. In this brief study we have concentrated on overall total event rates. An interesting next step would be to perform more detailed Monte Carlo studies of the various production processes, taking into account the W decays, experimental acceptance cuts, etc. In fact it would not be difficult to devise additional cuts to enhance the double scattering contribution. We see from Fig. 6.4, for example, that a cut of $p_T(W) < \mathcal{O}(20\text{ GeV})$ would remove most of the single scattering events while leaving the double scattering contribution largely intact.

Chapter 7

Conclusions and outlook

The main objective of this thesis has been to study theoretical aspects of electroweak boson production at hadron-hadron colliders in the framework of Quantum Chromodynamics. With the large data samples already gathered by the Tevatron collider, and even larger expected over the course of Run II and at the LHC, the accurate theoretical description of the production process becomes an imperative. In fixed-order perturbation theory, the differential distributions for the Drell-Yan process are known up to the NLO. Nevertheless, sufficiently less inclusive distributions may still demonstrate divergent behaviour in certain kinematical regions, no matter up to which order in perturbation theory they are calculated. The divergent behaviour arises as a mathematical reflection of the emission of soft gluons, predicted by QCD.

The key observation that was used in this thesis is that divergent contributions due to soft gluon radiation can be resummed, so that the distributions under investigation would recover finite values in the whole kinematical region available. This is a general statement that applies to many processes, examples of which we gave in Chapter 1. In that chapter we also explained how resummation is performed by the means of reorganizing the perturbative series in terms of towers of logarithms. Resummation of soft contributions can be understood as a successful attempt towards improving perturbative predictions, when the fixed-order perturbation theory calculations become precipitously difficult to

perform. When matched with available conventional, fixed-order in α_s results, the resummed expression encapsulates almost all the knowledge stemming from perturbation theory.

Much of the work presented in this thesis focused on theoretical predictions for one particular observable, that is for the transverse momentum distribution of electroweak gauge bosons produced in hadronic collisions. As we have shown in Chapter 2, the gluon emission manifests itself in the presence of logarithmic terms $\ln(Q^2/p_{\rm T}^2)$ in the $p_{\rm T}$ distribution. These terms diverge in the limit $p_{\rm T}\to 0$. In particular, radiation of soft and collinear gluons contributes double logarithmic factors $\sim \alpha_s^N \ln^{2N-1}(Q^2/p_{\rm T}^2)$. Resummation of all terms at least as singular as $1/p_{\rm T}^2$ has been proved to take place in the impact parameter b space, Fourier conjugated to $p_{\rm T}$ space. We have briefly presented a derivation of the b space formalism (CSS formalism) in Chapter 2. The b space method, although immensely successful theoretically, suffers from ambiguities when performing the matching procedure with the fixed-order result. Owing to the way in which the logarithms are resummed in b space, the matching is bound to fail. Moreover, there appear additional problems, related to the effects outside the perturbative regime. Therefore, in order to be applied phenomenologically, the CSS formalism needs to be enriched with arbitrary prescriptions, some of which we discussed in Chapter 2.

From the shortcomings of the original b space method arose the idea of utilising the b space expression for deriving a resummed expression which would sum logarithmic terms directly in $p_{\rm T}$ space. The ancestor of this idea, the $p_{\rm T}$ space DLLA resummation, was found very difficult to extend by including larger number of sub-leading logarithmic towers. In this light the b space method provides a way to improve the 'simple' double leading logarithm resummation in $p_{\rm T}$ space. The $p_{\rm T}$ space expression allows us to retain control over which $p_{\rm T}$ logarithms are resummed. Due to the form of the b space expression involving the Bessel function, the direct translation of the resummed expression from b space to $p_{\rm T}$ space is technically complicated.

In this thesis we proposed a $p_{\rm T}$ space approximation of the b expression, i.e. the resummed part in the CSS formalism. As demonstrated in Chapter 3, our formalism

resums fully the first four towers of logarithms, including the NNNLL series, the same as in the b space expression. In fact, at the level of the partonic subprocess, it can potentially resum all the known logarithmic terms for any specific finite number of towers. As such, our method differs from the original b space formalism only by terms coming from towers even more sub-leading than that specific number. In particular we argued that our approach correctly takes into account the effects of transverse momentum conservation. Furthermore, the form of our expression ensures that the resummation is valid for values of p_{T} where $\alpha_s \ln(Q^2/p_{\mathrm{T}}^2) \lesssim 1$. After carefully investigating the structure and the behaviour, especially the convergence properties, of our expression, we concluded that it is well suited for phenomenological purposes. This conclusion remains unchanged if sub-leading effects related to the running of the coupling or higher-order perturbative corrections are included. We found that the inclusion of the fourth tower does not change the distribution dramatically and the expected correction is of the order of 3% for Z boson production. When considered at the hadron level, the simplest form of our approach retains the potential of the full resummation of the first four towers of logarithms. The analytical formulae become lengthy but can be implemented into the FORTRAN program. The numerical results discussed in Chapter 5 generally show good agreement with recent sets of data on Z boson production from the Tevatron collider.

Since two other methods of performing resummation in p_{T} space have been proposed almost simultaneously to our method, part of this thesis, i.e. Chapter 4, has been devoted to clarifying differences between the three of them. In particular, our approach has been invented as a natural extension of the EV approach, in the sense of incorporating kinematical logarithms which are missing in the EV resummation. Since the first occurrence of such logarithmic terms takes place in the fourth tower, we differ from the EV method by logarithms coming from the towers more sub-leading than the fourth one. The second method, FNR, results in an expression which resums a different subset of terms: LL and NLL series if the classification is performed inside the Sudakov factor, i.e. in the argument of the exponential. However, it is found that the FNR method suffers from singular behaviour at certain small value of p_{T}. The attempts to systematically include more sub-leading terms in this classification do not improve that behaviour but rather make it even

worse. Hence we consider the theoretical validity, and certainly the phenomenological value of the FNR approach, as questionable.

No resummation formalism can provide predictions for the whole range of p_{T} values without an additional prescription for how to deal with the non-perturbative effects. This is equally true in case of the b space method where such a prescription is necessary for large values of b, or in case of the p_{T} space approach which naturally ceases to be reliable at very small values of p_{T}. Whereas in b space the form of the non-perturbative ansatz function is a topic of current theoretical debate with at least two different models proposed, an equivalent parameterization in p_{T} space has so far not been carefully analysed. In Chapter 5 we studied, first quantitatively at the parton level, then qualitatively for the hadronic process, the simplest possible method of including the non-perturbative effects, proposed by the EV collaboration. We found that their method, relying on the naive implementation of a Gaussian parameterization combined with the exponential 'freezing' method, describes the Tevatron data on Z boson production reasonably well. Assuming the EV non-perturbative prescription, we fitted the p_{T} distribution, calculated using our resummation formalism, to the data. In consequence we confirmed that the best fit is obtained with the EV values of the parameters $\tilde{a}$, $p_{\mathrm{T\,lim}}$. We also observed a strong correlation between these two parameters.

The problem of the accurate parameterization of the non-perturbative effects may need to wait for its resolution until the LHC experiments begin measurements. The cross sections for vector boson production are naturally expected to be much higher at the LHC than at the Tevatron. In Chapter 5, we presented the p_{T} space results for W and Z p_{T} distributions at the LHC. At the LHC energy, in addition to the single scattering processes, the phenomenon of double (multiple) scattering is predicted to take place. In Chapter 6 we investigated the like-sign W pair production process in the context of double scattering. We found that double scattering events significantly contribute to the final state like-sign W pair cross section, thus allowing calibration of the double scattering parameter σ_{eff}. The p_{T} distributions prove to be useful characteristics to distinguish between double scattering and single scattering events.

Outlook

In order to consider the p_{T} space formalism, presented in this thesis, as theoretically complete, some work still remains to be done. First of all, the analytical formulae and numerical programs give results only for the resummed part of the cross section. The matching with the fixed-order expressions, although as explained in Chapter 3 straightforward, still needs to be implemented into this formalism to make it valid for the whole range of p_{T}.

Reliable predictions for the p_{T} distributions at very small p_{T} require incorporating a parameterization of the non-perturbative effects. We believe that the method of including these effects needs to be re-examined, possibly along the lines of a new method proposed in Section 5.4, based on the theoretically more sound grounds than the phenomenological prescription of Section 5.3. The method should be investigated in more detail, specifically applied to the hadronic cross section, with all coefficients $A^{(1)}$, $A^{(2)}$, $B^{(1)}$, $B^{(2)}$ non-zero and the running coupling. $\tilde{F}^{NP}(p_{\mathrm{T}})$, the p_{T} space form of non-perturbative parameterization, needs to be studied more thoroughly too. The analysis done in Chapter 5, involving fits only to the Tevatron Z data, should be extended, allowing different parameterizations and including additional sets of data, also including data from fixed-target experiments. In particular it is important, especially for the LHC predictions, to correctly parameterize the dependence on Q and x.

A further development of the p_{T} space formalism could incorporate modifications allowing for its application to other processes involving emission of soft gluons. The production of vector boson pairs (e.g. W^+W^-, ZZ, $\gamma\gamma$) in hadron colliders is a straightforward example. Another exciting possibility opens up for the description of Higgs boson production. If the Higgs particle is produced via the vector boson fusion or the associated production channels, then soft gluons are radiated by incoming quarks. This results in the same Sudakov factor as for the vector boson production. The gluon fusion channel requires modifying the Sudákov factor entering the p_{T} space formalism. It also calls for a parameterization of the non-perturbative effects related to the emission of gluons off the initial gluon line. If the Higgs boson is found at the Tevatron or the LHC, the p_{T}

distribution will certainly be one of the first production characteristics to investigate. Given the current expectations of the relatively low Higgs boson mass, and the prospect of intensified searches at the Run II Tevatron and the LHC, we should look forward to revisiting the issue of the p_{T} space resummation in this new context.

Appendix A

Expressions for coefficients in the $p_{\rm T}$ method

In this appendix we list expressions for $\mathcal{S}_\eta$ and the c_i coefficients in (3.2.19), for the choice of the renormalization scale $\mu^2 = Q^{2/3} p_{\rm T}^{4/3}$. Here $L = \ln(Q^2/p_{\rm T}^2)$, $\alpha_s = \alpha_s(\mu^2)$.

$$
\begin{aligned}
\mathcal{S}_\eta \;=\; & -\frac{1}{2}\lambda\Bigg[\frac{1}{270}\,\frac{\alpha_s^5\,{\beta_0}^4\,A^{(2)}}{\pi^5\,A^{(1)}}\,L^6 \\
& + \Big(-\frac{1}{135}\,\frac{{\beta_0}^3\,\alpha_s^4\,A^{(2)}}{\pi^4\,A^{(1)}} - 4\,\pi\Big(\frac{1}{540}\,\frac{{\beta_0}^2\,\beta_1\,A^{(2)}}{\pi^6\,A^{(1)}} - \frac{11}{1620}\,\frac{{\beta_0}^4\,B^{(2)}}{\pi^6\,A^{(1)}}\Big)\,\alpha_s^5\Big)\,L^5 \\
& + \Big(\frac{1}{12}\,\frac{{\beta_0}^2\,\alpha_s^3\,A^{(2)}}{\pi^3\,A^{(1)}} - 4\,\pi\Big(-\frac{1}{144}\,\frac{{\beta_1}^2\,A^{(2)}}{\pi^6\,A^{(1)}} + \frac{5}{216}\,\frac{{\beta_0}^2\,\beta_1\,B^{(2)}}{\pi^6\,A^{(1)}}\Big)\,\alpha_s^5 \\
& \quad - 4\,\pi\Big(-\frac{1}{72}\,\frac{\beta_0\,\beta_1\,A^{(2)}}{\pi^5\,A^{(1)}} + \frac{5}{216}\,\frac{{\beta_0}^3\,B^{(2)}}{\pi^5\,A^{(1)}}\Big)\,\alpha_s^4 + \frac{1}{18}\,\frac{{\beta_0}^2\,\alpha_s^2}{\pi^2}\Big)L^4 \\
& + \Big(\frac{1}{9}\,\frac{{\beta_1}^2\,\alpha_s^5\,B^{(2)}}{\pi^5\,A^{(1)}} + \frac{2}{9}\,\frac{\beta_0\,\beta_1\,\alpha_s^4\,B^{(2)}}{\pi^4\,A^{(1)}} + \frac{1}{3}\,\frac{{\beta_0}^2\,\alpha_s^3\,B^{(2)}}{\pi^3\,A^{(1)}} + \frac{2}{9}\,\frac{\alpha_s^2\,{\beta_0}^2\,B^{(1)}}{\pi^2\,A^{(1)}}\Big)\,L^3 \\
& + \Big(-\frac{1}{3}\,\frac{\beta_1\,\alpha_s^3\,B^{(2)}}{\pi^3\,A^{(1)}} - 4\,\pi\Big(\frac{1}{12}\,\frac{\beta_0\,B^{(2)}}{\pi^3\,A^{(1)}} + \frac{1}{12}\,\frac{\beta_1\,B^{(1)}}{\pi^3\,A^{(1)}}\Big)\,\alpha_s^2 \\
& \quad -4\,\pi\Big(-\frac{1}{8}\,\frac{A^{(2)}}{\pi^2\,A^{(1)}} + \frac{1}{12}\,\frac{\beta_0\,B^{(1)}}{\pi^2\,A^{(1)}}\Big)\,\alpha_s + 1\Big)L^2 \\
& + \Big(\frac{\alpha_s\,B^{(2)}}{\pi\,A^{(1)}} + 2\,\frac{B^{(1)}}{A^{(1)}}\Big)\,L\Bigg],
\end{aligned}
$$

$$
\begin{aligned}
c_1 = & \left(\frac{1}{18} \frac{\beta_1^2 B^{(2)} L^2}{\pi^5 A^{(1)}} + \frac{1}{30} \frac{\left(\frac{10}{9} \frac{\beta_0^2 \beta_1 B^{(2)}}{A^{(1)}} + \frac{5}{3} \frac{\beta_1^2 A^{(2)}}{A1^{(1)}} \right) L^3}{\pi^5} \right. \\
& + \frac{1}{30} \frac{\left(\frac{5}{27} \frac{\beta_0^4 B^{(2)}}{A^{(1)}} + \frac{10}{9} \frac{\beta_0^2 \beta_1 A^{(2)}}{A^{(1)}} \right) L^4}{\pi^5} + \frac{1}{162} \frac{L^5 \beta_0^4 A^{(2)}}{\pi^5 A^{(1)}} \Bigg) \alpha_s^5 \\
& + \left(\frac{1}{9} \frac{\beta_0 \beta_1 B^{(2)} L^2}{\pi^4 A^{(1)}} + \frac{1}{27} \frac{\beta_0^3 A^{(2)} L^4}{\pi^4 A^{(1)}} + \frac{1}{30} \frac{\left(\frac{10}{9} \frac{\pi \beta 0^3 B^{(2)}}{A^{(1)}} + \frac{10}{3} \frac{\pi \beta_0 \beta_1 A^{(2)}}{A^{(1)}} \right) L^3}{\pi^5} \right) \alpha_s^4 \\
& + \left(\frac{1}{3} \frac{\beta_1 B^{(2)} L}{\pi^3 A^{(1)}} + \frac{1}{30} \frac{\left(5 \frac{\pi^2 \beta_0^2 B^{(2)}}{A^{(1)}} + 10 \frac{\pi^2 \beta_1 A^{(2)}}{A^{(1)}} \right) L^2}{\pi^5} + \frac{1}{6} \frac{\beta_0^2 A^{(2)} L^3}{\pi^3 A^{(1)}} \right) \alpha_s^3 \\
& + \left(\frac{1}{30} \frac{\left(10 \frac{\pi^3 \beta_0 B^{(2)}}{A^{(1)}} + 10 \frac{\pi^3 \beta_1 B^{(1)}}{A^{(1)}} \right) L}{\pi^5} \right. \\
& + \frac{1}{30} \frac{\left(\frac{10}{3} \frac{\pi^3 \beta_0^2 B^{(1)}}{A^{(1)}} + 10 \frac{\pi^3 \beta_0 A^{(2)}}{A^{(1)}} + 10 \pi^3 \beta_1 \right) L^2}{\pi^5} + \frac{1}{9} \frac{\beta_0^2 L^3}{\pi^2} \Bigg) \alpha_s^2 \\
& + \left(\frac{1}{30} \frac{\left(10 \frac{\pi^4 \beta 0 B^{(1)}}{A^{(1)}} + 15 \frac{\pi^4 A^{(2)}}{A^{(1)}} \right) L}{\pi^5} + \frac{1}{3} \frac{\beta_0 L^2}{\pi} + \frac{1}{2} \frac{B^{(2)}}{\pi A^{(1)}} \right) \alpha_s + L + \frac{B^{(1)}}{A^{(1)}} ,
\end{aligned}
$$

$$
\begin{aligned}
c_2 = & \left(\frac{1}{3} \frac{\beta_1^2 B^{(2)} L}{\pi^5 A^{(1)}} + \frac{13}{162} \frac{\beta_0^4 A^{(2)} L^4}{\pi^5 A^{(1)}} + \frac{1}{30} \frac{\left(10 \frac{\beta_0^2 \beta_1 B^{(2)}}{A^{(1)}} + \frac{35}{3} \frac{\beta_1^2 A^{(2)}}{A^{(1)}} \right) L^2}{\pi^5} \right. \\
& + \frac{1}{30} \frac{\left(\frac{20}{9} \frac{\beta_0^4 B^{(2)}}{A^{(1)}} + \frac{100}{9} \frac{\beta_0^2 \beta_1 A^{(2)}}{A^{(1)}} \right) L^3}{\pi^5} \Bigg) \alpha_s^5 \\
& + \left(\frac{2}{3} \frac{\beta_0 \beta_1 B^{(2)} L}{\pi^4 A^{(1)}} + \frac{1}{30} \frac{\left(10 \frac{\pi \beta_0^3 B^{(2)}}{A^{(1)}} + \frac{70}{3} \frac{\pi \beta_0 \beta_1 A^{(2)}}{A^{(1)}} \right) L^2}{\pi^5} + \frac{10}{27} \frac{\beta_0^3 A^{(2)} L^3}{\pi^4 A^{(1)}} \right) \\
& \alpha_s^4 + \left(\frac{\beta_1 B^{(2)}}{\pi^3 A^{(1)}} + \left(\frac{1}{30} \frac{\left(30 \frac{\pi^2 \beta_0^2 B^{(2)}}{A^{(1)}} + 40 \frac{\pi^2 \beta_1 A^{(2)}}{A^{(1)}} \right) L}{\pi^5} + \frac{7}{6} \frac{\beta_0^2 A^{(2)} L^2}{\pi^3 A^{(1)}} \right) \alpha_s^3 \right. \\
& + \left(\frac{1}{30} \frac{30 \frac{\pi^3 \beta_0 B^{(2)}}{A^{(1)}} + 30 \frac{\pi^3 \beta_1 B^{(1)}}{A^{(1)}}}{\pi^5} + \frac{7}{9} \frac{\beta_0^2 L^2}{\pi^2} \right. \\
& \left. \left. + \frac{1}{30} \frac{\left(20 \frac{\pi^3 \beta_0^2 B^{(1)}}{A^{(1)}} + 40 \frac{\pi^3 \beta_0 A^{(2)}}{A^{(1)}} + 40 \pi^3 \beta_1 \right) L}{\pi^5} \right) \alpha_s^2 \right)
\end{aligned}
$$

$$+\left(\frac{1}{30}\,\frac{30\,\frac{\pi^4\,\beta_0\,B^{(1)}}{A^{(1)}}+15\,\frac{\pi^4\,A^{(2)}}{A^{(1)}}}{\pi^5}+\frac{4}{3}\,\frac{\beta_0\,L}{\pi}\right)\,\alpha_s+1\,,$$

$$\begin{aligned}
c_3 = &\left(\frac{1}{30}\,\frac{\left(\frac{40}{3}\,\frac{\beta_0^4\,B^{(2)}}{A^{(1)}}+\frac{160}{3}\,\frac{\beta_0^2\,\beta_1\,A^{(2)}}{A^{(1)}}\right)L^2}{\pi^5}+\frac{44}{81}\,\frac{\beta_0^4\,A^{(2)}\,L^3}{\pi^5\,A^{(1)}}\right.\\
&\left.+\frac{1}{30}\,\frac{\left(40\,\frac{\beta_0^2\,\beta_1\,B^{(2)}}{A^{(1)}}+\frac{100}{3}\,\frac{\beta_1^2\,A^{(2)}}{A^{(1)}}\right)L}{\pi^5}+\frac{2}{3}\,\frac{\beta_1^2\,B^{(2)}}{\pi^5\,A^{(1)}}\right)\alpha_s^5\\
&+\left(\frac{4}{3}\,\frac{\beta_0\,\beta_1\,B^{(2)}}{\pi^4\,A^{(1)}}+\frac{16}{9}\,\frac{\beta_0^3\,A^{(2)}\,L^2}{\pi^4\,A^{(1)}}+\frac{1}{30}\,\frac{\left(40\,\frac{\pi\,\beta_0^3\,B^{(2)}}{A^{(1)}}+\frac{200}{3}\,\frac{\pi\,\beta_0\,\beta_1\,A^{(2)}}{A^{(1)}}\right)L}{\pi^5}\right)\alpha_s^4\\
&+\left(\frac{1}{30}\,\frac{60\,\frac{\pi^2\,\beta_0^2\,B^{(2)}}{A^{(1)}}+40\,\frac{\pi^2\,\beta_1\,A^{(2)}}{A^{(1)}}}{\pi^5}+\frac{10}{3}\,\frac{\beta_0^2\,A^{(2)}\,L}{\pi^3\,A^{(1)}}\right)\alpha_s^3\\
&+\left(\frac{1}{30}\,\frac{40\,\frac{\pi^3\,\beta_0^2\,B^{(1)}}{A^{(1)}}+40\,\frac{\pi^3\,\beta_0\,A^{(2)}}{A^{(1)}}+40\,\pi^3\,\beta_1}{\pi^5}+\frac{20}{9}\,\frac{\beta_0^2\,L}{\pi^2}\right)\alpha_s^2+\frac{4}{3}\,\frac{\beta_0\,\alpha_s}{\pi}\,,
\end{aligned}$$

$$\begin{aligned}
c_4 = &\left(\frac{1}{30}\,\frac{60\,\frac{\beta_0^2\,\beta_1\,B^{(2)}}{A^{(1)}}+30\,\frac{\beta_1^2\,A^{(2)}}{A^{(1)}}}{\pi^5}+2\,\frac{\beta_0^4\,A^{(2)}\,L^2}{\pi^5\,A^{(1)}}\right.\\
&\left.+\frac{1}{30}\,\frac{(40\,\frac{\beta_0^4\,B^{(2)}}{A^{(1)}}+120\,\frac{\beta_0^2\,\beta_1\,A^{(2)}}{A^{(1)}})\,L}{\pi^5}\right)\alpha_s^5\\
&+\left(\frac{1}{30}\,\frac{60\,\frac{\pi\,\beta_0^3\,B^{(2)}}{A^{(1)}}+60\,\frac{\pi\,\beta_0\,\beta_1\,A^{(2)}}{A^{(1)}}}{\pi^5}+4\,\frac{\beta_0^3\,A^{(2)}\,L}{\pi^4\,A^{(1)}}\right)\alpha_s^4+3\,\frac{\alpha_s^3\,\beta_0^2\,A^{(2)}}{\pi^3\,A^{(1)}}\\
&+2\,\frac{\beta_0^2\,\alpha_s^2}{\pi^2}\,,
\end{aligned}$$

$$c_5=\left(\frac{56}{15}\,\frac{\beta_0^4\,A^{(2)}\,L}{\pi^5\,A^{(1)}}+\frac{1}{30}\,\frac{48\,\frac{\beta_0^4\,B^{(2)}}{A^{(1)}}+96\,\frac{\beta_0^2\,\beta_1\,A^{(2)}}{A^{(1)}}}{\pi^5}\right)\alpha_s^5+\frac{16}{5}\,\frac{\alpha_s^4\,\beta_0^3\,A^{(2)}}{\pi^4\,A^{(1)}}\,,$$

$$c_6=\frac{8}{3}\,\frac{\beta_0^4\,A^{(2)}\,\alpha_s^5}{\pi^5\,A^{(1)}}\,.$$

Appendix B

The modified parton distribution functions

According to the factorization theorem for the Drell-Yan process [13], see also Chapter 1, all collinear singularities at every order in perturbation theory can be factorised out into universal parton distribution functions. Various factorization schemes (e.g. $\overline{\rm MS}$, DIS) differ by how much of the finite, non-logarithmic contribution to the cross section is included in the parton distributions. A change in the set of the parton distribution functions generates modifications of the finite perturbative corrections to the cross section.

The parton distribution functions used for the Drell-Yan process, f', are related to the $\overline{\rm MS}$ structure functions, f, by a convolution [21, 35, 37], cf. (2.4.52)

$$f'_{a/H}(x_A,\mu) = \sum_c \int_{x_A}^1 \frac{dz}{z} C_{ac}\left(\frac{x_A}{z},\mu\right) f_{c/H}\left(z,\mu\right) \ , \tag{B.0.1}$$

where $(a, b \neq g)$

$$\begin{aligned} C_{ab}(z,\mu) &= \delta_{ab}\Big\{\delta(1-z) + \bar{\alpha}_s(\mu) C_F \left[1 - z + \left(\frac{\pi^2}{2} - 4\right)\delta(1-z)\right]\Big\} \ , \\ C_{ag}(z,\mu) &= \bar{\alpha}_s(\mu) T_R\Big[2z(1-z)\Big] \ , \end{aligned}$$

and $\bar{\alpha}_s(\mu) = \frac{\alpha_s(\mu)}{2\pi}$, $C_F = 4/3$, $T_R = 1/2$.

The scale dependence of the parton distribution functions is determined by the DGLAP

evolution equation, i.e. for the moments of the non-singlet (NS) parton distributions, $\tilde{f}_{q/H} = f_{q/H} - f_{\bar{q}/H}$, we have

$$\frac{d}{d\ln\mu^2}\tilde{f}_{q/H}(N,\mu) = \gamma_N \tilde{f}_{q/H}(N,\mu)\,, \tag{B.0.2}$$

where $\tilde{f}_{q/H}(N,\mu) = \int_0^1 dx x^N \tilde{f}_{q/H}(x,\mu)$ and the solution is

$$\tilde{f}_{q/H}(N,\mu_1) = \exp\left[-\int_{\mu_1}^{\mu_2}\frac{d\bar{\mu}^2}{\bar{\mu}^2}\gamma_N(\alpha_s(\bar{\mu}))\right]\tilde{f}_{q/H}(N,\mu_2)\,. \tag{B.0.3}$$

The anomalous dimension γ_N is defined as

$$\gamma_N(\alpha_s) = \bar{\alpha_s}\int_0^1 dz\, z^N P_{qq}(z)$$

where P_{qq} is the quark-quark Altarelli-Parisi splitting function. Thus the anomalous dimension inherits the perturbative character of the splitting function

$$\gamma_N(\alpha_s) = \sum_{i=1}\bar{\alpha_s}^i\gamma_N^{(i)}\,,$$

the first coefficient (in the $\overline{\text{MS}}$ scheme) being

$$\gamma_N^{(1)} = C_F\left[-\frac{1}{2} + \frac{1}{(N+1)(N+2)} - 2\sum_{j=2}^{N+1}\frac{1}{j}\right].$$

For the modified NS parton distributions, $\tilde{f}'$, the DGLAP equation has an identical form

$$\frac{d}{d\ln\mu^2}\tilde{f}'_{q/H}(N,\mu) = \gamma'_N\tilde{f}'_{q/H}(N,\mu)\,, \tag{B.0.4}$$

where now

$$\tilde{f}'_{q/H}(N,\mu) = C_{qq}(N,\mu)\tilde{f}_{q/H}(N,\mu)\,, \tag{B.0.5}$$

and $C_{qq}(N,\mu) = \int_0^1 dz z^N C_{qq}(z,\mu)$. The modified anomalous dimension γ' differs in a calculable way from the $\overline{\text{MS}}$ anomalous dimension γ. Comparing DGLAP equations for the case of modified parton distribution functions (B.0.4) and for the unmodified case (B.0.2) gives

$$\exp\left\{\int_{\mu_1}^{\mu_2}\frac{d\bar{\mu}^2}{\bar{\mu}^2}\left[\gamma'_N(\alpha_s(\bar{\mu})) - \gamma_N(\alpha_s(\bar{\mu}))\right]\right\} = \frac{C_{qq}(N,\mu_2)}{C_{qq}(N,\mu_1)}$$

which when solved perturbatively yields

$$\begin{aligned}\gamma_N'^{(1)} &= \gamma_N^{(1)} \\ \gamma_N'^{(2)} &= \gamma_N^{(2)} - 2\beta_0 C_F \left[\frac{\pi^2}{2} - 4 + \frac{1}{(N+2)(N+1)}\right] .\end{aligned}$$

Appendix C

Ansatz function

For completeness we present here details of the ansatz functions used to obtain numerical predictions. Their task is to parameterize the integration over parton distribution functions in (5.1.12). The expression for the cross section (5.3.20) can be rearranged to give

$$\begin{aligned}\frac{d\sigma}{dp_{\rm T}} &= \left\{ -\frac{1}{p_{\rm T*}}\frac{dp_{\rm T*}}{dp_{\rm T}}\Sigma_1(p_{\rm T*},M_V)\mathcal{A}^V(p_{\rm T*},M_V)\tilde{F}^{NP}(p_{\rm T}) \right. \\ &+ \Sigma_2(p_{\rm T*},M_V)\frac{dp_{\rm T*}}{dp_{\rm T}}\frac{d\mathcal{A}^V(p_{\rm T*},M_V)}{dp_{\rm T*}}\tilde{F}^{NP}(p_{\rm T}) \\ &+ \left. \Sigma_2(p_{\rm T*},M_V)\mathcal{A}^V(p_{\rm T*},M_V)\frac{d}{dp_{\rm T}}\tilde{F}^{NP}(p_{\rm T}) \right\}, \end{aligned} \tag{C.0.1}$$

where

$$\mathcal{A}^V(p_{\rm T*},Q) = \sigma_0 \sum_{qq'} U^V_{qq'} \int_0^1 dx_A\, dx_B\, \delta\left(x_A x_B - \frac{Q^2}{s}\right) f_{q/A}(x_A,p_{\rm T*})\, f_{q'/B}(x_B,p_{\rm T*}) \tag{C.0.2}$$

is the ansatz function.

We find $\mathcal{A}^V(p_{\rm T*},Q)$ can be very accurately parameterized in the range $1.2 \le p_{\rm T*} \le 1000$ GeV with a 5th order polynomial in $\ln(p^2_{\rm T*}/Q^2)$, in particular

$$\begin{aligned}\mathcal{A}^V(p_{\rm T*},Q) &= 10^4 \times (\, a(Q) + b(Q)\, L(p_{\rm T*}) + c(Q)\, L^2(p_{\rm T*}) + d(Q)\, L^3(p_{\rm T*}) \\ &\quad + e(Q)\, L^4(p_{\rm T*}) + f(Q)\, L^5(p_{\rm T*}))\end{aligned} \tag{C.0.3}$$

with $L(p_{T*}) = \ln(p_{T*}/1.2)$. For $Q = M_Z$ and MRST99 parton distribution functions [74], option 1 (central gluon, $\alpha_s = 0.1175$) we have

$$\mathcal{A}^Z(p_{T*}, M_Z)|_{MRST99} = 10^4 \times (0.463402 + 0.115187\, L(p_{T*}) - 0.044319\, L^2(p_{T*}) + 0.008582\, L^3(p_{T*}) - 0.000905\, L^4(p_{T*}) + 4 \times 10^{-5}\, L^5(p_{T*})), \quad \text{(C.0.4)}$$

A similar exercise can be performed for different values of α_s, gluon distributions or for an entirely different set of parton distribution functions, see Fig. C.1 and Fig. C.2. Examining the accuracy of the approximation of the MC results by the ansatz function we find a difference less than 0.15% for the highest values of p_{T*}, cf. Fig C.3. (In practice $A^V(p_{T*}, Q)$ is never calculated for such high values of p_{T*}.) Consequently, the biggest error introduced by replacing the Monte Carlo integration with the ansatz function in (5.3.20) does not exceed 0.6% and appears mostly at the intermediate p_T range, see Fig. C.4.

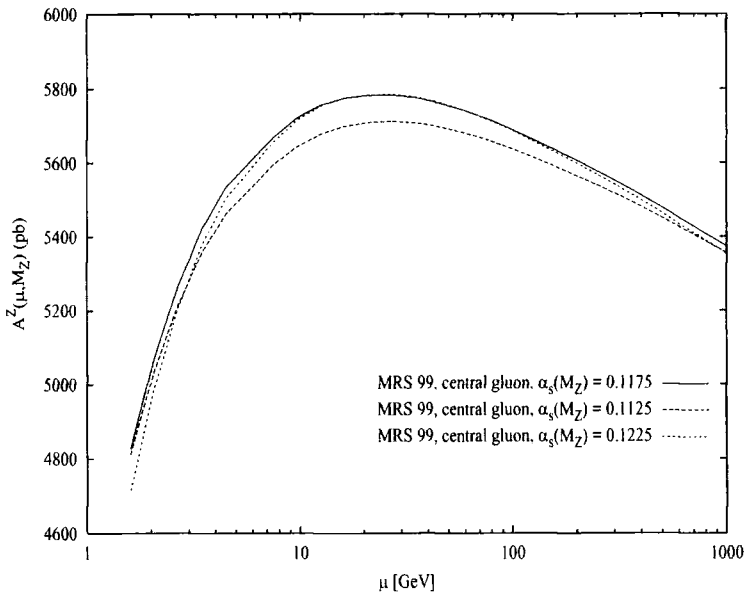

Figure C.1: MRST99 ansatz functions (C.0.3) for $Q = M_Z$ and different values of α_s. Here N_f changes in a step-like manner.

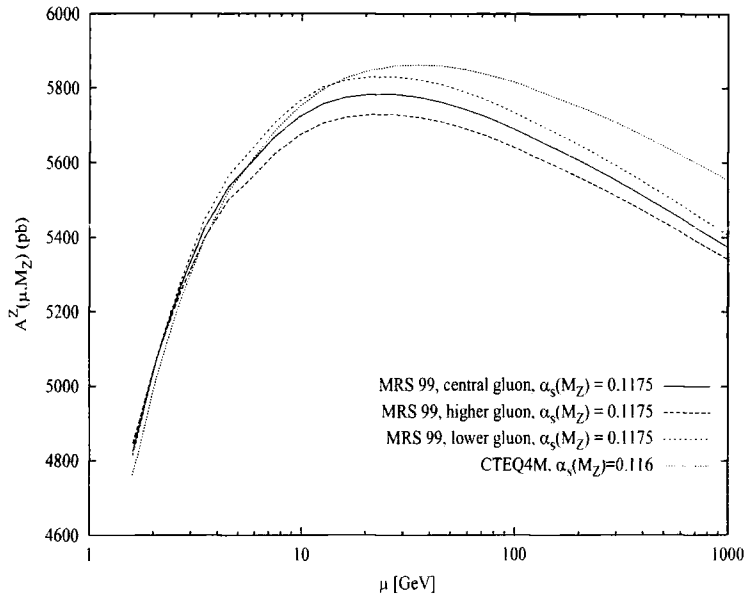

Figure C.2: Ansatz functions (C.0.3) for $Q = M_Z$. Here N_f changes in a step-like manner.

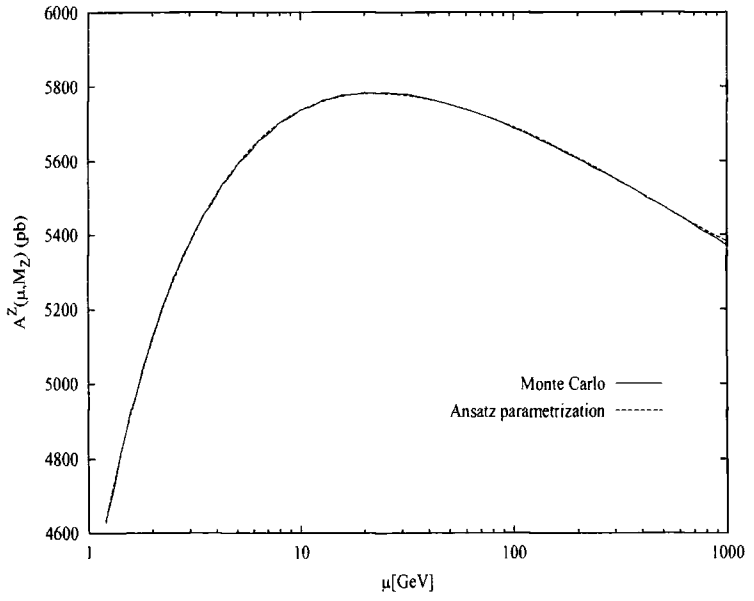

Figure C.3: Quality of the approximation of the Monte Carlo results by the ansatz parameterization for MRST99 parton distribution functions (central gluon, $\alpha_s = 0.1175$). Here N_f changes in a continuous manner described in section 5.2.

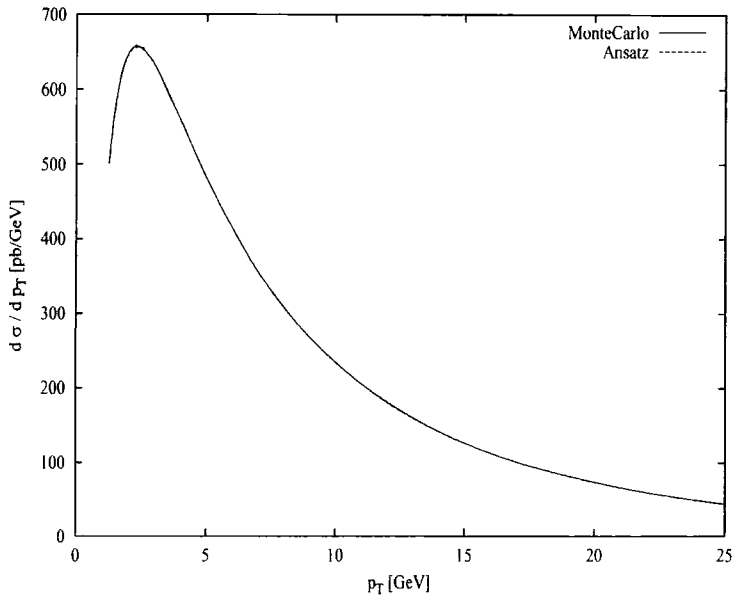

Figure C.4: Quality of the approximation of the Monte Carlo results by the ansatz parameterization for the Z p_{T} distribution in the KS approach ($\mu_R = p_{\mathrm{T}}^{2/3} Q^{1/3}$); MRST99 parton distribution functions (central gluon, $\alpha_s = 0.1175$). Here N_f changes in a continuous manner described in section 5.2 and no non-perturbative contribution is assumed.

References

[1] S.L. Glashow, *Nucl. Phys.* **22** (1961) 579;
S. Weinberg, *Phys. Rev. Lett.* **19** (1967) 1264;
A. Salam, in *Elementary Particle Theory*, ed. N. Svartholm, Almquist and Forlag (1968);
for a pedagogical introduction to the Standard Model see also:
T.P. Cheng and L.F. Li, *Gauge Theory of Elementary Particle Physics*, Oxford University Press (1991);
J. Donoghue, E. Golovich and B.R. Holstein, *Dynamics of the Standard Model*, Cambridge University Press (1994).

[2] M. Peskin and D.V. Schroeder, *An Introduction to Quantum Field Theory*, Addison-Wesley (1995);
L.H. Ryder, *Quantum Field Theory*, Cambridge University Press (1992);
G. Sterman, *An Introduction to Quantum Field Theory*, Cambridge University Press (1993);
S. Weinberg, *The Quantum Theory of Fields*, Cambridge University Press (1995).

[3] R.K. Ellis, W.J. Stirling and B.R. Webber, *QCD and Collider Physics*, Cambridge University Press (1996).

[4] The CTEQ Collaboration, *Handbook of Perturbative QCD*, *Rev. Mod. Phys.* **67** (1995) 157.

[5] M.R. Pennington, *Reports in Progress in Physics* **46** (1983) 393.

[6] T. Muta, *Foundations of Quantum Chromodynamics*, World Scientific (1987).

[7] R.D. Field, *Applications of Perturbative QCD*, Addison-Wesley (1989).

[8] G. Leibbrant, *Rev. Mod. Phys.* **59** (1987) 1067.

[9] J. Collins, *Renormalization*, Cambridge University Press (1992).

[10] G. 't Hooft and M. Veltman, *Nucl. Phys.* **B44** (1972) 199.

[11] D.E. Groom *et al.* [Particle Data Group] *Eur. Phys. J.* **15** (2000) 1.

[12] T. Kinoshita, *J. Math. Phys.* **3** (1962) 650.
T.D. Lee and M. Naunenberg, *Phys. Rev.* **133B** (1964) 1549.

[13] J. Collins, D. Soper, G. Sterman in *Perturbative Quantum Chromodynamics*, ed. by A.H. Mueller, World Scientific (1989).

[14] S.D. Drell and T.M. Yan, *Ann. Phys.* **66** (1971) 578.

[15] S. Catani, Lectures at the 1998 CTEQ Summer School, Courmayeur, Italy, July 1998.

[16] S. Catani *et al.*, CERN-TH-2000-131, preprint hep-ph/0005025.

[17] B. I. Ermolaev and V. S. Fadin, *JETP Lett.* **33**, (1981) 269;
A. Bassetto, M. Ciafaloni and G. Marchesini, *Phys. Rep.* **100** (1983) 201, and references therein.

[18] S. Catani, L. Trentadue, G. Turnock, B.R. Webber *Phys. Lett.* **B263** (1991) 491; *Nucl. Phys.* **B407** (1993) 3.

[19] G. Sterman, *Nucl. Phys.* **B281** (1987) 310;
S. Catani and L. Trentadue, *Nucl. Phys.* **B327** (1989) 323; *Nucl. Phys.* **B353** (1991) 183;

[20] J. Collins and D. Soper, *Nucl. Phys.* **B193** (1981) 381; Erratum *Nucl. Phys.* **B213** (1983) 545; *Nucl. Phys.* **B197** (1982) 446.

[21] J. Collins, D. Soper and G. Sterman, *Nucl. Phys.* **B250** (1985) 199.

[22] B. Abbott *et al.* [D0 Collaboration], *Phys. Rev. Lett.* **80** (1998) 3008.

[23] W.J. Stirling and M.R. Whalley, *J. Phys.* **G19** (1993) D1, and references therein.

[24] G. Altarelli, R.K. Ellis, M. Greco and G. Martinelli, *Nucl. Phys.* **B246** (1984) 12.

[25] S.D. Ellis and W.J. Stirling, *Phys. Rev.* **D23** (1981) 214.

[26] W.J. Stirling, private communication.

[27] S.D. Ellis, N. Fleishon and W.J. Stirling, *Phys. Rev.* **D24** (1981) 1386.

[28] P.E.L Rakov, B.R. Webber, *Nucl. Phys.* **B187** (1981) 254.

[29] Yu.L. Dokshitzer, D.I. Dyakonov and S.I. Troyan, *Phys. Rep.* **58** (1980) 269.

[30] H. Fritzsch and P. Minkowski, *Phys. Lett.* **B73** (1978) 80;
K. Kajantie and R. Ratio, *Nucl. Phys.* **B139** (1978) 72.

[31] R.K. Ellis, G. Martinelli and R. Petronzio, *Nucl. Phys.* **B211** (1983) 106.

[32] P. Arnold and M.H. Reno, *Nucl. Phys.* **B319** (1989) 37, Erratum *Nucl. Phys.* **B330** (1990) 284;
P. Arnold, R.K. Ellis and M.H. Reno, *Phys. Rev.* **D40** (1989) 912,

[33] G. Parisi and R. Petronzio, *Nucl. Phys.* **B154** (1979) 427.

[34] J. Collins, D. Soper and G. Sterman, *Phys. Lett.* **B109** (1982) 388; *Nucl. Phys.* **B223** (1983) 381; *Phys. Lett.* **B126** (1983) 275.

[35] C. Davies and W.J. Stirling, *Nucl. Phys.* **B244** (1984) 337.

[36] P.B. Arnold and R.P. Kauffman, *Nucl. Phys.* **B349** (1991) 381.

[37] R.K. Ellis, D.A. Ross and S. Veseli, *Nucl. Phys.* **B503** (1997) 309.

[38] C. Davies, Ph.D. Thesis (Cambridge University), 1984.

[39] C. Davies, W.J. Stirling and B.R. Webber, *Nucl. Phys.* **B256** (1985) 413.

[40] G. P. Korchemsky and G. Sterman, *Nucl. Phys.* **B437** (1995) 415.

[41] A. Guffanti and G.E. Smye, preprint hep-ph/0007190.

[42] D.W. Duke and J.F. Owens, *Phys. Rev.* **D30** (1984) 49.

[43] G.A. Ladinsky and C.-P. Yuan, *Phys. Rev.* **D50** (1994) 4239.

[44] R. Brock, G. Ladinsky, F. Landry and C. P. Yuan, preprint hep-ph/9905391.

[45] B. Abbott *et al.*, [D0 Collaboration], *Phys. Rev.* **D61** (2000) 032004;
B. Abbott *et al.* [D0 Collaboration], *Phys. Rev. Lett.* **84** (2000) 2792.

[46] T. Affolder *et al.*, [CDF Collaboration], *Phys. Rev. Lett.* **84** (2000) 845.

[47] A.D. Martin, R.G. Roberts, W.J. Stirling and R.S. Thorne, *Eur. Phys. J.* **C4** (1998) 463.

[48] H. Lai *et al.*, *Phys. Rev.* **D55** (1997) 1280.

[49] C. Balazs and C.-P. Yuan, *Phys. Rev.* **D56** (1997) 5558.

[50] G. Marchesini, B.R. Webber, G. Abbiendi, I.G. Knowles, M.H. Seymour and L. Stanco, *Comp. Phys. Comm.* **67** (1992) 465.

[51] F.E. Paige and S.D. Protopopescu, in *Proc. UCLA Workshop*, ed. H.-U. Bengtsson *at al.*, World Scientific (1986).

[52] T. Sjöstrand, *Comp. Phys. Comm.* **82** (1994) 74.

[53] G. Corcella and M.H. Seymour, *Nucl. Phys.* **565** (2000) 227.

[54] G. Miu and T. Sjöstrand, *Phys. Lett.* **B449** (1999) 313.

[55] S. Mrenna, preprint hep-ph/9902471.

[56] S. Veseli, preprint FERMILAB-PUB-97/271-T, physics/9710017.

[57] R.K. Ellis and S. Veseli, *Nucl. Phys.* **B511** (1998) 649.

[58] S. Frixione, P. Nason and G. Ridolfi, *Nucl. Phys.* **B542** (1999) 311.

[59] N. Brown and W.J. Stirling, *Zeit. Phys.* **C53** (1992) 629.

[60] C. Balazs, Ph.D. Thesis (Michigan State University), 1999, hep-ph/9906422.

[61] S.J. Brodsky, M.S. Gill, M. Melles and J. Rathsman, *Phys. Rev.* **D58** (1998) 116006; S.J. Brodsky, M. Melles and J. Rathsman, *Phys. Rev.* **D60** (1999) 096006.

[62] B. Abbott *et al.* (CDF Collaboration), *Phys. Rev.* **D61** (2000) 072001.

[63] M. Lancaster and D.S. Waters, *J. Phys.* **G26** (2000) 646.

[64] F. Abe *et al.* [CDF Collaboration], *Phys. Rev. Lett.* **66** (1991) 2951.

[65] B. Abbott *et al.* [D0 Collaboration], *Phys. Rev. Lett.* **80** (1998) 5498.

[66] M. Lancaster, talk at the *UK Phenomenology Workshop on Collider Physics*, Durham, September 1999.

[67] S. Catani *et al.*, preprint hep-ph/0005114.

[68] A. Del Fabbro and D. Treleani, *Phys. Rev.* **D61** (2000) 077502.

[69] P.V. Landshoff and J.C. Polkinghorne, *Phys. Rev.* **D18** (1978) 3344;
C. Goebel, F. Halzen and D.M. Scott, *Phys. Rev.* **D22** (1980) 2789;
N. Paver and D. Treleani, *Nuovo Cimento* **A70** (1982) 215;
B. Humpert, *Phys. Lett.* **B131** (1983) 461;
B. Humpert and R. Odorico *Phys. Lett.* **B154** (1985) 211;
F. Halzen, P. Hoyer and W.J. Stirling, *Phys. Lett.* **B188** (1987) 375;
M. Mangano, *Zeit. Phys.* **C42** (1989) 331;
R.M. Godbole, S. Gupta and J. Lindfors, *Zeit. Phys.* **C47** (1990) 69;
M. Drees and T. Han, *Phys. Rev. Lett.* **77** (1996) 4142.

[70] F. Abe et al. (CDF Collaboration), *Phys. Rev. Lett.* **79** (1997) 584; *Phys. Rev.* **D56** (1997) 3811.

[71] V. Barger, Kingman Cheung, T. Han and R.J.N. Phillips, *Phys. Rev.* **D42** (1990) 3052.

[72] D.A. Dicus and R. Vega, *Phys. Lett.* **B217** (1989) 194; *Nucl. Phys.* **B329** (1990) 533;
M.S. Chanowitz and M. Golden, *Phys. Rev. Lett.* **61** (1988) 1053;
M.S. Berger and M.S. Chanowitz, *Phys. Lett.* **B263** (1991) 509;
D.A. Dicus, J.F. Gunion, L.H. Orr and R. Vega, *Nucl. Phys.* **B377** (1991) 31.

[73] G. Calucci and D. Treleani, *Phys. Rev.* **D57** (1998) 503; *Phys. Rev.* **D60** (1999) 054023.

[74] A.D. Martin, R.G. Roberts, W.J. Stirling and R.S. Thorne, *Eur. Phys. J.* **C14** (2000) 133.

[75] R. Hamberg, T. Matsuura and W.L. van Neerven, *Nucl. Phys.* **B345** (1990) 331; *Nucl. Phys.* **B359** (1991) 343;
W.L. van Neerven and E.B. Zijlstra, *Nucl. Phys.* **B382** (1992) 11.

[76] J. Ohnemus, *Phys. Rev.* **D44** (1991) 1403;
S. Frixione, *Nucl. Phys.* **B410** (1993) 280;
J. Ohnemus, *Phys. Rev.* **D50** (1994) 1931;
L. Dixon, Z. Kunszt and A. Signer, *Nucl. Phys.* **B531** (1998) 23; *Phys. Rev.* **D60** (1999) 114037;
J.M. Campbell and R.K. Ellis, *Phys. Rev.* **D60** (1999) 113006.

[77] T. Stelzer and W.F. Long, *Comp. Phys. Comm.* **81** (1994) 357.

[78] E. Murayama, I. Watanabe and K. Hagiwara, *KEK report* 91-11, January 1992.

[79] G.P. Lepage, *Jou. Comp. Phys.* **27** (1978) 192.

[80] G. Calucci and D. Treleani, *Phys. Rev.* **D60** (1999) 054023.

[81] A. Del Fabbro and D. Treleani, preprint hep-ph/0005273.

[82] T. Affolder *et al.* [CDF Collaboration], preprint hep-ex/0007044.